

RTD-TDR-63-4179  
PART I

**PRESSURE MEASUREMENTS FOR MACH FIVE FLOWS  
OVER WINGED RE-ENTRY CONFIGURATIONS  
WITH AERODYNAMIC CONTROLS**

**PART I. BLUNT CABIN CONFIGURATION**

TECHNICAL DOCUMENTARY REPORT No. RTD-TDR-63-4179, PART I

FEBRUARY 1964

**DEPARTMENT OF AERONAUTICS  
U. S. Naval Postgraduate School  
Monterey, California**

AF FLIGHT DYNAMICS LABORATORY  
RESEARCH AND TECHNOLOGY DIVISION  
AIR FORCE SYSTEMS COMMAND  
WRIGHT-PATTERSON AIR FORCE BASE, OHIO

Project No. 8219, Task No. 821902

(Prepared under Contract No. AF 33(616)-8130 by  
Grumman Aircraft Engineering Corporation, Bethpage, New York  
Louis G. Kaufman, II, author)

## NOTICES

When Government drawings, specifications, or other data are used for any purpose other than in connection with a definitely related Government procurement operation, the United States Government thereby incurs no responsibility nor any obligation whatsoever; and the fact that the Government may have formulated, furnished, or in any way supplied the said drawings, specifications, or other data, is not to be regarded by implication or otherwise as in any manner licensing the holder or any other person or corporation, or conveying any rights or permission to manufacture, use, or sell any patented invention that may in any way be related thereto.

Qualified requesters may obtain copies of this report from the Defense Documentation Center (DDC), (formerly ASTIA), Cameron Station, Bldg. 5, 5010 Duke Street, Alexandria 4, Virginia

This report has been released to the Office of Technical Services, U.S. Department of Commerce, Washington 25, D.C., in stock quantities for sale to the general public.

Copies of this report should not be returned to the Aeronautical Systems Division unless return is required by security considerations, contractual obligations, or notice on a specific document.

## FOREWORD

This report, written in two parts, presents the results of a portion of the experimental program for the investigation of hypersonic flow separation and control characteristics being conducted by the Research Department of Grumman Aircraft Engineering Corporation, Bethpage, New York. Mr. Donald E. Hoak of the Flight Dynamics Laboratory, Research and Technology Division, at Wright-Patterson Air Force Base, Ohio, is the Air Force Project Engineer for the program, which is being supported primarily under Contract AF33(616)-8130, Air Force Task 821902.

The author wishes to express his appreciation to the staff of the von Karman Facility for their helpfulness in conducting the tests; and particularly to Messrs. Schueler, Baer and Uselton for providing the machine plotted graphs of the experimental data included in this report. Ozaalid reproducible copies of the tabulated data are available on loan from the Flight Control Division of the Flight Dynamics Laboratory.

The parts of this report are:

Part I: Blunt Cabin Configuration

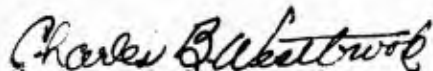
Part II: Conical Cabin Configuration

## ABSTRACT

Pressure data were obtained for Mach five flows over winged re-entry configurations composed of cylindrical cabins mounted on a 60 degree sweepback delta wing with a cylindrical leading edge, clipped tips, and trailing edge flaps. The model was tested with spherical and conical fronts on the cabin, with and without tip fins, and with and without a trailing edge spoiler. Flap deflections were varied from -40 to +40 degrees and the model was pitched at angles of attack from -30 to +45 degrees for a free stream Reynolds number, based on model length of 3,575,000.

## PUBLICATION REVIEW

This report has been reviewed and is approved.



Charles B. Westbrook  
Chief, Control Criteria Branch  
Flight Control Division  
Air Force Flight Dynamics Laboratory

## TABLE OF CONTENTS

ITEM	PAGE
Introduction . . . . .	1
Model . . . . .	1
Test Conditions . . . . .	2
Data Reduction and Accuracy . . . . .	2
Results . . . . .	3
References . . . . .	4

# LIST OF ILLUSTRATIONS

Figure		Page
1	General Outline of Models and Remarks for Over-all Program . . . . .	9
2	Photograph of Upper Surface of Model, with Tip Fins, Installed in the AEDC 40-inch Supersonic Tunnel . . . . .	10
3	Photograph of Lower Surface of Model, with Tip Fins, Installed in the AEDC 40-inch Supersonic Tunnel . . . . .	11
4	Instrumentation on Upper Surface of Model . . . . .	12
5	Instrumentation on Lower Surface of Model . . . . .	13
6 - 42	Pressure Coefficient Data Plots* . . . . .	14

\*See Table II, page 6, for figure numbers corresponding to particular test conditions.

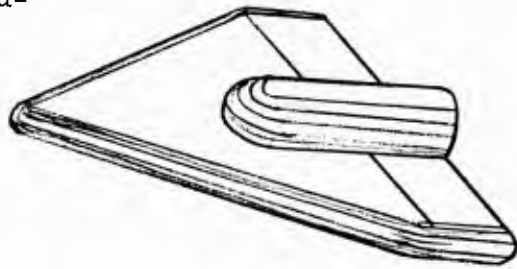
# LIST OF SYMBOLS

$C_p$	Pressure coefficient, $C_p = (p - p_\infty) / q_\infty$
$M_\infty$	Free stream Mach number
$p$	Pressure (psia)
$p_o$	Stagnation pressure (psia)
$p_\infty$	Free stream static pressure (psia)
$q_\infty$	Free stream dynamic pressure (psia)
$Re_\infty / \text{ft}$	Reynolds number per foot, $Re_\infty / \text{ft} = \rho_\infty U_\infty / \mu_\infty$
$T_o$	Stagnation temperature ( $^{\circ}\text{R}$ )
$T_\infty$	Free stream static temperature ( $^{\circ}\text{R}$ )
$U_\infty$	Free stream velocity (ft/sec)
$X'$	Nondimensional streamwise distance measured downstream of the virtual apex of the delta wing
$Y'$	Nondimensional spanwise distance measured outboard from the model centerline
$\alpha$	Angle of attack of model (degrees)
$\mu_\infty$	Viscosity of air in the free stream (slugs/ft sec)
$\rho_\infty$	Density of air in the free stream (slugs/ft <sup>3</sup> )

## INTRODUCTION

The experimental data generated for an investigation of hypersonic flow separation and aerodynamic control characteristics are to be presented in a series of reports, of which this is one. Pressure, heat transfer, and force data are to be obtained for hypersonic flows over "basic geometries," such as a wedge mounted on a flat plate, and for "typical" hypersonic flight configurations with aerodynamic control surfaces. The experimental portion of the program requires a total of eleven models (see Fig. 1, page 9); eight for tests in the von Karman Facility of the Arnold Engineering Development Center and three for tests in the Grumman Hypersonic Shock Tunnel (Refs. 1 and 2). Data obtained from AEDC tests of one of the models are given in this two part report (see "Foreword").

This report presents pressure data obtained in the AEDC 40-inch Supersonic Tunnel for Mach 5 flows over winged re-entry configurations having three, remotely controlled, trailing edge flaps. Alterations to one basic model, such as adding tip fins, provided the different configurations. The same model is to be tested in the AEDC 50-inch Mach 8 Tunnel to obtain pressure and aerodynamic heating rate distributions at the same free stream Reynolds number. Six component force data were obtained on a geometrically similar model in both the 40-inch and 50-inch AEDC Tunnels at the same model length Reynolds number as for the pressure tests. A third geometrically similar model, with limited pressure instrumentation, was tested in the AEDC Hotshot 2 Tunnel (see Fig. 1).



This part of the report presents the data obtained on the basic model with a spherically capped, cylindrical cabin mounted on top of the wing. The second part of this report presents the data obtained on the model with a conically capped cabin and with and without tip fins and a trailing edge spoiler.

## MODEL

Photographs of the model installed in the AEDC 40-inch Supersonic Tunnel are shown in Figs. 2 and 3. The model consists of a spherically capped cylindrical cabin mounted on top of a blunt delta wing with  $60^\circ$

Manuscript released by author in October 1963 for publication as an RTD Technical Documentary Report.



sweepback. The delta wing has clipped tips and a thickness equal to 10 per cent of the virtual length of the model (see Figs. 4 and 5). The cabin height is equal to the wing thickness and the radius of the spherical apex and cylindrical leading edges of the wing is the same as for the 70° sweepback wing of Configuration "D" (Fig. 1).

The model has three, remotely controlled, trailing edge flaps. Two outboard flaps, extending from the cabin-wing junctions to the shoulders of the cylindrical wing tips, and one "split" flap on the lower surface of the wing, extending spanwise between the outboard flaps (Fig. 5). The flaps are rectangular and have chords equal to 15 per cent of the virtual length of the model.

Each flap is individually controllable; the outboard flaps have a travel of  $\pm 40$  degrees and the "center" flap on the lower surface has a travel of  $+20$  degrees. Flap deflections are defined positive for downward deflections of the flap trailing edges. The three electrical motors for the flaps are enclosed in a water cooled housing immediately behind the model (see Figs. 2 and 3), and actuate the flaps through drive screws and push-pull rods connected to the flap bell cranks.

Pressure tap locations on the upper and lower surfaces of the model are shown in Figs. 4 and 5. Eight taps are located on the spherical-cylindrical cabin, six on the upper and lower surfaces of the outboard flaps, two on the center flap, and the remaining are positioned in streamwise and spanwise lines on the upper and lower surfaces of the wing.

## TEST CONDITIONS

The data presented herein were obtained from Mach five tests in the AEDC 40-inch Supersonic Tunnel (Ref. 3). The model was pitched from 30 degrees nose down to 45 degrees nose up for various flap settings for a free stream Reynolds number per foot of 3.3 million (corresponding to a Reynolds number of 3.6 million, based on free stream conditions and the model reference length). Tunnel test conditions, flap settings, and angles of attack are shown in Table I.

## DATA REDUCTION AND ACCURACY

The data were reduced to standard pressure coefficient form:

$$C_p = \frac{p - p_\infty}{q_\infty}$$

where:  $p$  is the measured pressure,  $p_\infty$  is the free stream static pressure, and  $q_\infty$  is the free stream dynamic pressure. The inaccuracy in the

measured pressure varies from  $\pm 0.005$  psia for pressures below 1.00 psia, to  $\pm 0.075$  psia for pressures greater than 15 psia. Whence, depending upon the values of  $C_p$  and  $Re_\infty/ft$ , the pressure coefficient accuracy varies from about  $\pm 0.009$  to  $\pm 0.020$ . Variations in the tunnel conditions affect the accuracy of the tabulated pressure coefficient data to a negligible extent; the tunnel conditions shown in Table I were kept constant to well within one per cent of the values shown.

The automatic plotting machines, used in presenting the data herein, introduce another source of possible error. The discrepancy in the plotted pressure coefficients due to this machine error should not exceed  $\pm 0.01$ . Nevertheless, there is always the rare possibility that a point will be completely misplotted. Each graph has been inspected and questionable points checked with the tabulated pressure coefficients.

Finally, the remotely controlled flap settings were estimated to be accurate to well within half a degree.

## RESULTS

Table II summarizes the Mach five flow data obtained on the model and indicates the corresponding figure numbers where the sets of data are presented. The AEDC group number is presented in the last column. This number indicates the order in which the data were obtained and is to be used when referring to the tabulated data.

Four pages are required for each figure containing pressure coefficient plots. Streamwise plots of the pressure coefficients on the lower surface, at four spanwise stations, are presented on the first page of each figure. Streamwise plots along the upper surface, at six spanwise stations, are presented on the second page. Spanwise plots, at five streamwise stations on the lower and upper surfaces, are presented on the third and fourth pages of each figure.

The pressure coefficients for the tap in the spherical apex and for the taps in the cylindrical leading edges of the wing are presented in both the lower and upper surface plots. An outline of the model, showing the position of the streamwise and spanwise lines of pressure taps and the associated symbols, appears on each page. As indicated in the figures,  $X'$  is the nondimensional streamwise distance from the virtual apex to the projection of a pressure tap on the planform, and  $Y'$  is the nondimensional spanwise distance of the planform projection of the tap measured outboard from the centerline.

Although the accuracy of the plotted data should suffice for engineering purposes, ozalid reproducible copies of the tabulated data are available on loan (see "Foreword"). The plotted data may be read accurately using standard 20/inch grid, tracing graph paper overlays. The positions of the planform projections of the pressure taps are given in Table III.

## REFERENCES

1. Kaufman, Louis G. II, et al., A Review of Hypersonic Flow Separation and Control Characteristics, ASD-TDR-62-168, March 1962.
2. Evans, W. J. and Kaufman, L. G. II, Pretest Report on Hypersonic Flow Separation and Control Models for AEDC Tunnels A, B. Hotshot 2 and Grumman Hypersonic Shock Tunnel, Grumman Research Department Memorandum RM-209, July 1962.
3. Arnold Center, Test Facilities Handbook, Arnold Air Force Station, January 1961.
4. Kaufman, Louis G. II, Pressure and Heat Transfer Measurements for Hypersonic Flows Over Expansion Corners and Ahead of Ramps, Part I: Mach 5 and 8 Data for Expansion Corner Flows, Part II: Mach 5 Pressure Data for Flows Ahead of Ramps, Part III: Mach 8 Pressure Data for Flows Ahead of Ramps, Part IV: Mach 8 Heat Transfer Data for Flows Ahead of Ramps, ASD-TDR-63-679, July 1963.
5. Kaufman, Louis G. II, Pressure Measurements for Mach 8 Flows Over Expansion Corners and Ramps on an Internally Cooled Model, Part I: Expansion Corner Flows, Part II: Flows Over a Flat Plate with and without a Partial Span Ramp, Part III: Flows Over Full Span Ramps Mounted on a Flat Plate, to be published as an ASD Technical Documentary Report.
6. Kaufman, L. G. II and Meckler, L., Pressure and Heat Transfer Measurements at Mach 5 and 8 for a Fin Flat Plate Model, ASD-TDR-63-235, April 1963.
7. Kaufman, Louis G. II, Pressure Distributions and Oil Film Photographs for Mach 5 Flows Past Fins Mounted on a Flat Plate, to be published as an ASD Technical Documentary Report.
8. Hartofilis, Stavros A., Pressure Measurements at Mach 19 for a Winged Re-entry Configuration, ASD-TDR-63-319, May 1963.
9. Meckler, Lawrence, Longitudinal and Lateral Characteristics at Mach 5 and 8 for an Aerodynamically Controllable Winged Re-entry Configuration, to be published as an ASD Technical Documentary Report.
10. Kaufman, Louis G. II, Pressure and Heat Transfer Measurements for Hypersonic Flows Over a Blunt Pyramidal Configuration with Aerodynamic Controls, to be published as an ASD Technical Documentary Report.

TABLE I

## TEST CONDITIONS

Tunnel	$M_\infty=5.01$		$p_\infty=0.134\text{psia}$	$p_o=72\text{psia}$
Conditions	$Re_\infty/\text{ft}=3,300,000$		$q_\infty=2.35\text{psia}$	$T_o=620^\circ\text{R.}$
Flap Settings (deg)			ANGLES OF ATTACK (degrees)	
Center	Left	Right		
0	-40	-40	0	20 33 45
0	-30	-30	0	
0	-20	-20	-20	0 20 33 45
0	-10	-10	0	
0	0	0	-30 -20 -10 0 10 20 33 45	
0	+10	+10	0	
0	+20	+20	-30 -20 -10 0 10	45
0	+30	+30	0	
0	+40	+40	-30 -20 -10 0 10	
0	+20	-20	0	
+20	+20	+20	-10 0 10	45

A similar configuration, but with a conical cabin front instead of the spherical one, was tested at the same tunnel conditions for  $-30^\circ \leq \alpha \leq +10^\circ$ . The configuration was tested with and without tip fins and a full span spoiler at the trailing edge. The data are presented in Part II of this report.

TABLE II

## PRESSURE DATA FIGURE NUMBERS

FLAP SETTINGS (deg.)			$\alpha$ (deg.)	C <sub>p</sub> Plots Figure Numbers	AEDC Group Number
Center	Left	Right			
0	0	0	-30	6	49
0	+20	+20	-30	7	50
0	+40	+40	-30	8	59
0	-20	-20	-20	9	67
0	0	0	-20	10	48
0	+20	+20	-20	11	51
0	+40	+40	-20	12	58
0	0	0	-10	13	47
0	+20	+20	-10	14	52
+20	+20	+20	-10	15	63
0	+40	+40	-10	16	57
0	-40	-40	0	17	77
0	-30	-30	0	18	78
0	-20	-20	0	19	66
0	-10	-10	0	20	65
0	0	0	0	21	46
0	+10	+10	0	22	64
0	+20	-20	0	23	79
0	+20	+20	0	24	53
+20	+20	+20	0	25	62
0	+30	+30	0	26	60
0	+40	+40	0	27	56



TABLE II (contd.)

## PRESSURE DATA FIGURE NUMBERS

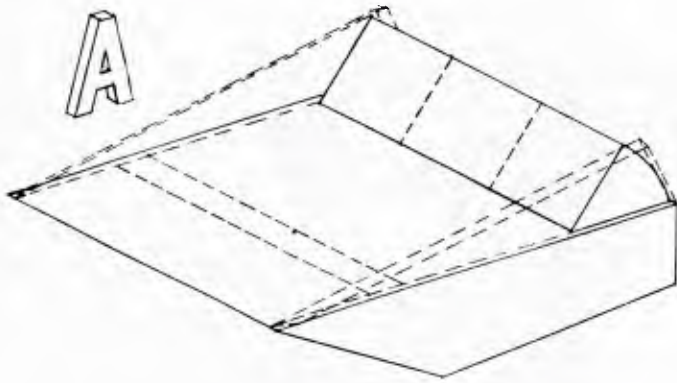
FLAP SETTINGS (deg.)			$\alpha$ (deg.)	$C_p$ Plots Figure Numbers	AEDC Group Number
Center	Left	Right			
0	0	0	+10	28	45
0	+20	+20	+10	29	54
+20	+20	+20	+10	30	61
0	+40	+40	+10	31	55
0	-40	-40	+20	32	76
0	-20	-20	+20	33	71
0	0	0	+20	34	70
0	-40	-40	+33	35	75
0	-20	-20	+33	36	72
0	0	0	+33	37	69
0	-40	-40	+45	38	74
0	-20	-20	+45	39	73
0	0	0	+45	40	68
0	+20	+20	+45	41	80
+20	+20	+20	+45	42	81

TABLE III

COORDINATES OF PLATFORM PROJECTIONS  
OF PRESSURE TAPS

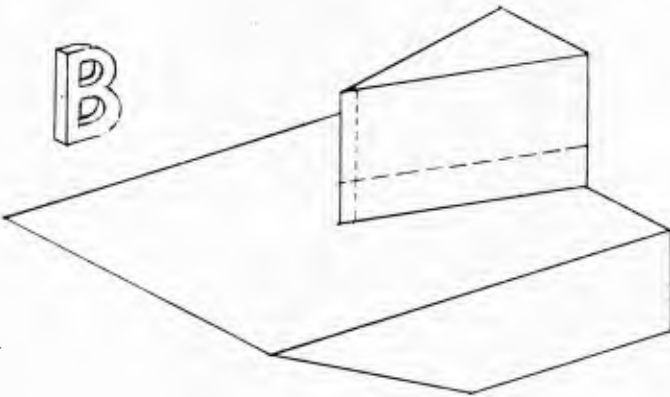
Tap No.	X'	Y'
78	0.0500	0
79	0.1000	↓
80	0.2596	
81	0.4038	
82	0.5481	
84	0.6923	
86	0.8077	0
87	0.9173	0.0313
88	0.9750	0.0313
42	0.5481	0.3125
43	0.6347	↓
44	0.6923	
45	0.7500	
46	0.8077	
47	0.9173	
48	0.9750	0.3125
31	0.4423	0.5625
32	0.5481	↓
33	0.6347	
34	0.6923	
35	0.7500	
36	0.8077	
37	0.9173	↓
38	0.9750	
26	0.8077	0.8020
27	0.9173	0.8020
28	0.9750	0.8020

Tap No.	X'	Y'
177	0.1000	0
178	0.2654	↓
179	0.3346	
180	0.4038	
181	0.4731	
182	0.5481	
183	0.5851	↓
184	0.6274	
164	0.6923	0.1083
166	0.7846	0.1083
167	0.9173	0.1083
154	0.6923	0.1877
156	0.7846	0.1877
157	0.9173	0.1877
141	0.4904	0.3125
142	0.5481	0.4375
143	0.6058	0.3125
146	0.7846	0.3125
147	0.9173	0.3125
148	0.9750	0.3125
131	0.4423	0.5625
132	0.5481	↓
134	0.6923	
136	0.7846	
137	0.9173	
138	0.9750	
126	0.7846	0.8020
127	0.9173	0.8020
128	0.9750	0.8020



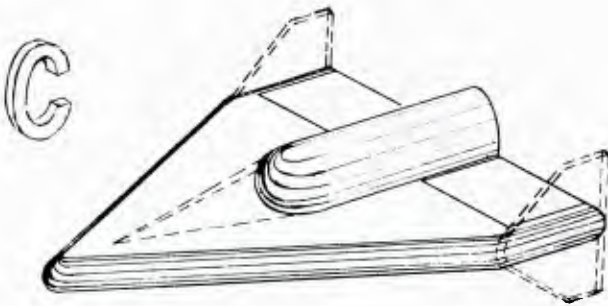
Separated Flows ahead of a Ramp  
Fore and aft flaps, end plates  
3 separate models:

- 1) Pressure and heat transfer, AEDC Tunnels A & B,  $M = 5$  &  $8$ , results in Ref. 4.
- 2) Controlled wall temperature, pressure, AEDC Tunnel B,  $M = 8$ , results in Ref. 5.
- 3) Pressure and heat transfer, Grumman Shock Tunnel,  $M \approx 13$  &  $19$ , results not available yet.



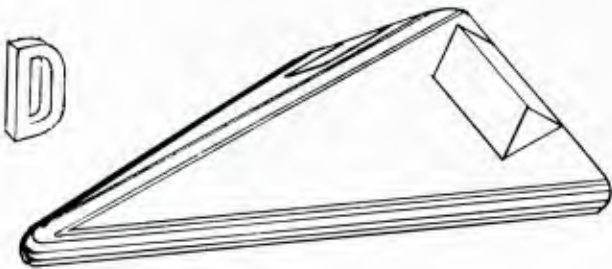
Wedge - Plate Interaction  
Small and large fins with sharp and blunt leading edges  
2 separate models:

- 1) Pressure and heat transfer, AEDC Tunnels A & B,  $M = 5$  &  $8$ , results in Refs. 6 and 7.
- 2) Pressure and heat transfer, Grumman Shock Tunnel,  $M \approx 13$  &  $19$ , results not available yet.



Clipped Delta, Blunt L.E.  
Center body, T.E. flaps, drooped nose, spoiler, tip fins  
3 separate models:

- 1) Pressure and heat transfer, AEDC Tunnels A & B,  $M = 5$  &  $8$ , results herein.
- 2) Pressure, AEDC Hotshot 2,  $M \approx 19$ , results in Ref. 8.
- 3) Six component force, AEDC Tunnels A & B,  $M = 5$  &  $8$ , results in Ref. 9.



Delta, Blunt L.E., Dihedral  
T.E. flaps, canard, ventral fin  
3 separate models:

- 1) Pressure and heat transfer, AEDC Tunnels A & B,  $M = 5$  &  $8$ , results in Ref. 10.
- 2) Pressure and heat transfer, Grumman Shock Tunnel,  $M \approx 19$ , results not available yet.
- 3) Six component force, AEDC Tunnels A & B,  $M = 5$  &  $8$ , results not available yet.

Fig. 1 General Outline of Models and Remarks for Over-all Program



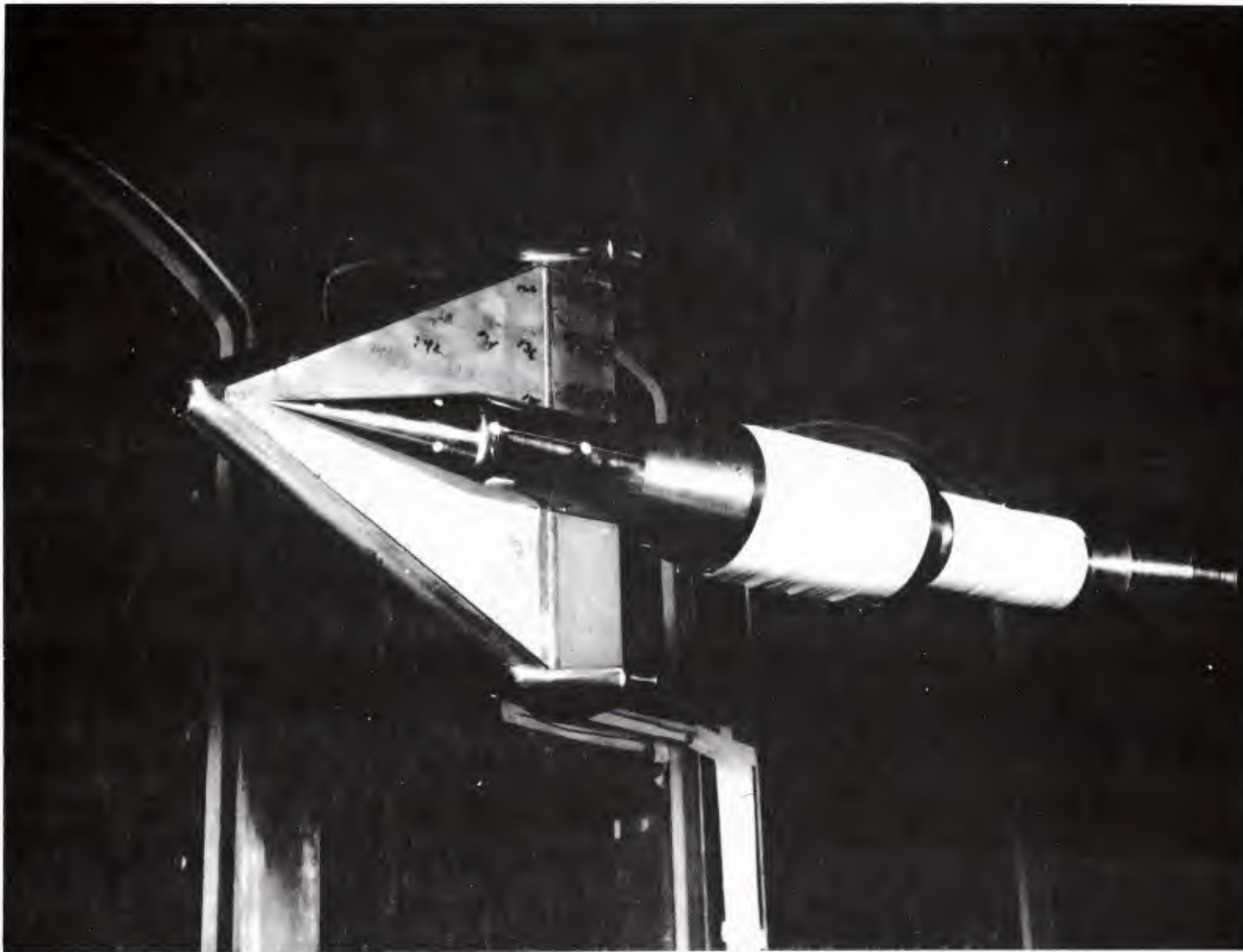


Fig. 2 Photograph of Upper Surface of Model, with Tip Fins,  
Installed in the AEDC 40-inch Supersonic Tunnel

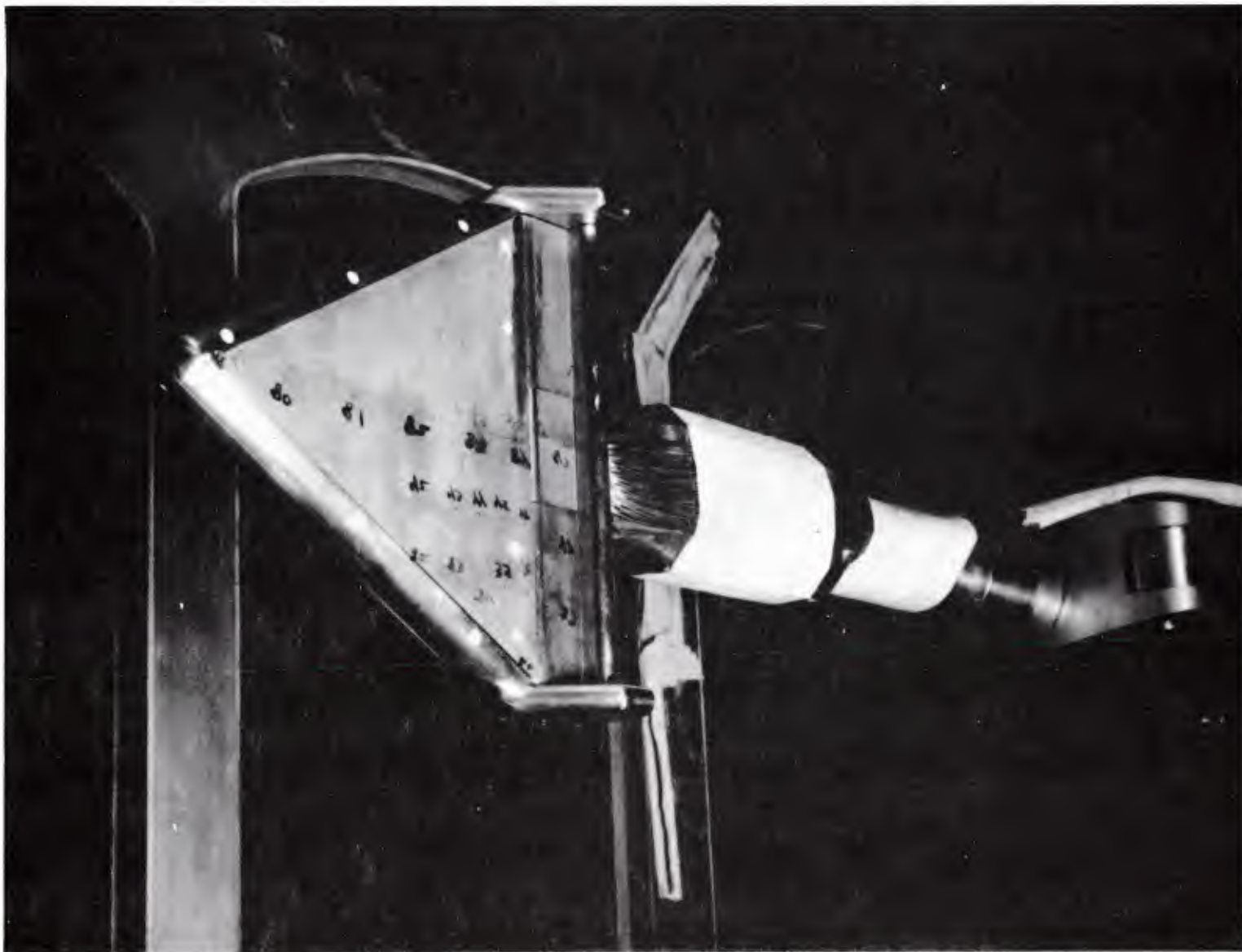


Fig. 3 Photograph of Lower Surface of Model, with Tip Fins and Trailing Edge Spoiler, Installed in the AEDC 40-inch Supersonic Tunnel

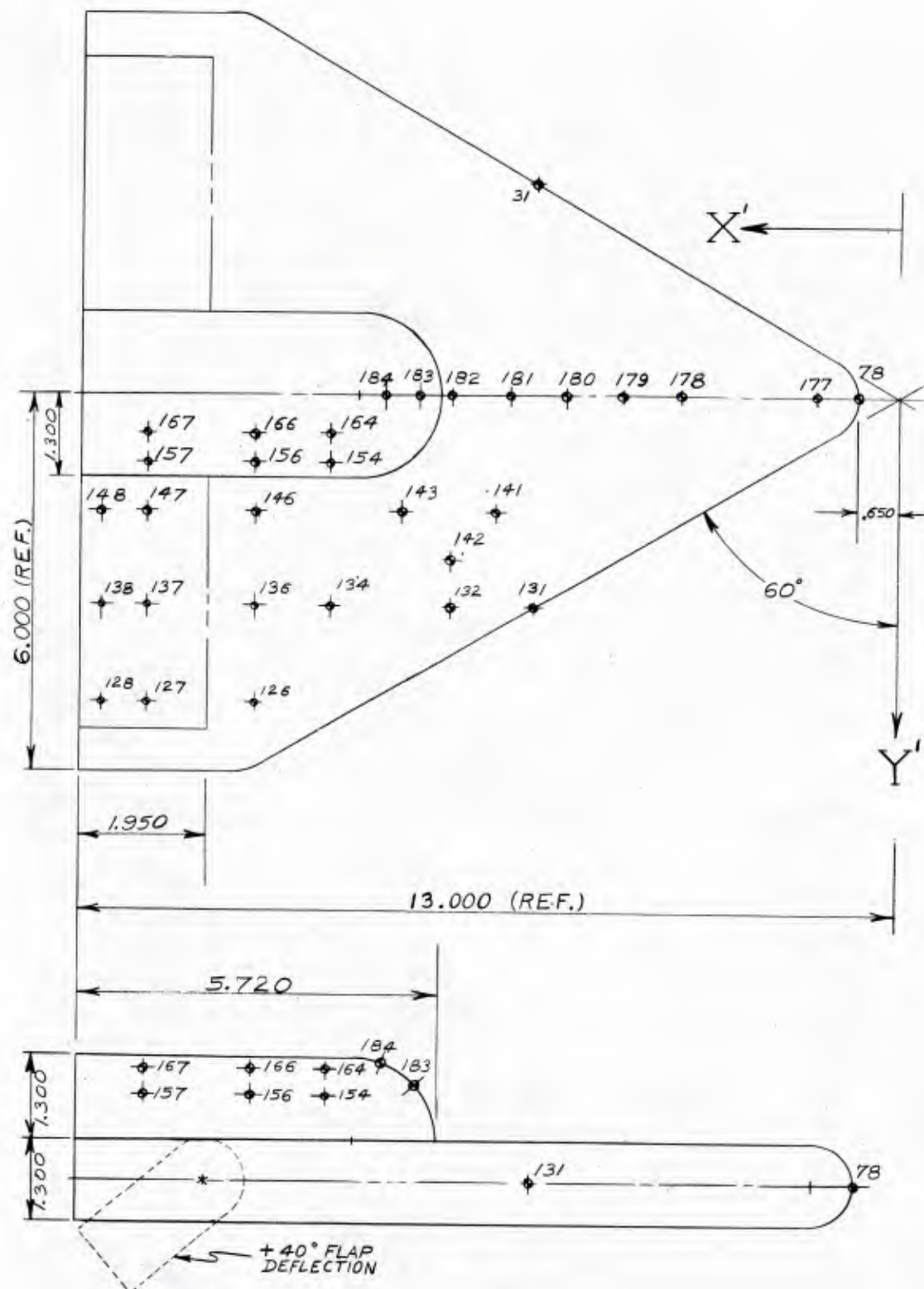


Fig. 4 Instrumentation on Upper Surface of Model  
(Top and Side Views)

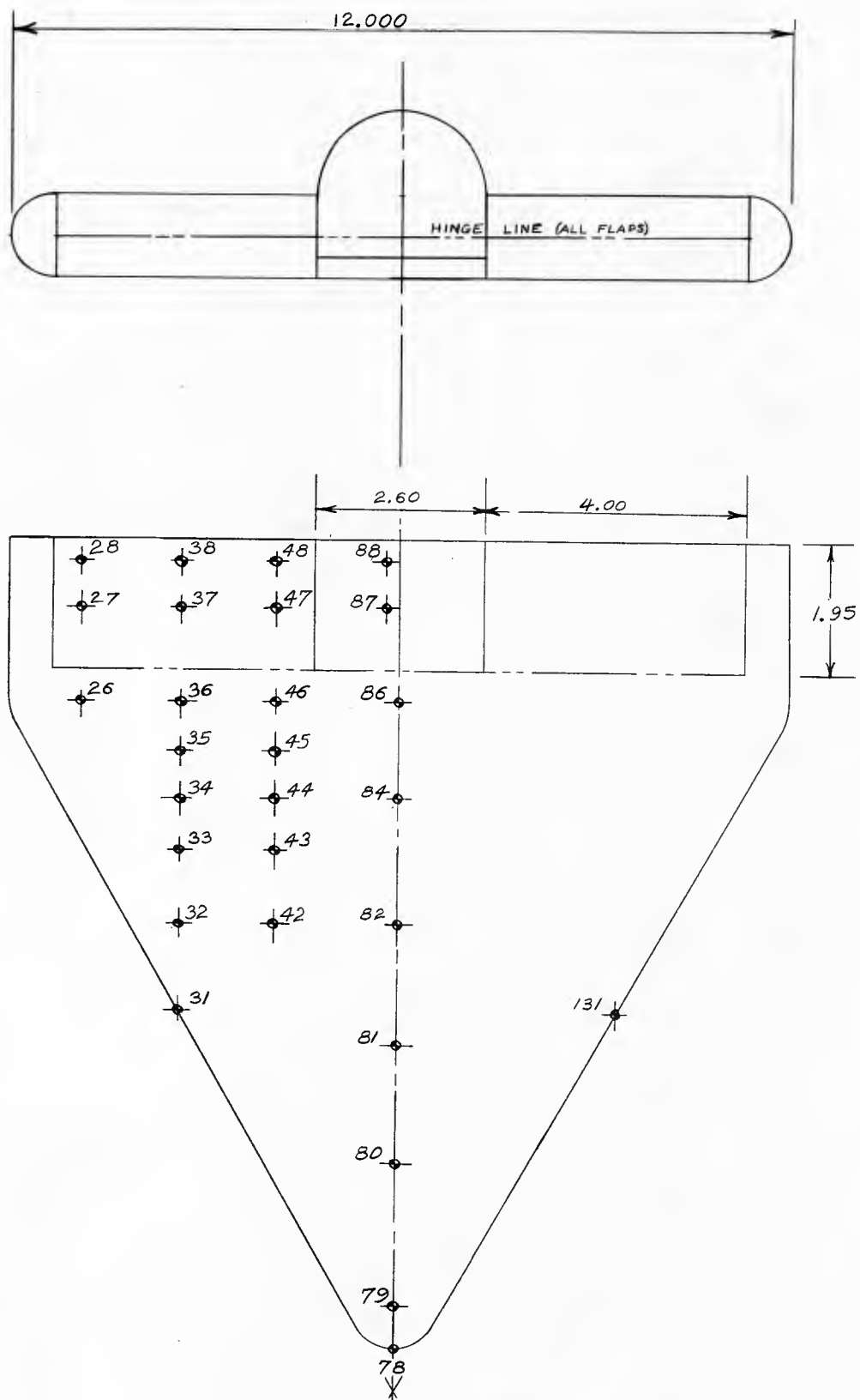
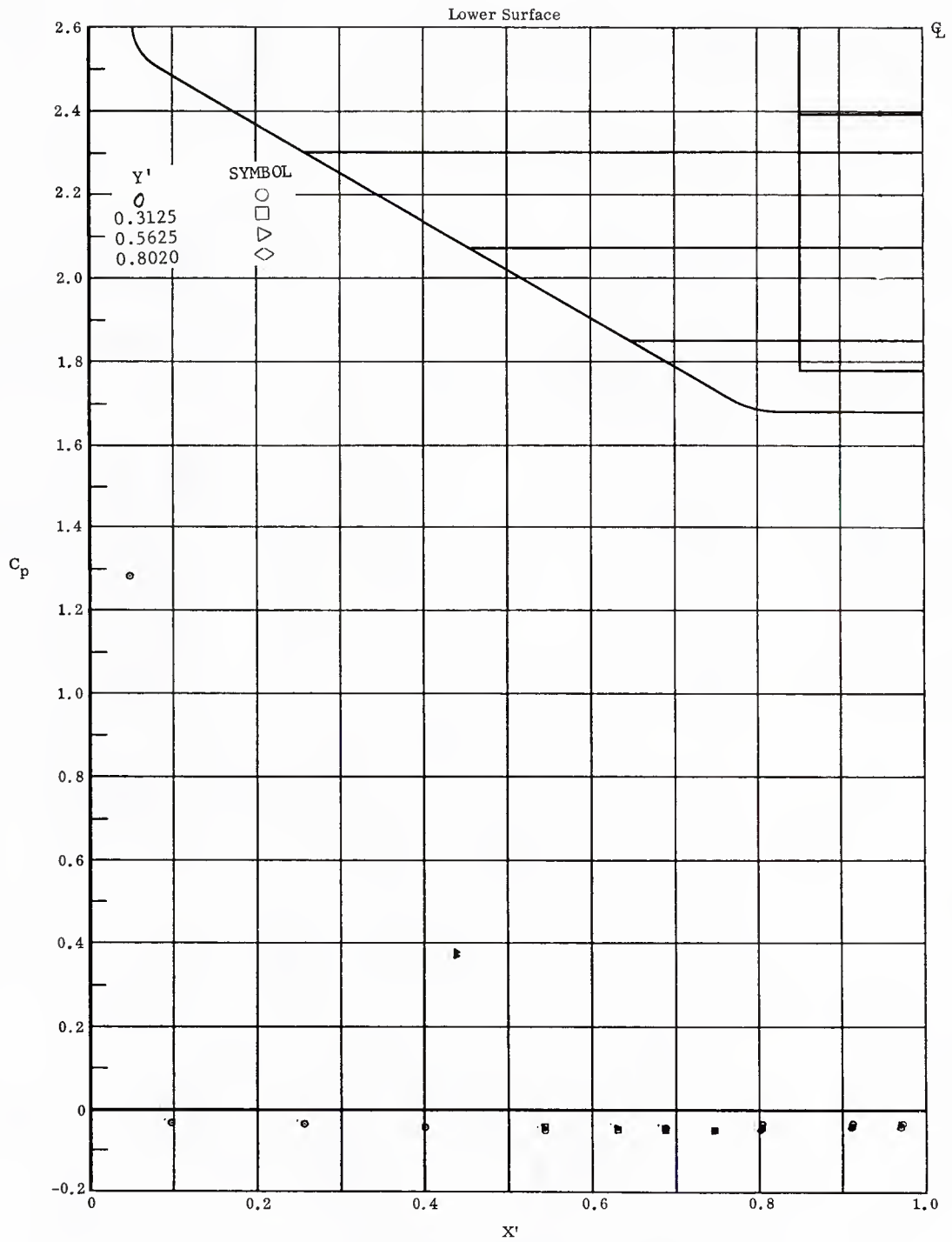
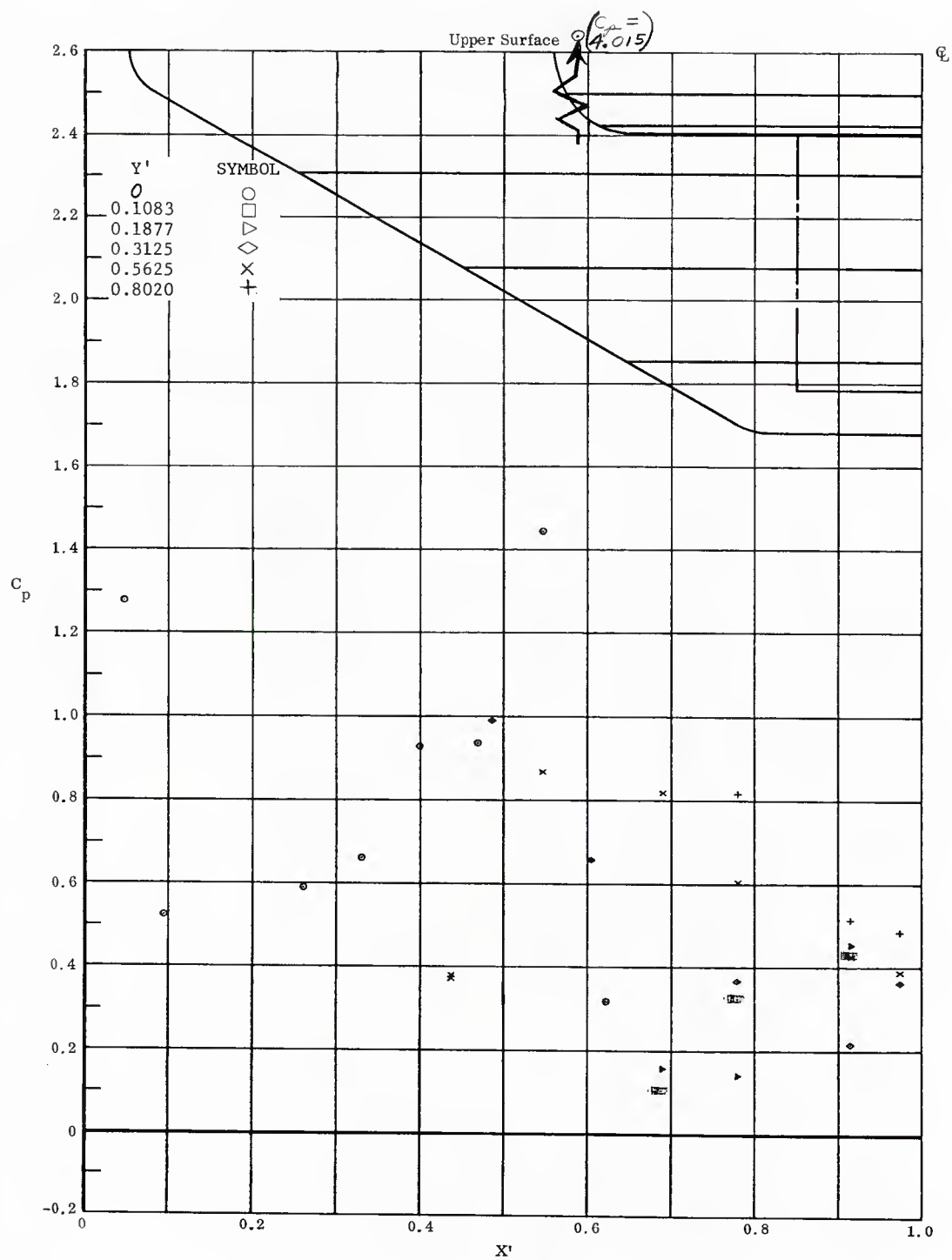


Fig. 5 Instrumentation on Lower Surface of Model  
(Base and Bottom Views)



(NONDIMENSIONAL STREAMWISE DISTANCE FROM VIRTUAL APEX)

Fig. 6 Streamwise Pressure Distributions on Lower Surface; No Flap Deflections,  $\alpha = -30^\circ$ .



( NONDIMENSIONAL STREAMWISE DISTANCE FROM VIRTUAL APEX )

Fig. 6 Streamwise Pressure Distributions on Upper Surface; No Flap Deflections,  $\alpha = -30^\circ$ .



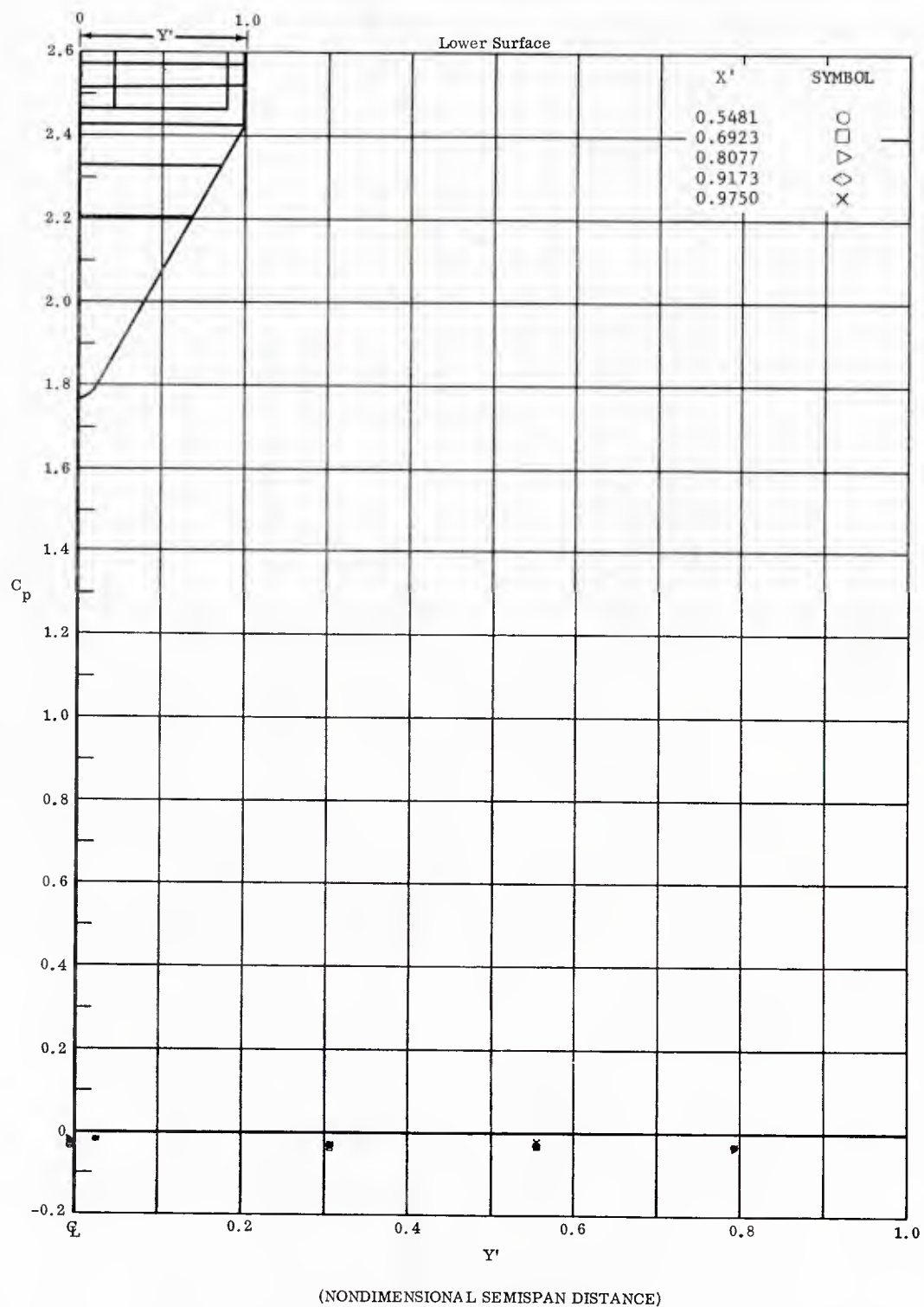


Fig. 6 Spanwise Pressure Distributions on Lower Surface; No Flap Deflections,  
 $\alpha = -30^\circ$ .

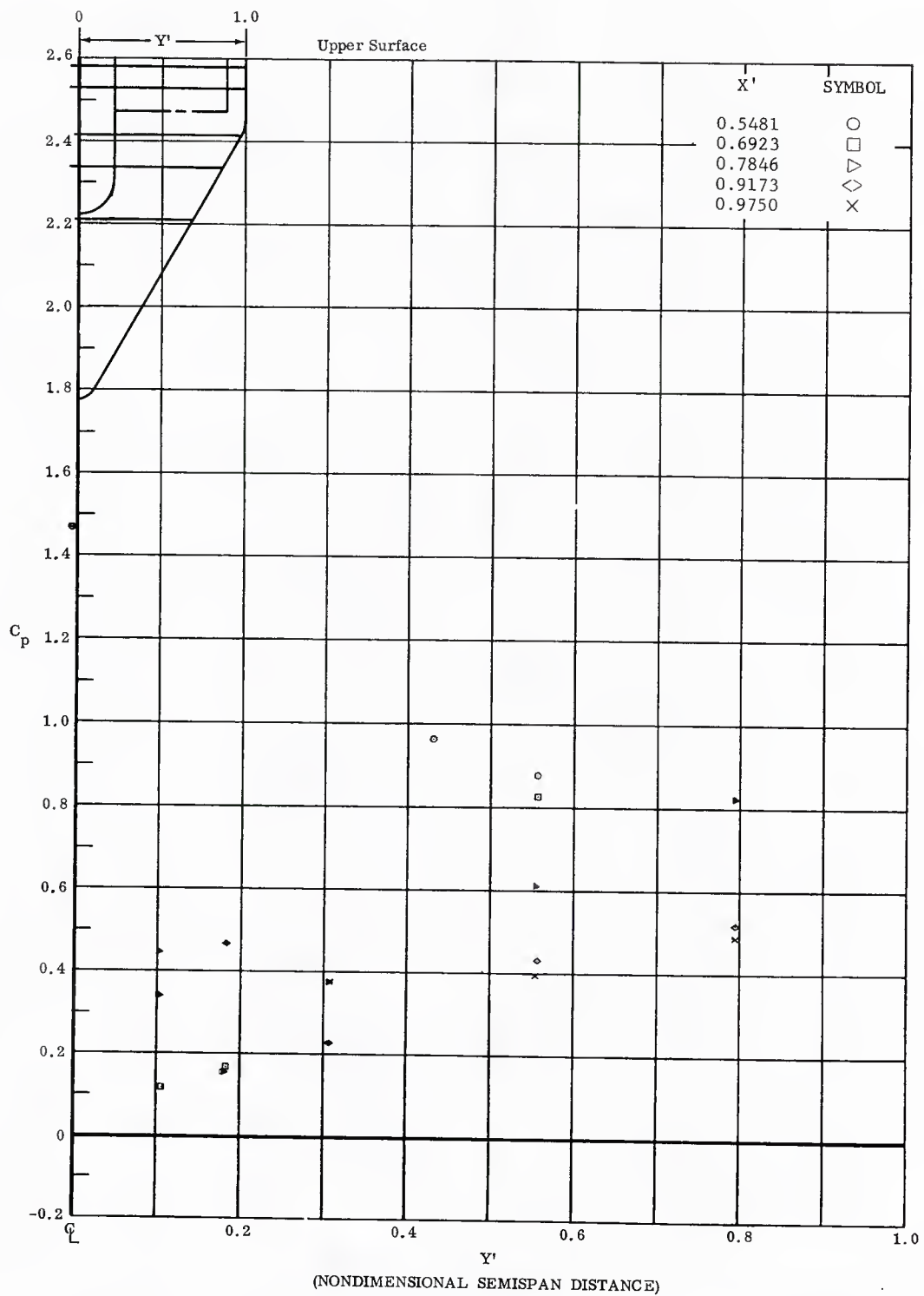


Fig. 6 Spanwise Pressure Distributions on Upper Surface; No Flap Deflections,  $\alpha = -30^\circ$ .



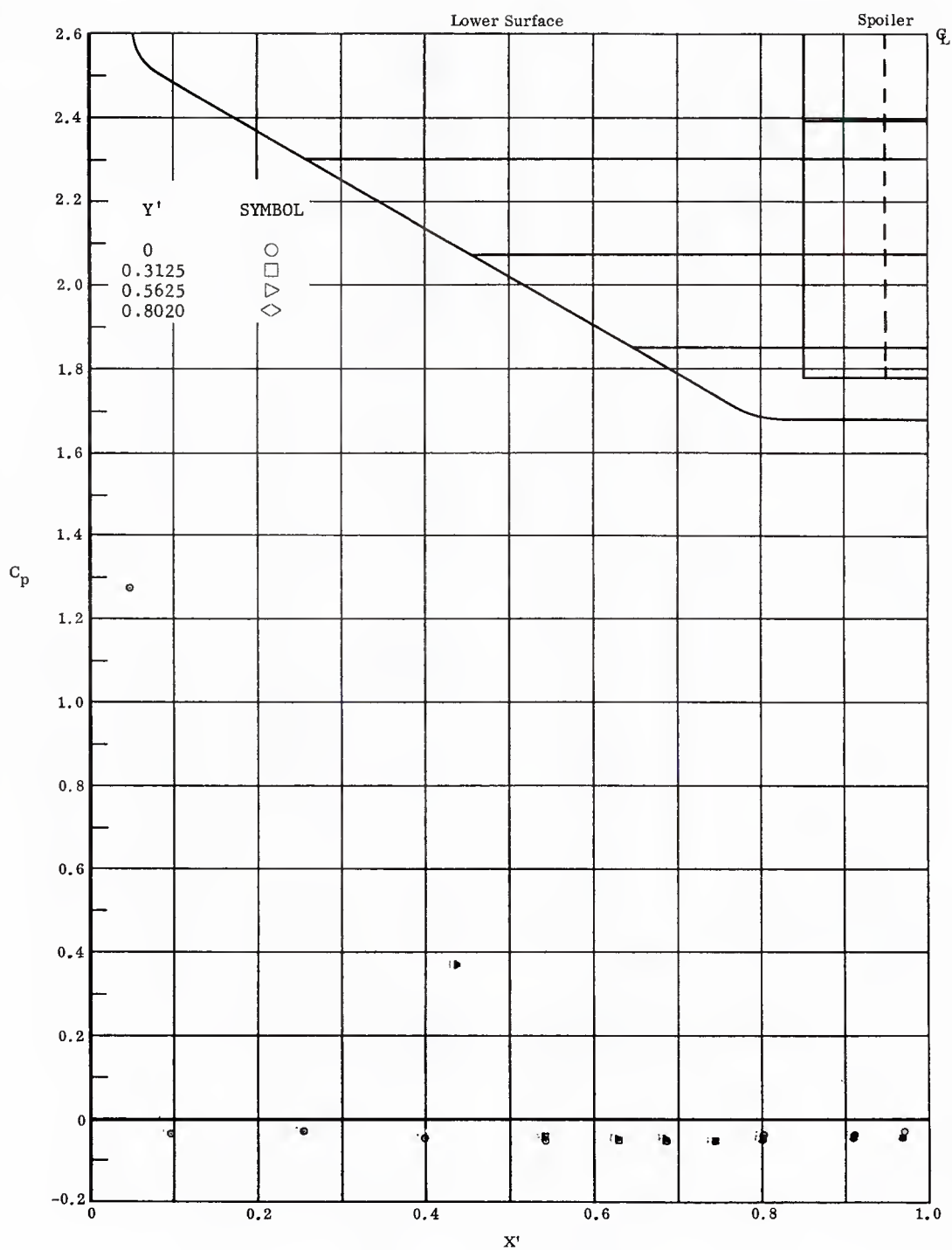
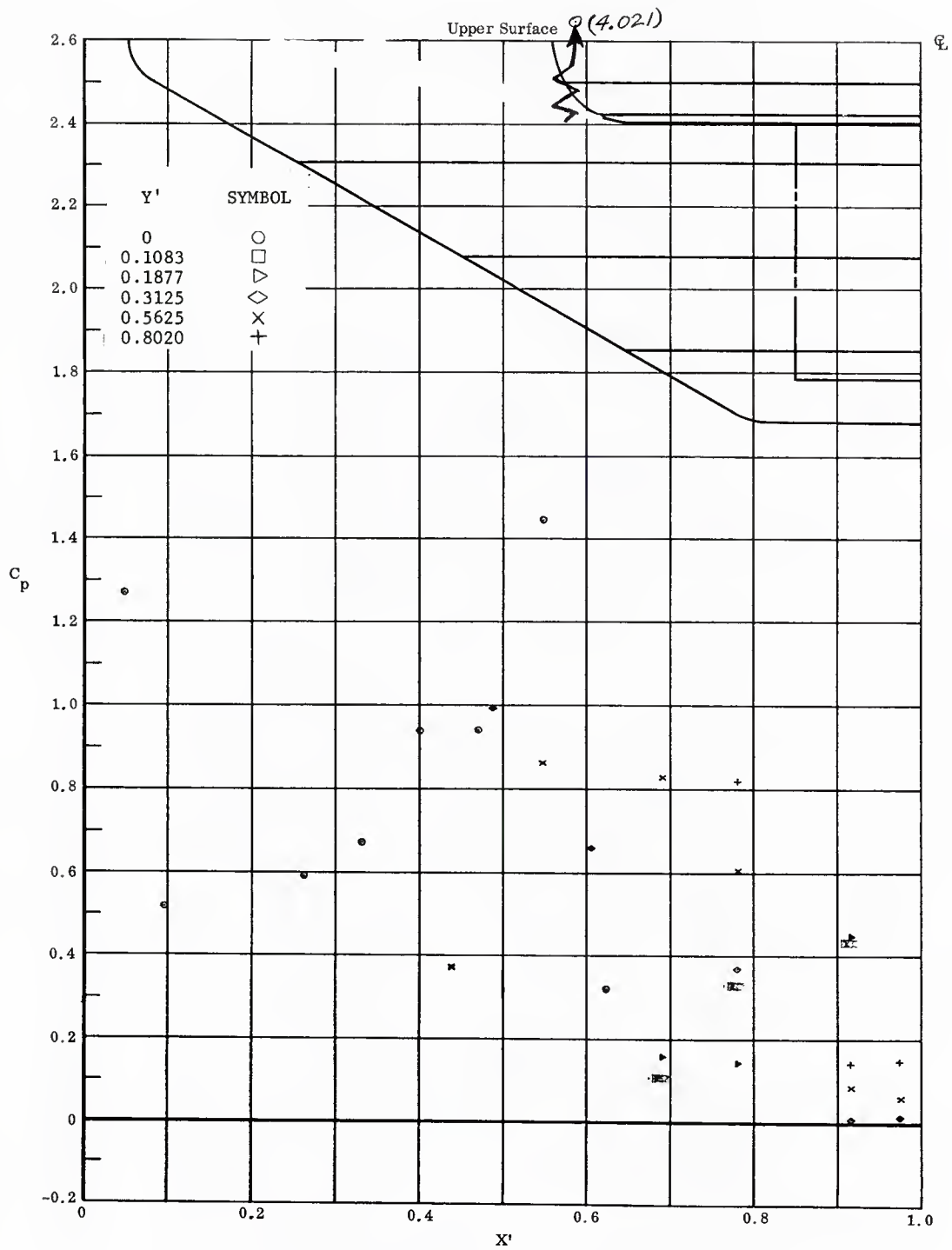


Fig. 7 Streamwise Pressure Distributions on Lower Surface; Left and Right Flaps Deflected  $+20^\circ$ ,  $\alpha = -30^\circ$ .



( NONDIMENSIONAL STREAMWISE DISTANCE FROM VIRTUAL APEX )

Fig. 7 Streamwise Pressure Distributions on Upper Surface; Left and Right Flaps Deflected  $+20^\circ$ ,  $\alpha = -30^\circ$ .

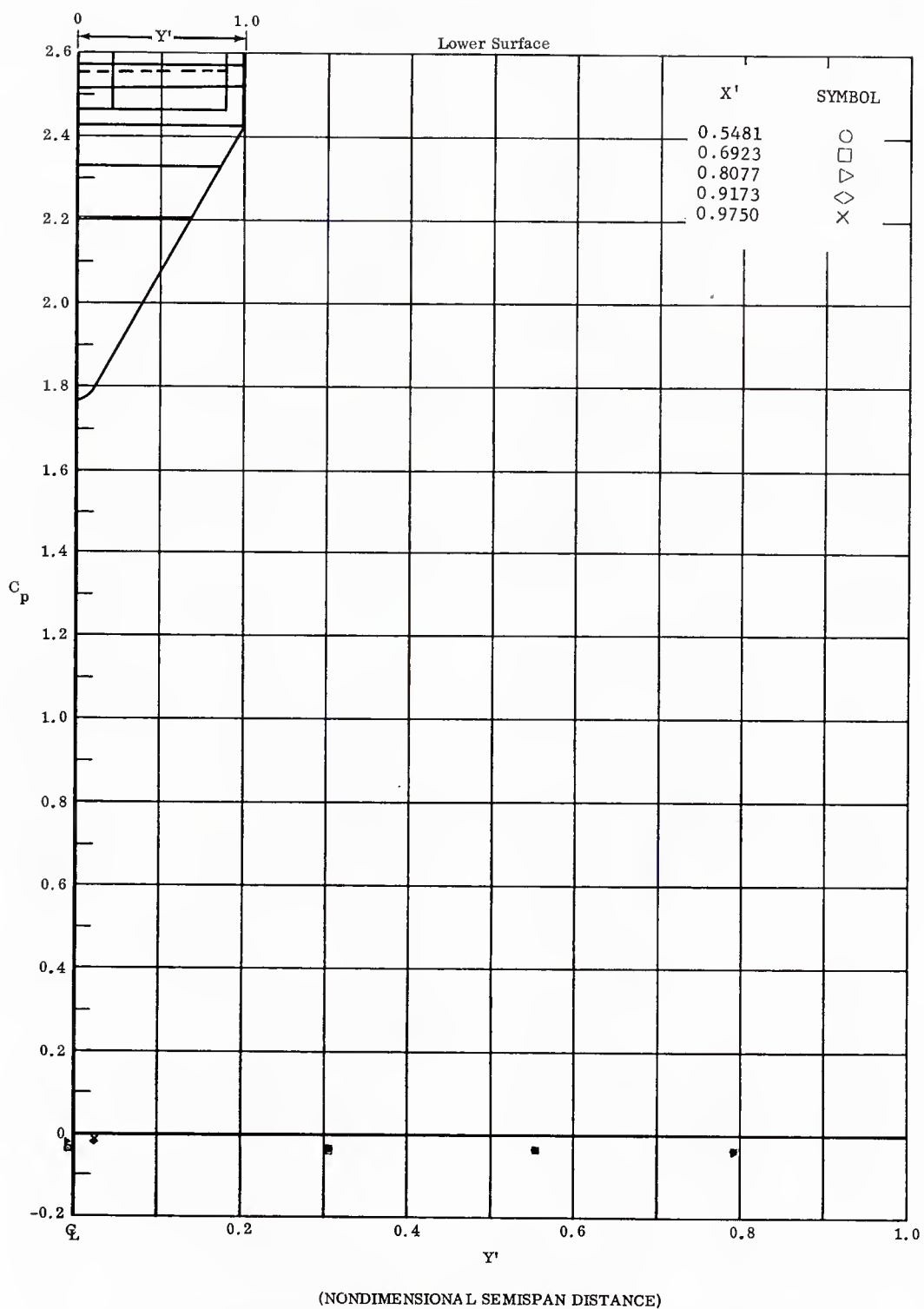


Fig. 7 Spanwise Pressure Distributions on Lower Surface; Left and Right Flaps Deflected  $+20^\circ$ ,  $\alpha = -30^\circ$ .

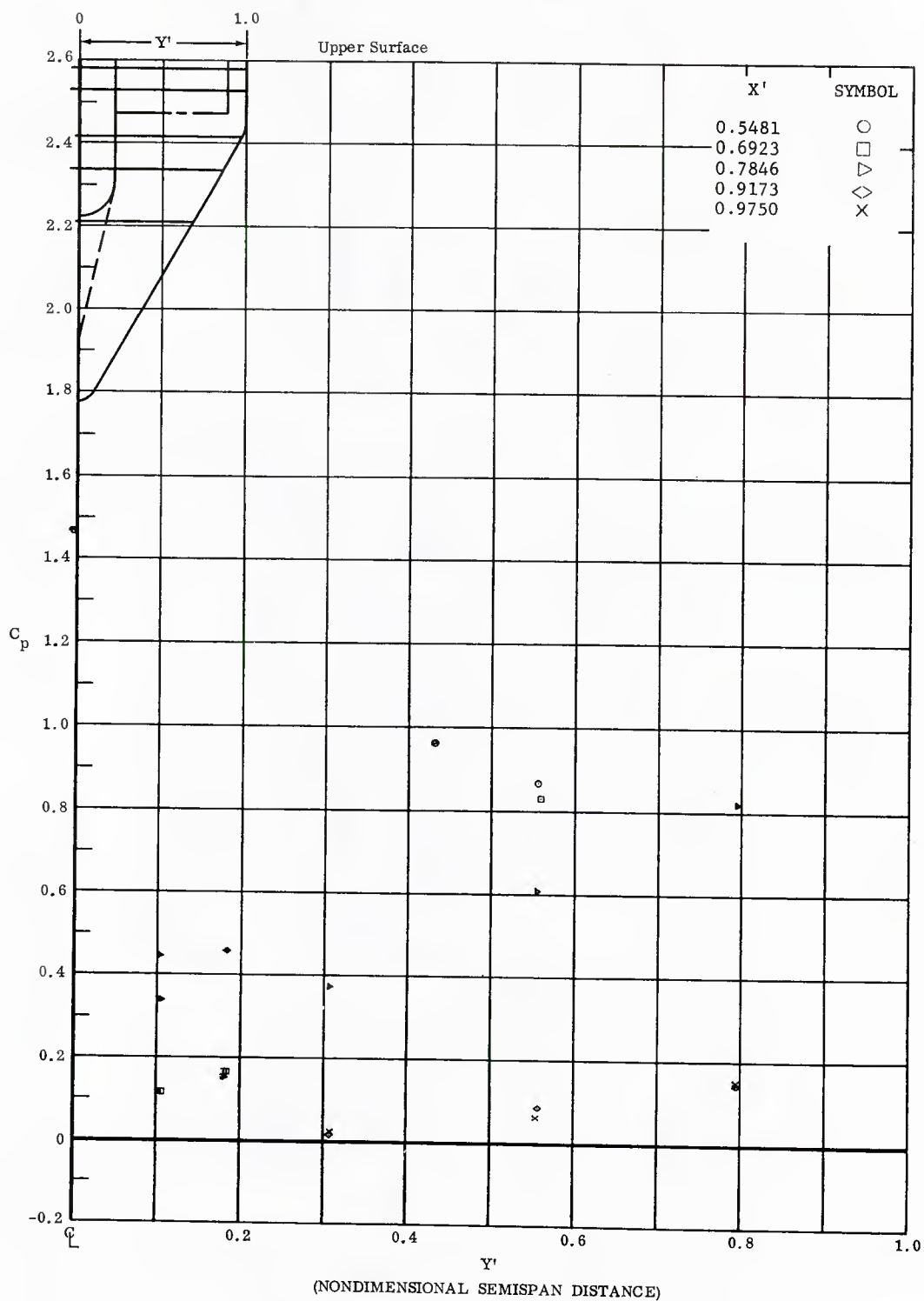


Fig. 7 Spanwise Pressure Distribution on Upper Surface; Left and Right Flaps Deflected  $+20^\circ$ ,  $\alpha = -30^\circ$ .

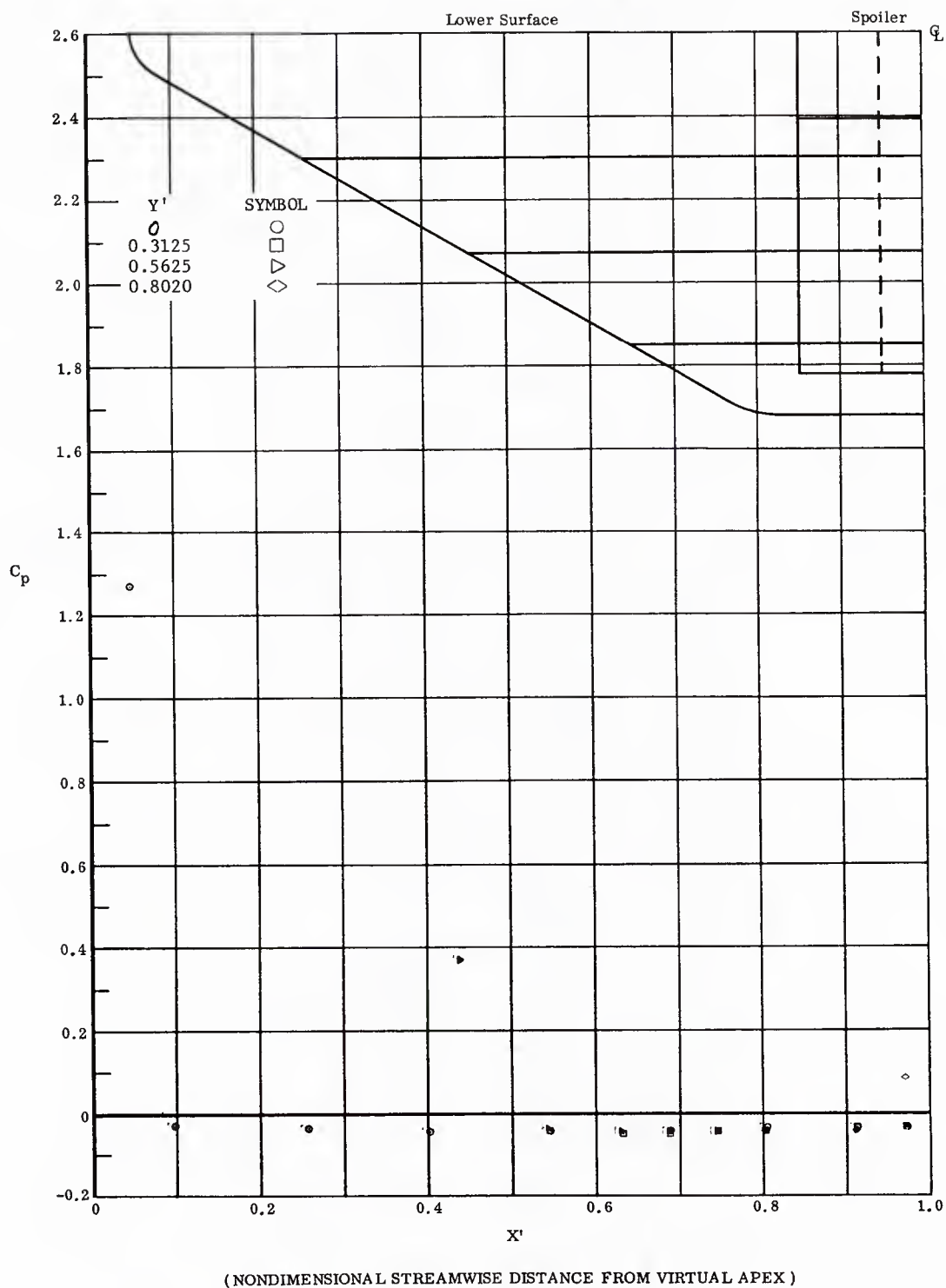


Fig. 8 Streamwise Pressure Distributions on Lower Surface; Left and Right Flaps Deflected  $+40^\circ$ ,  $\alpha = -30^\circ$ .

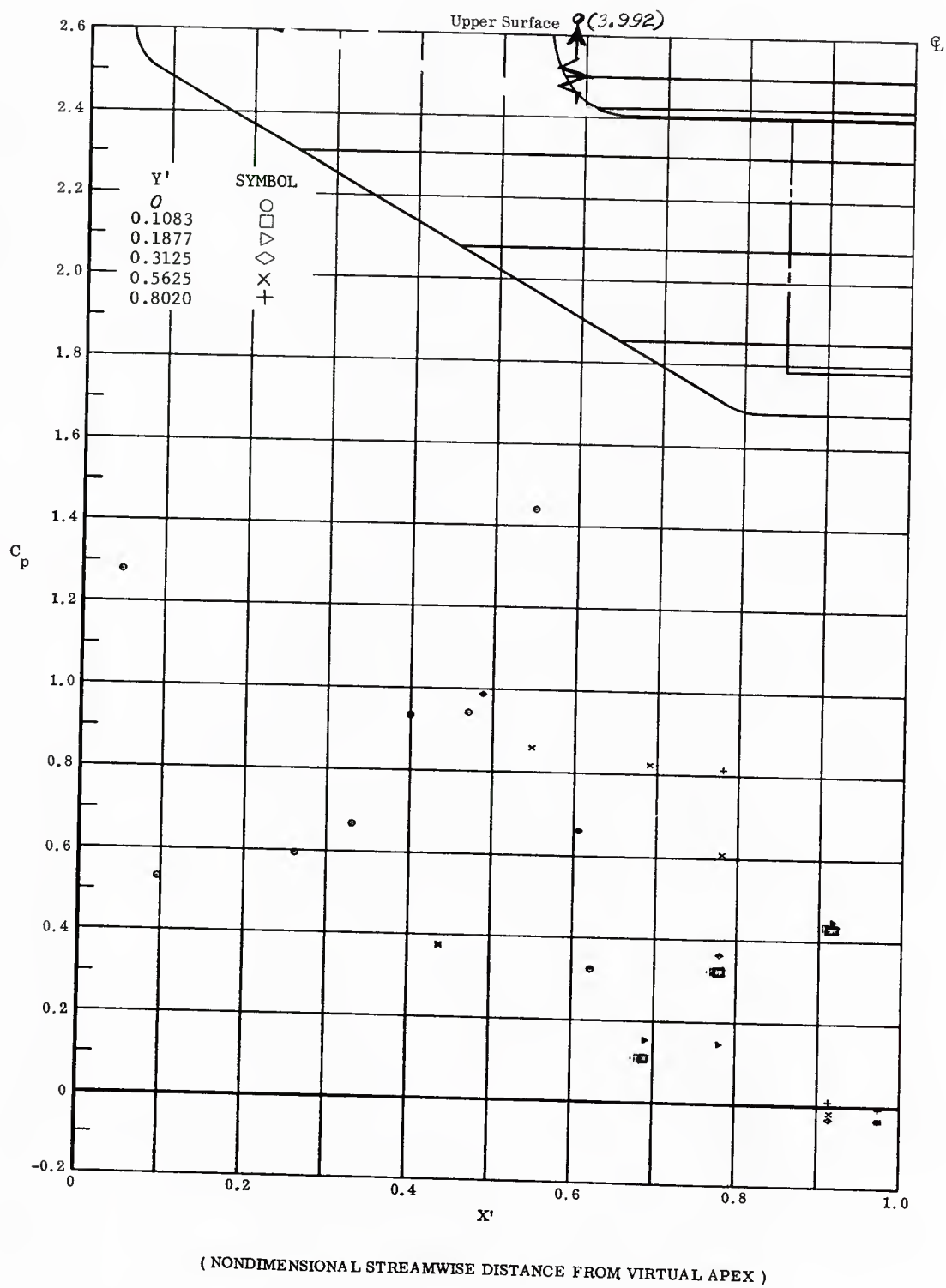


Fig. 8 Streamwise Pressure Distributions on Upper Surface; Left and Right Flaps Deflected  $+40^\circ$ ,  $\alpha = -30^\circ$ .

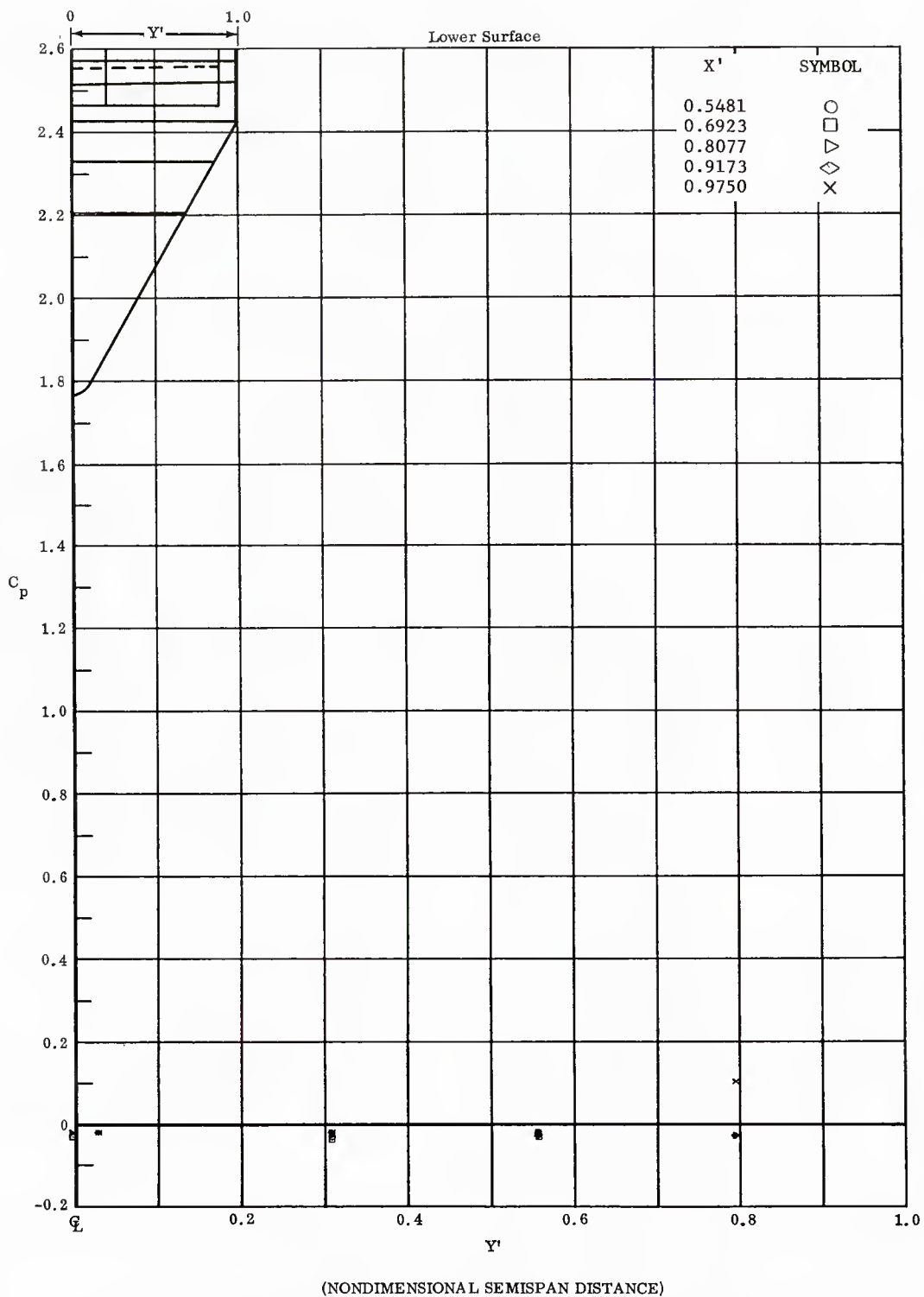


Fig. 8 Spanwise Pressure Distributions on Lower Surface; Left and Right Flaps Deflected  $+40^\circ$ ,  $\alpha = -30^\circ$ .

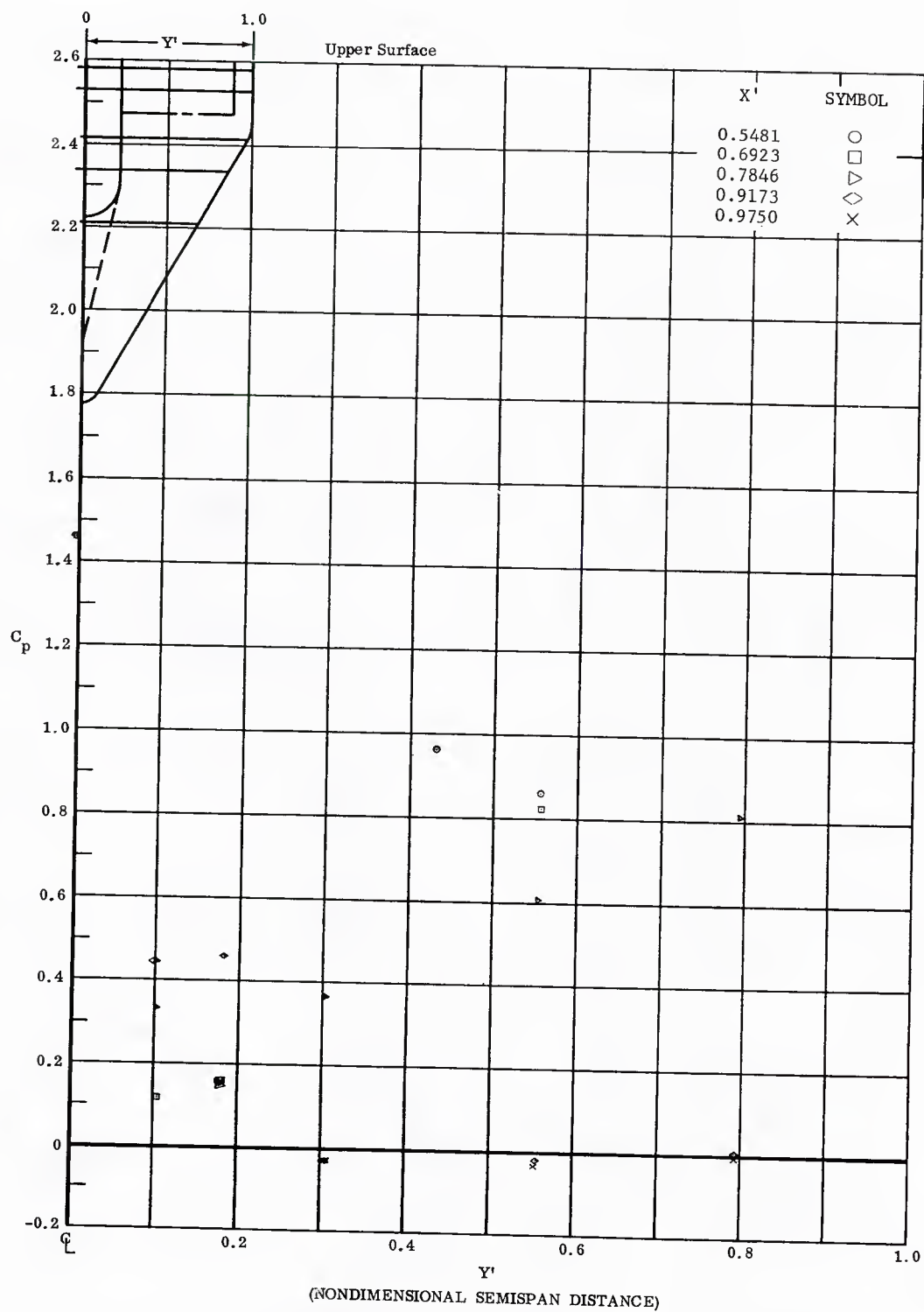


Fig. 8 Spanwise Pressure Distributions on Upper Surface; Left and Right Flaps Deflected  $+40^\circ$ ,  $\alpha = -30^\circ$ .



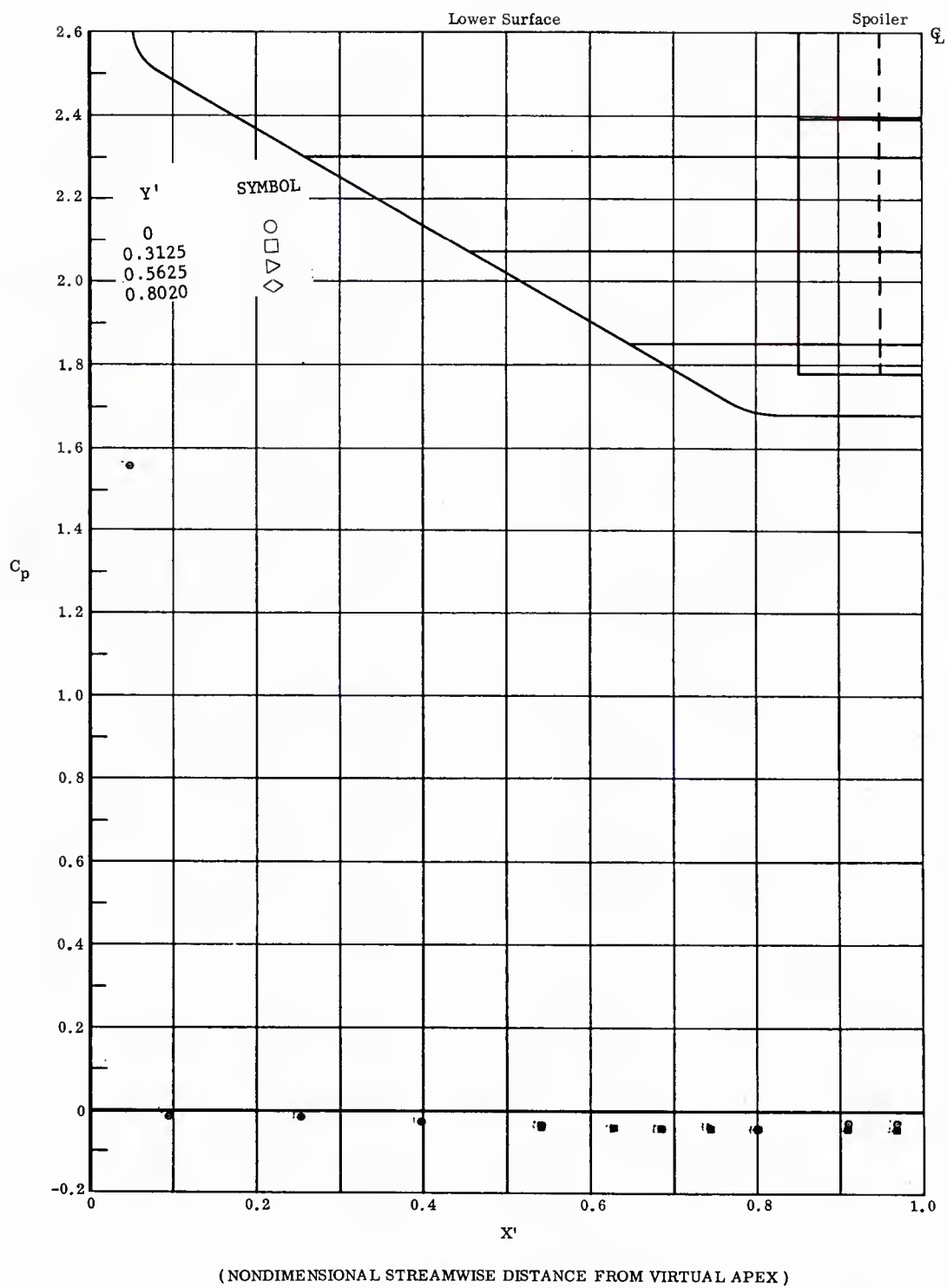
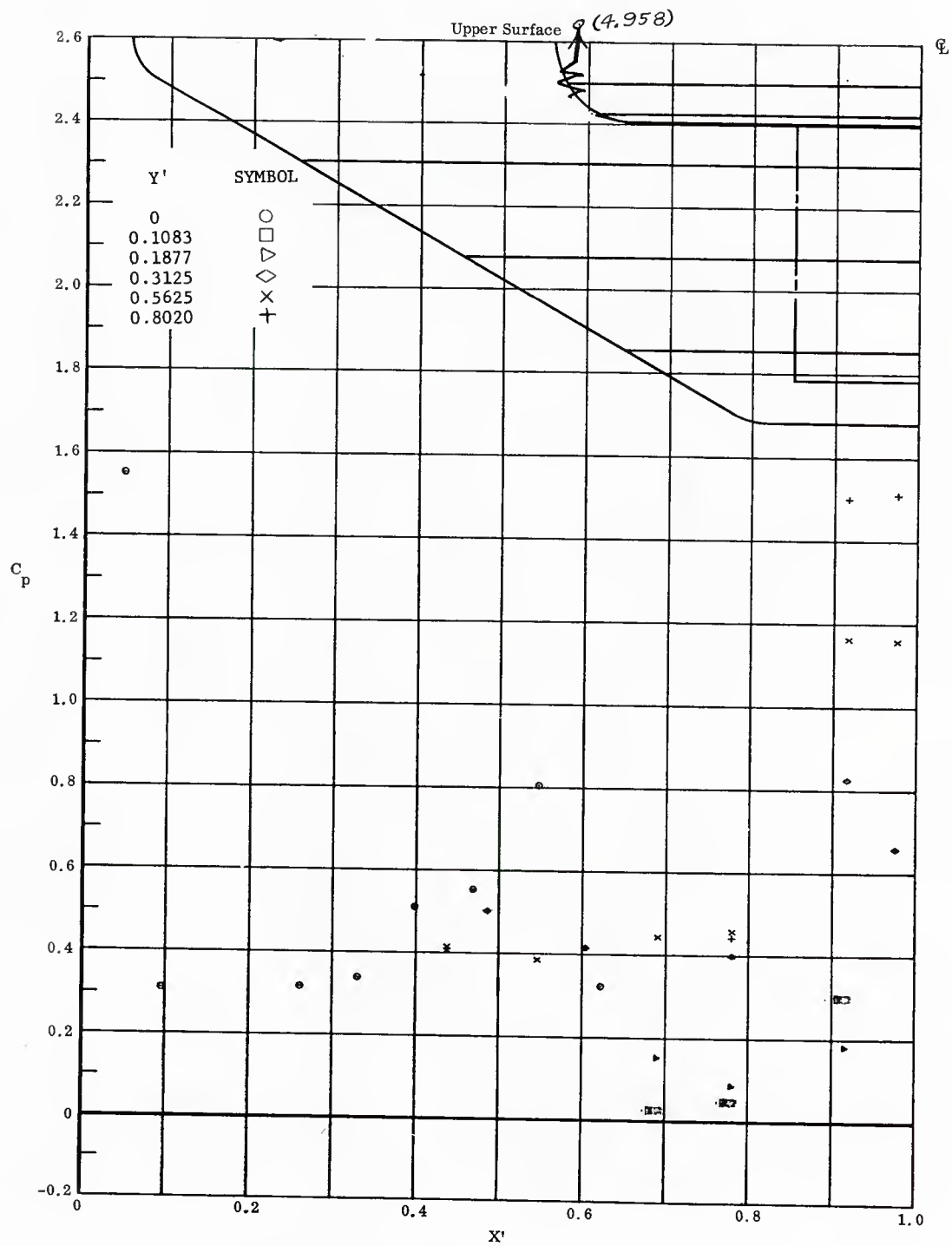


Fig. 9 Streamwise Pressure Distributions on Lower Surface; Left and Right Flaps Deflected  $-20^\circ$ ,  $\alpha = -20^\circ$ .



( NONDIMENSIONAL STREAMWISE DISTANCE FROM VIRTUAL APEX )

Fig. 9 Streamwise Pressure Distributions on Upper Surface; Left and Right Flaps Deflected  $-20^\circ$ ,  $\alpha = -20^\circ$ .

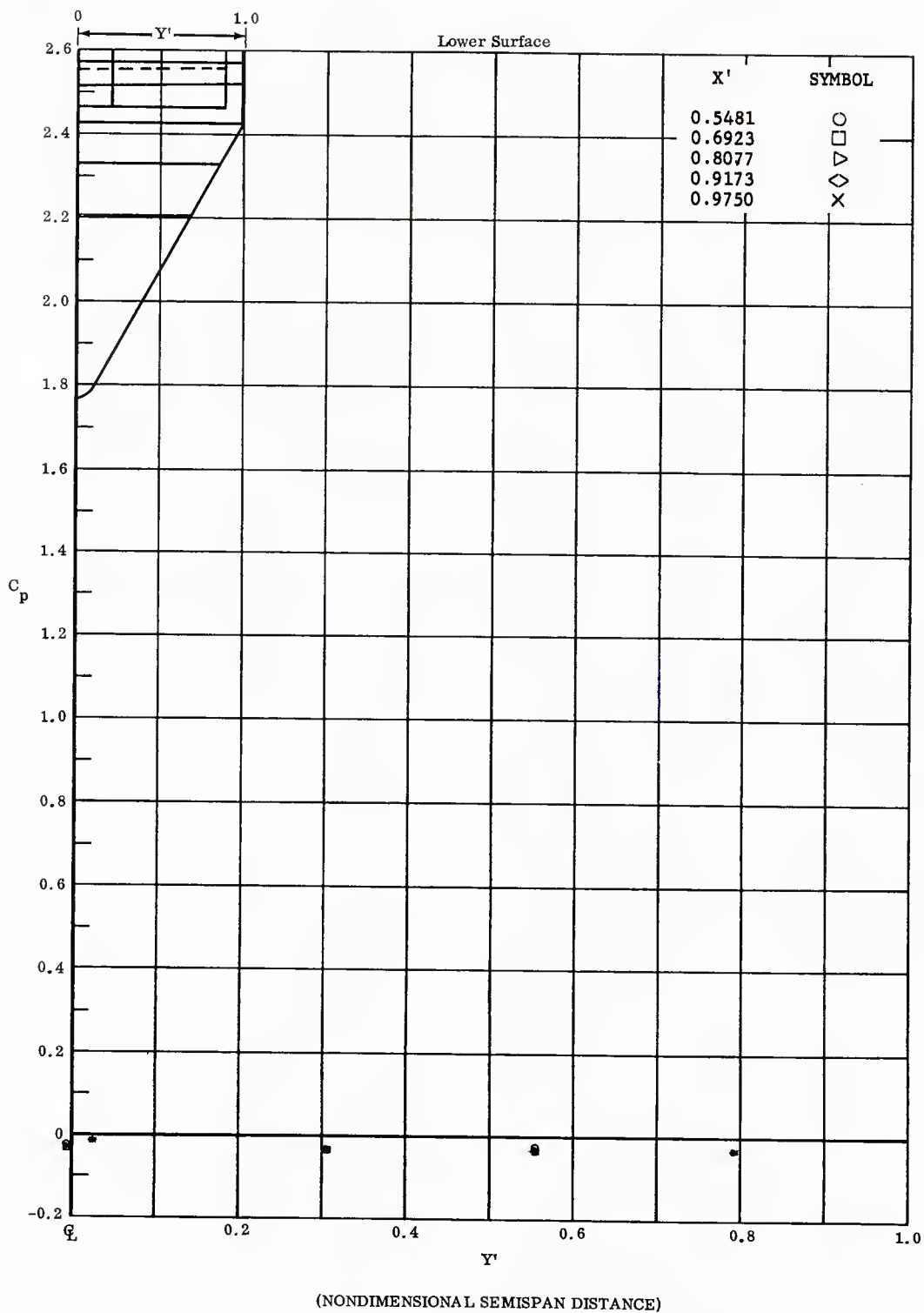


Fig. 9 Spanwise Pressure Distributions on Lower Surface; Left and Right Flaps Deflected  $-20^\circ$ ,  $\alpha = -20^\circ$ .

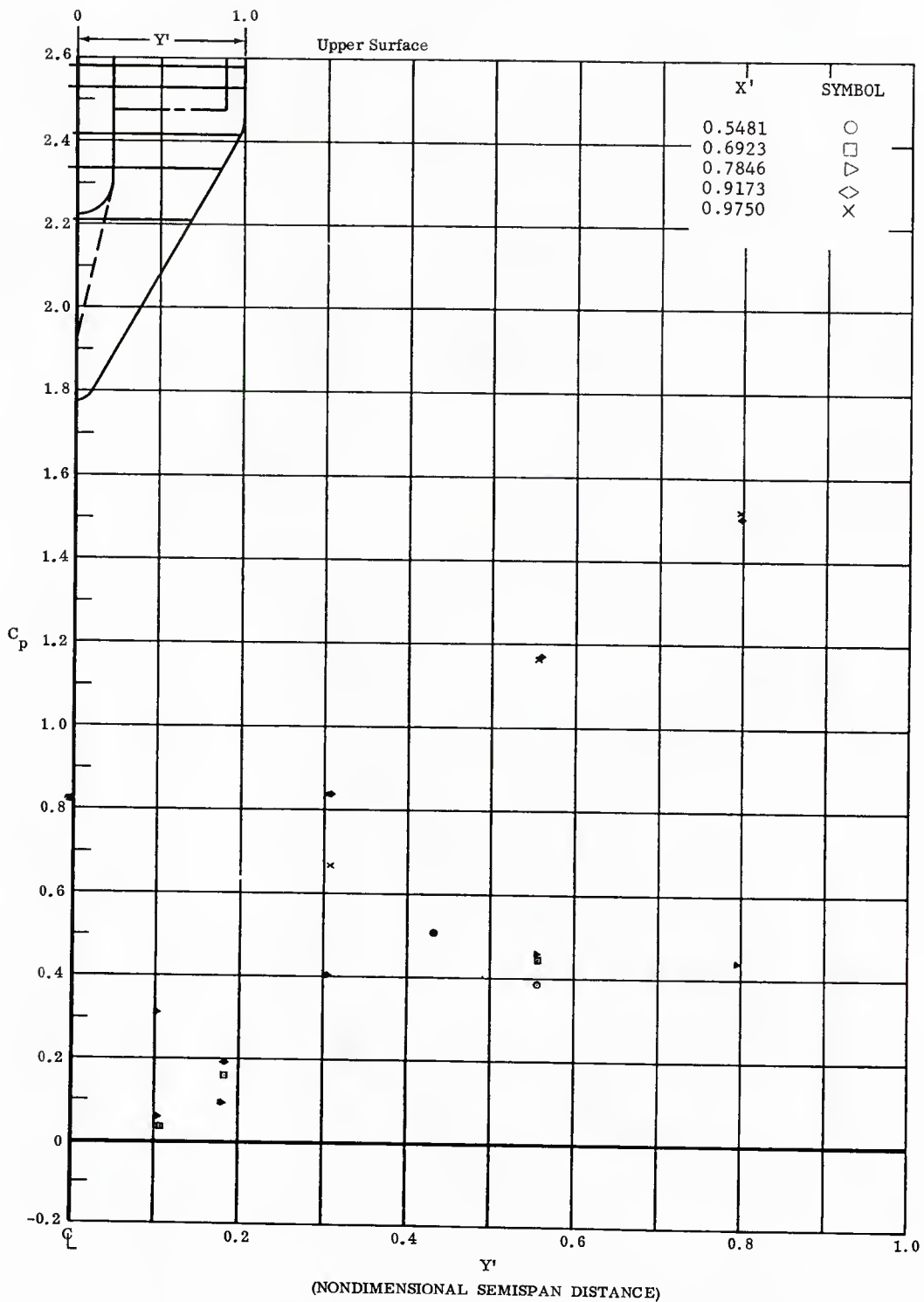


Fig. 9 Spanwise Pressure Distributions on Upper Surface; Left and Right Flaps Deflected  $-20^\circ$ ,  $\alpha = -20^\circ$ .

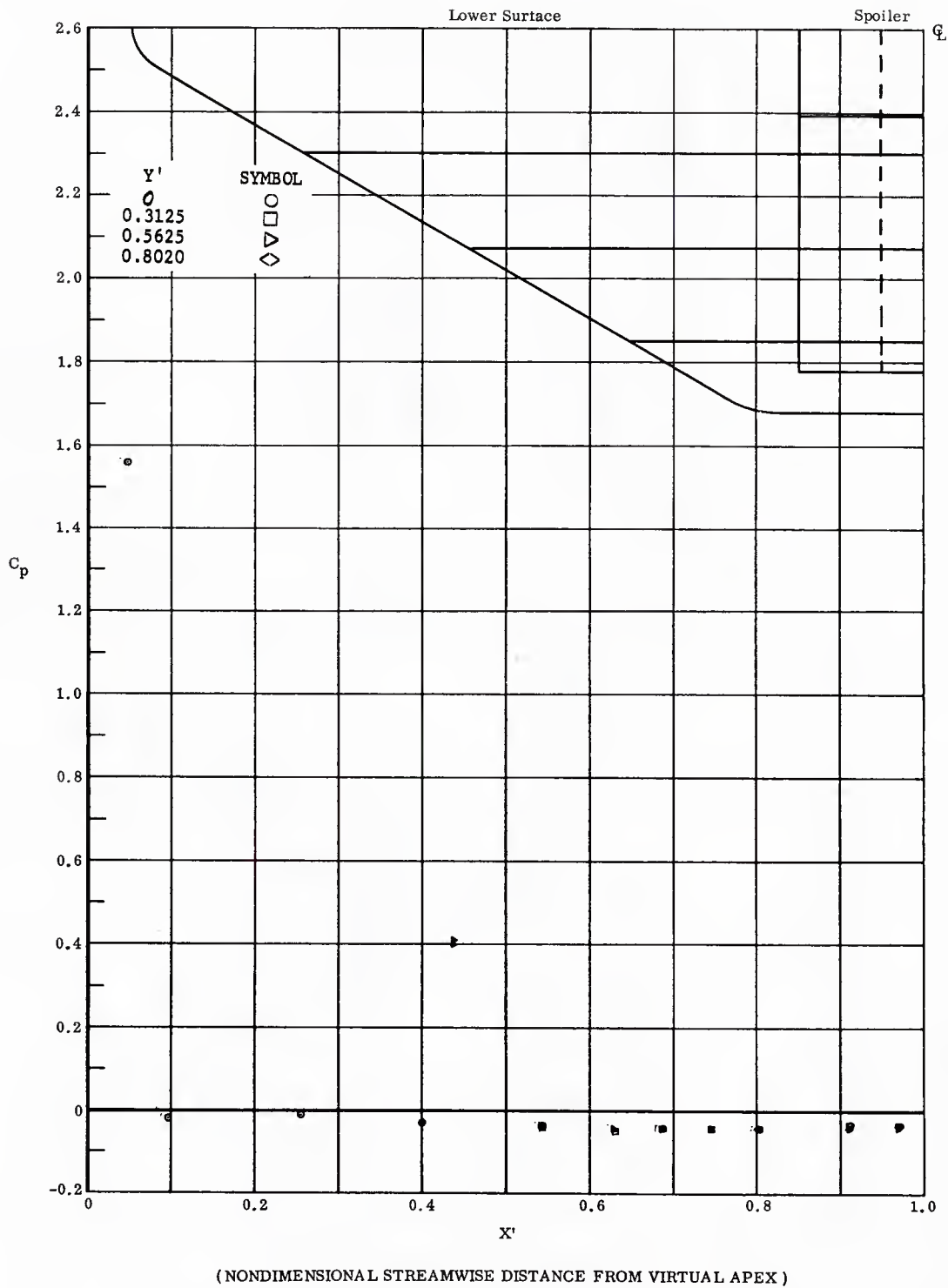


Fig. 10 Streamwise Pressure Distributions on Lower Surface; No Flap Deflections,  $\alpha = -20^\circ$ .

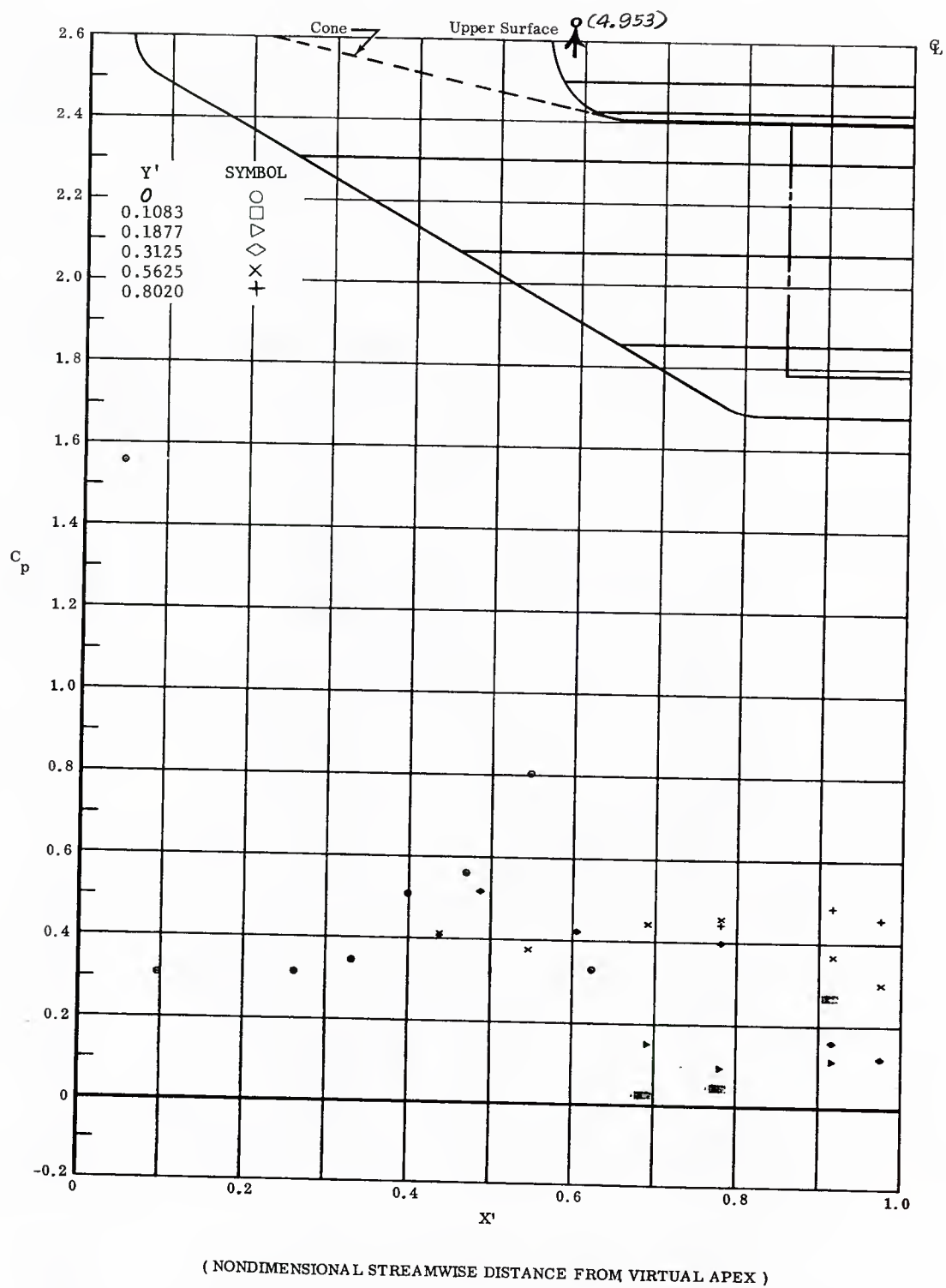


Fig. 10 Streamwise Pressure Distributions on Upper Surface; No Flap Deflections,  $\alpha = -20^\circ$ .

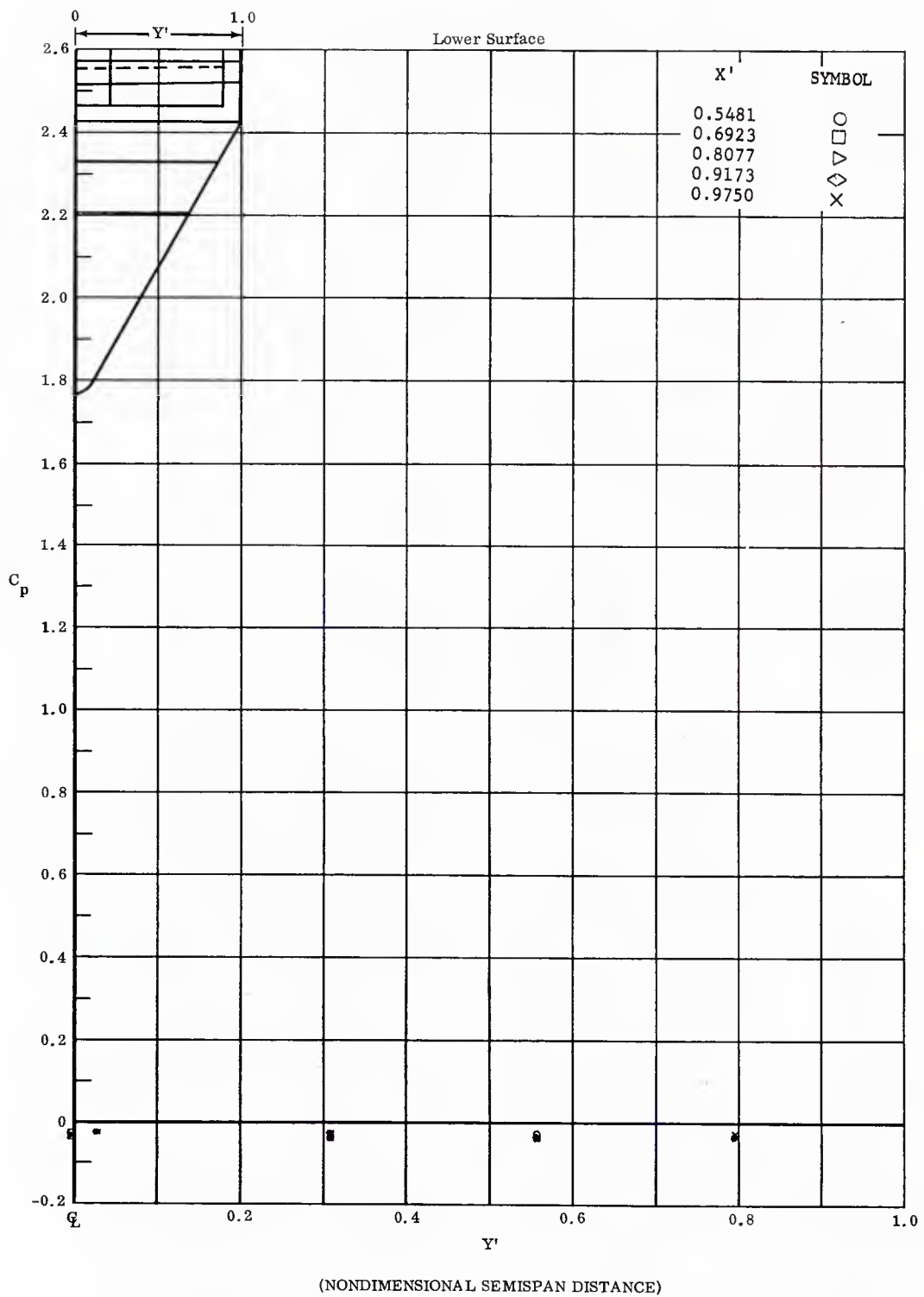


Fig. 10 Spanwise Pressure Distributions on Lower Surface; No Flap Deflections,  $\alpha = -20^\circ$ .

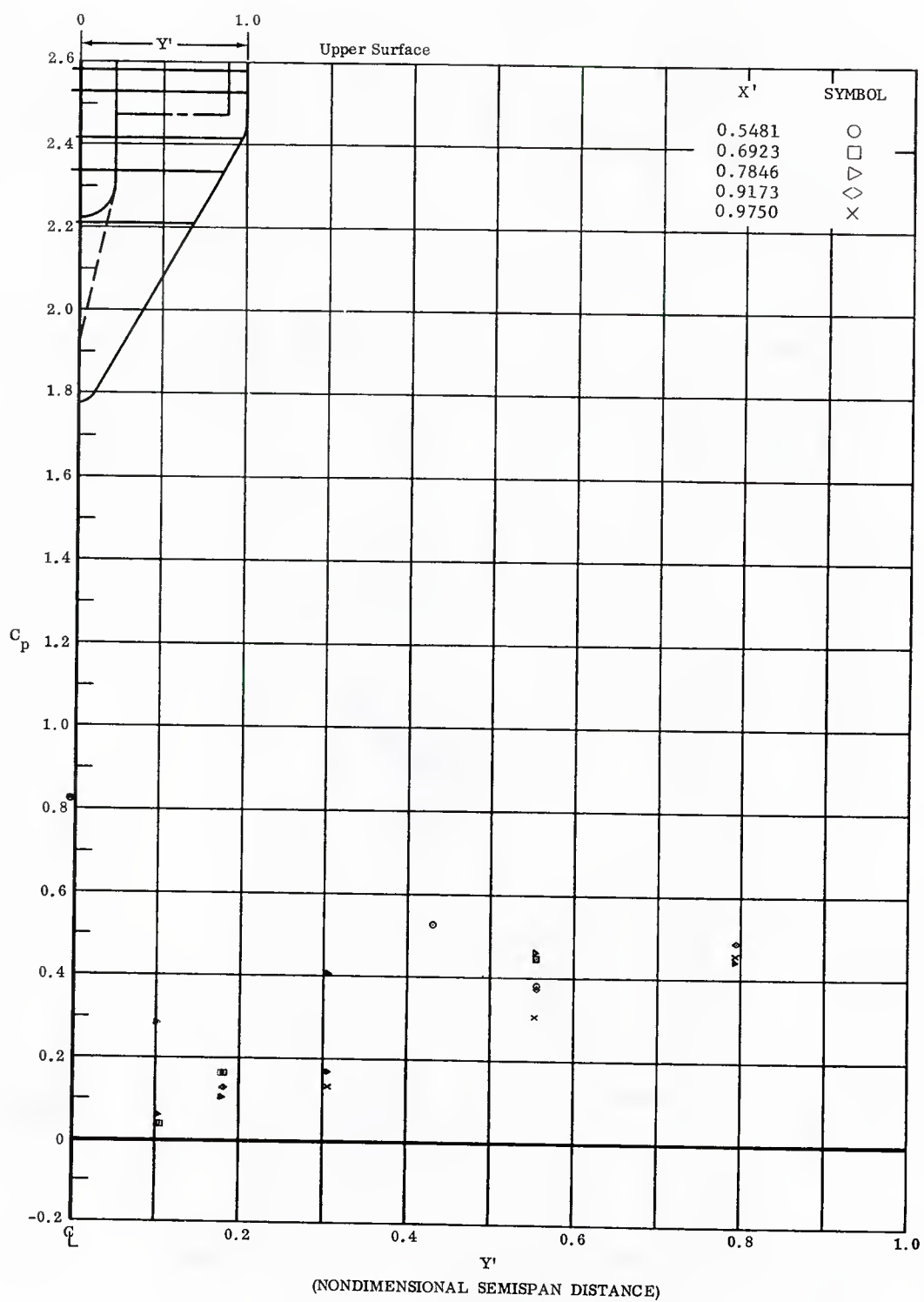


Fig. 10 Spanwise Pressure Distributions on Upper Surface; No Flap Deflections,  $\alpha = -20^\circ$ .



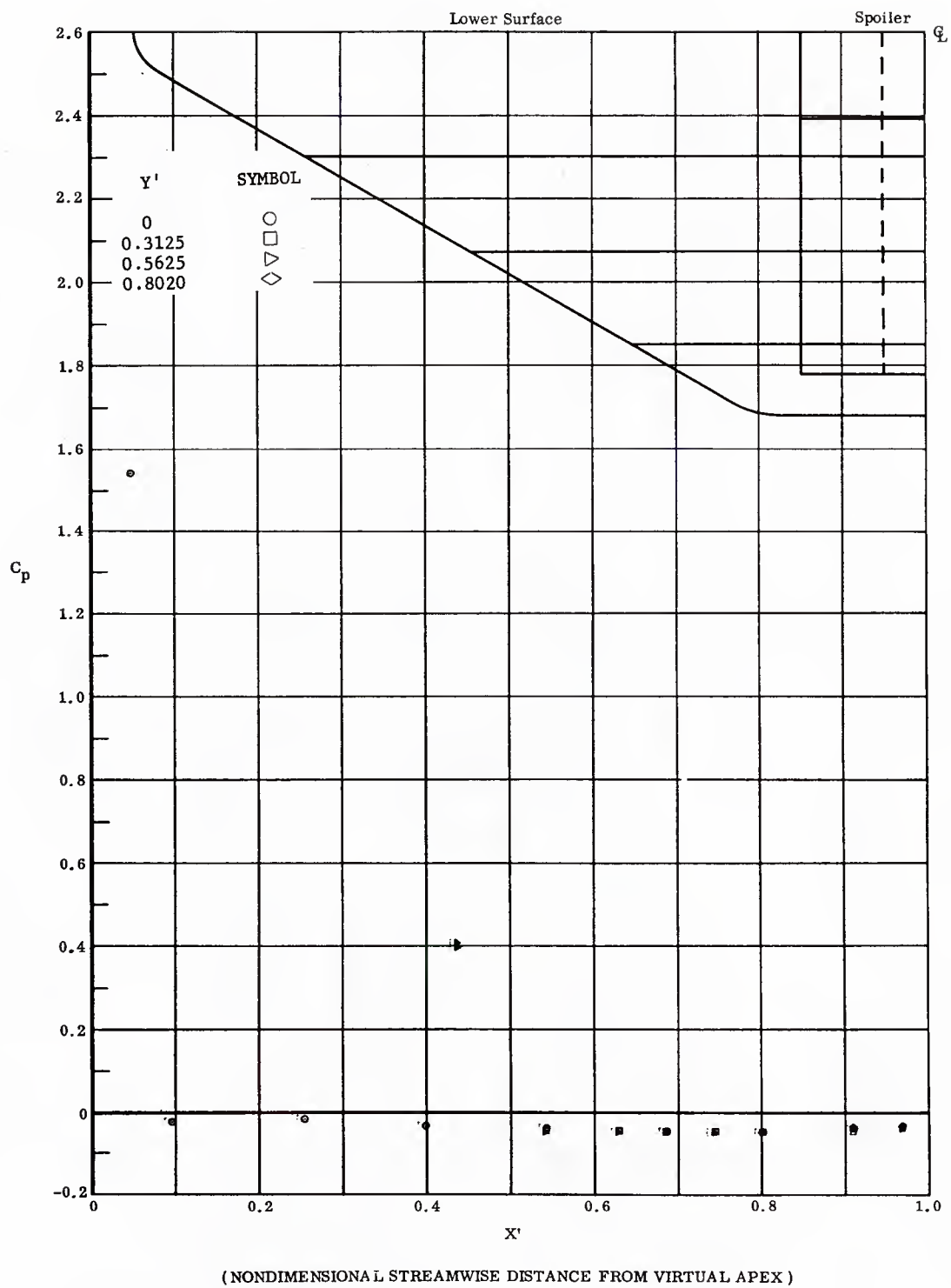
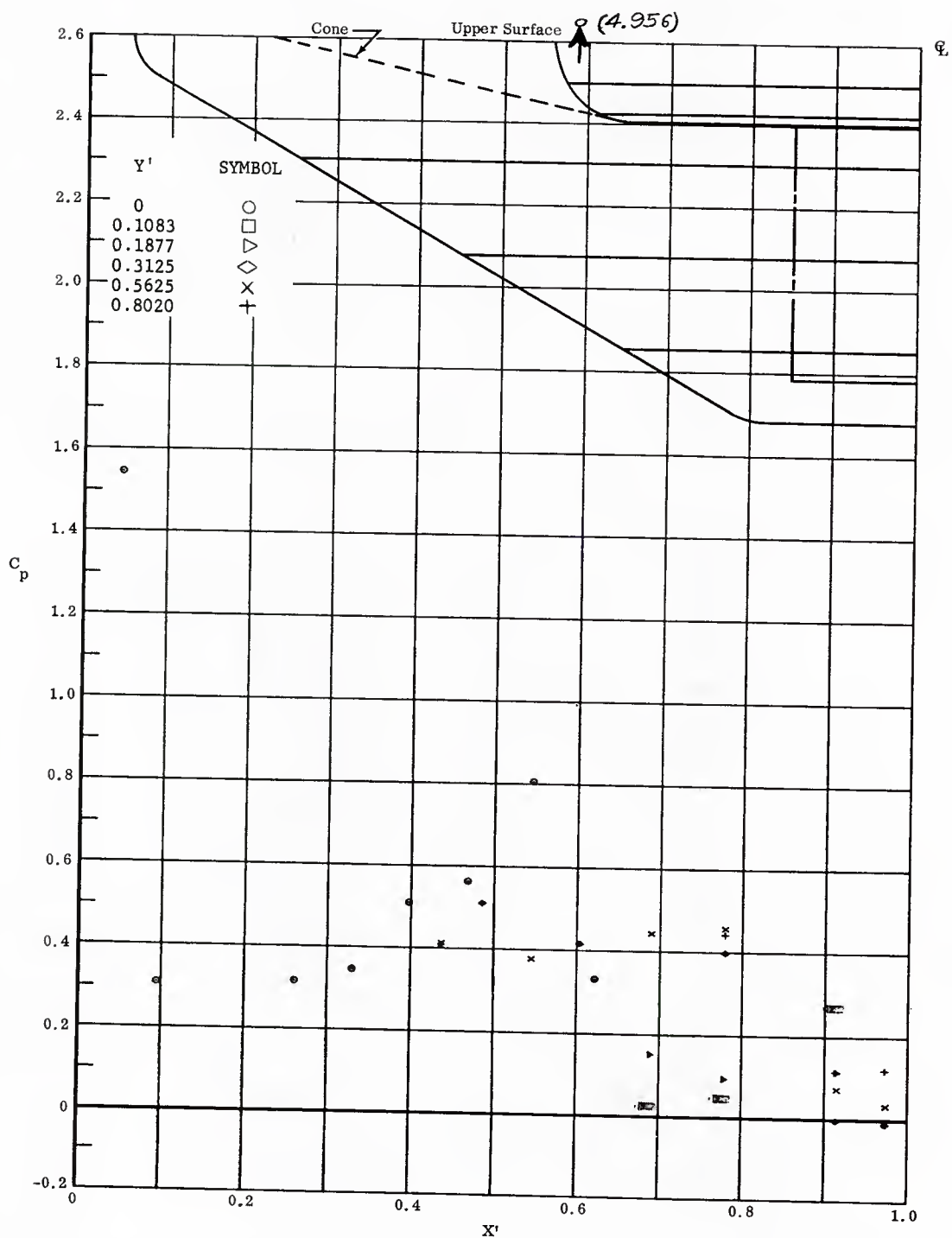


Fig. 11 Streamwise Pressure Distributions on Lower Surface; Left and Right Flaps Deflected  $+20^\circ$ ,  $\alpha = -20^\circ$ .



( NONDIMENSIONAL STREAMWISE DISTANCE FROM VIRTUAL APEX )

Fig. 11 Streamwise Pressure Distributions on Upper Surface; Left and Right Flaps Deflected  $+20^\circ$ ,  $\alpha = -20^\circ$ .

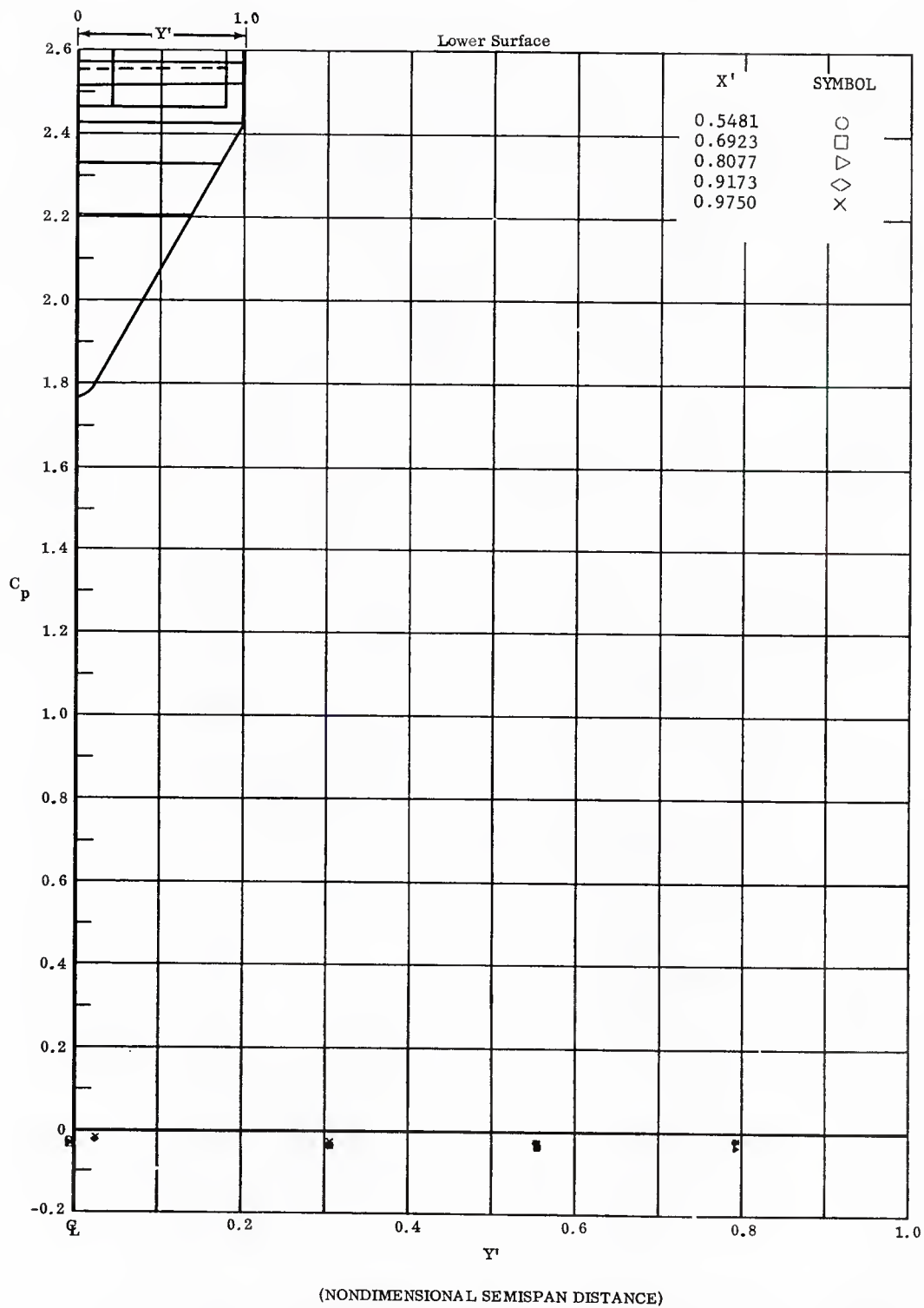


Fig. 11 Spanwise Pressure Distributions on Lower Surface; Left and Right Flaps Deflected  $+20^\circ$ ,  $\alpha = -20^\circ$ .

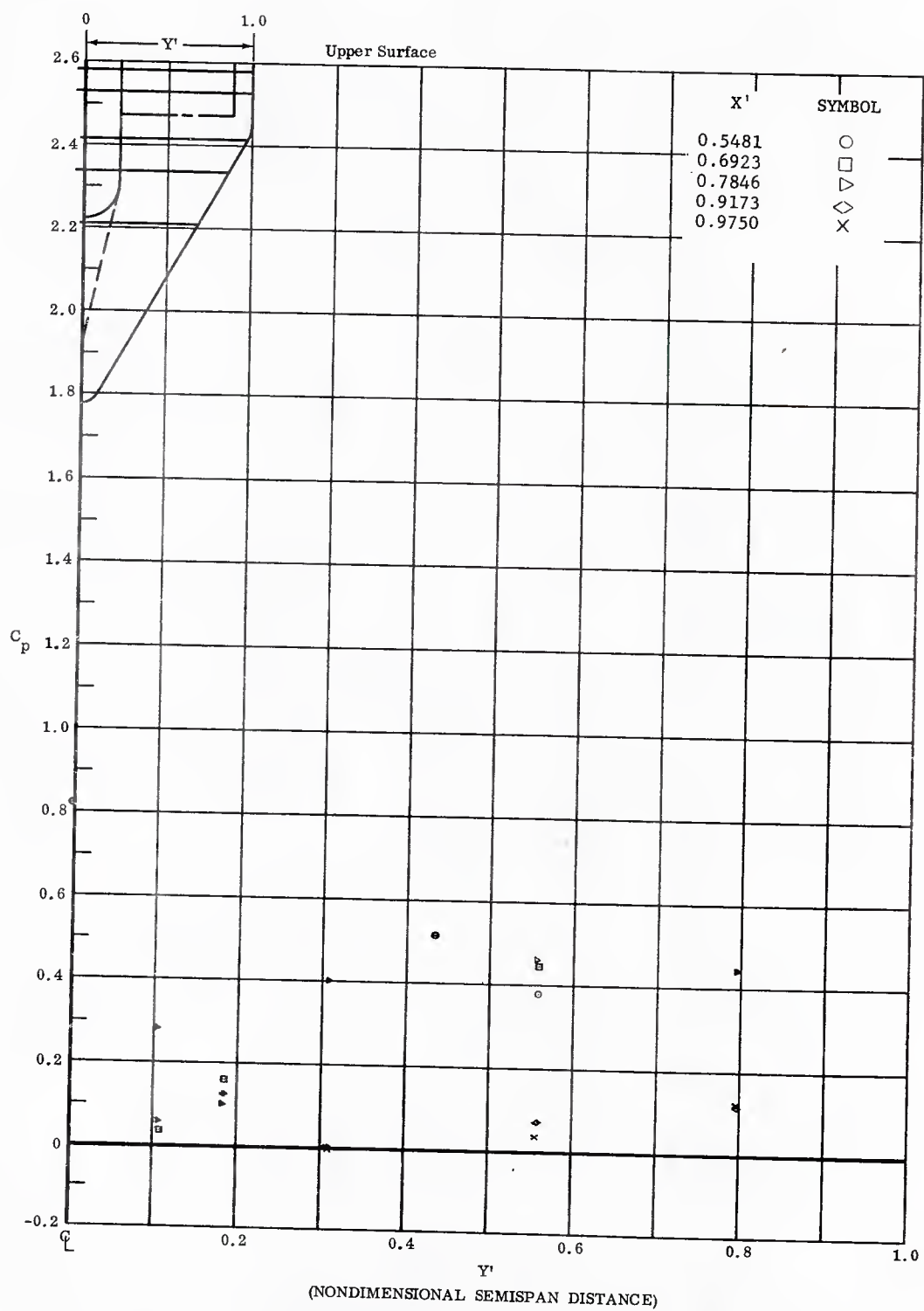


Fig. 11 Spanwise Pressure Distributions on Upper Surface; Left and Right Flaps Deflected  $+20^\circ$ ,  $\alpha = -20^\circ$ .

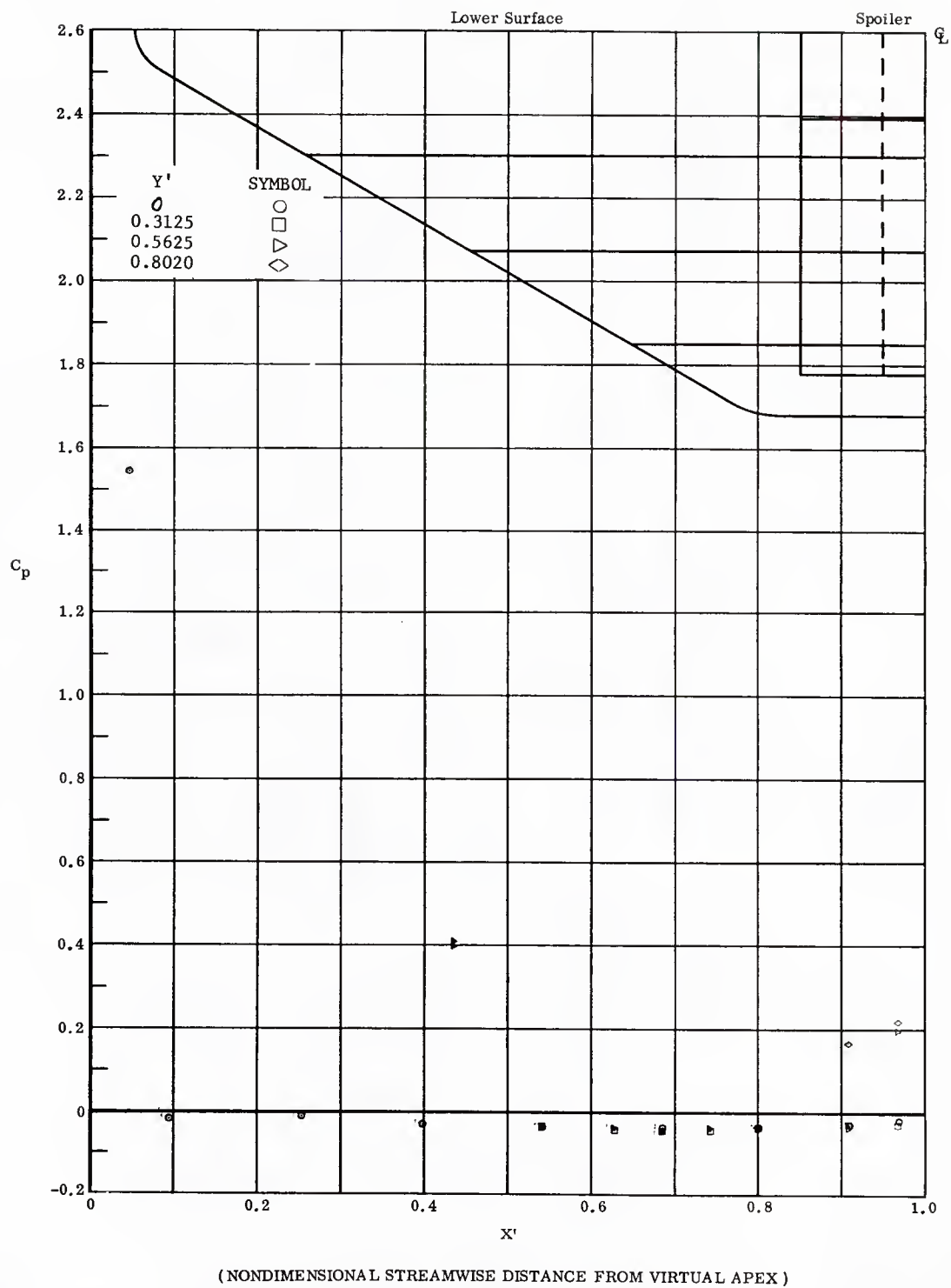


Fig. 12 Streamwise Pressure Distributions on Lower Surface; Left and Right Flaps Deflected  $+40^\circ$ ,  $\alpha = -20^\circ$ .

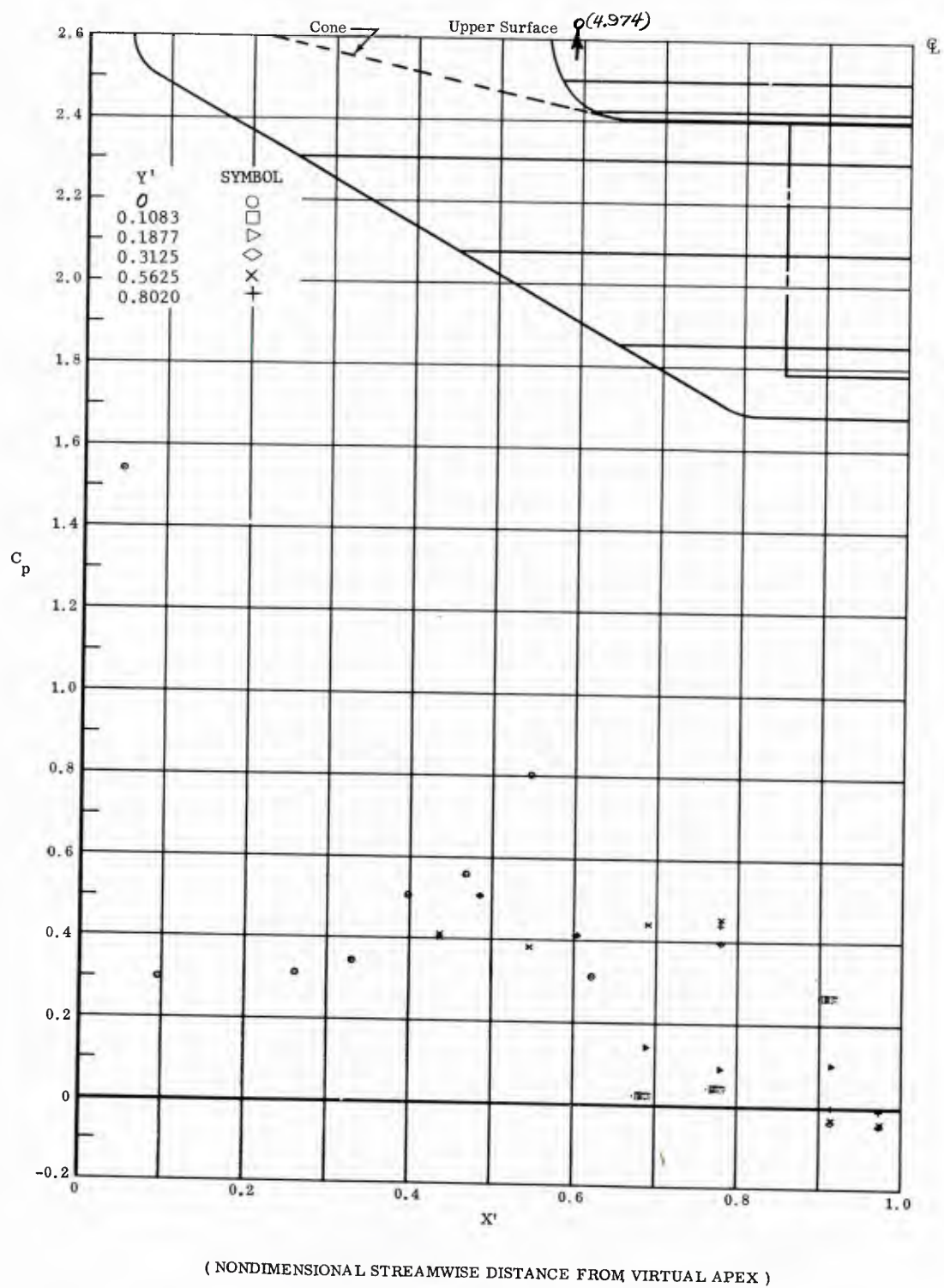


Fig. 12 Streamwise Pressure Distributions on Upper Surface; Left and Right Flaps Deflected  $+40^\circ$ ,  $\alpha = -20^\circ$ .

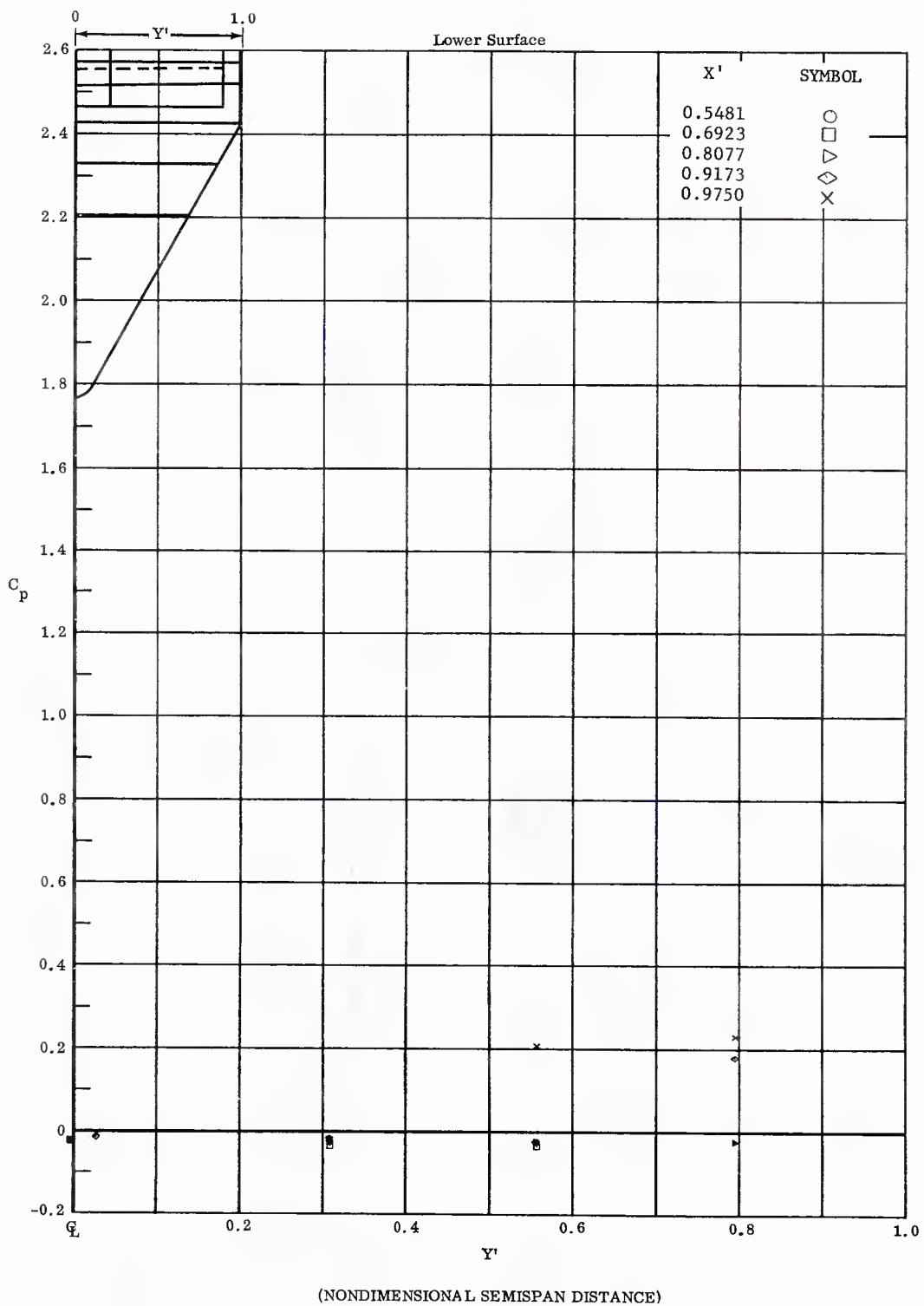


Fig. 12 Spanwise Pressure Distributions on Lower Surface; Left and Right Flaps Deflected  $+40^\circ$ ,  $\alpha = -20^\circ$ .



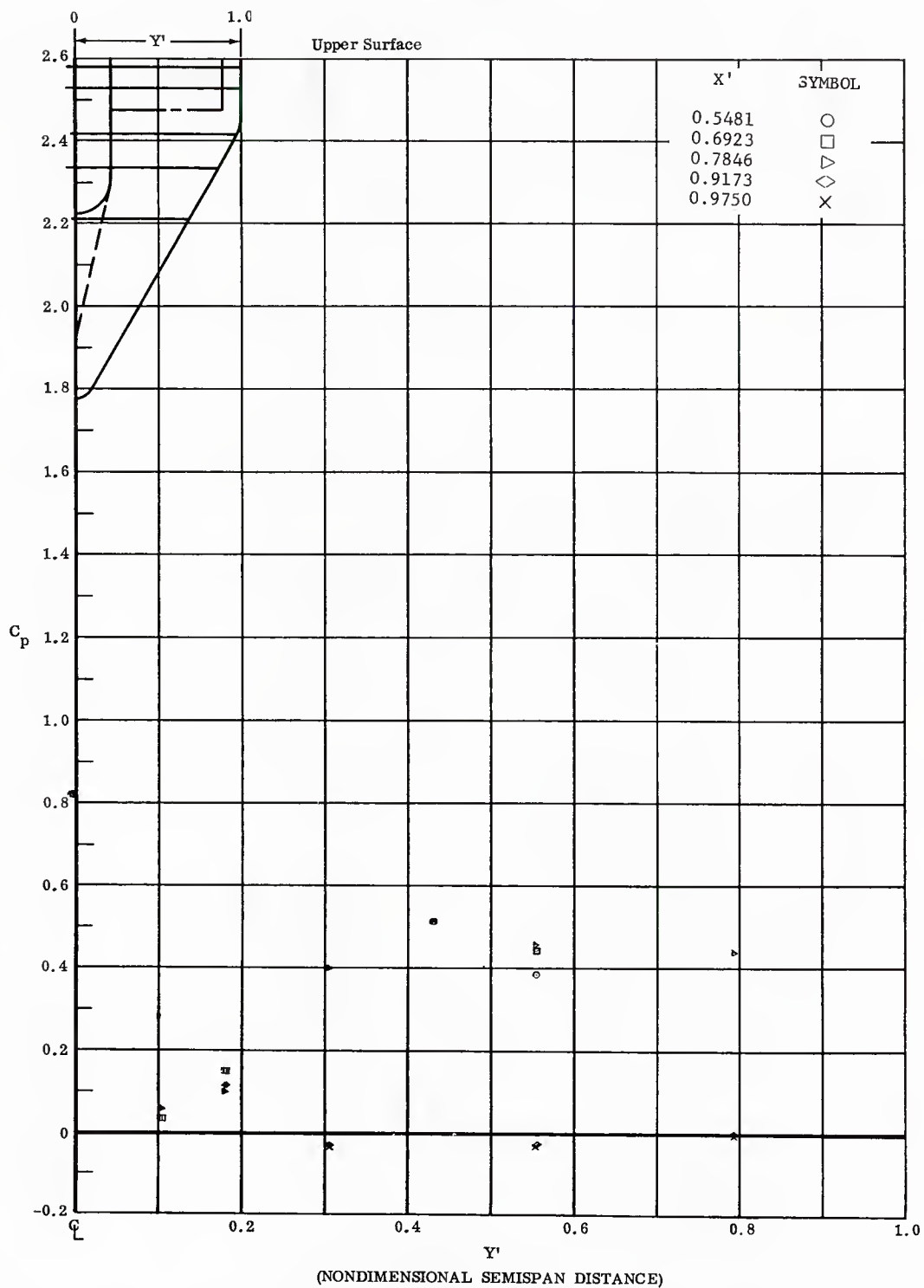


Fig. 12 Spanwise Pressure Distributions on Upper Surface; Left and Right Flaps Deflected  $+40^\circ$ ,  $\alpha = -20^\circ$ .

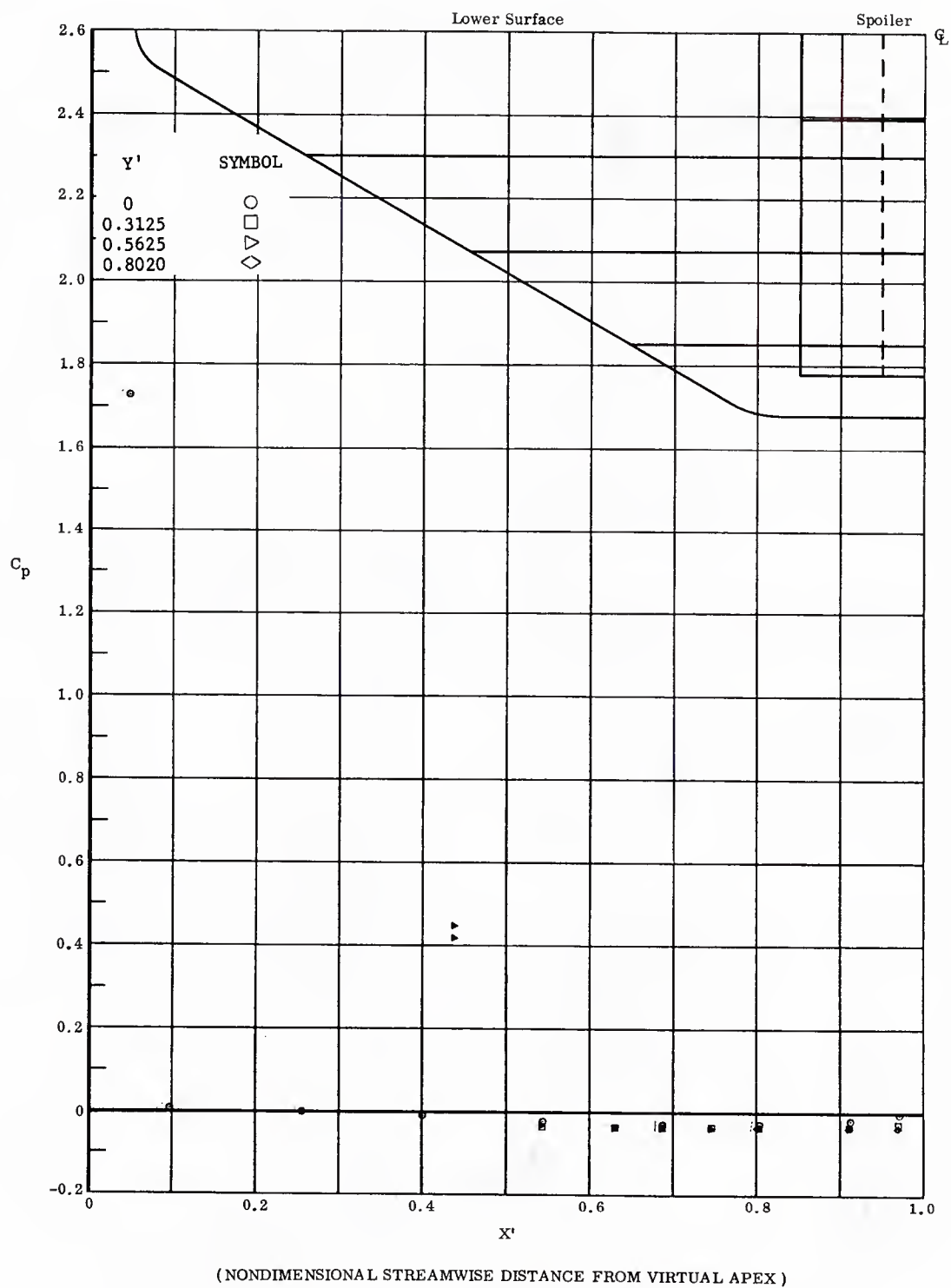
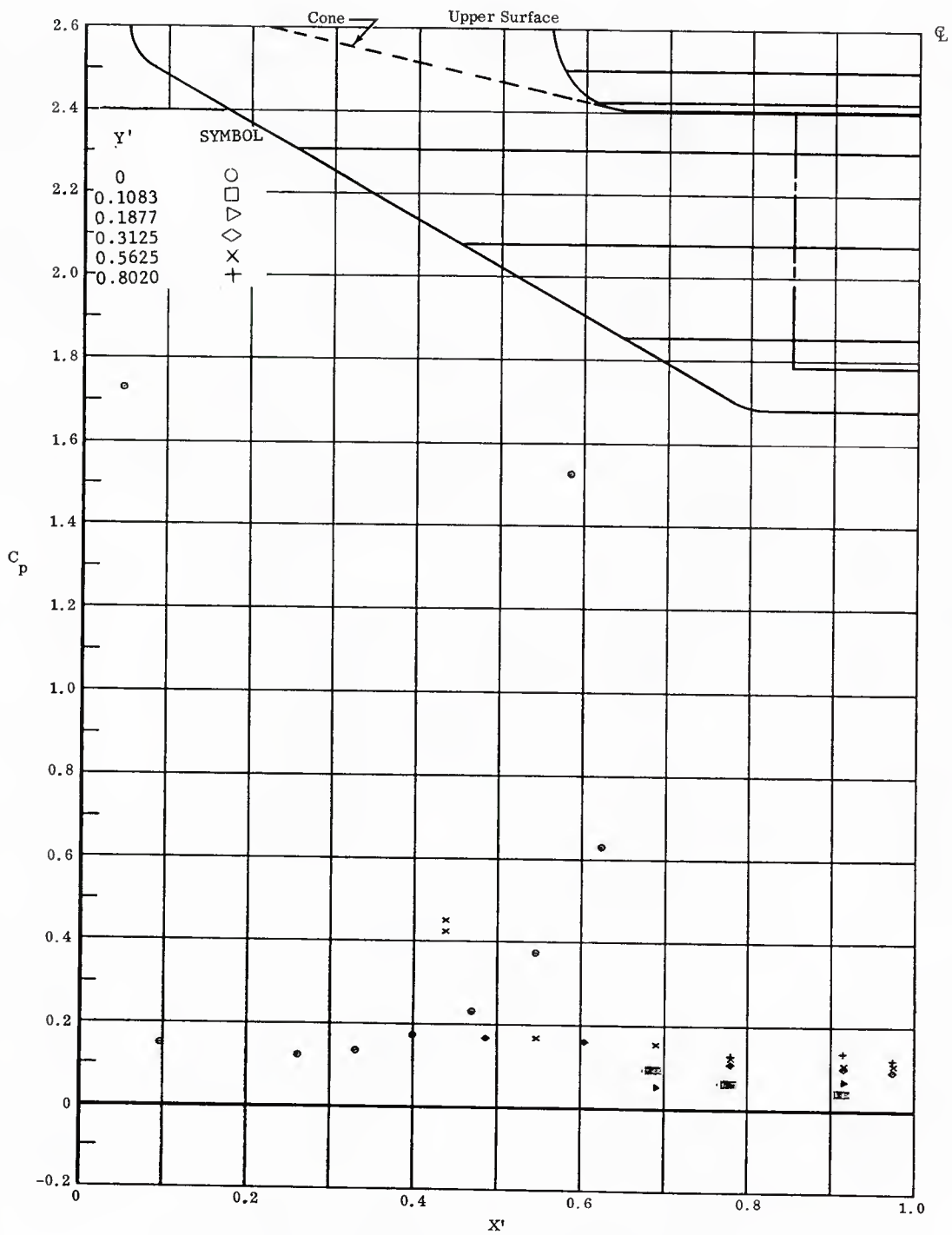


Fig. 13 Streamwise Pressure Distributions on Lower Surface; No Flap Deflections,  $\alpha = -10^\circ$ .



( NONDIMENSIONAL STREAMWISE DISTANCE FROM VIRTUAL APEX )

Fig. 13 Streamwise Pressure Distributions on Upper Surface; No Flap Deflections,  $\alpha = -10^\circ$ .

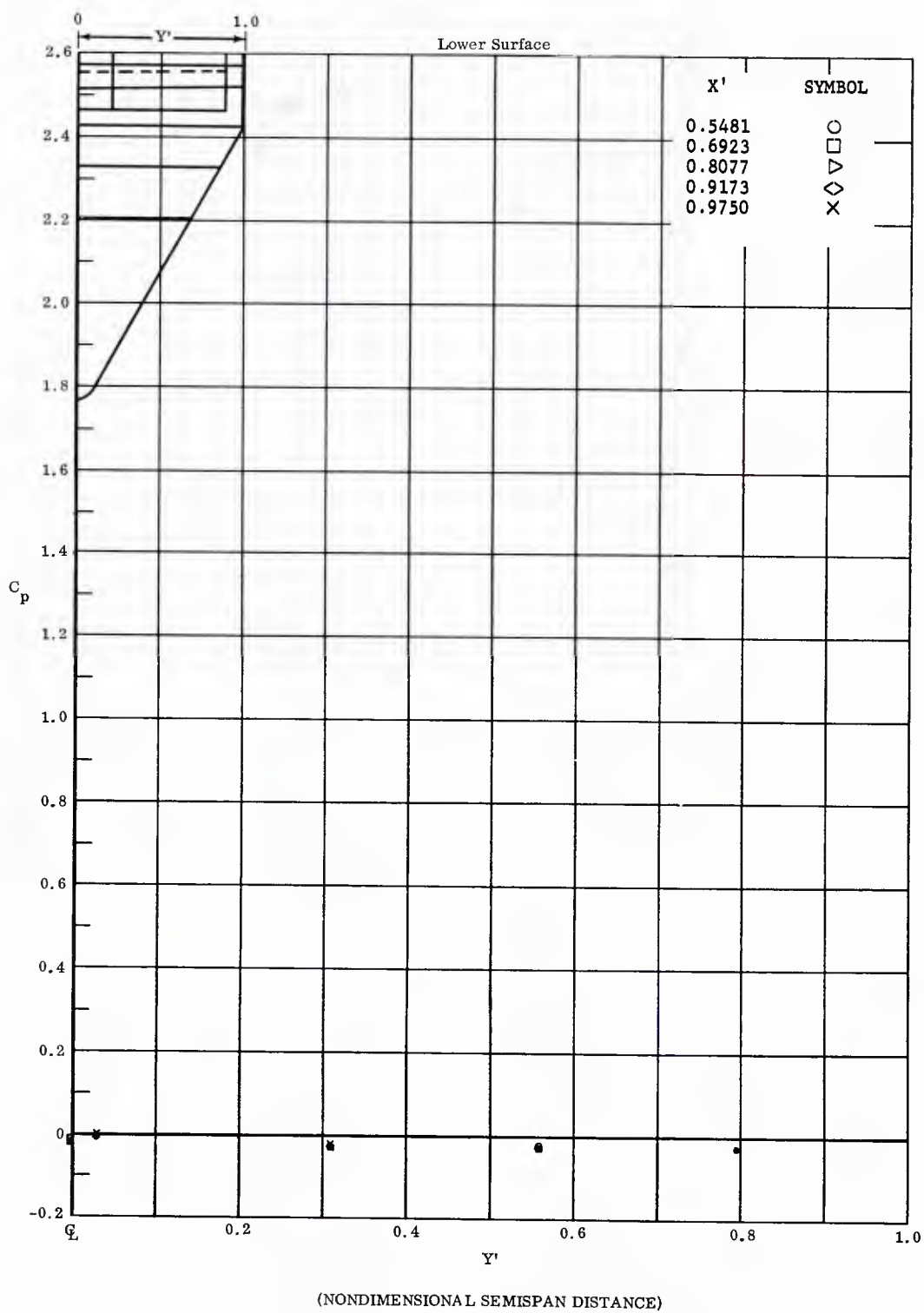


Fig. 13 Spanwise Pressure Distributions on Lower Surface; No Flap Deflections,  $\alpha = -10^\circ$ .

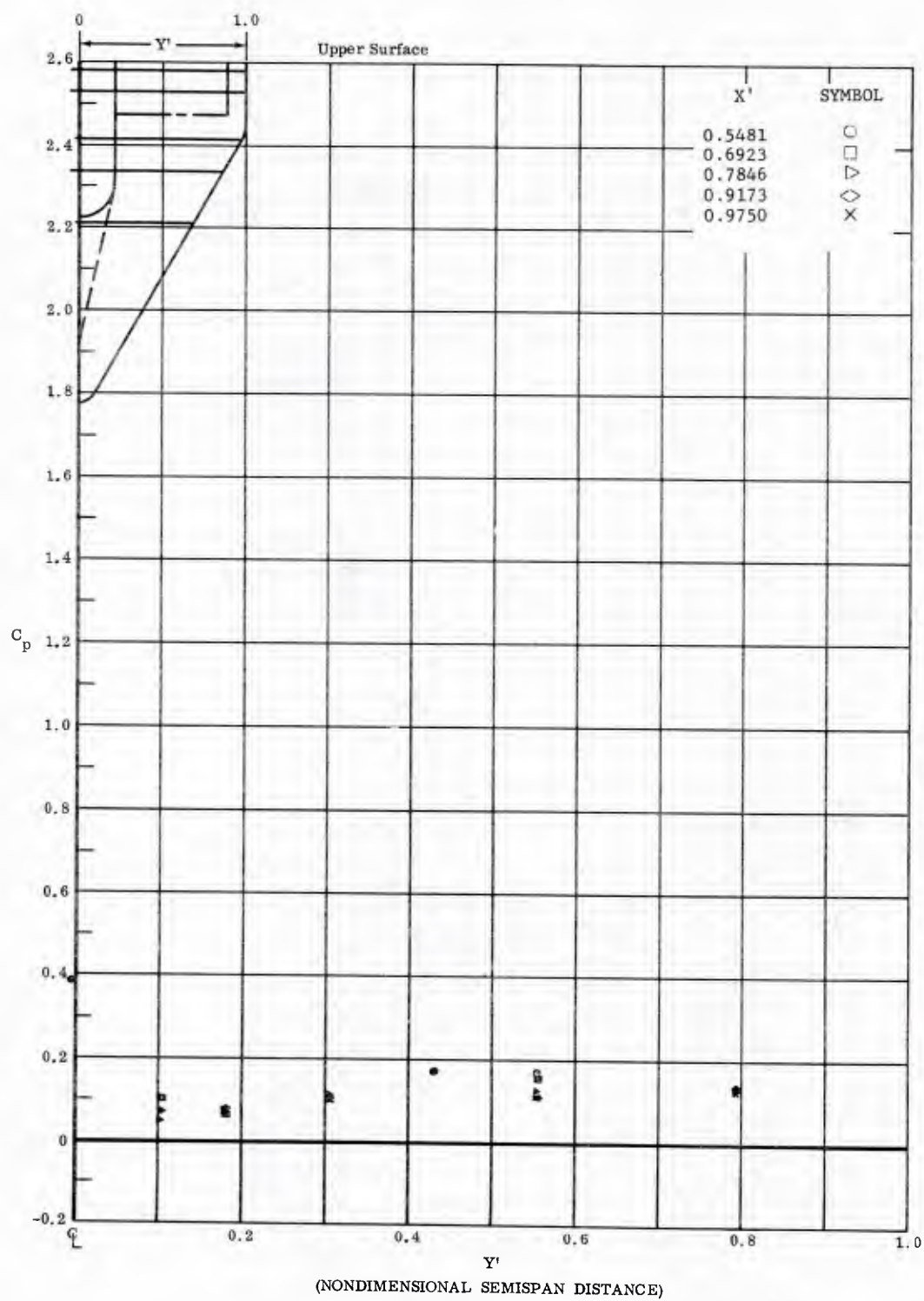


Fig. 13 Spanwise Pressure Distributions on Upper Surface; No Flap Deflections,  $\alpha = -10^\circ$ .

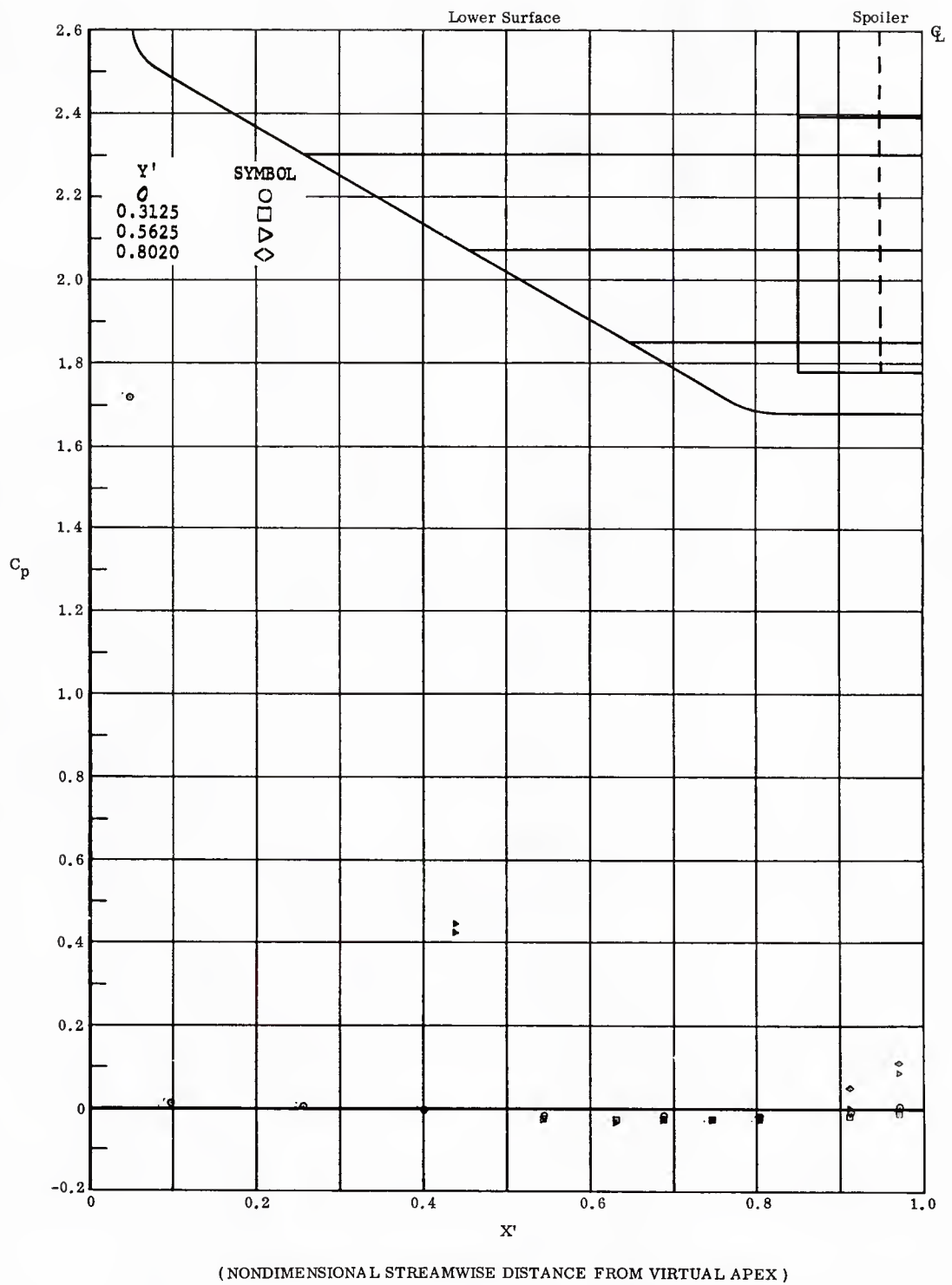
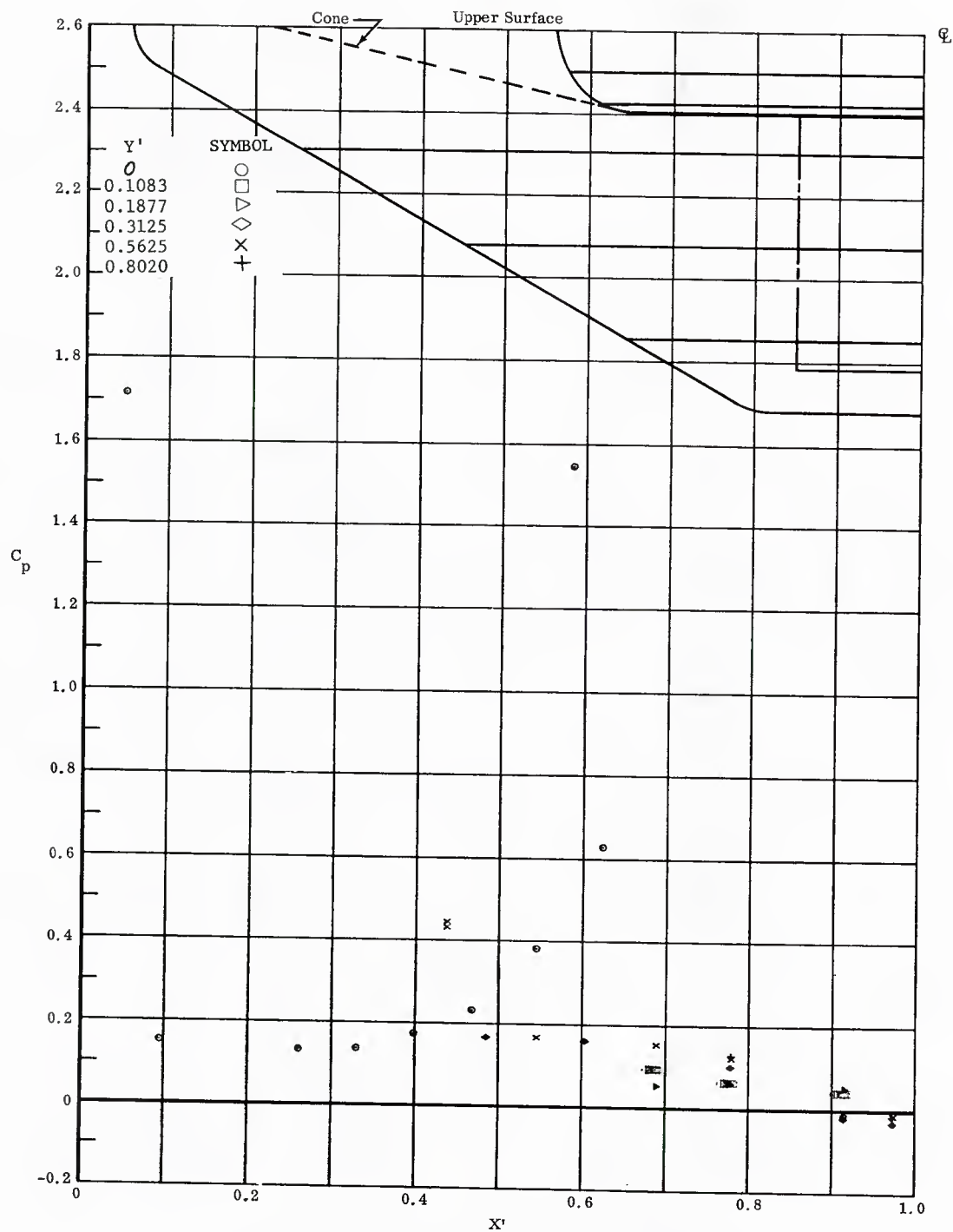


Fig. 14 Streamwise Pressure Distributions on Lower Surface; Left and Right Flaps Deflected +20,  $\alpha = -10^\circ$ .



( NONDIMENSIONAL STREAMWISE DISTANCE FROM VIRTUAL APEX )

Fig. 14 Streamwise Pressure Distributions on Upper Surface; Left and Right Flaps Deflected  $+20^\circ$ ,  $\alpha = -10^\circ$ .

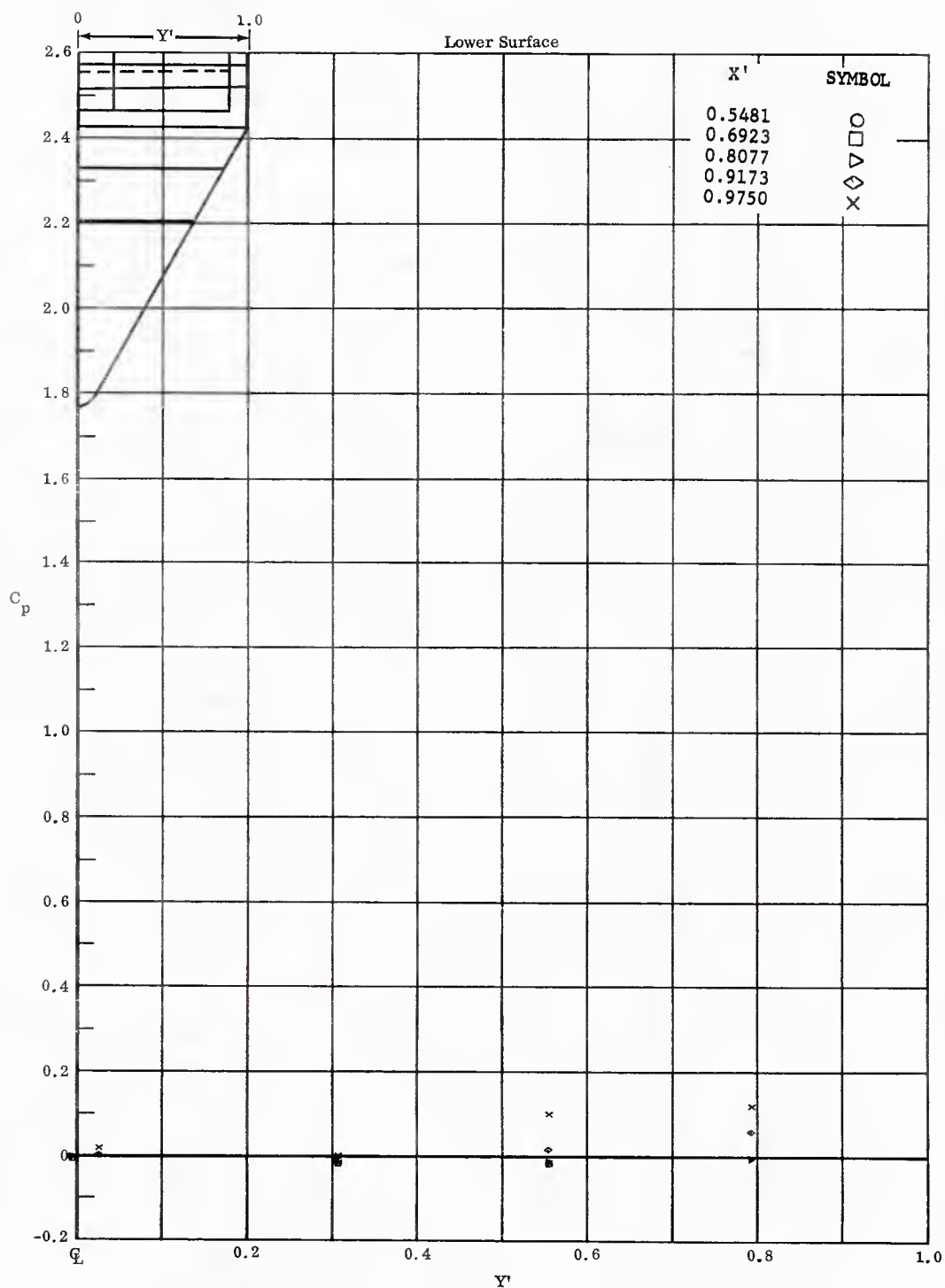


Fig. 14 Spanwise Pressure Distributions on Lower Surface; Left and Right Flaps Deflected  $+20^\circ$ ,  $\alpha = -10^\circ$ .



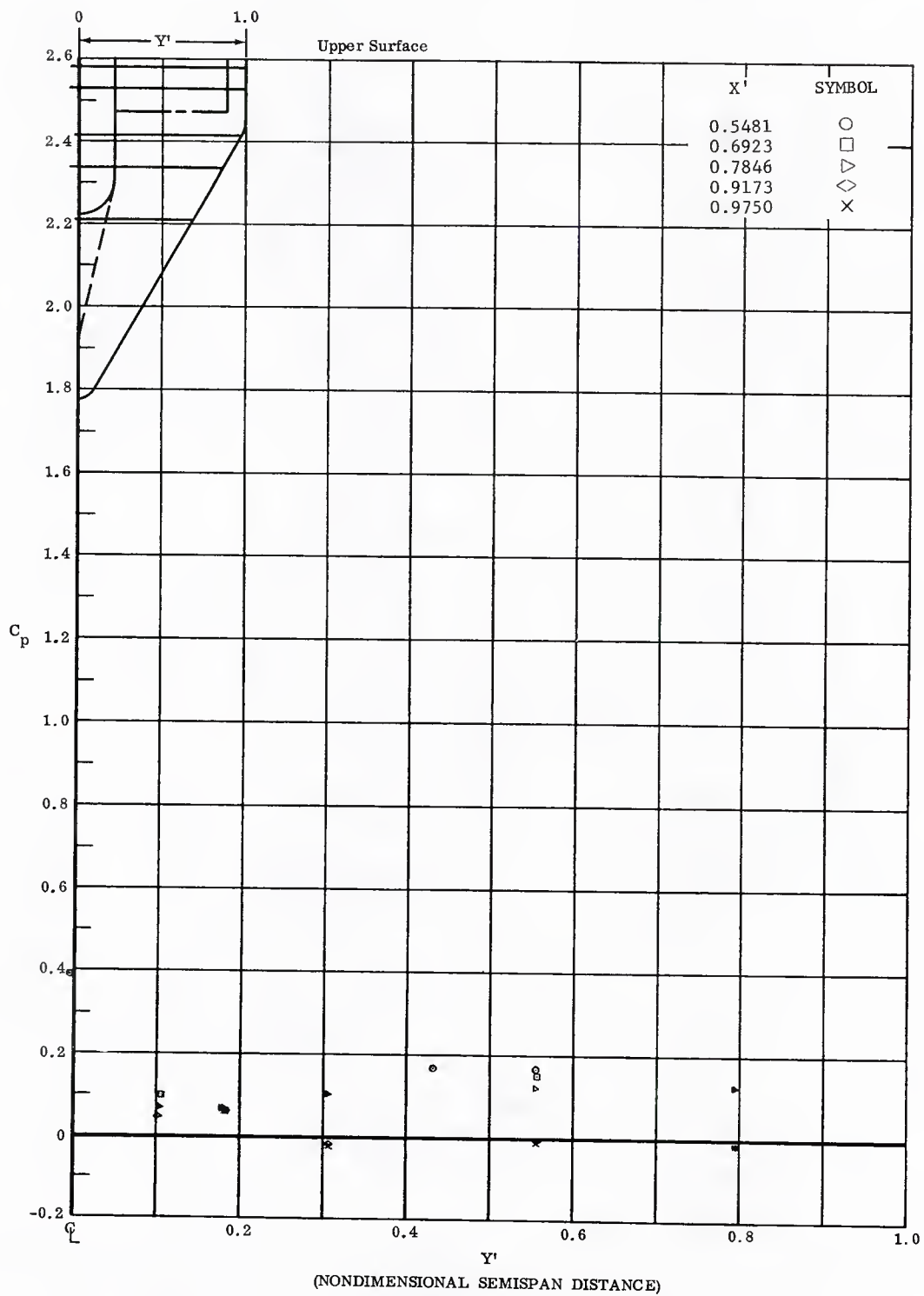


Fig. 14 Spanwise Pressure Distributions on Upper Surface; Left and Right Flaps Deflected  $+20^\circ$ ,  $\alpha = -10^\circ$ .

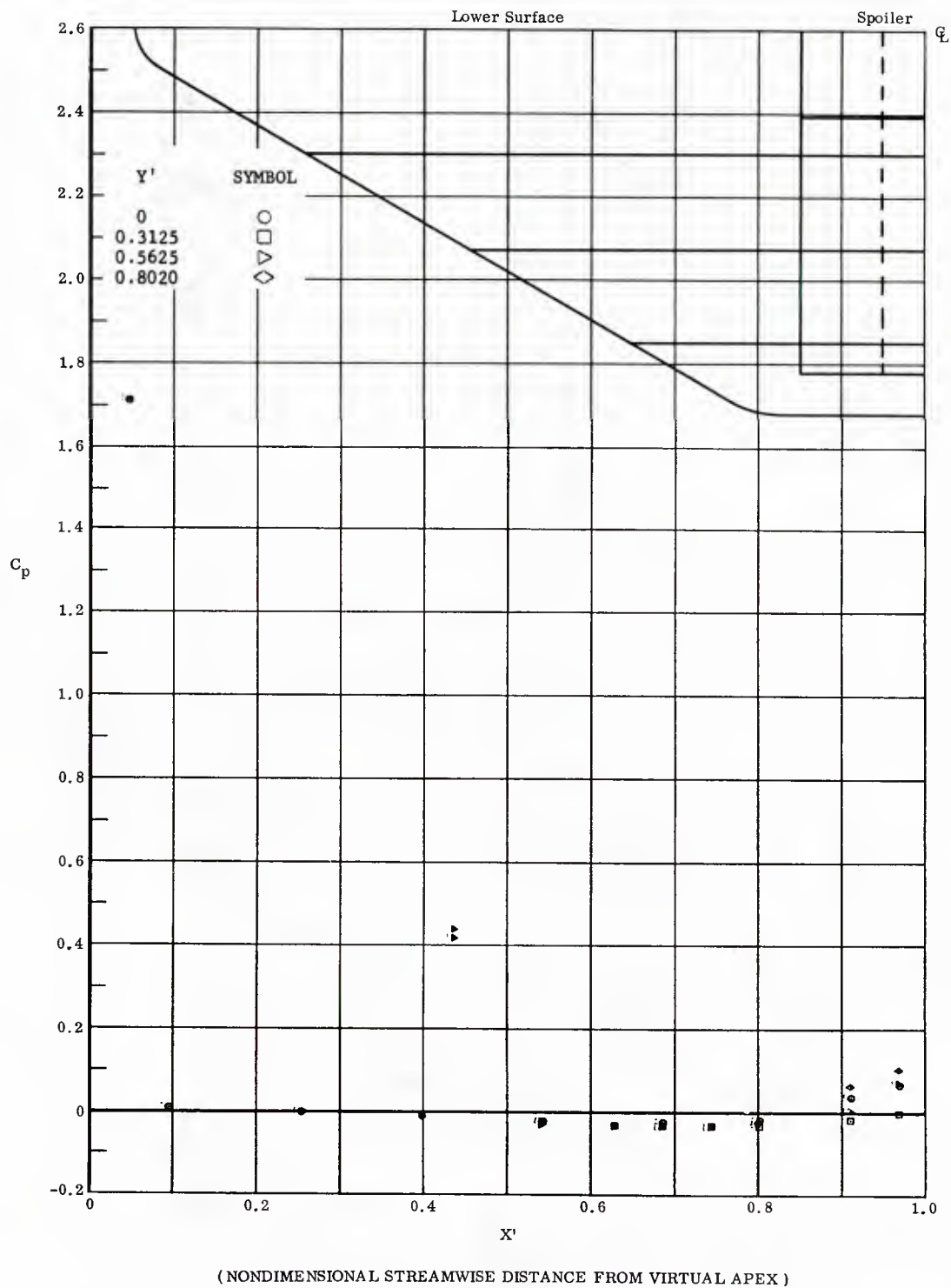
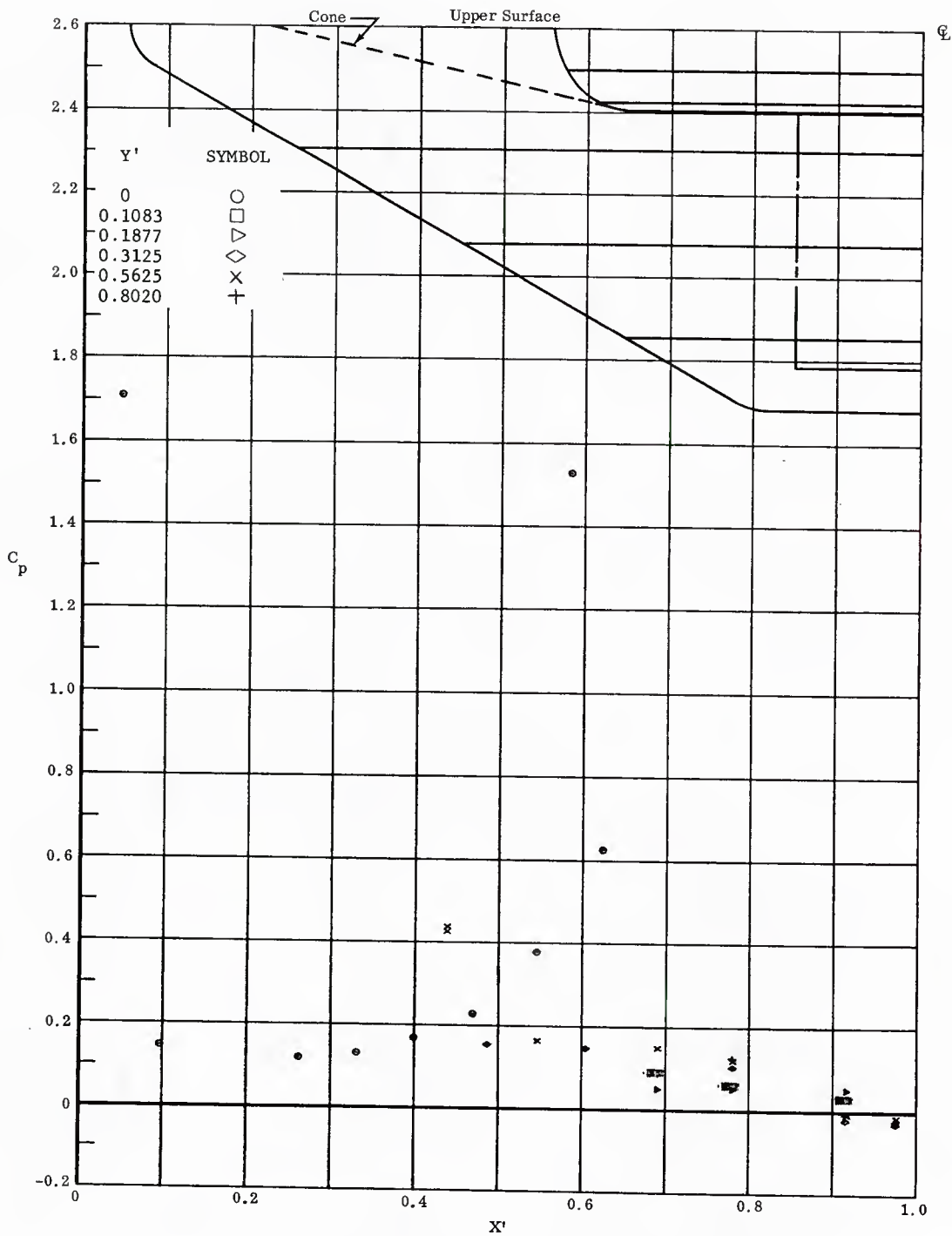
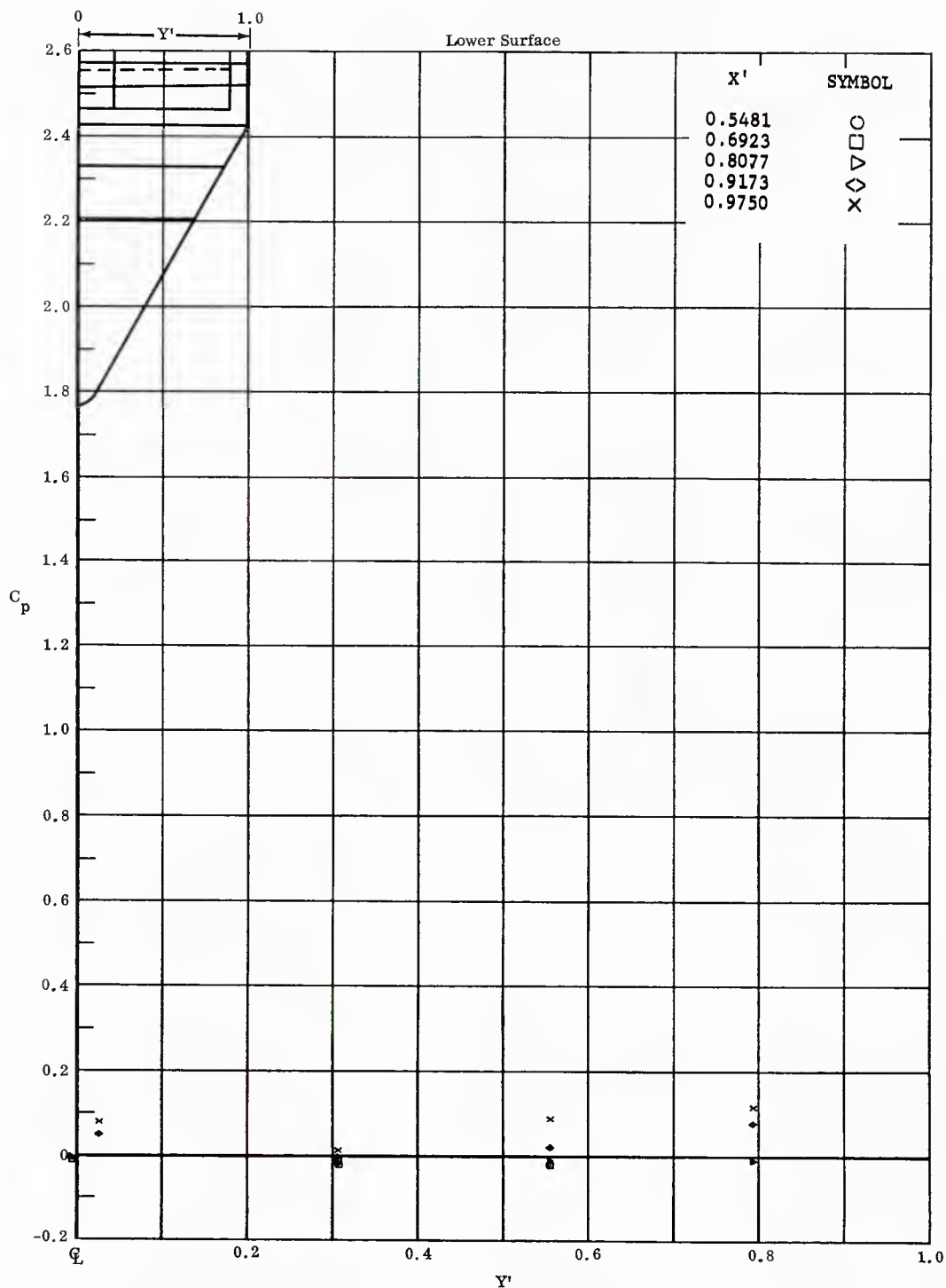


Fig. 15 Streamwise Pressure Distributions on Lower Surface; Center, Left and Right Flaps All Deflected  $+20^\circ$ ,  $\alpha = -10^\circ$ .



( NONDIMENSIONAL STREAMWISE DISTANCE FROM VIRTUAL APEX )

Fig. 15 Streamwise Pressure Distributions on Upper Surface; Center, Left and Right Flaps All Deflected  $+20^\circ$ ,  $\alpha = -10^\circ$ .



(NONDIMENSIONAL SEMISPAN DISTANCE)

Fig. 15 Spanwise Pressure Distributions on Lower Surface; Center, Left and Right Flaps All Deflected  $+20^\circ$ ,  $\alpha = -10^\circ$ .

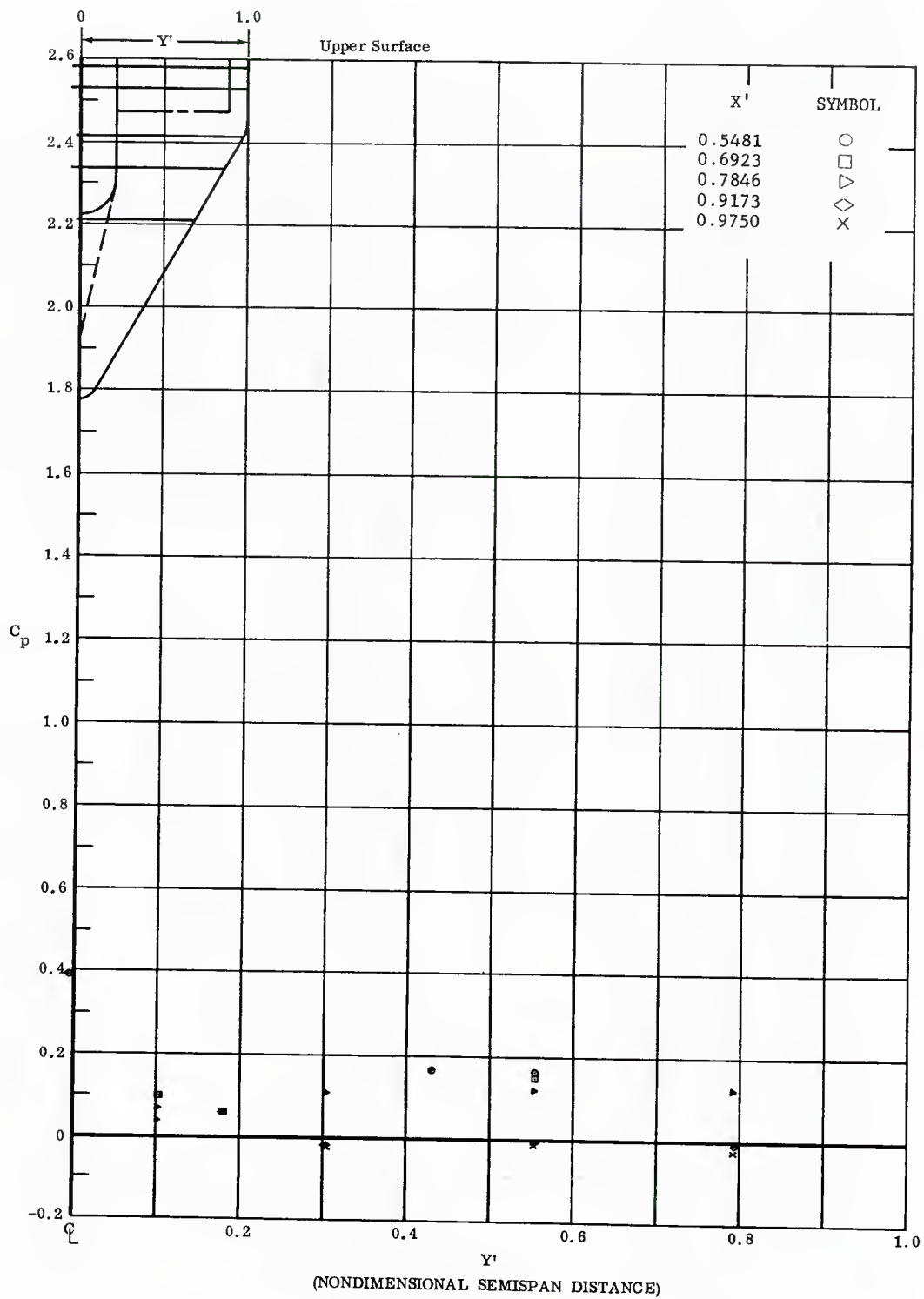


Fig. 15 Spanwise Pressure Distributions on Upper Surface; Center, Left and Right Flaps All Deflected  $+20^\circ$ ,  $\alpha = -10^\circ$ .

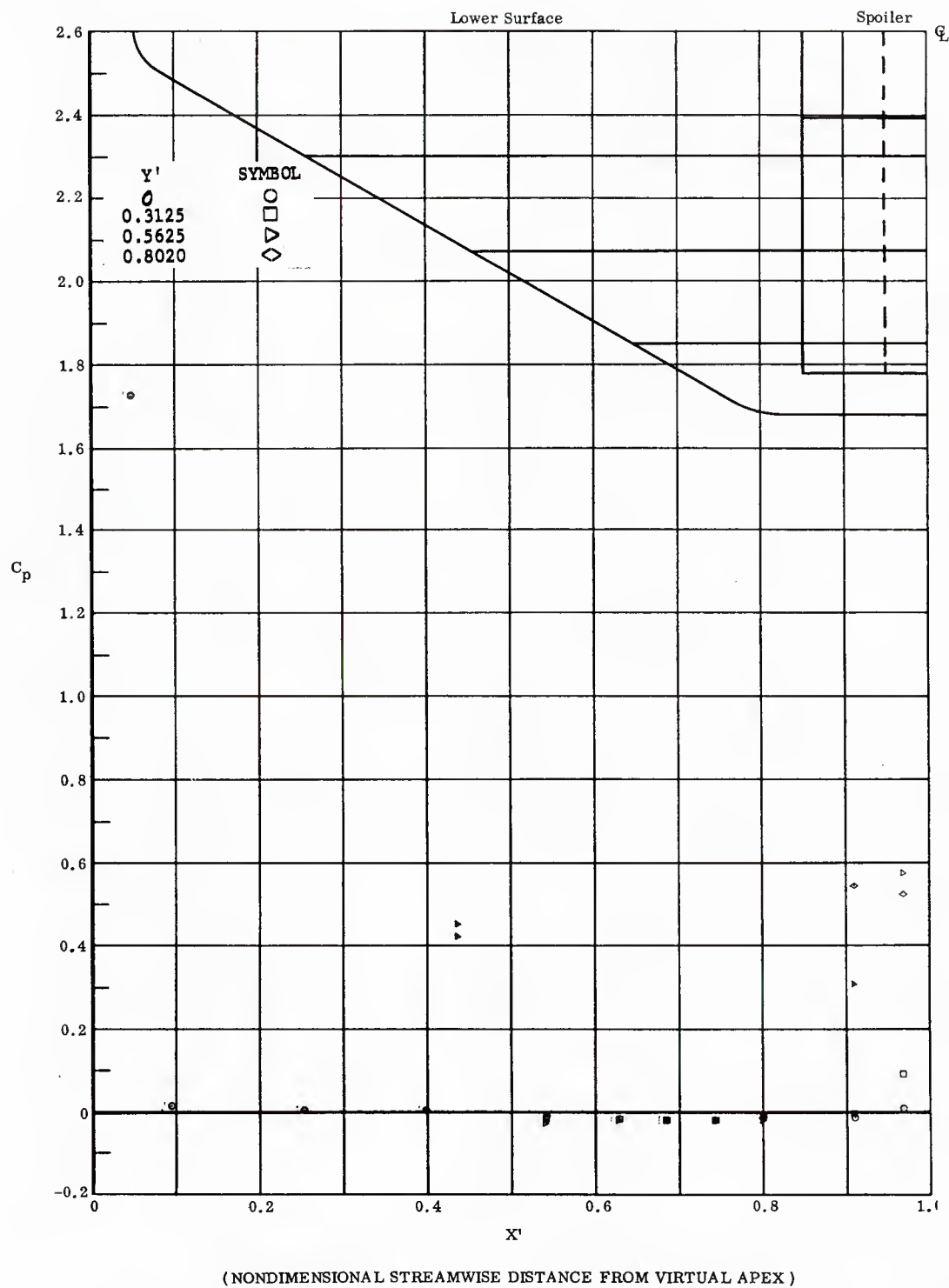
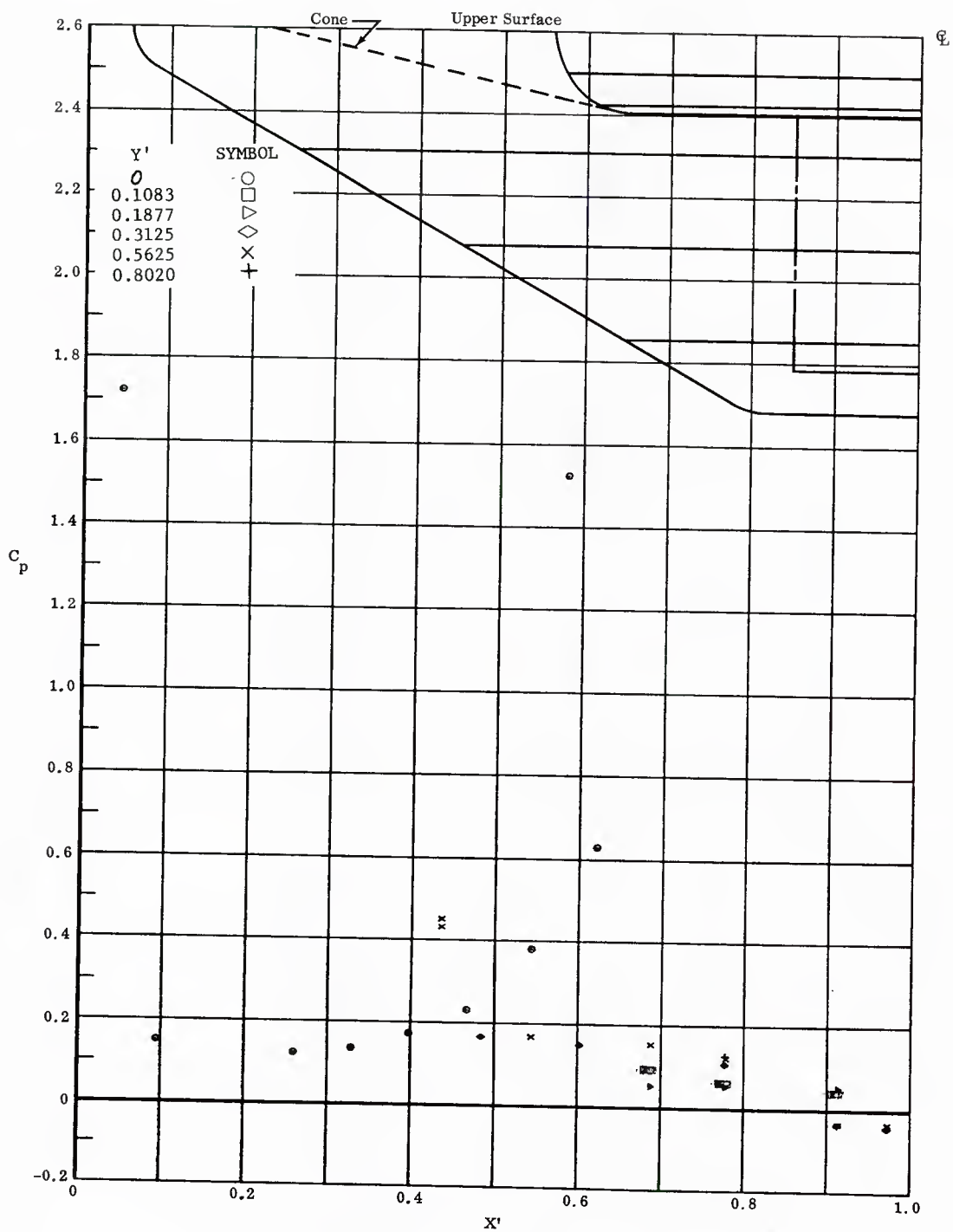


Fig. 16 Streamwise Pressure Distributions on Lower Surface; Left and Right Flaps Deflected  $+40^\circ$ ,  $\alpha = -10^\circ$ .



(NONDIMENSIONAL STREAMWISE DISTANCE FROM VIRTUAL APEX)

Fig. 16 Streamwise Pressure Distributions on Upper Surface; Left and Right Flaps Deflected  $+40^\circ$ ,  $\alpha = -10^\circ$ .

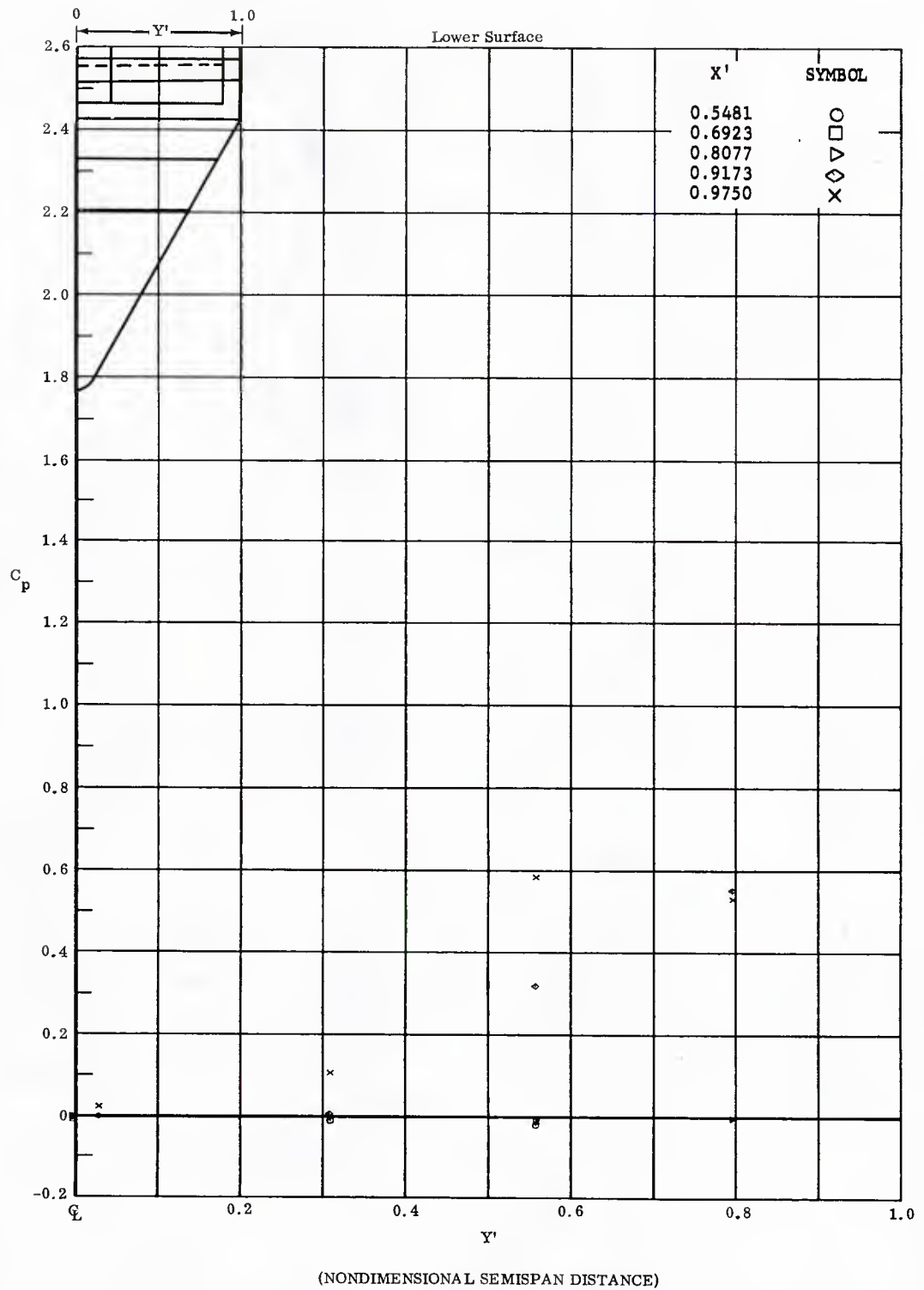


Fig. 16 Spanwise Pressure Distributions on Lower Surface; Left and Right Flaps Deflected  $+40^\circ$ ,  $\alpha = -10^\circ$ .



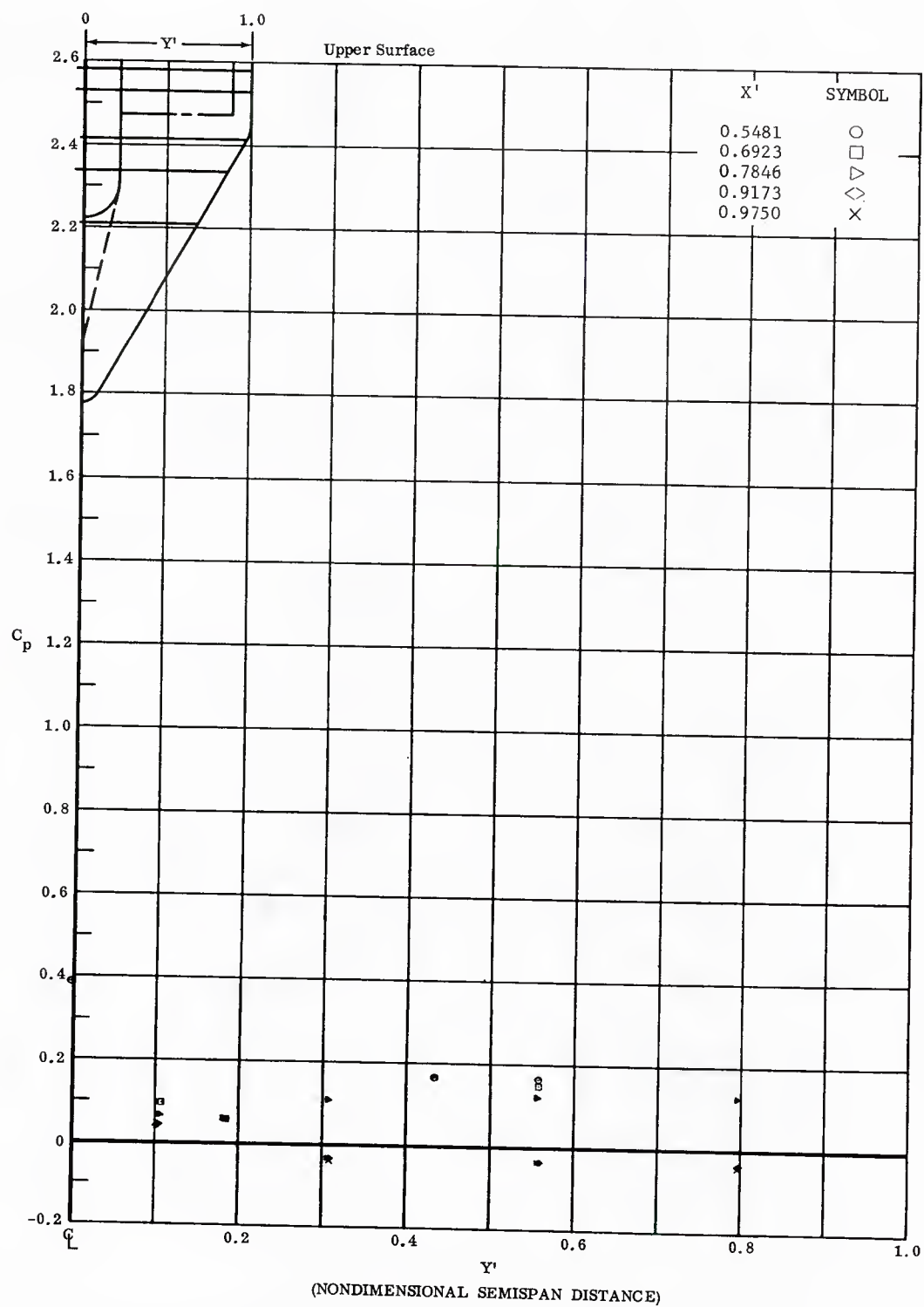


Fig. 16, Spanwise Pressure Distributions on Upper Surface; Left and Right Flaps Deflected  $+40^\circ$ ,  $\alpha = -10^\circ$ .

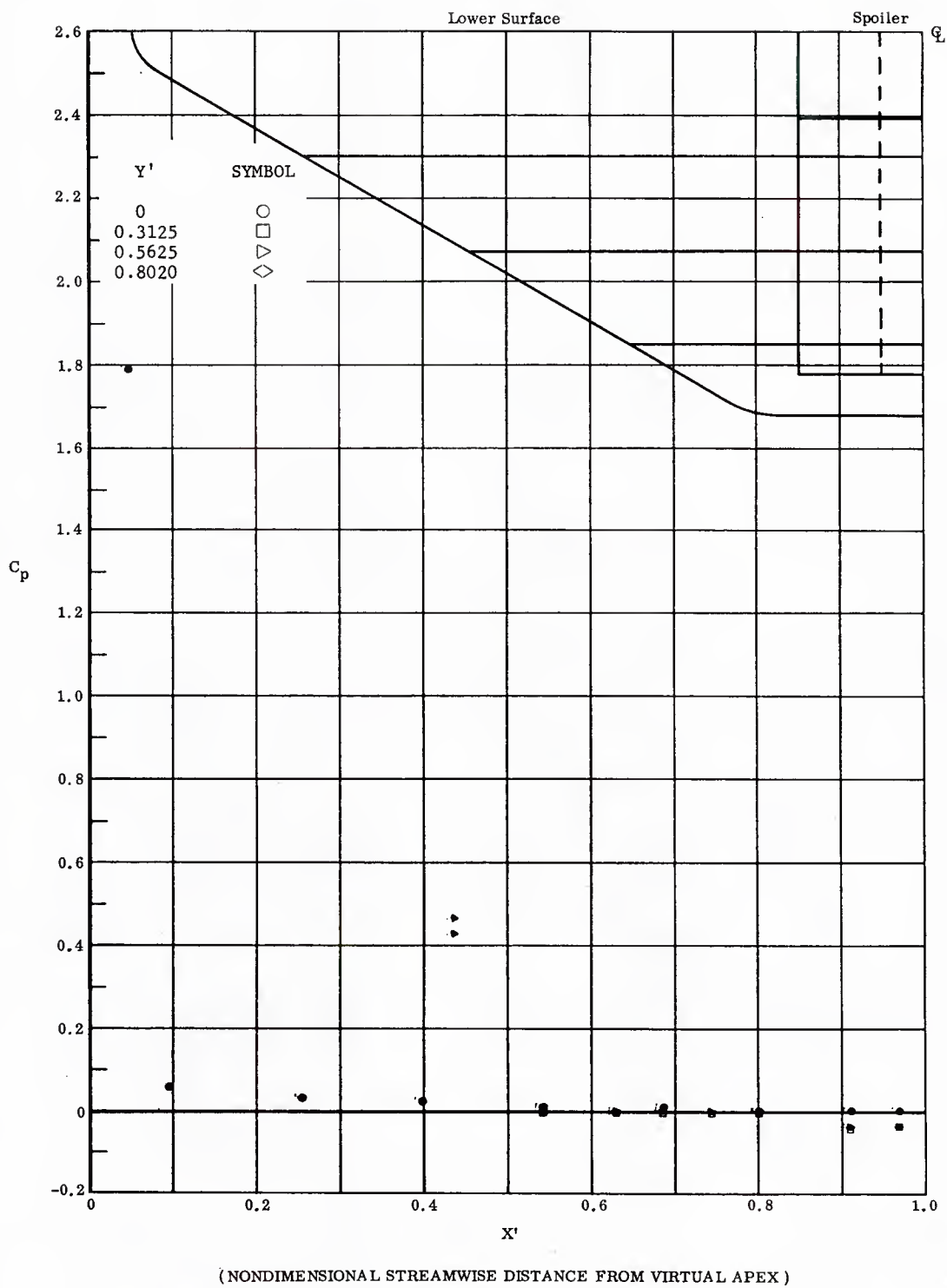


Fig. 17 Streamwise Pressure Distributions on Lower Surface; Left and Right Flaps Deflected  $-40^\circ$ ,  $\alpha = 0^\circ$ .

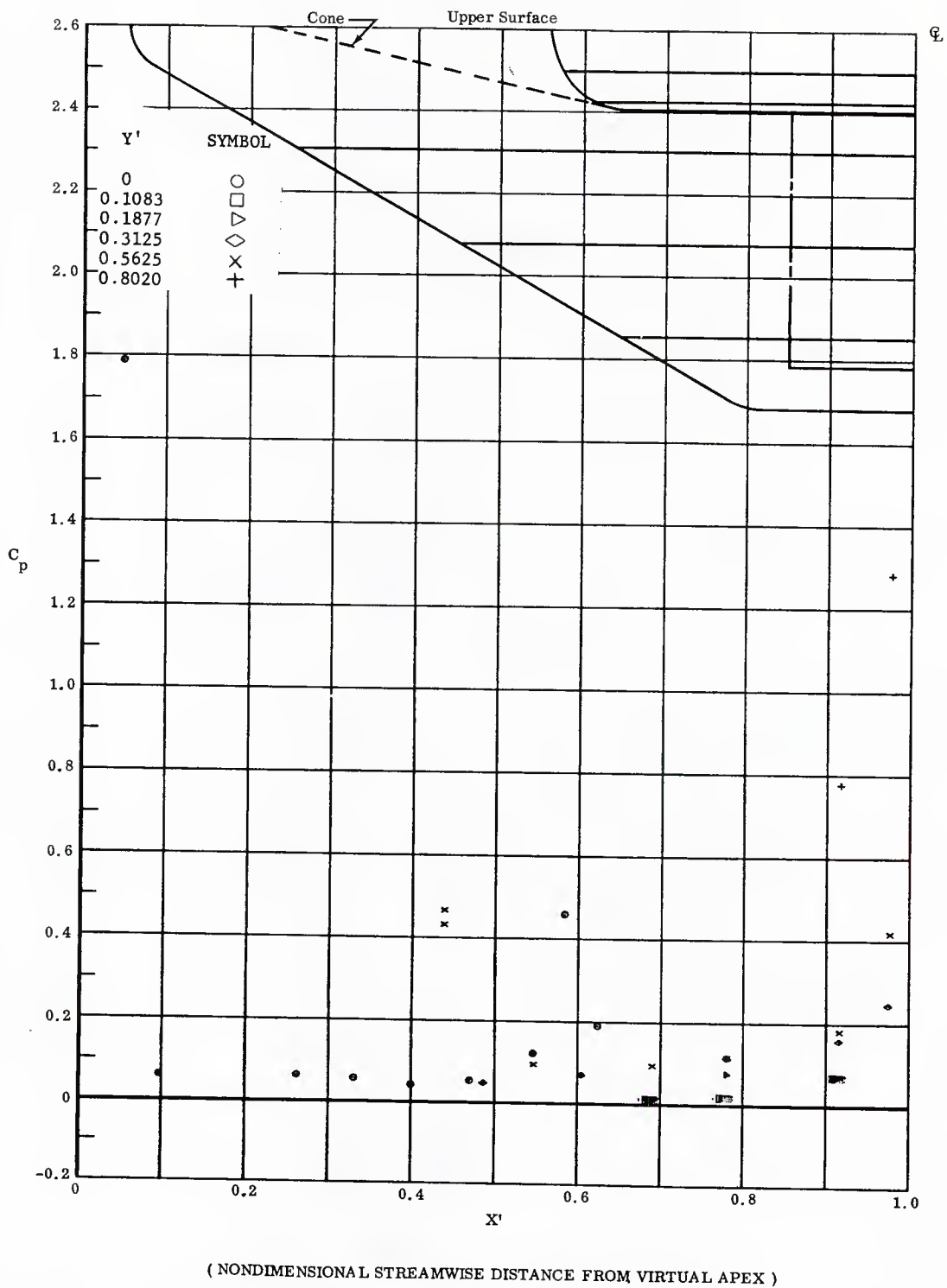


Fig. 17 Streamwise Pressure Distributions on Upper Surface; Left and Right Flaps Deflected  $-40^\circ$ ,  $\alpha = 0^\circ$ .

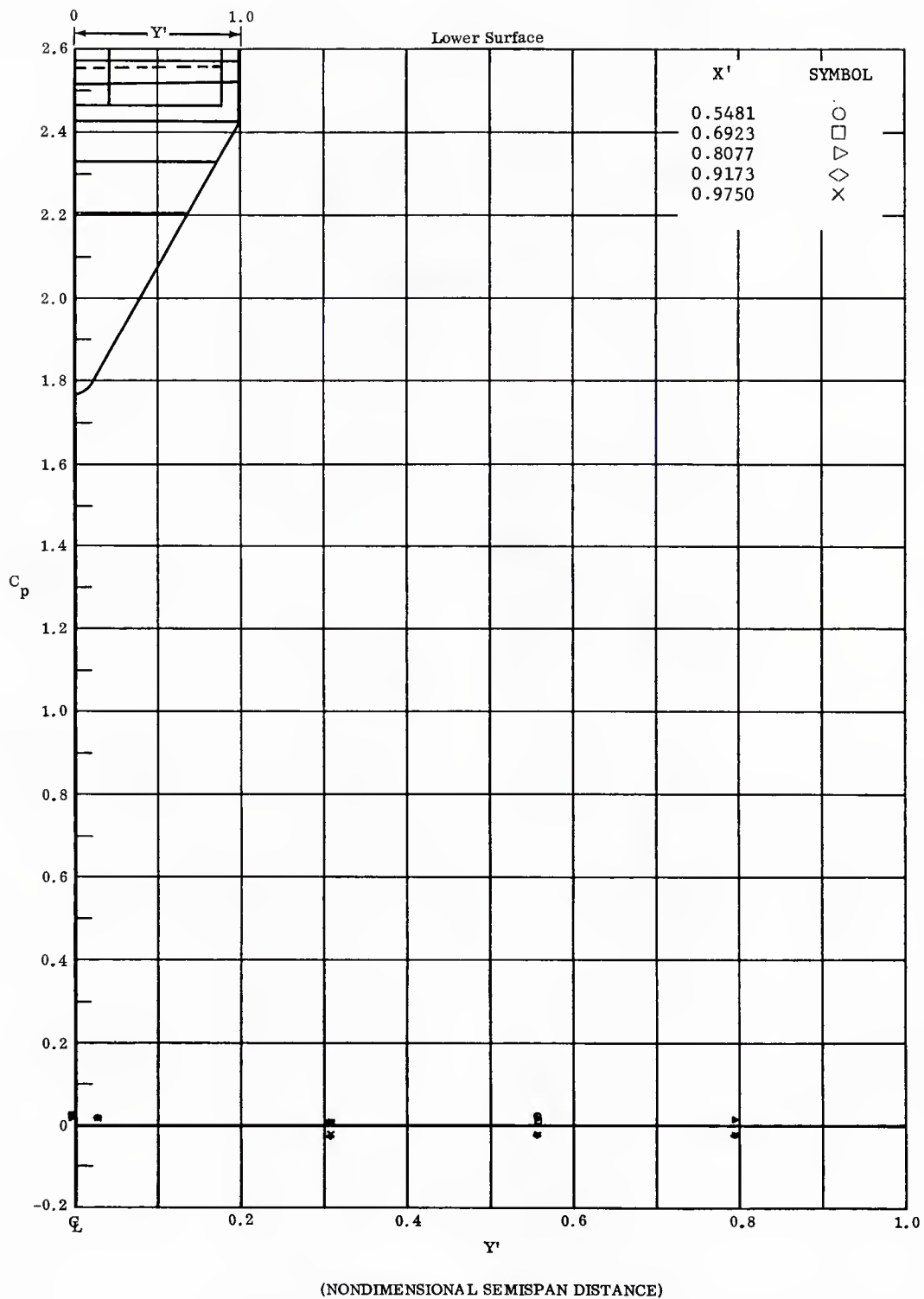


Fig. 17 Spanwise Pressure Distributions on Lower Surface; Left and Right Flaps Deflected  $-40^\circ$ ,  $\alpha = 0^\circ$ .

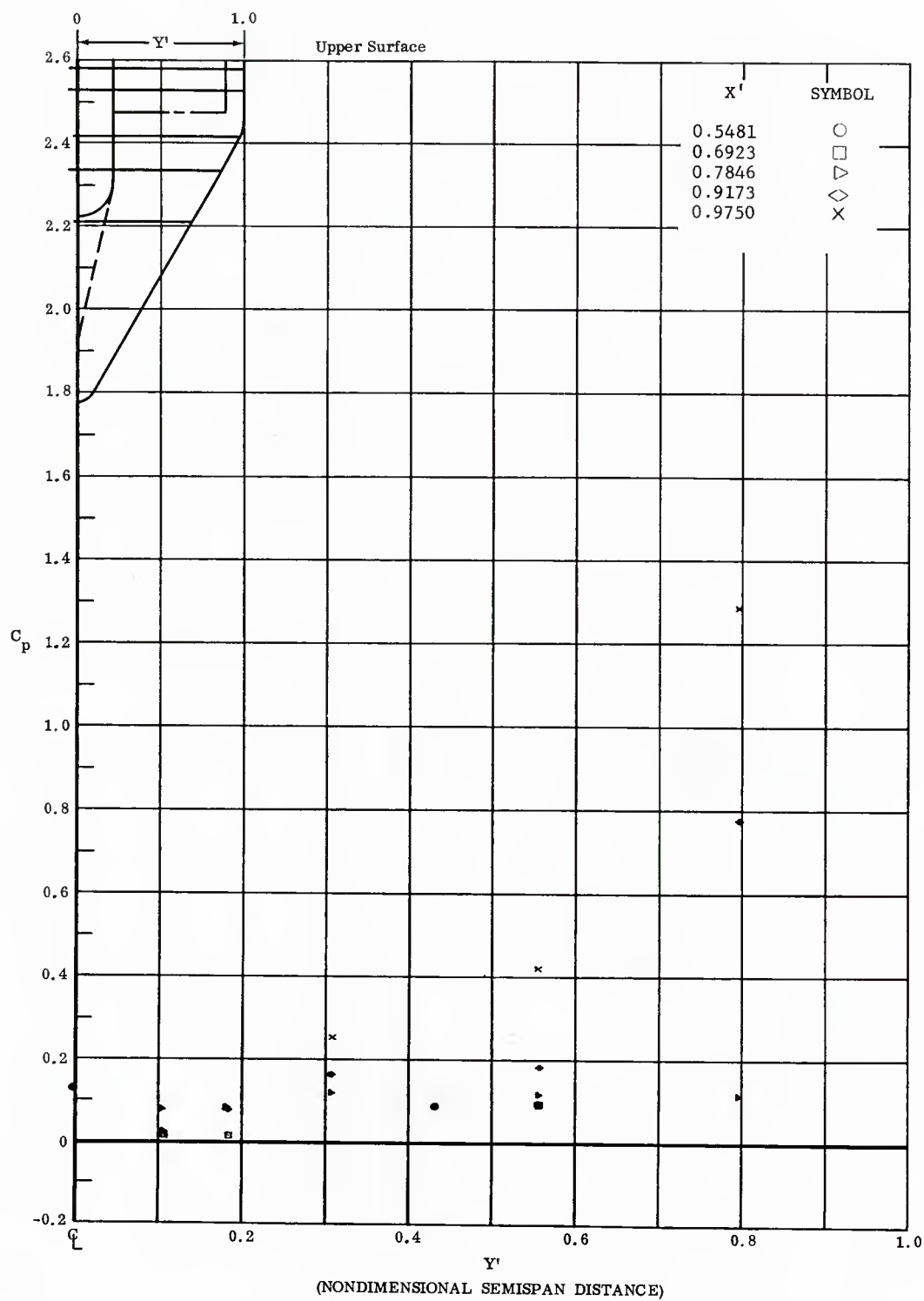


Fig. 17 Spanwise Pressure Distributions on Upper Surface; Left and Right Flaps Deflected  $-40^\circ$ ,  $\alpha = 0^\circ$ .

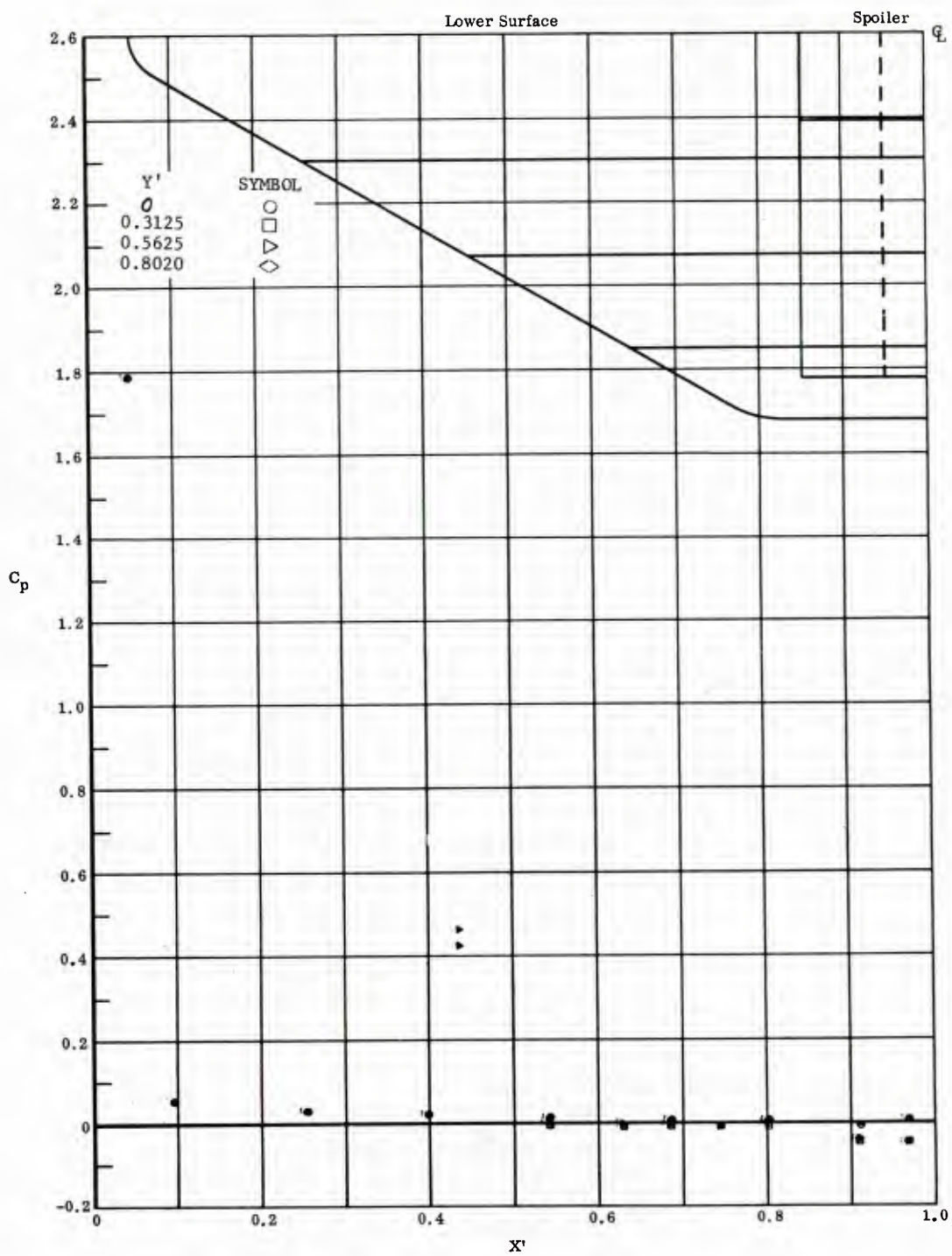
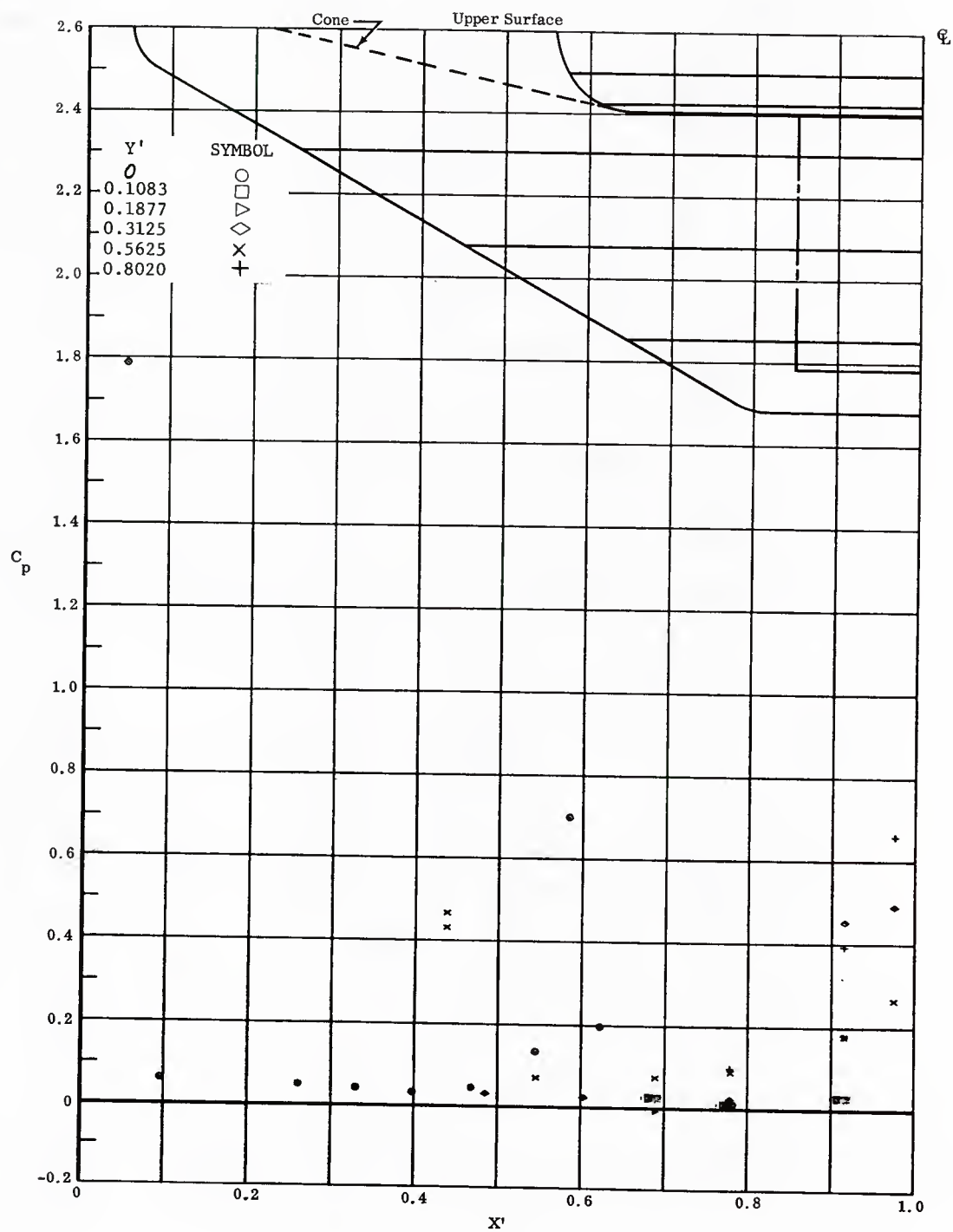


Fig. 18 Streamwise Pressure Distributions on Lower Surface; Left and Right Flaps Deflected  $-30^\circ$ ,  $\alpha = 0^\circ$ .



( NONDIMENSIONAL STREAMWISE DISTANCE FROM VIRTUAL APEX )

Fig. 18 Streamwise Pressure Distributions on Upper Surface; Left and Right Flaps Deflected  $-30^\circ$ ,  $\alpha = 0^\circ$ .

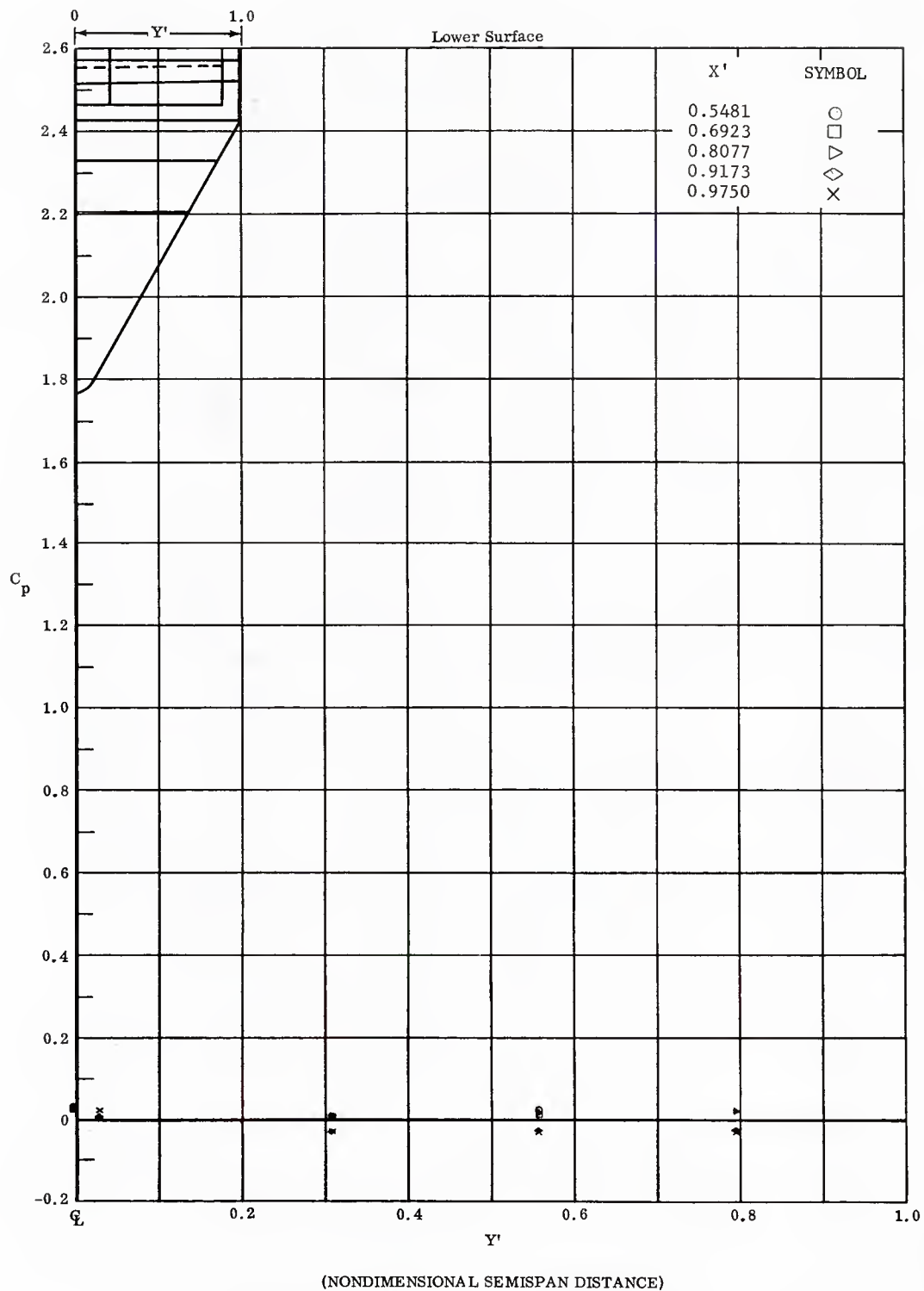


Fig. 18 Spanwise Pressure Distributions on Lower Surface; Left and Right Flaps Deflected  $-30^\circ$ ,  $\alpha = 0^\circ$ .



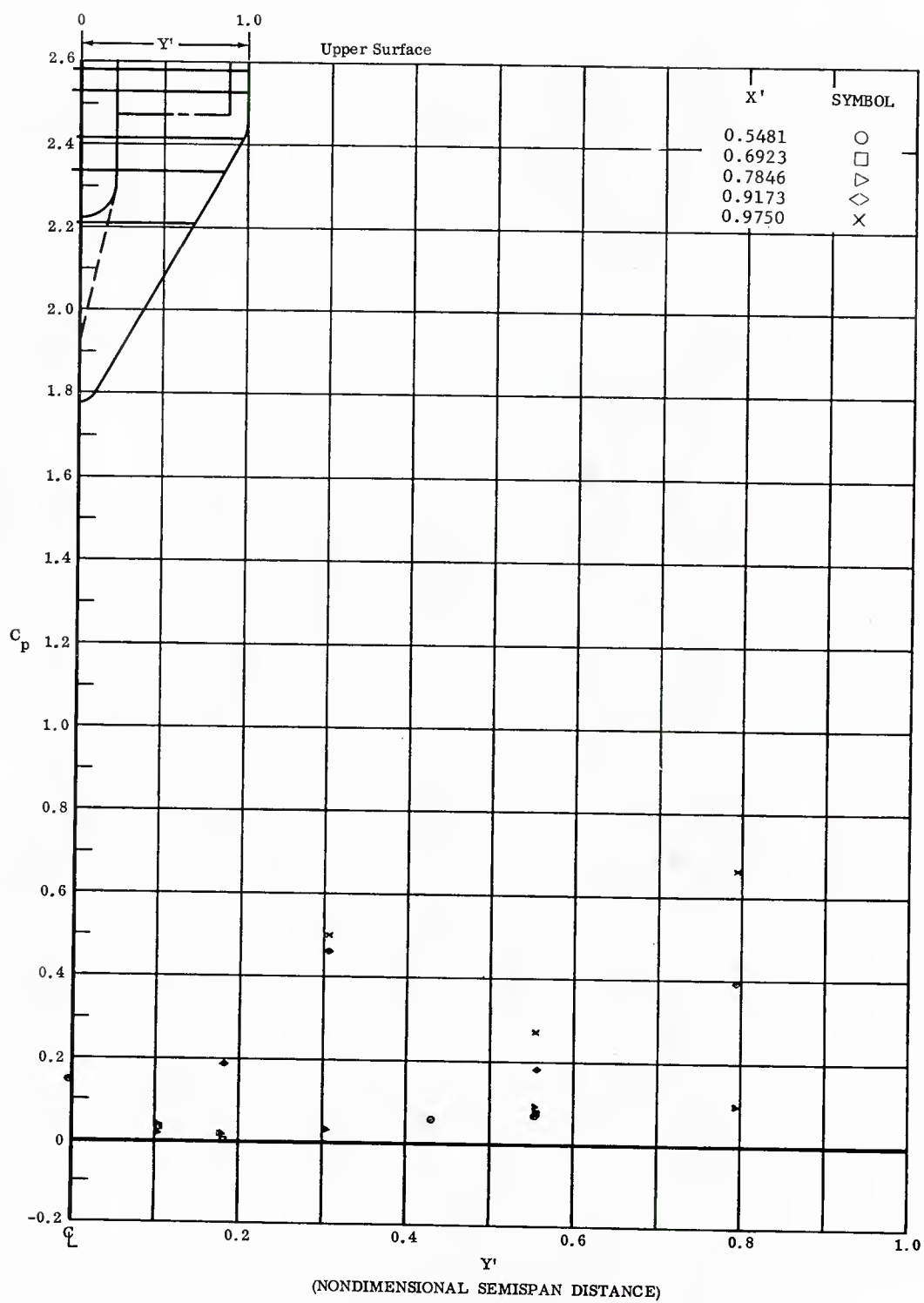


Fig. 18 Spanwise Pressure Distributions on Upper Surface; Left and Right Flaps Deflected  $-30^\circ$ ,  $\alpha = 0^\circ$ .

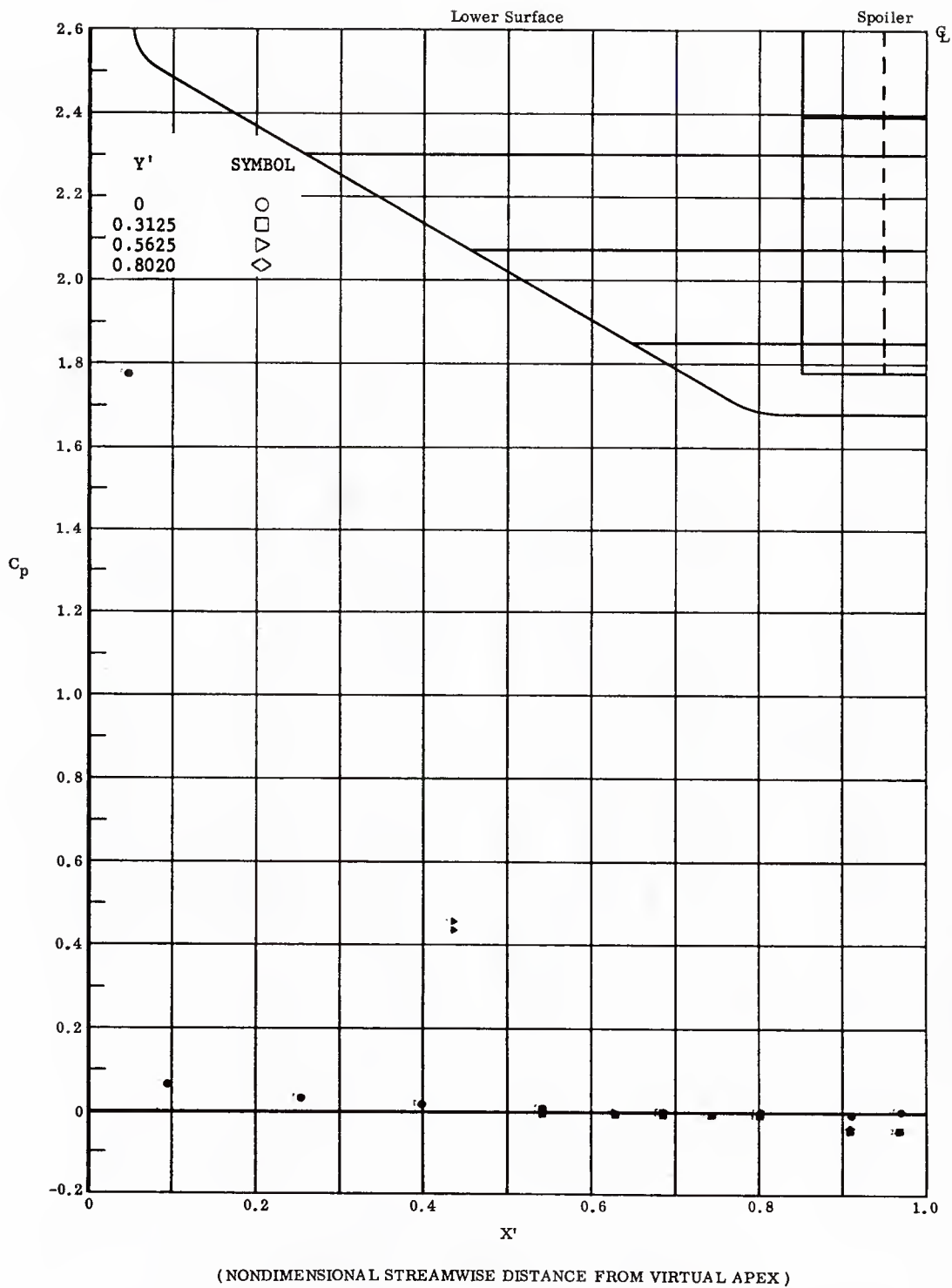
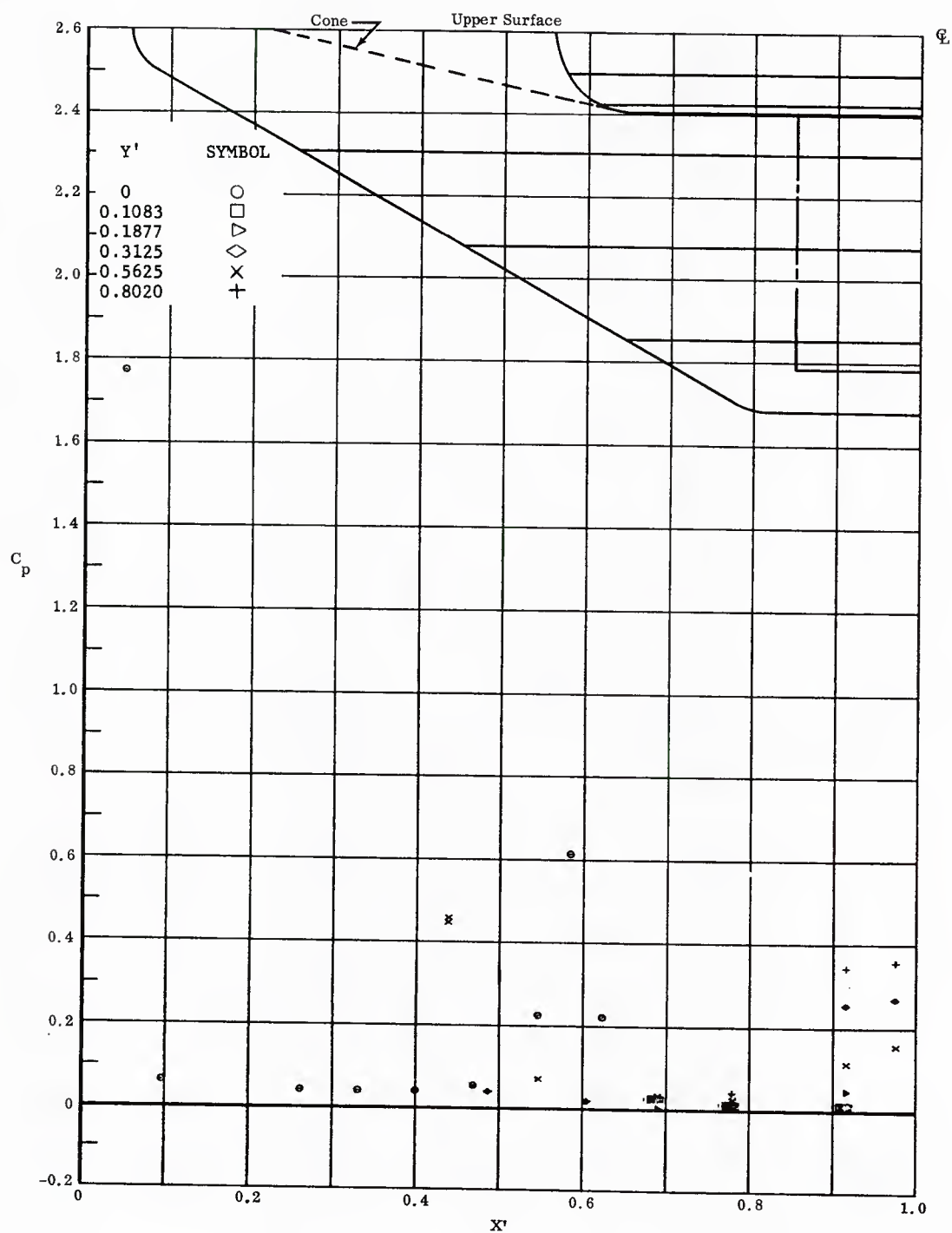


Fig. 19 Streamwise Pressure Distributions on Lower Surface; Left and Right Flaps Deflected  $-20^\circ$ ,  $\alpha = 0^\circ$ .



( NONDIMENSIONAL STREAMWISE DISTANCE FROM VIRTUAL APEX )

Fig. 19 Streamwise Pressure Distributions on Upper Surface; Left and Right Flaps Deflected  $-20^\circ$ ,  $\alpha = 0^\circ$ .

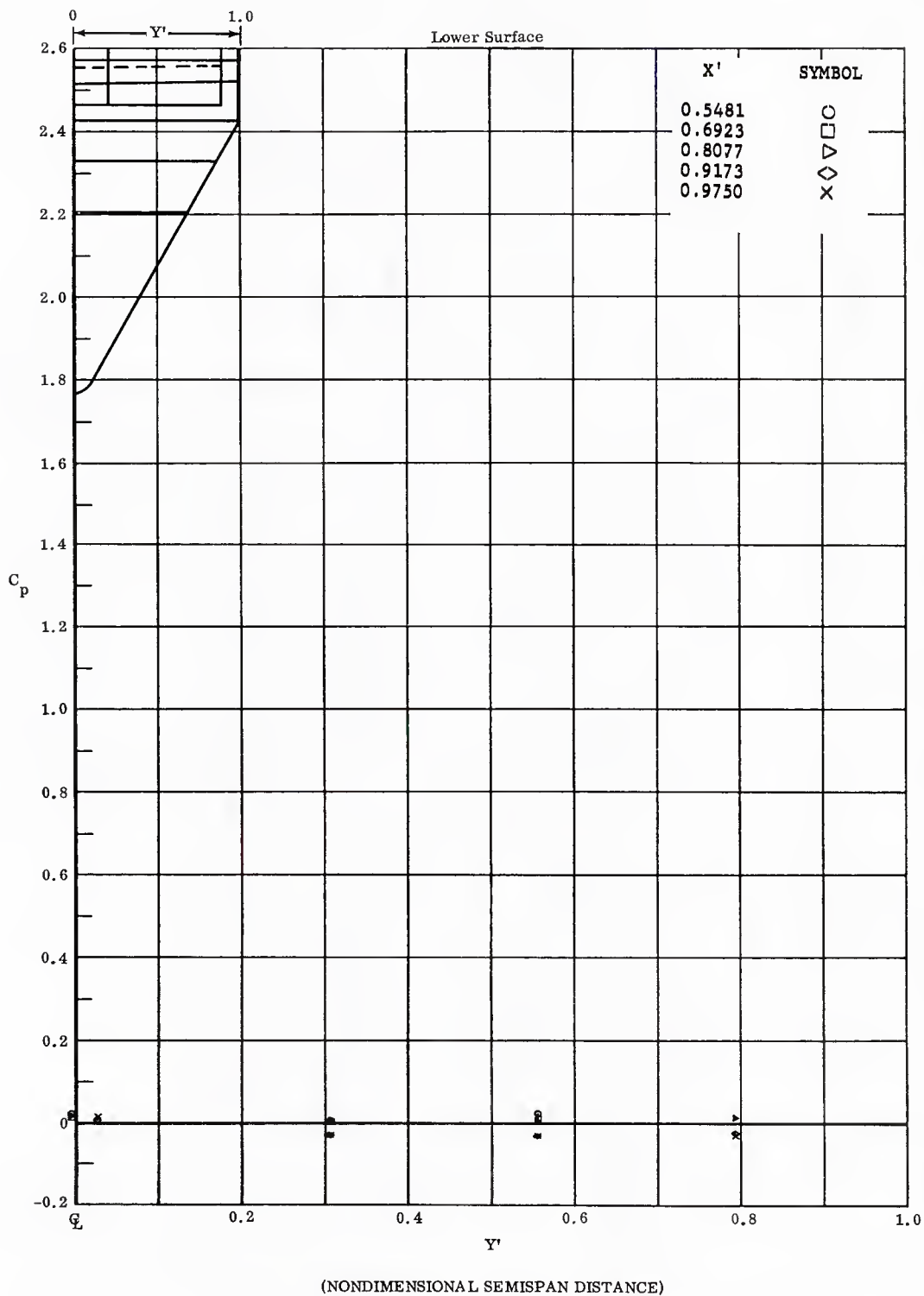


Fig. 19 Spanwise Pressure Distributions on Lower Surface; Left and Right Flaps Deflected  $-20^\circ$ ,  $\alpha = 0^\circ$ .

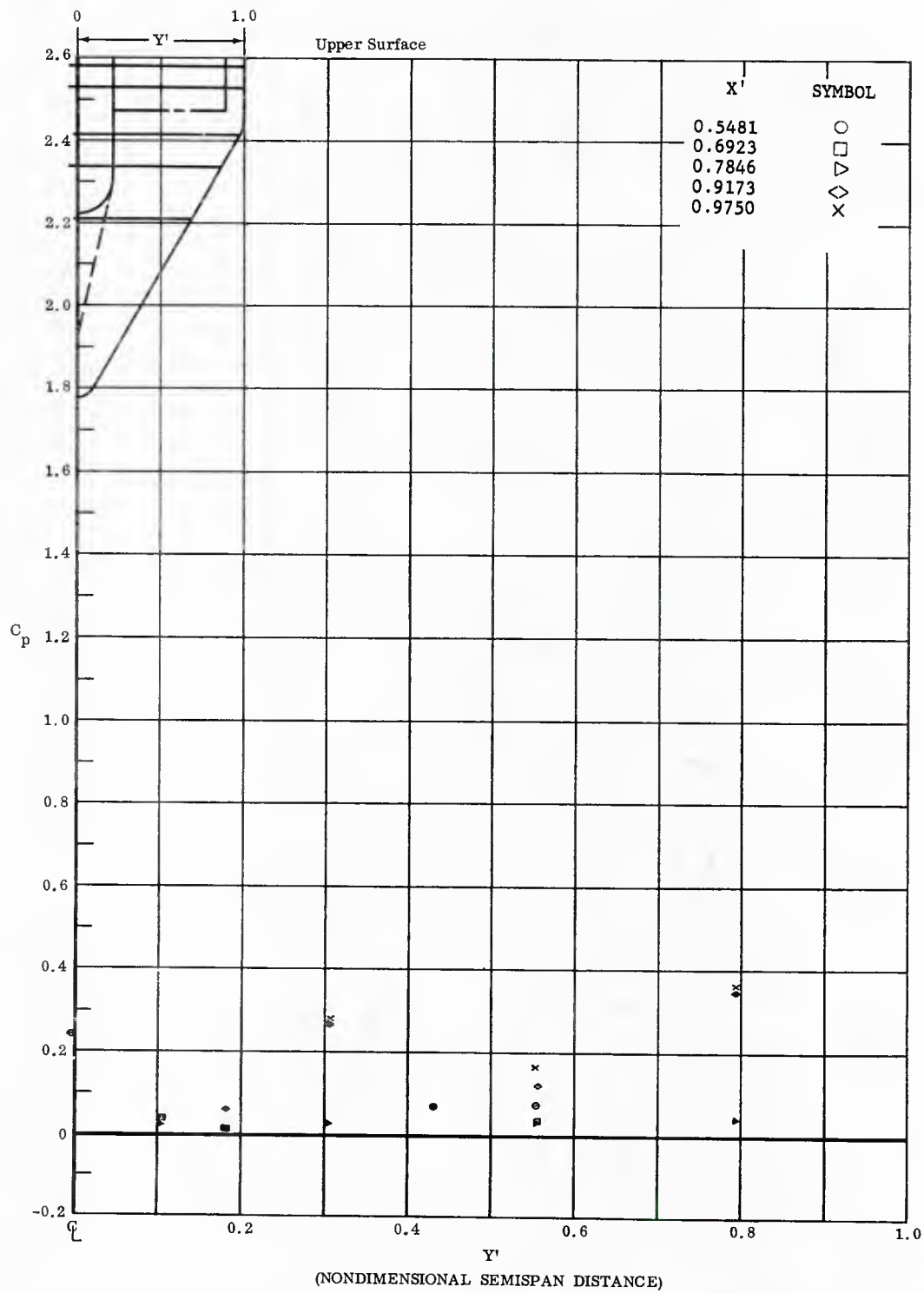


Fig. 19 Spanwise Pressure Distributions on Upper Surface; Left and Right Flaps Deflected  $-20^\circ$ ,  $\alpha = 0^\circ$ .

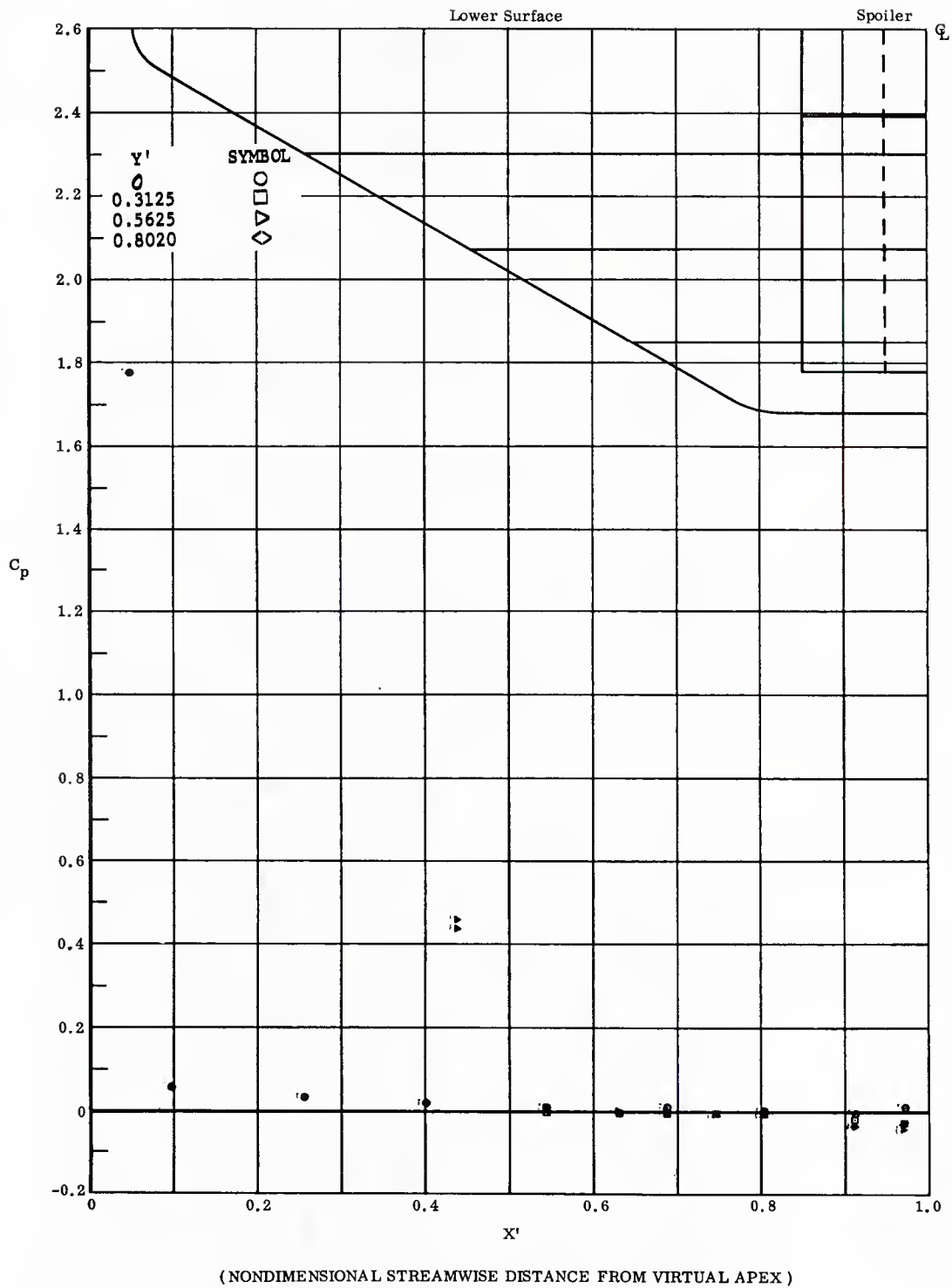
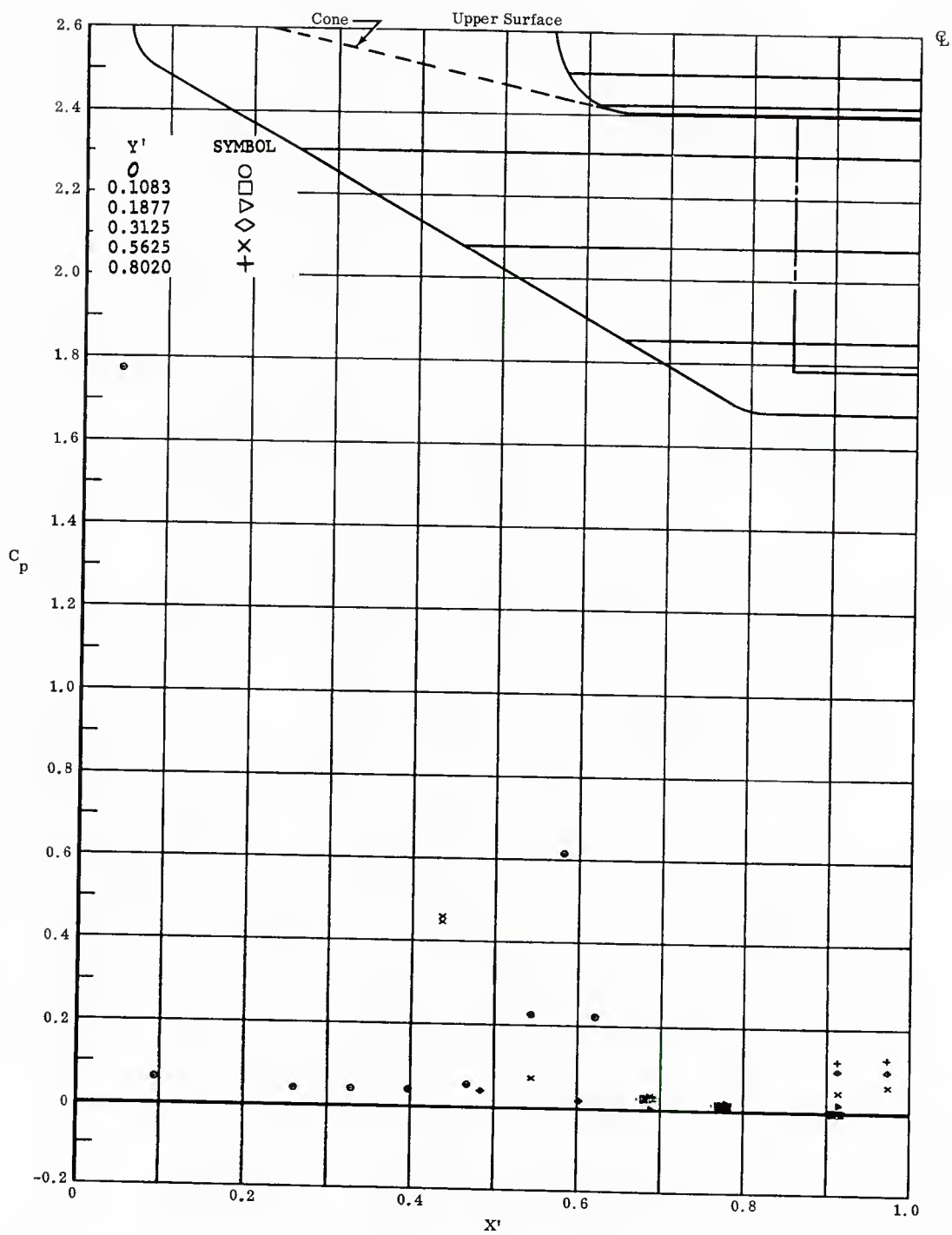


Fig. 20 Streamwise Pressure Distributions on Lower Surface; Left and Right Flaps Deflected  $-10^\circ$ ,  $\alpha = 0^\circ$ .



( NONDIMENSIONAL STREAMWISE DISTANCE FROM VIRTUAL APEX )

Fig. 20 Streamwise Pressure Distributions on Upper Surface; Left and Right Flaps Deflected  $-10^\circ$ ,  $\alpha = 0^\circ$ .

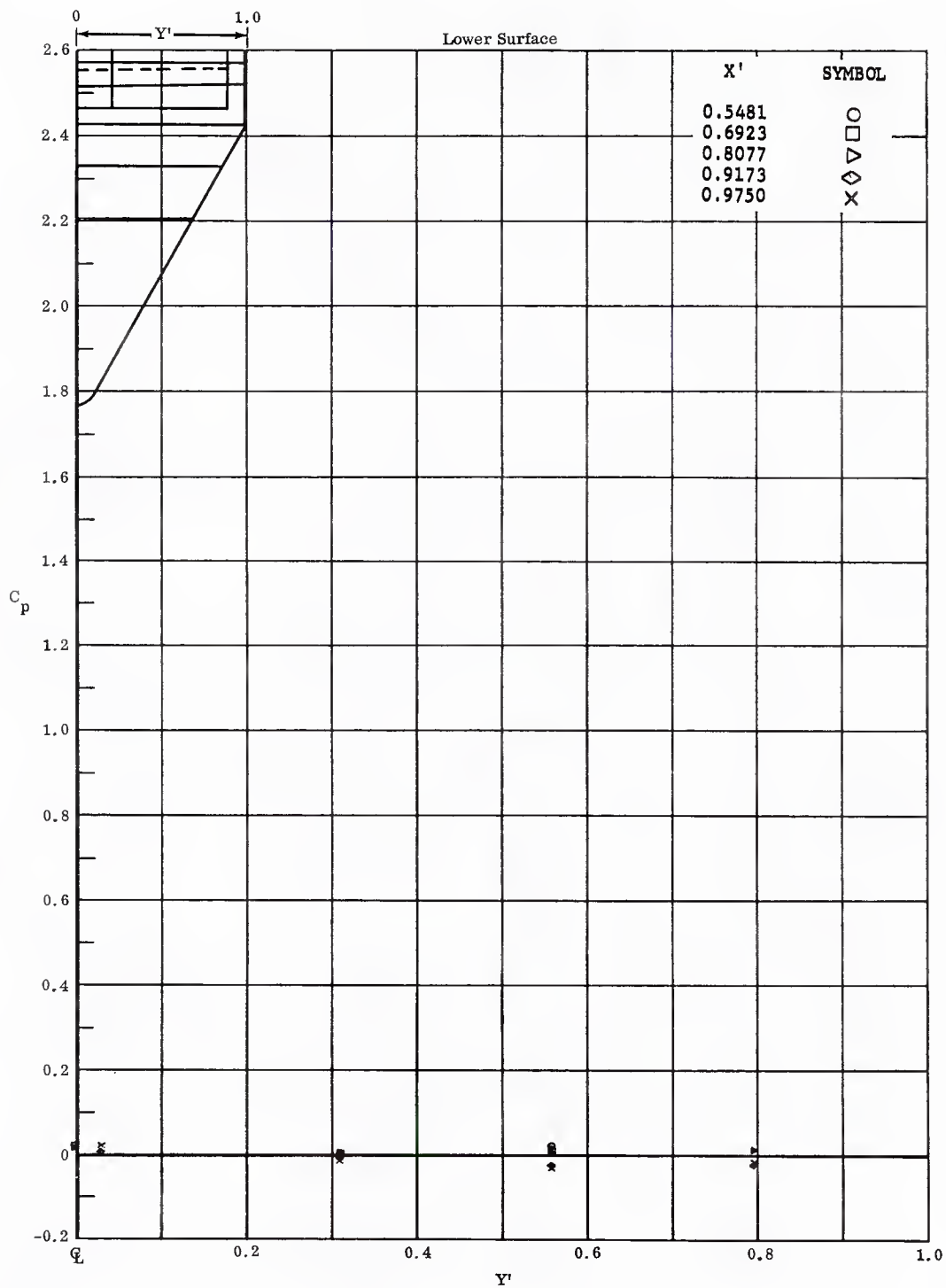


Fig. 20 Spanwise Pressure Distributions on Lower Surface; Left and Right Flaps Deflected  $-10^\circ$ ,  $\alpha = 0^\circ$ .



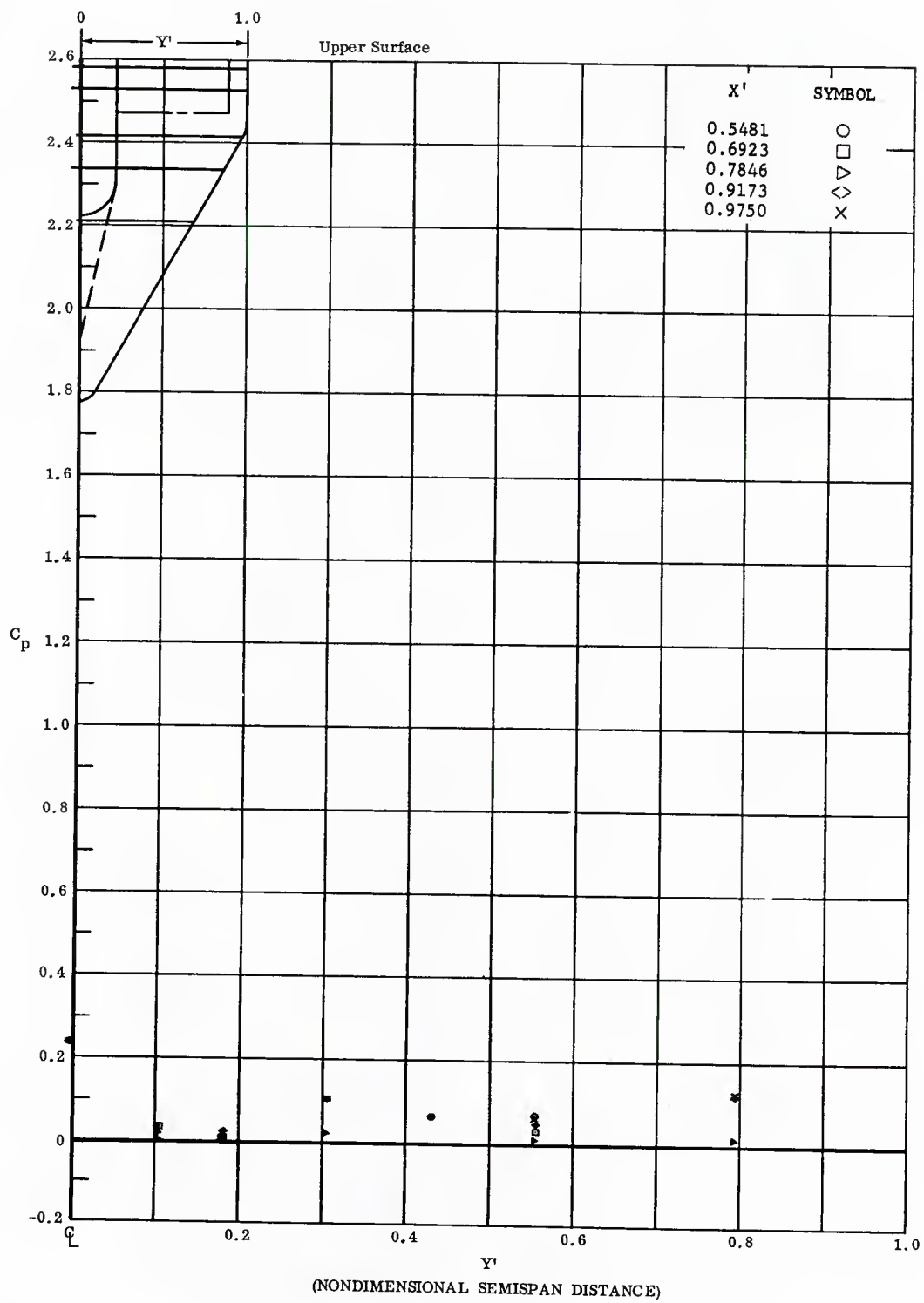


Fig. 20 Spanwise Pressure Distributions on Upper Surface; Left and Right Flaps Deflected  $-10^\circ$ ,  $\alpha = 0^\circ$ .

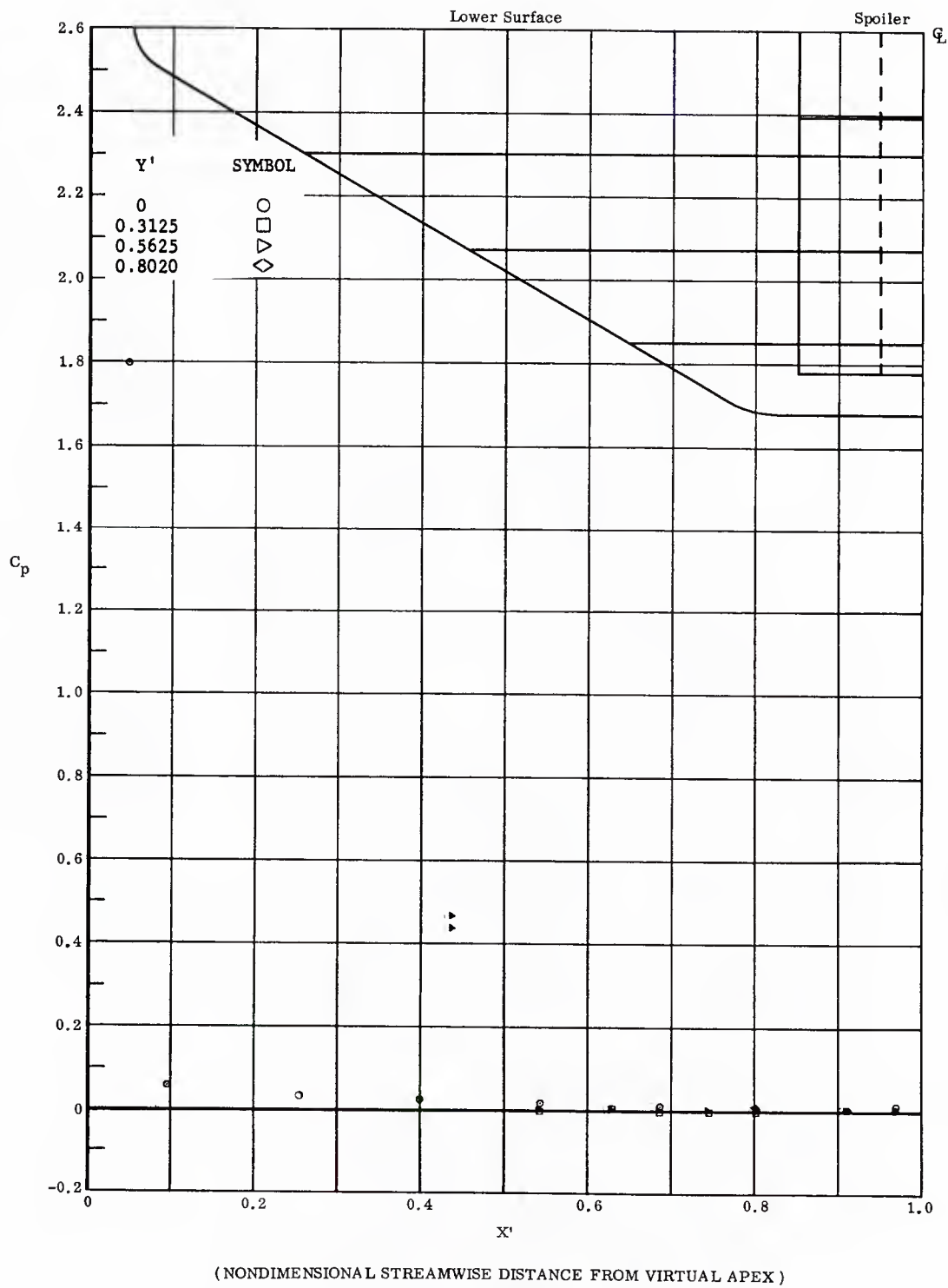


Fig. 21 Streamwise Pressure Distributions on Lower Surface; No Flap Deflections,  
 $\alpha = 0^\circ$ .

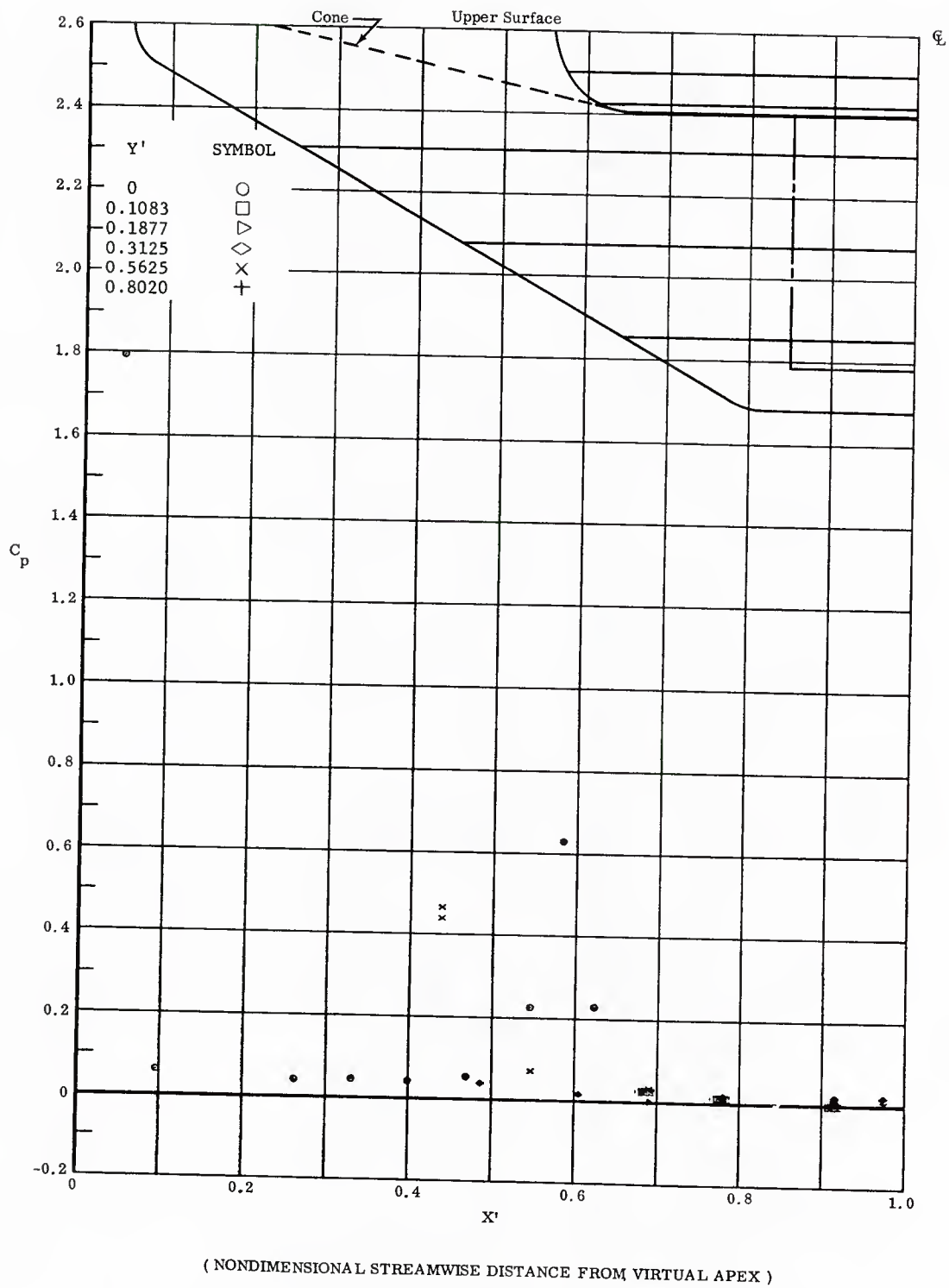


Fig. 21 Streamwise Pressure Distributions on Upper Surface; No Flap Deflections,  $\alpha = 0^\circ$ .

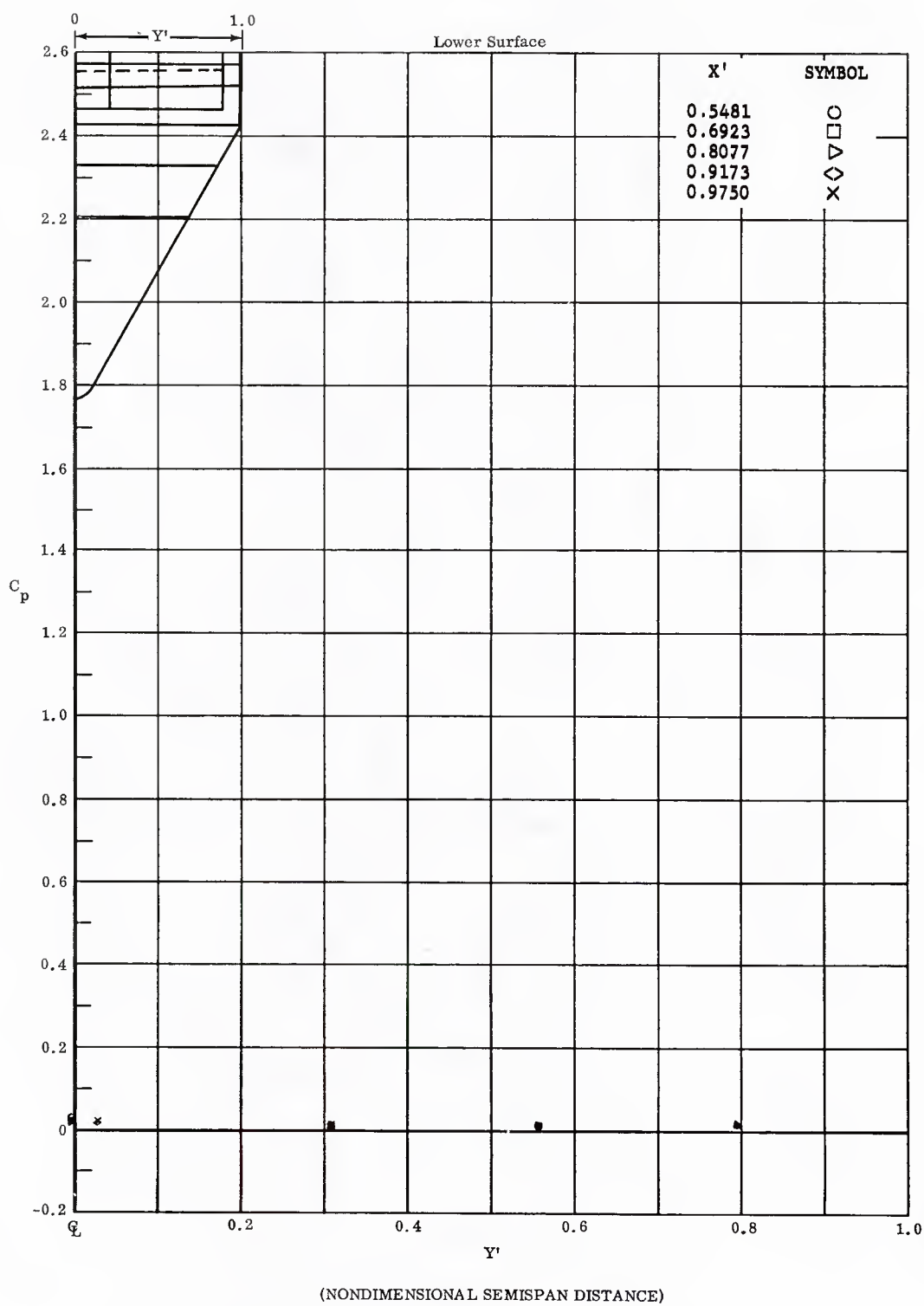


Fig. 21 Spanwise Pressure Distributions on Lower Surface; No Flap Deflections,  $\alpha = 0^\circ$ .

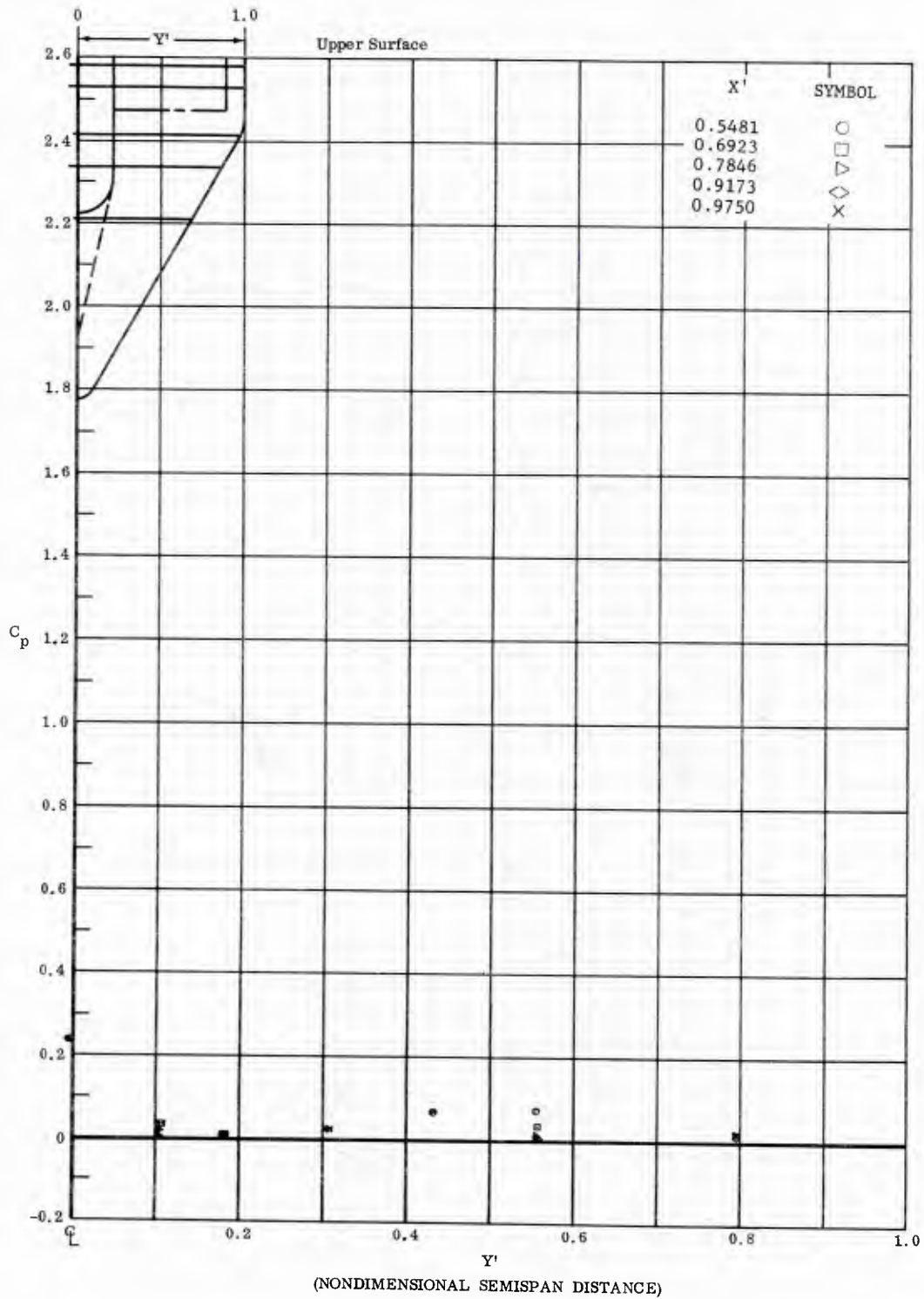


Fig. 21 Spanwise Pressure Distributions on Upper Surface; No Flap Deflections,  $\alpha = 0^\circ$ .

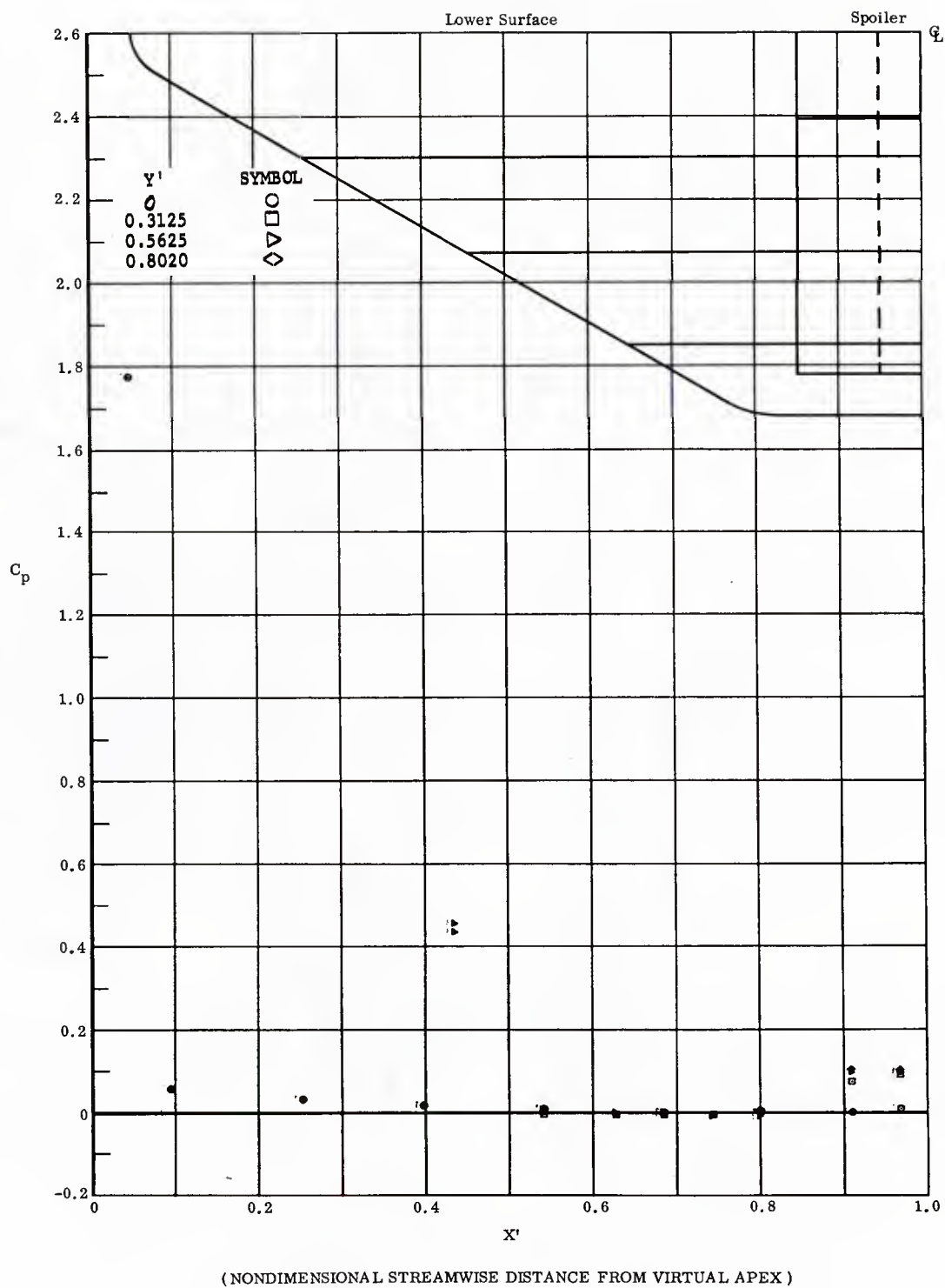


Fig. 22 Streamwise Pressure Distributions on Lower Surface; Left and Right Flaps Deflected  $+10^\circ$ ,  $\alpha = 0^\circ$ .

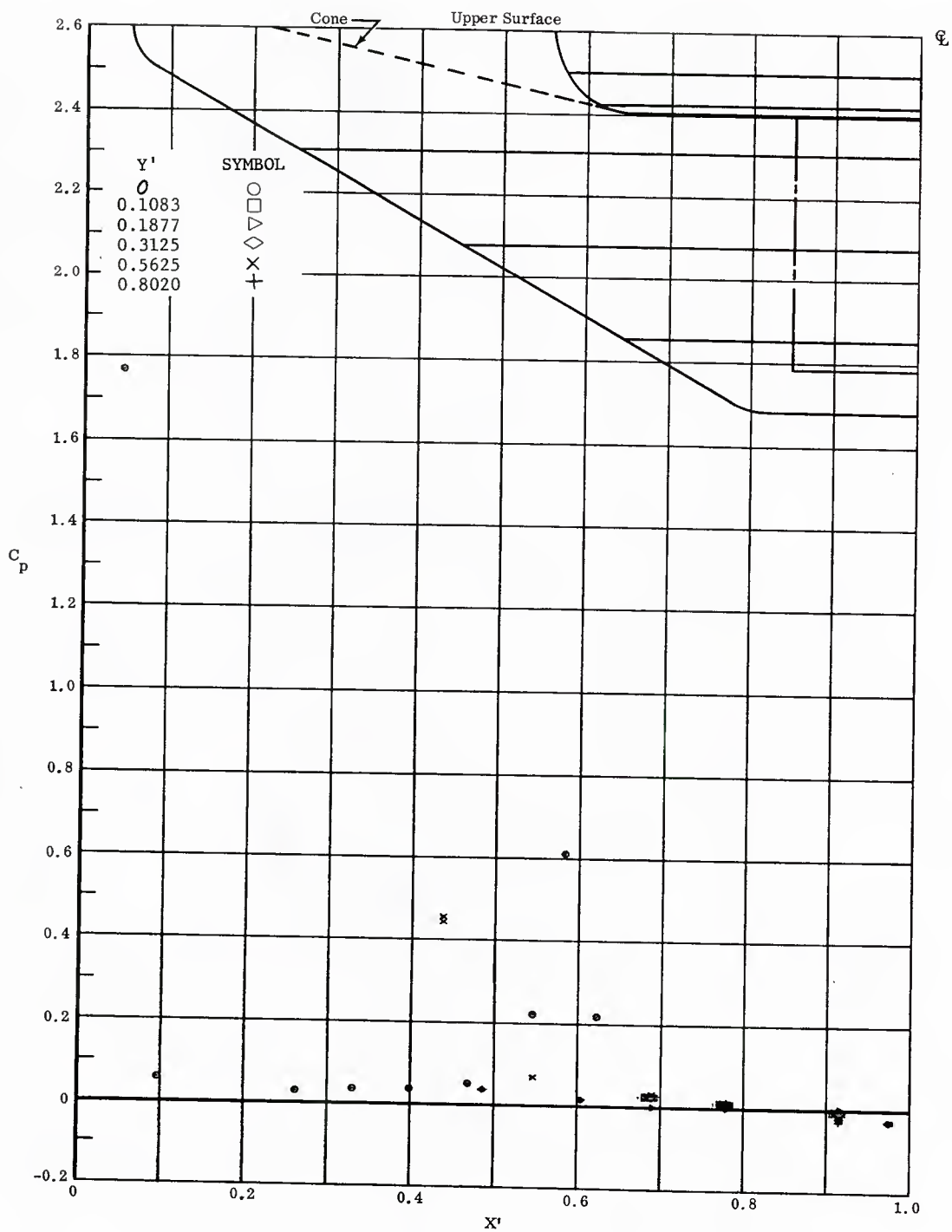


Fig. 22 Streamwise Pressure Distributions on Upper Surface; Left and Right Flaps Deflected  $+10^\circ$ ,  $\alpha = 0^\circ$ .

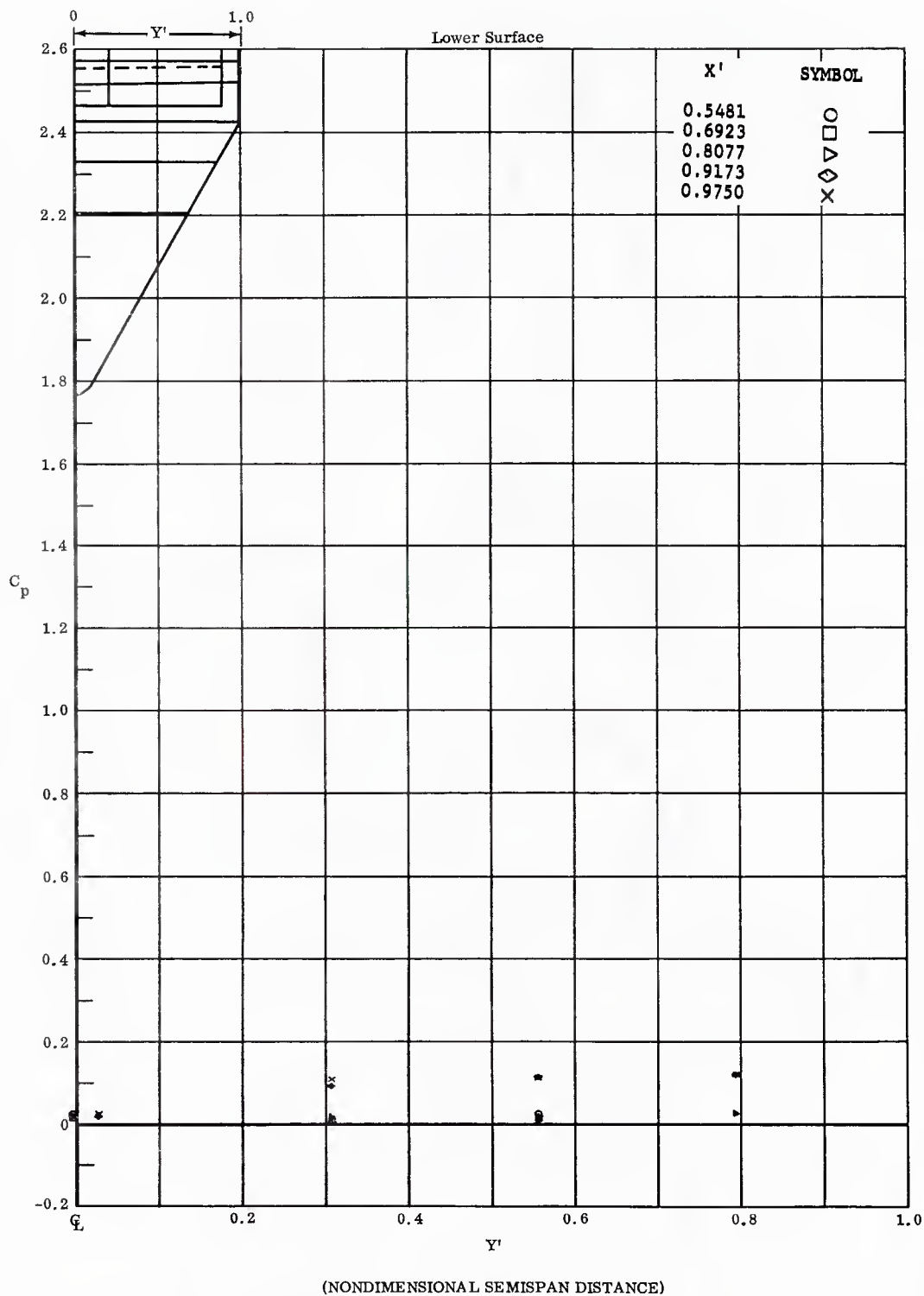


Fig. 22 Spanwise Pressure Distributions on Lower Surface; Left and Right Flaps Deflected  $+10^\circ$ ,  $\alpha = 0^\circ$ .



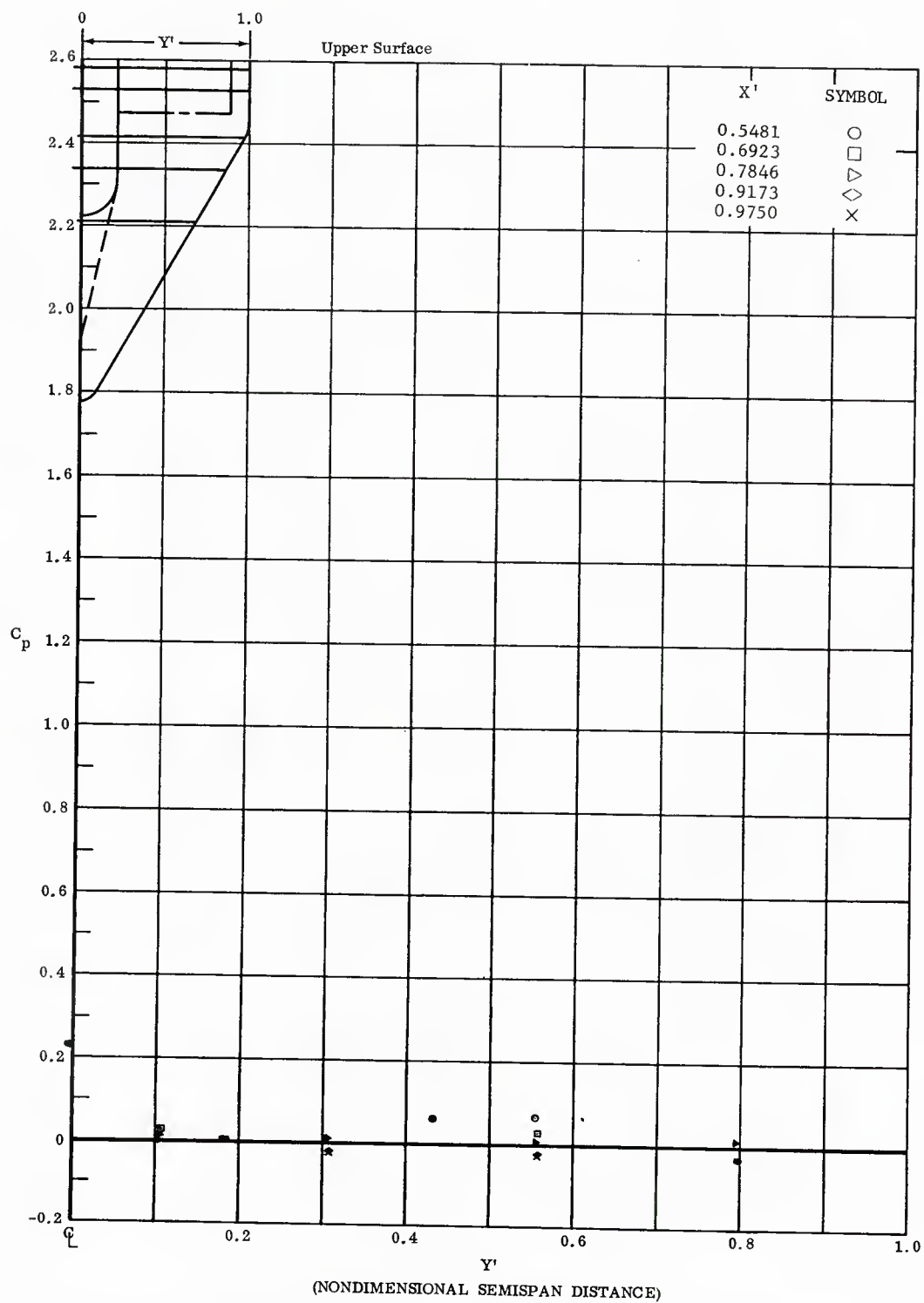


Fig. 22 Spanwise Pressure Distributions on Upper Surface; Left and Right Flaps Deflected  $+10^\circ$ ,  $\alpha = 0^\circ$ .

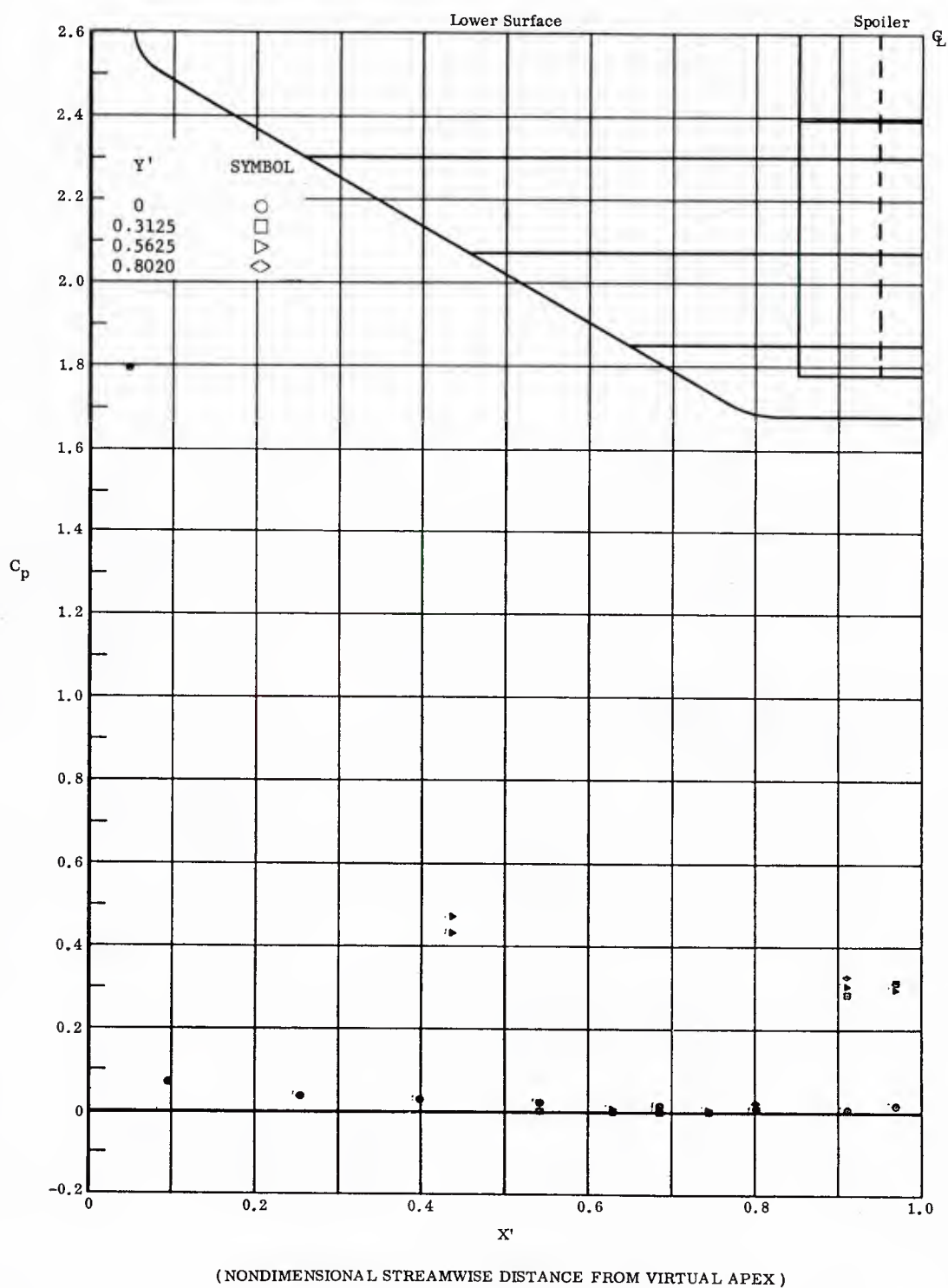
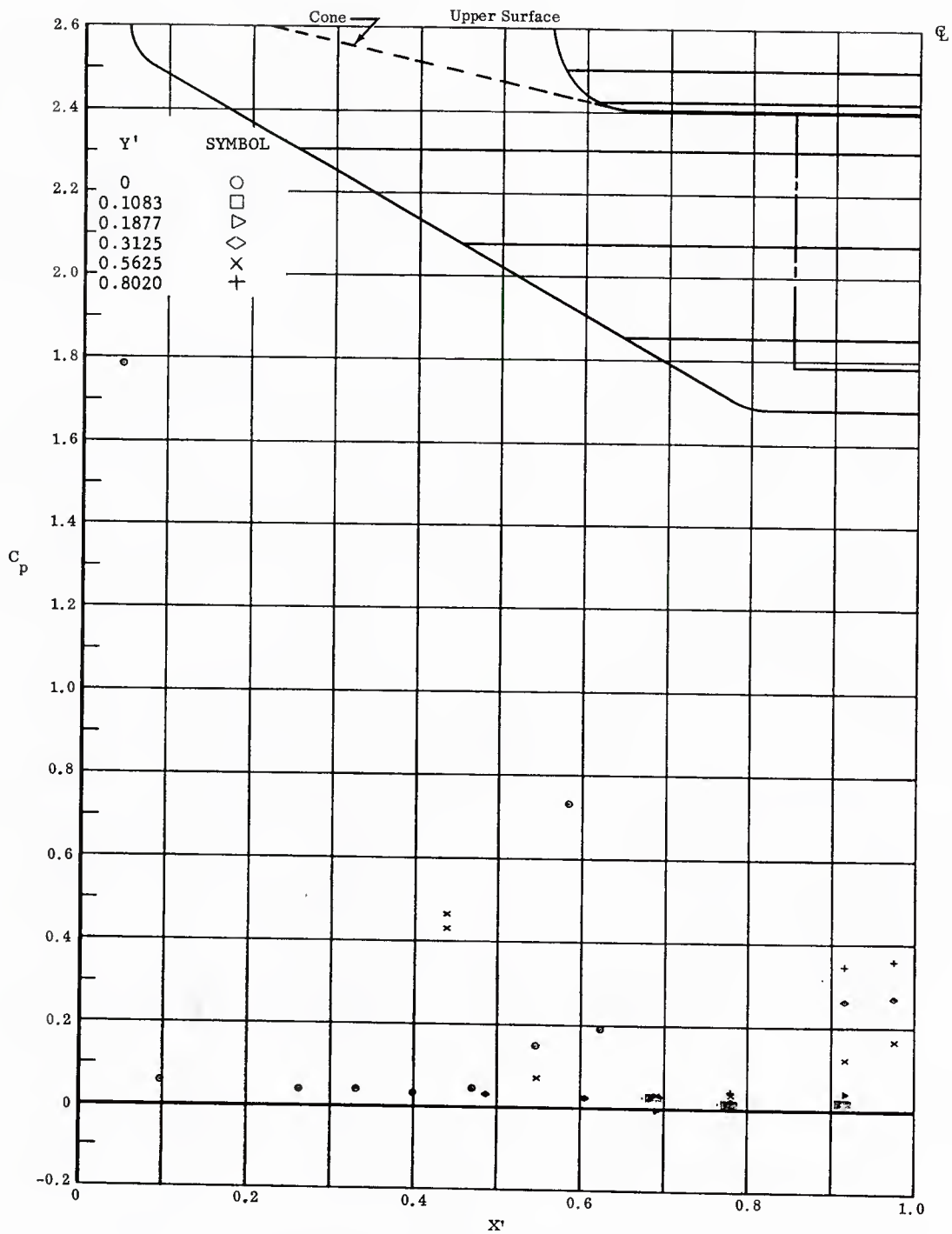


Fig. 23 Streamwise Pressure Distributions on Lower Surface; Left Flap Deflected  $+20^\circ$ , Right Flap Deflected  $-20^\circ$ ,  $\alpha = 0^\circ$ .



( NONDIMENSIONAL STREAMWISE DISTANCE FROM VIRTUAL APEX )

Fig. 23 Streamwise Pressure Distributions on Upper Surface; Left Flap Deflected  $+20^\circ$ , Right Flap Deflected  $-20^\circ$ ,  $\alpha = 0^\circ$ .

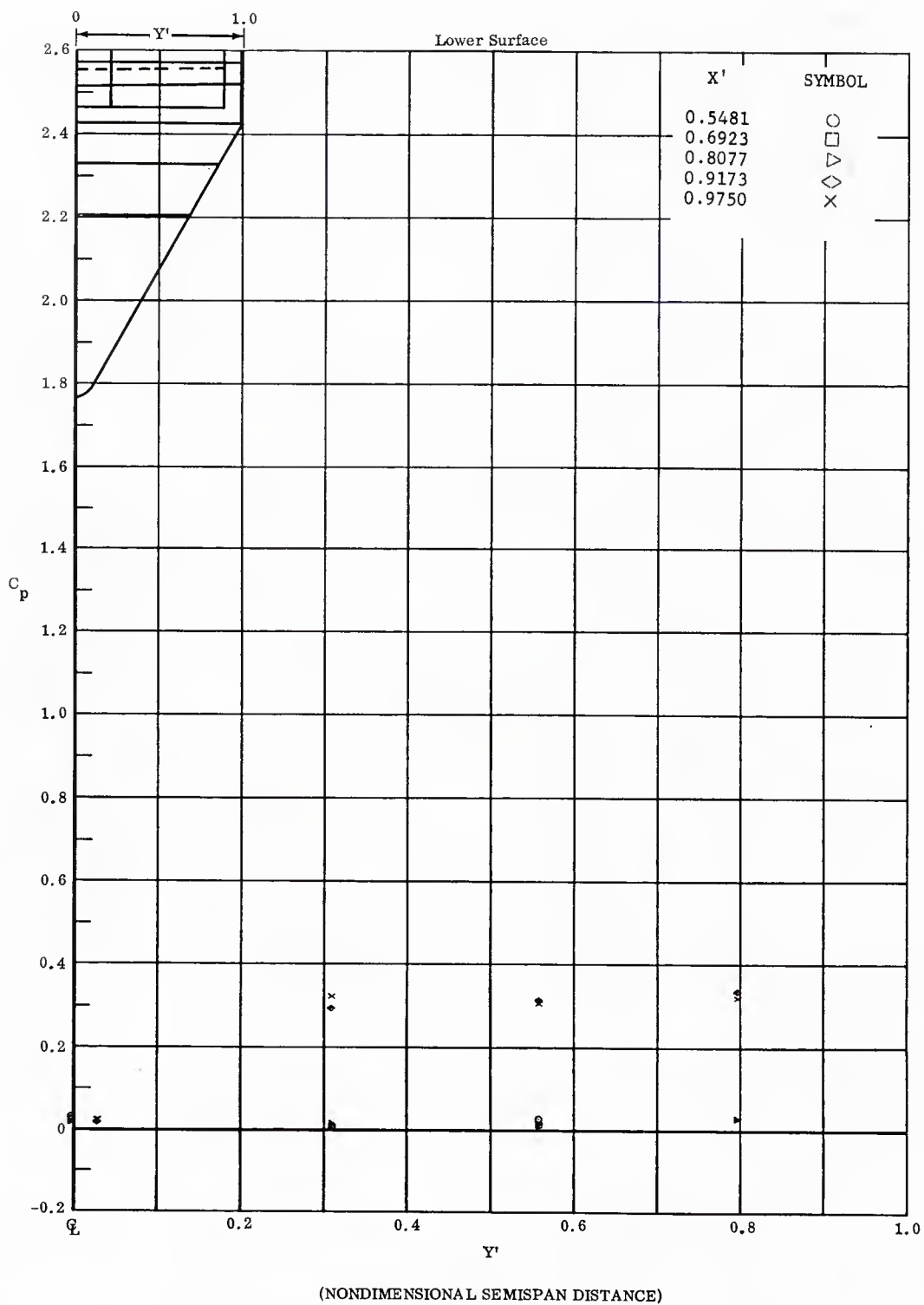


Fig. 23 Spanwise Pressure Distributions on Lower Surface; Left Flap Deflected  $+20^\circ$ , Right Flap Deflected  $-20^\circ$ ,  $\alpha = 0^\circ$ .

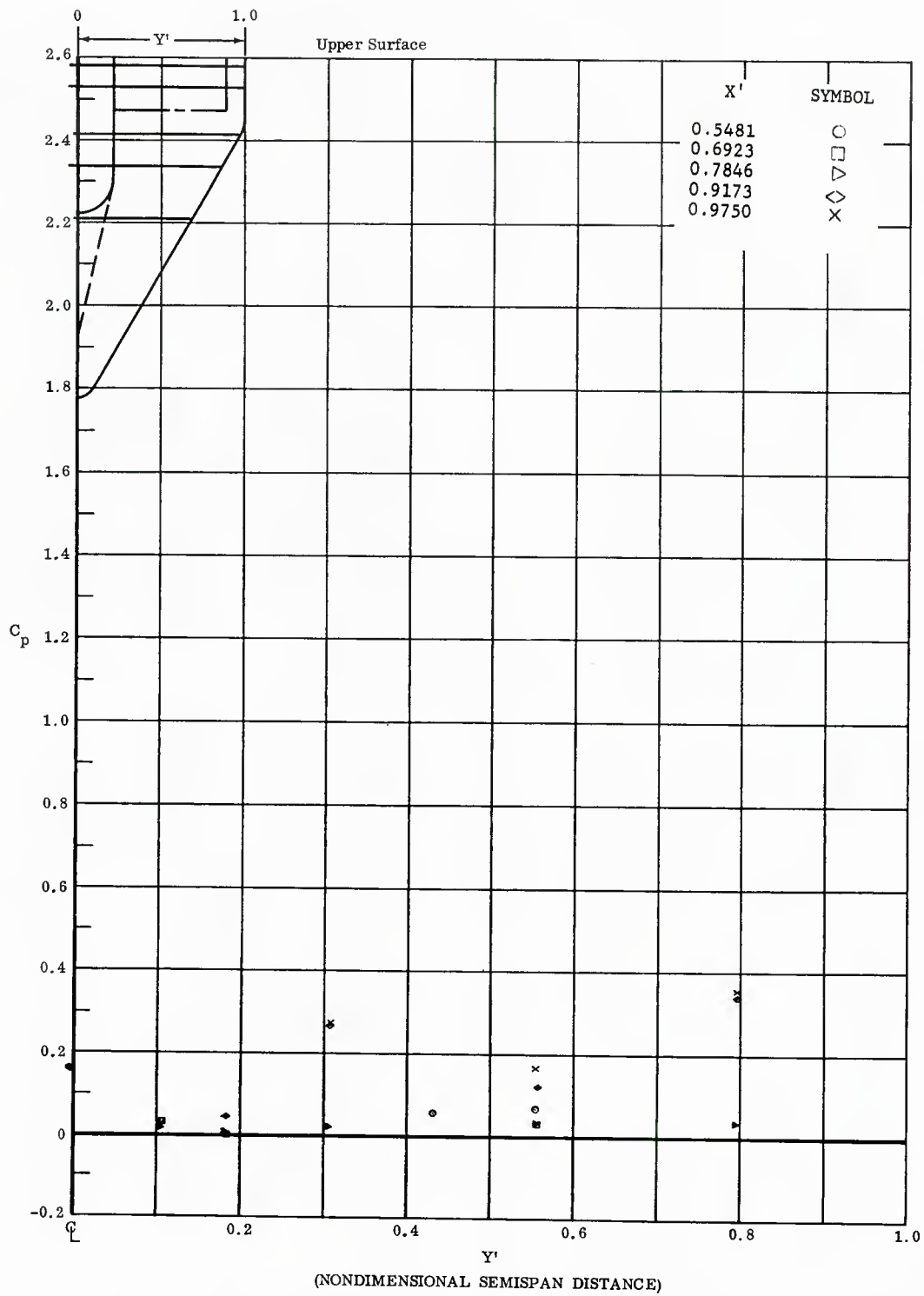


Fig. 23 Spanwise Pressure Distributions on Upper Surface; Left Flap Deflected  $+20^\circ$ , Right Flap Deflected  $-20^\circ$ ,  $\alpha = 0^\circ$ .

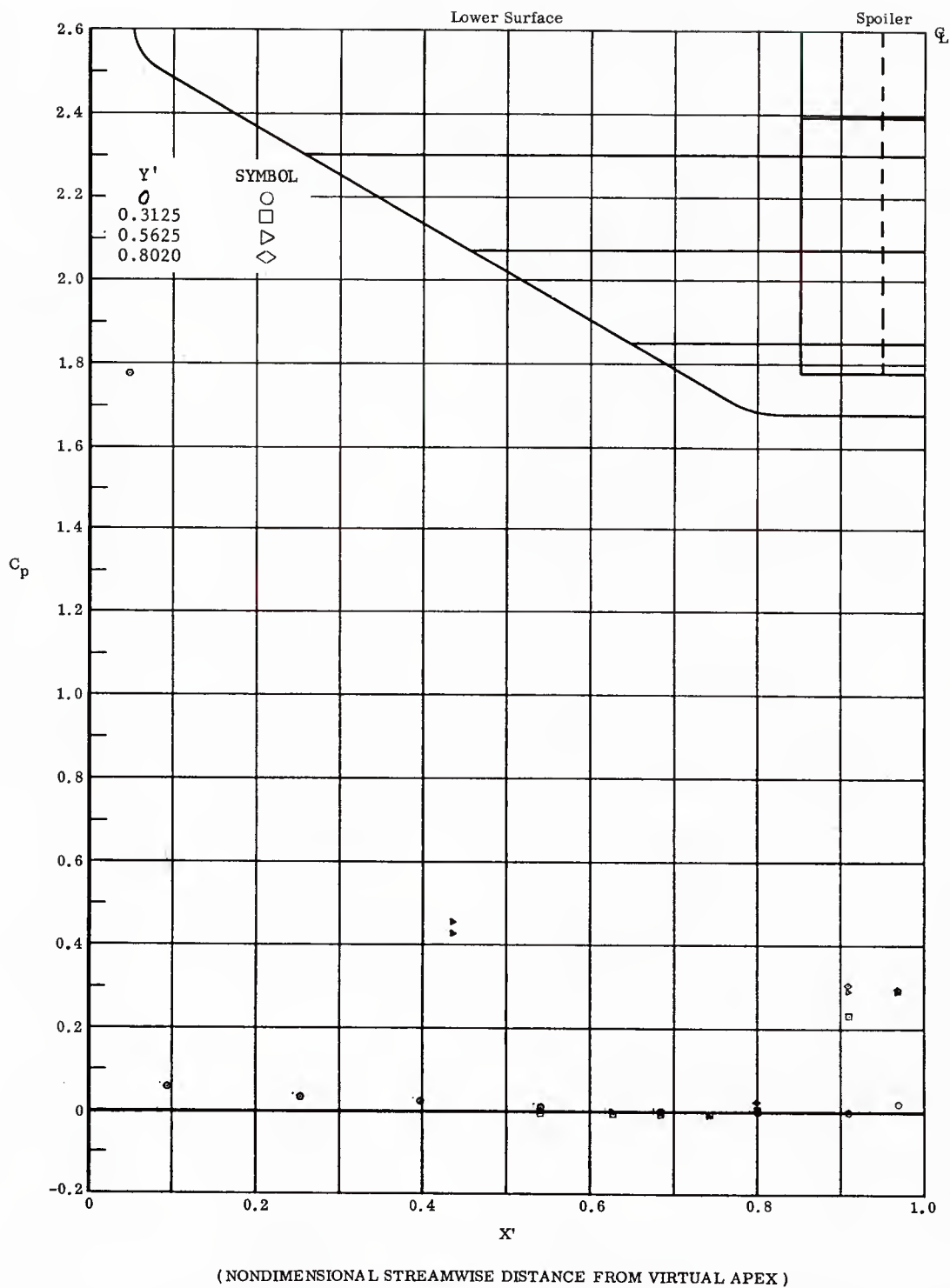


Fig. 24 Streamwise Pressure Distributions on Lower Surface; Left and Right Flaps Deflected  $+20^\circ$ ,  $\alpha = 0^\circ$ .

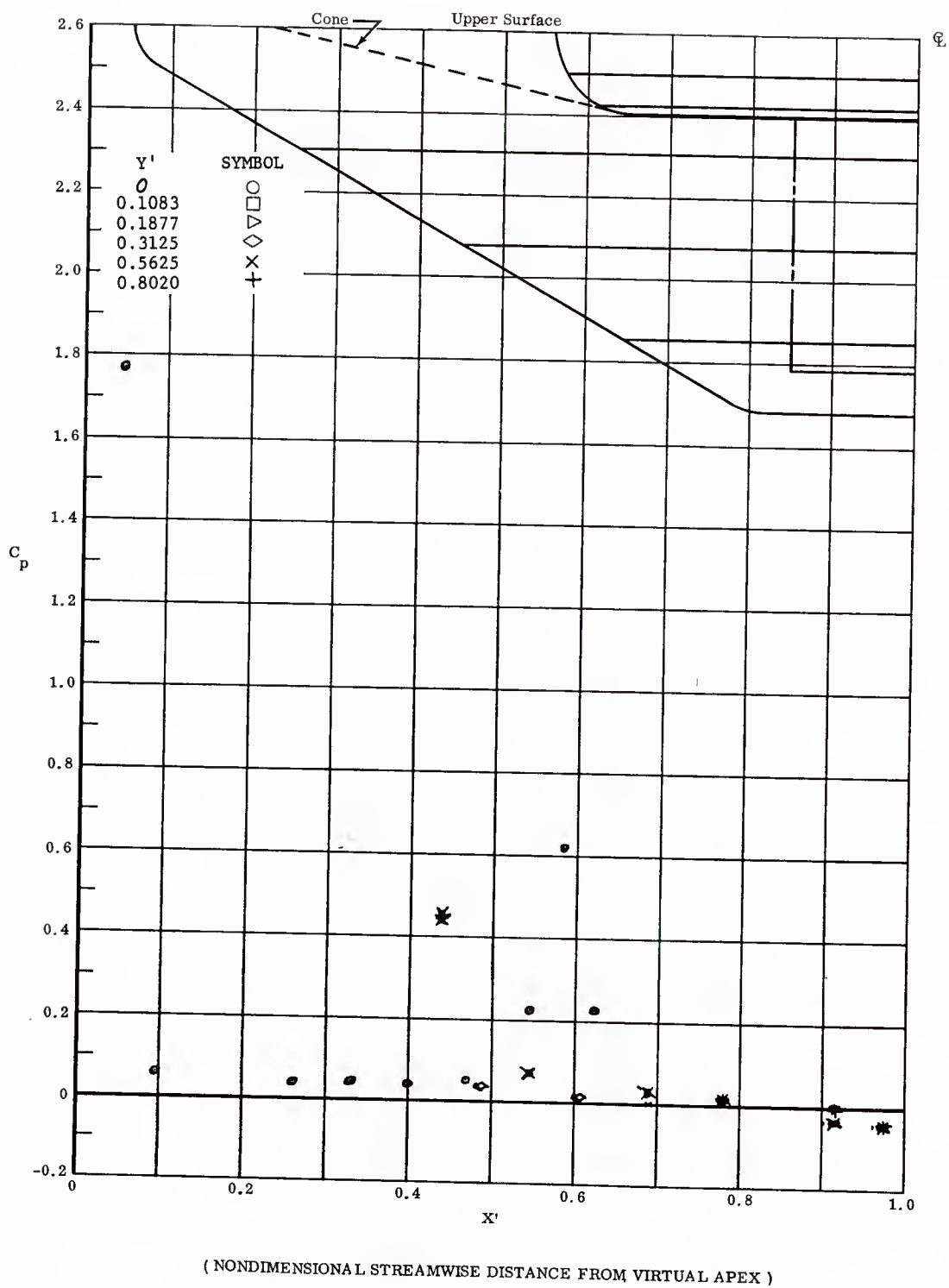


Fig. 24 Streamwise Pressure Distributions on Upper Surface; Left and Right Flaps Deflected  $+20^\circ$ ,  $\alpha = 0^\circ$ .

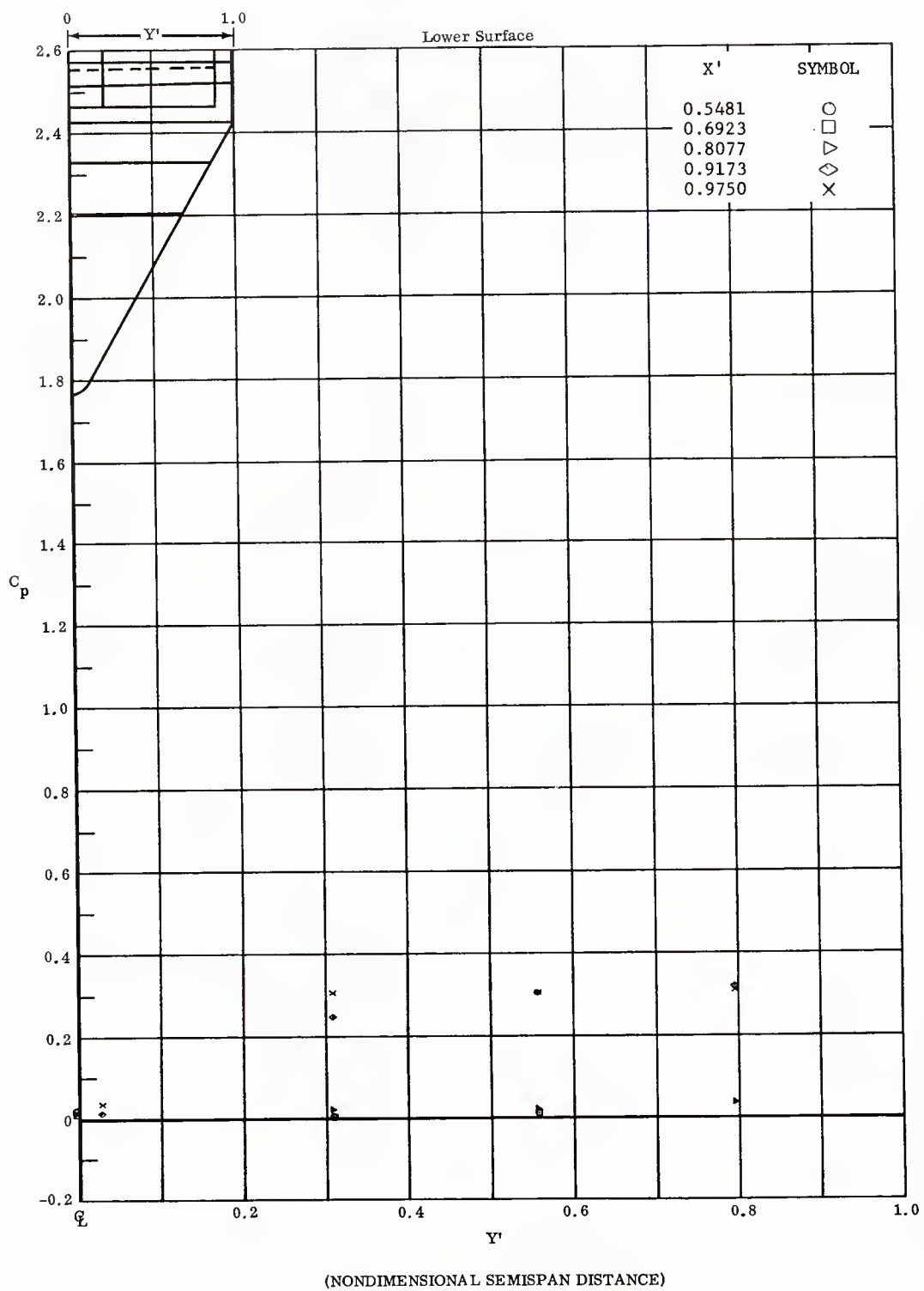


Fig. 24 Spanwise Pressure Distributions on Lower Surface; Left and Right Flaps Deflected  $+20^\circ$ ,  $\alpha = 0^\circ$ .



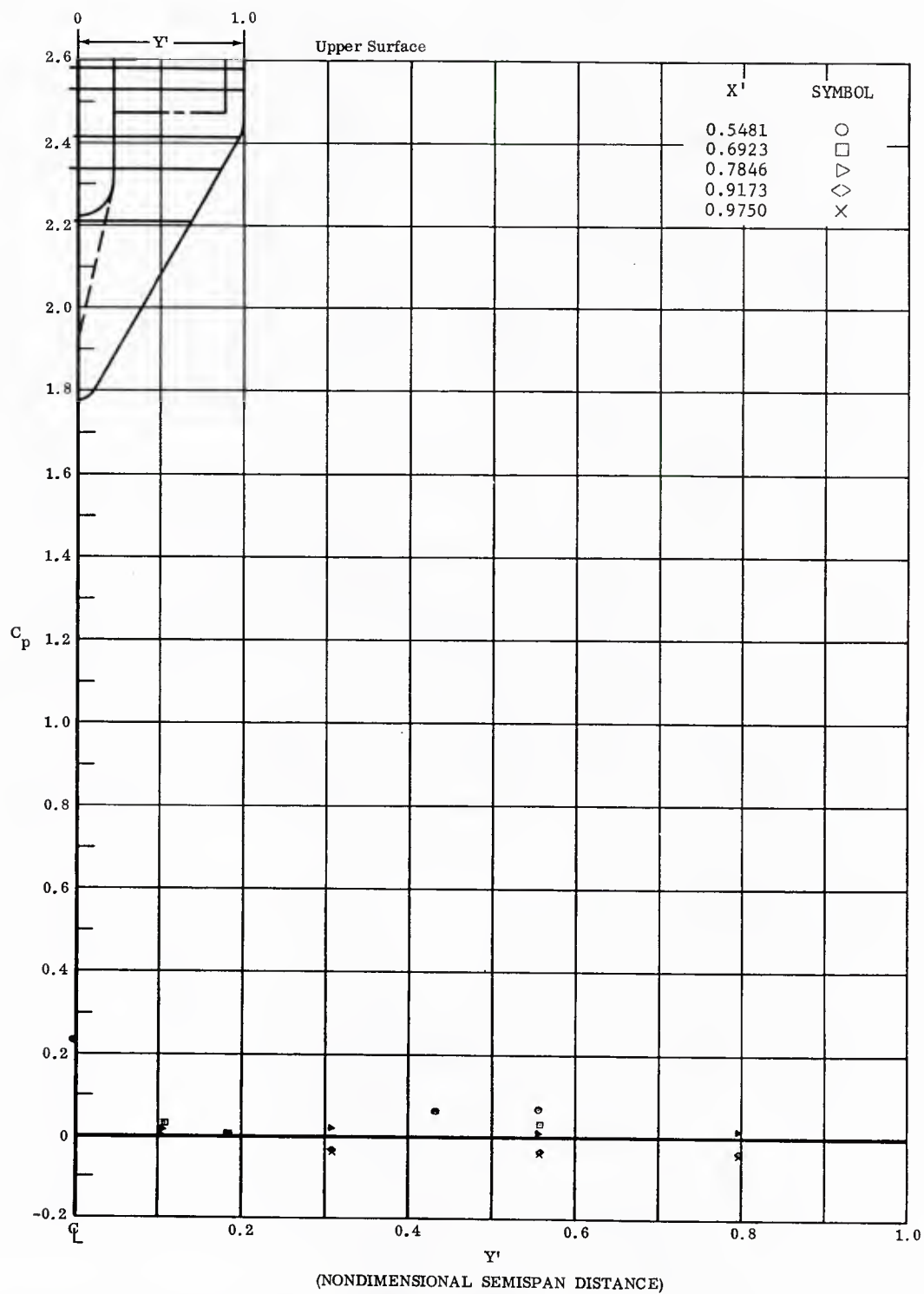


Fig. 24 Spanwise Pressure Distributions on *Upper Surface*; Left and Right Flaps Deflected  $+20^\circ$ ,  $\alpha = 0^\circ$ .

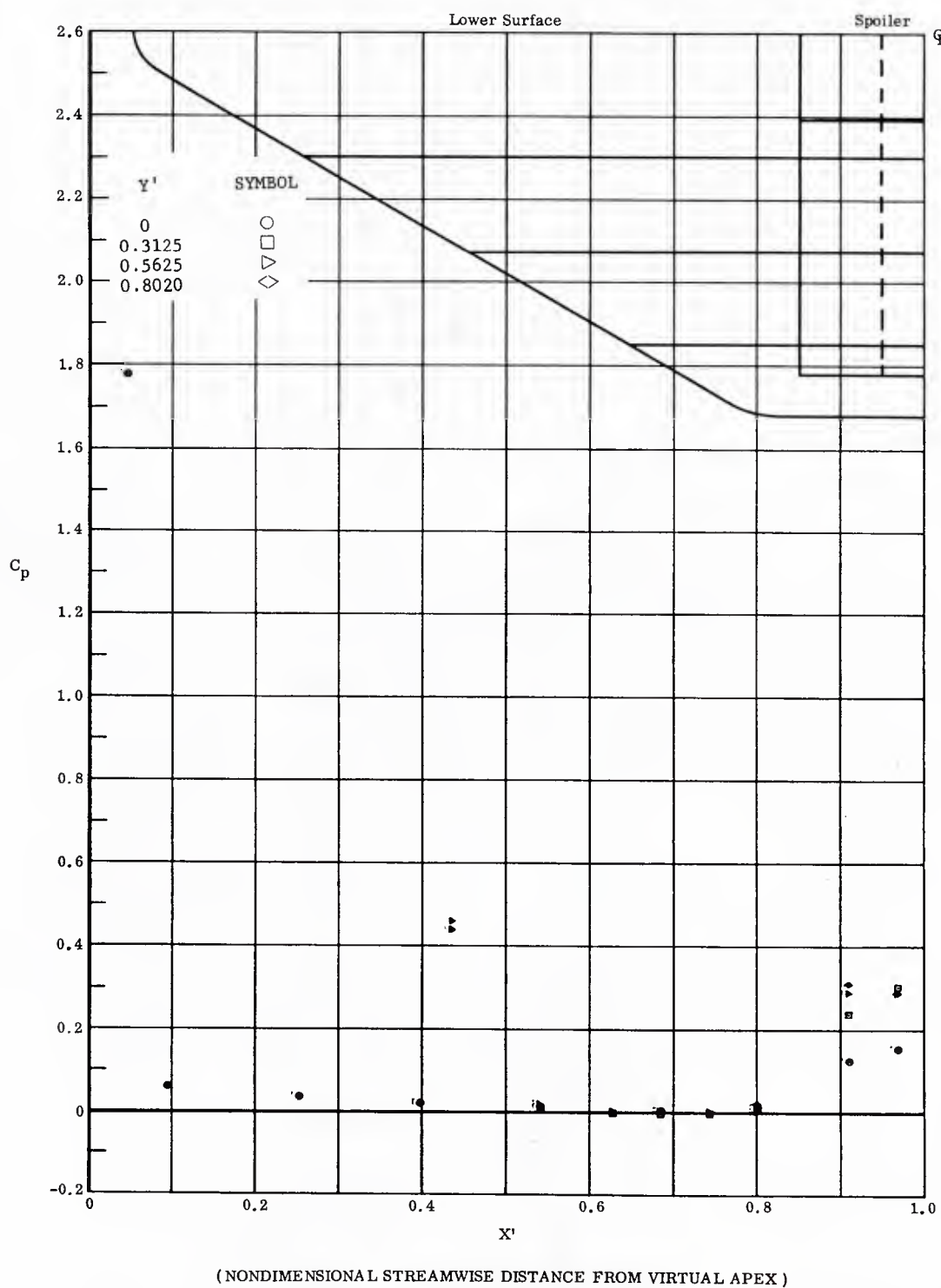


Fig. 25 Streamwise Pressure Distributions on Lower Surface; Center, Left and Right Flaps Deflected  $+20^\circ$ ,  $\alpha = 0^\circ$ .

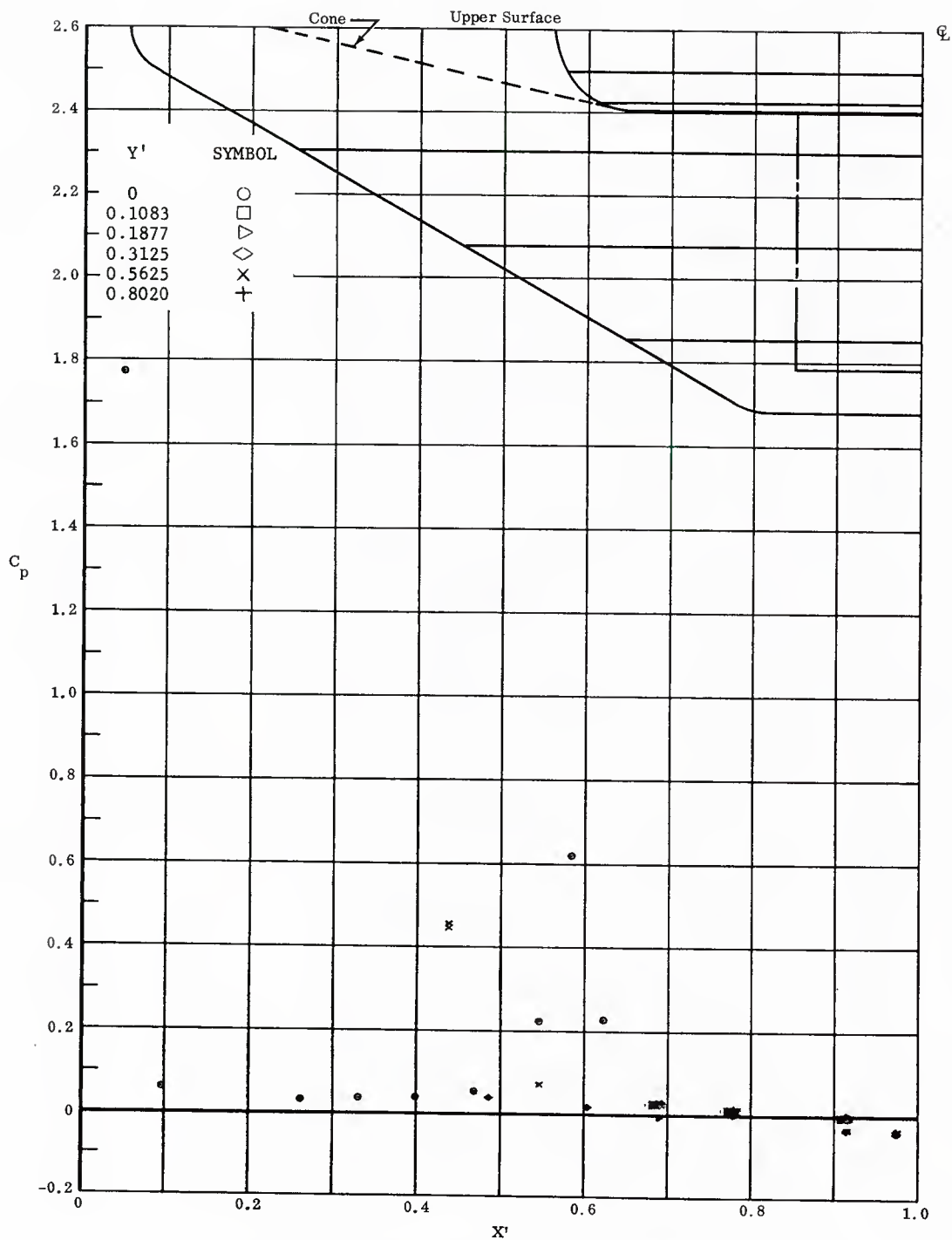


Fig. 25 Streamwise Pressure Distributions on Upper Surface; Center, Left and Right Flaps Deflected  $+20^\circ$ ,  $\alpha = 0^\circ$ .

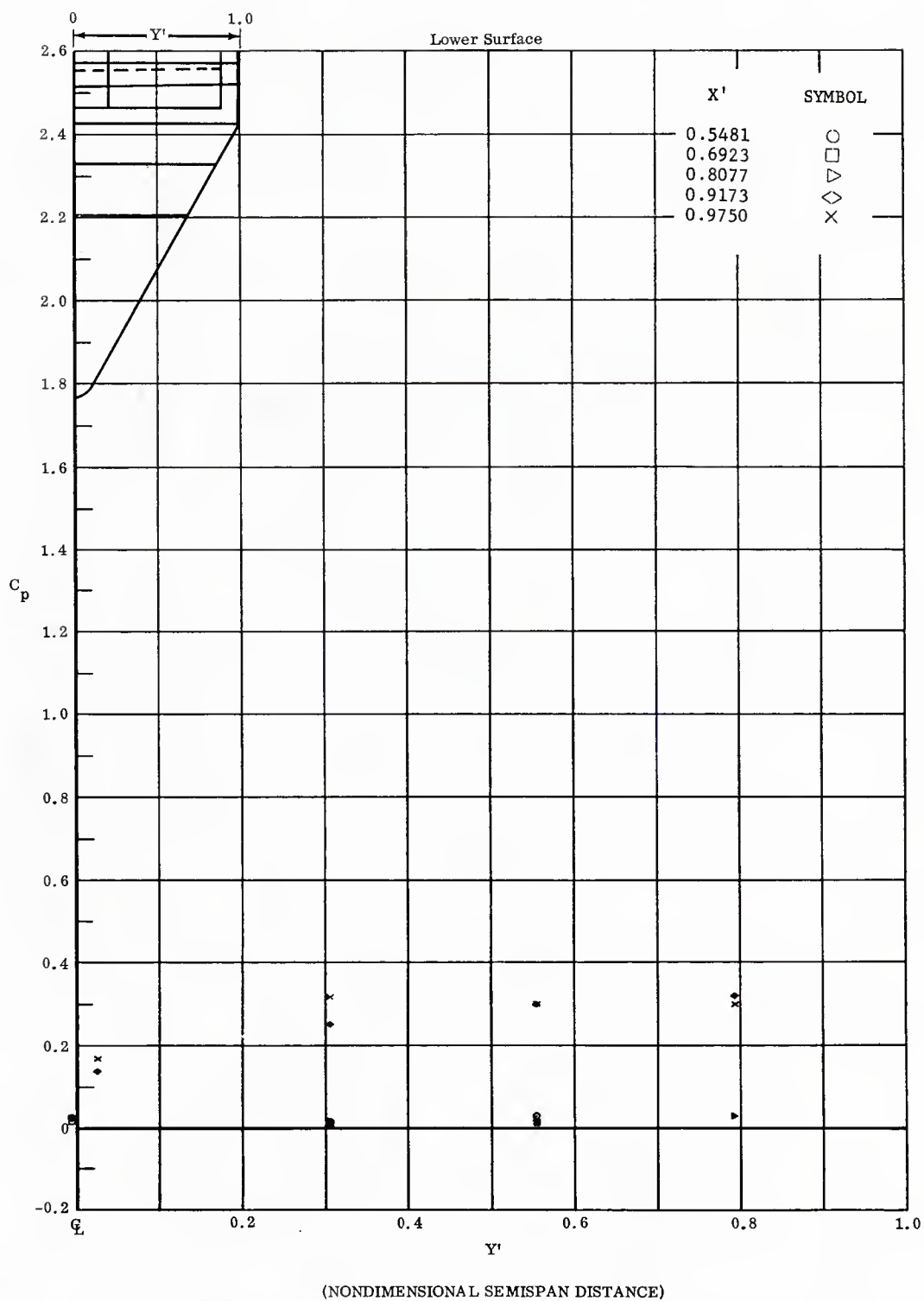


Fig. 25 Spanwise Pressure Distributions on Lower Surface; Center, Left and Right Flaps Deflected  $+20^\circ$ ,  $\alpha = 0^\circ$ .

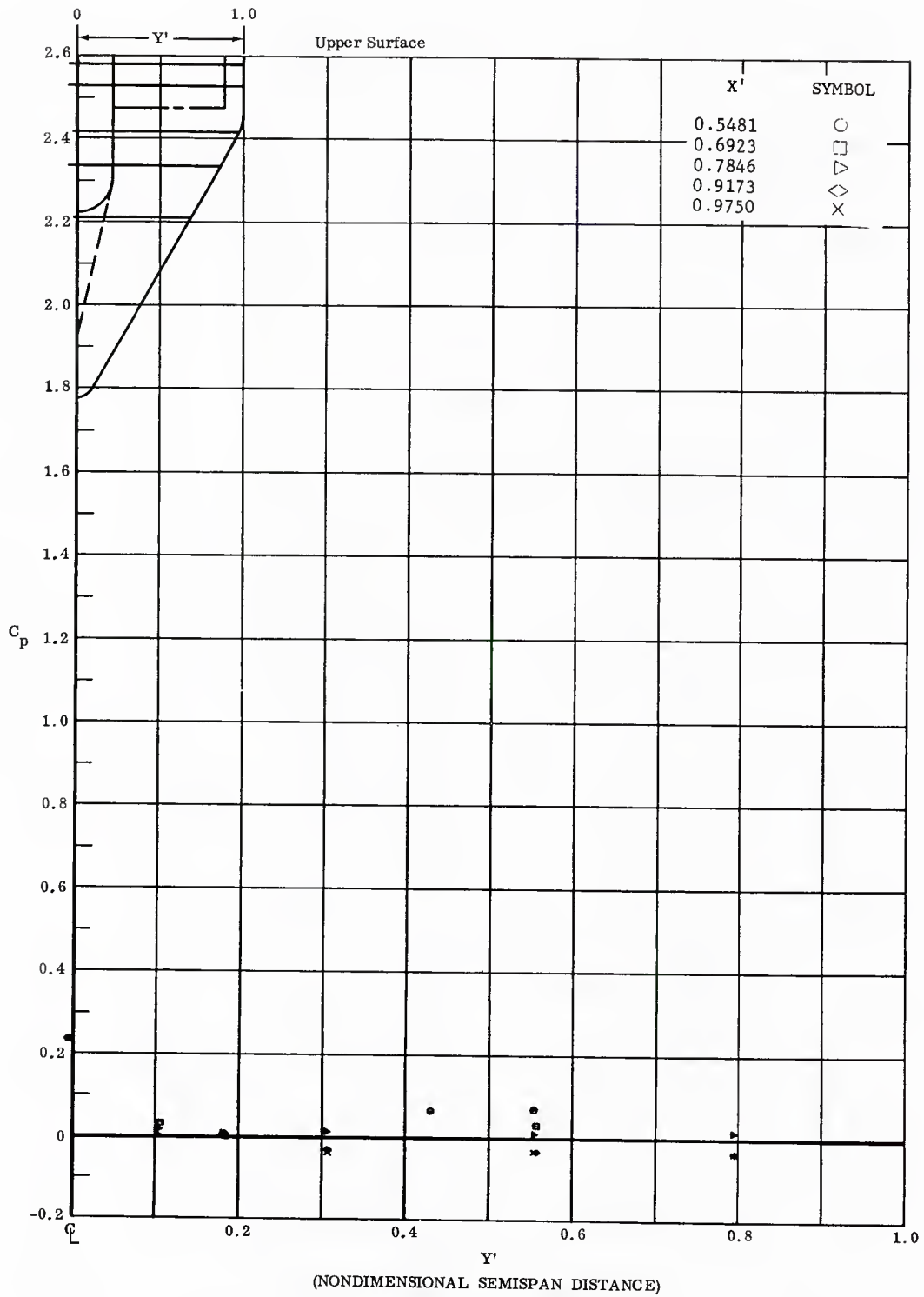


Fig. 25 Spanwise Pressure Distributions on Upper Surface; Center, Left and Right Flaps Deflected  $+20^\circ$ ,  $\alpha = 0^\circ$ .

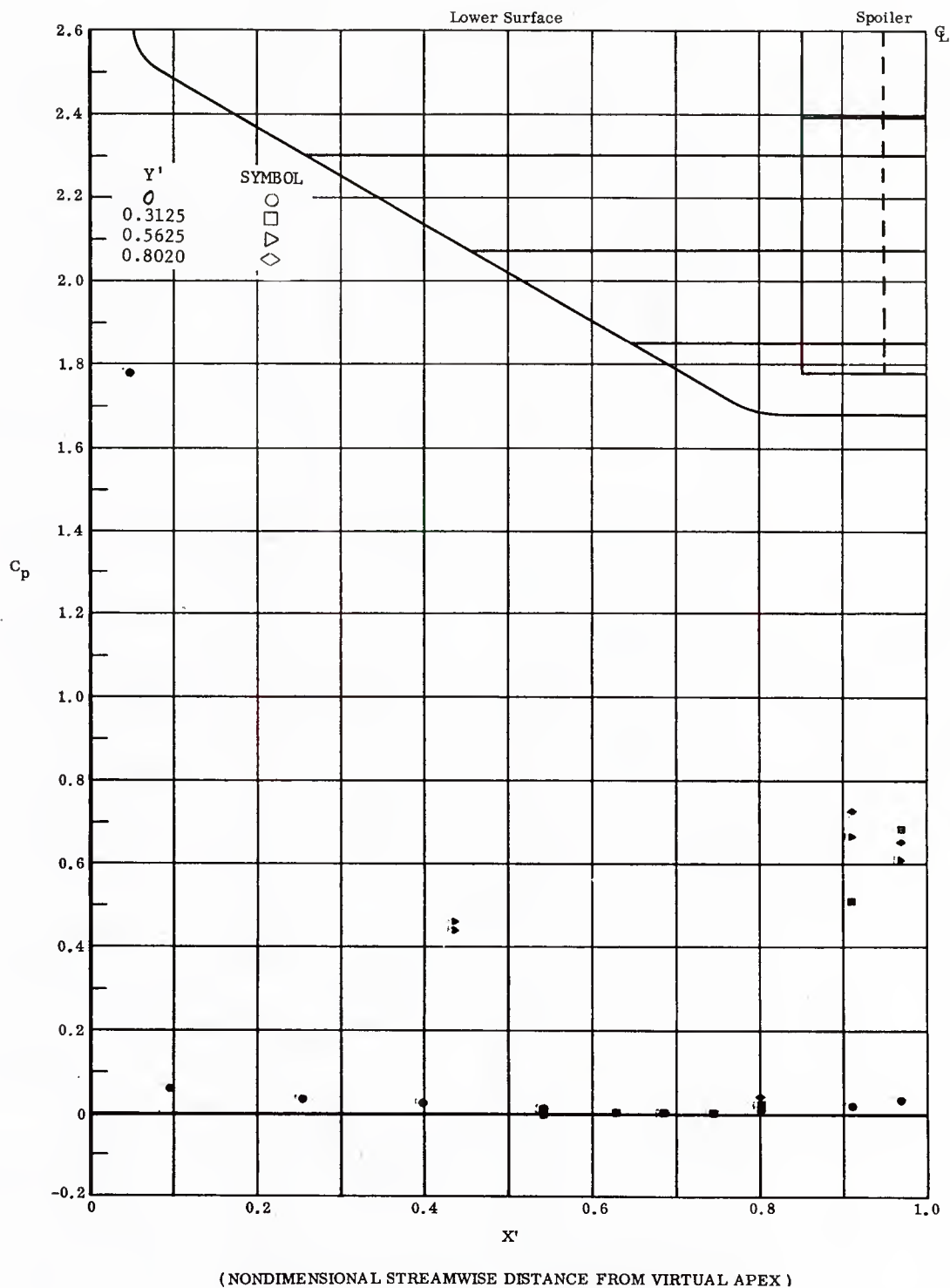


Fig. 26 Streamwise Pressure Distributions on Lower Surface; Left and Right Flaps Deflected  $+30^\circ$ .  $\alpha = 0^\circ$ .

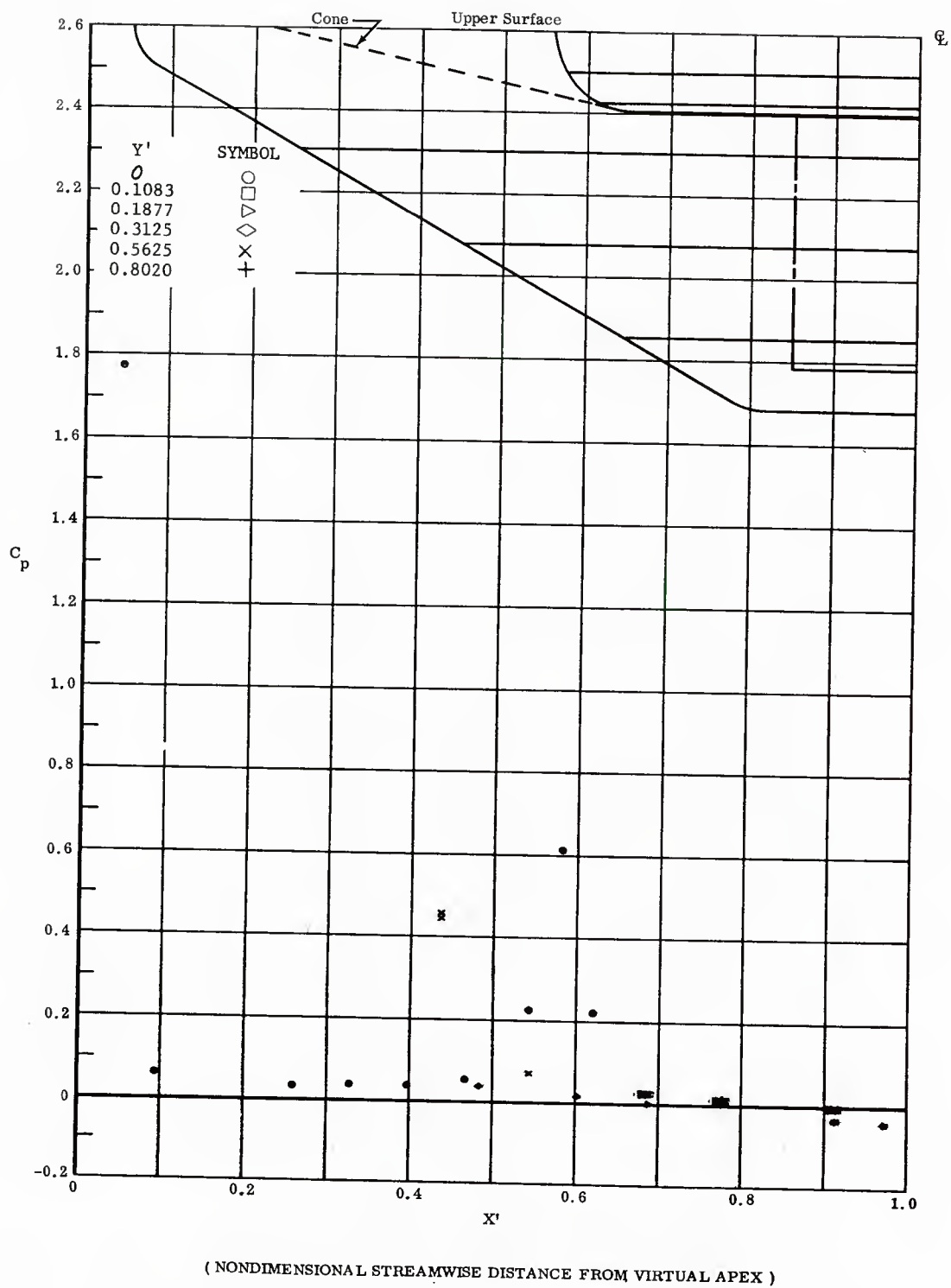


Fig. 26 Streamwise Pressure Distributions on Upper Surface; Left and Right Flaps Deflected  $+30^\circ$ ,  $\alpha = 0^\circ$ .

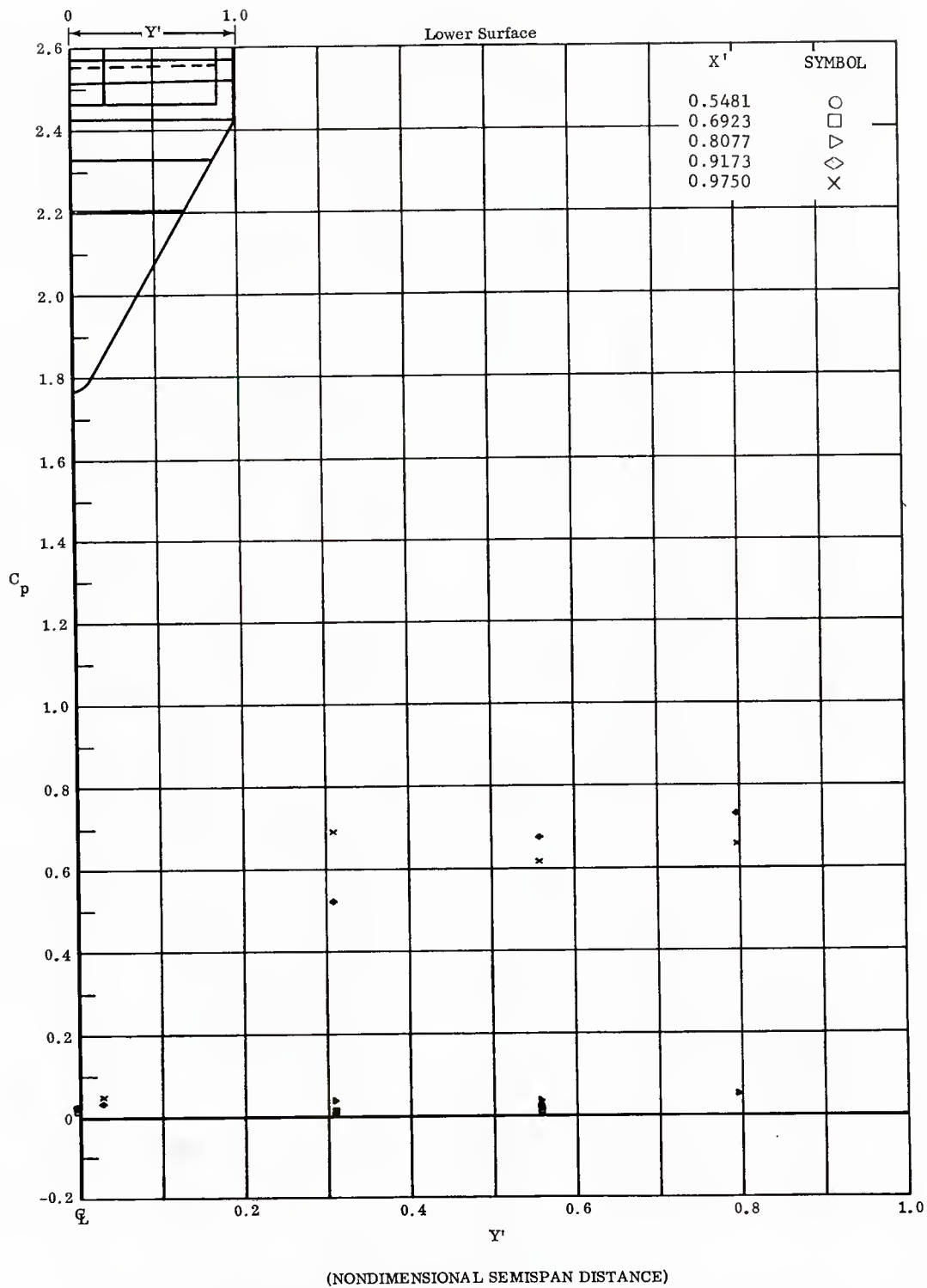


Fig. 26 Spanwise Pressure Distributions on Lower Surface; Left and Right Flaps Deflected  $+30^\circ$ ,  $\alpha = 0^\circ$ .



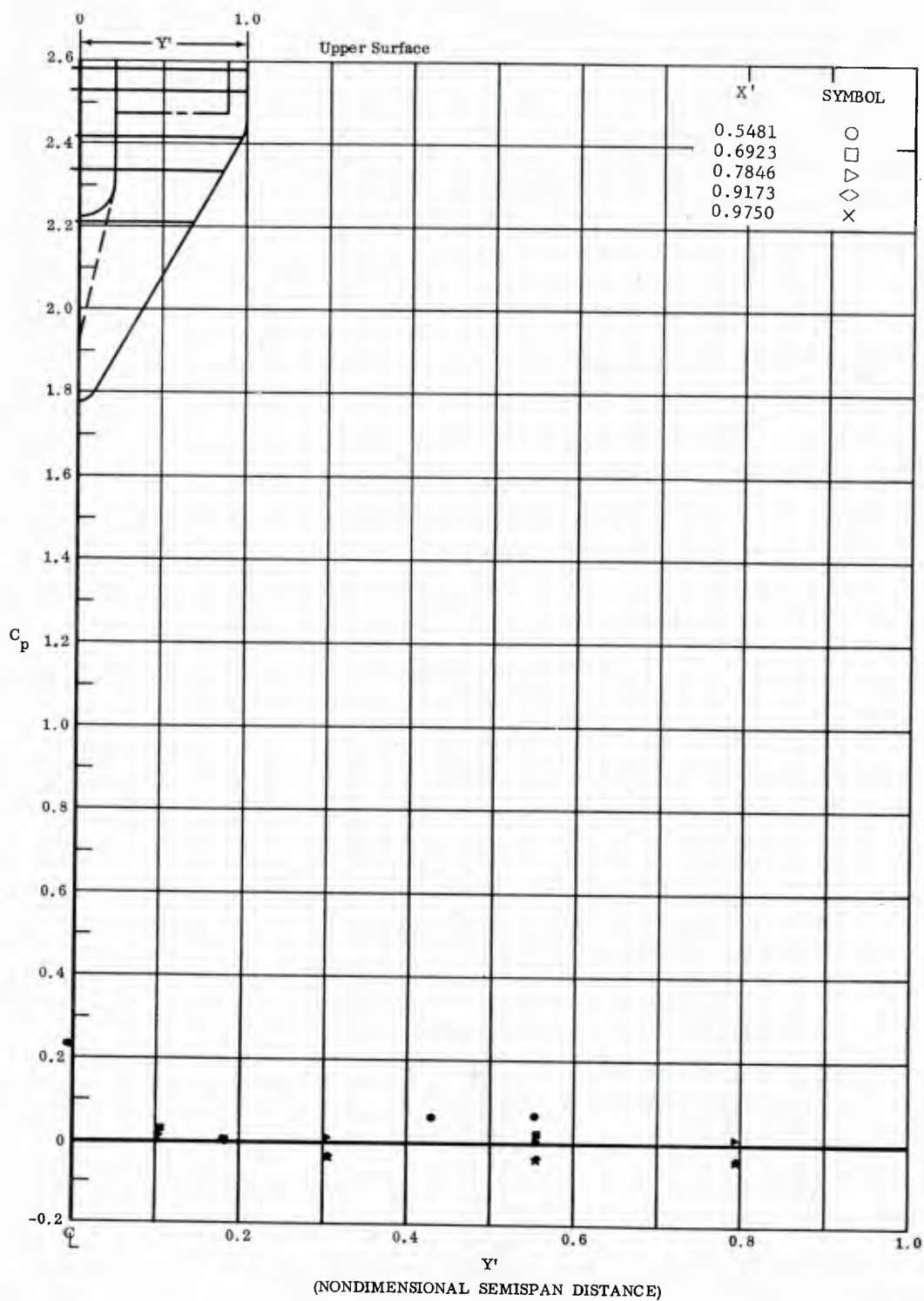


Fig. 26 Spanwise Pressure Distributions on Upper Surface; Left and Right Flaps Deflected  $+30^\circ$ ,  $\alpha = 0^\circ$ .

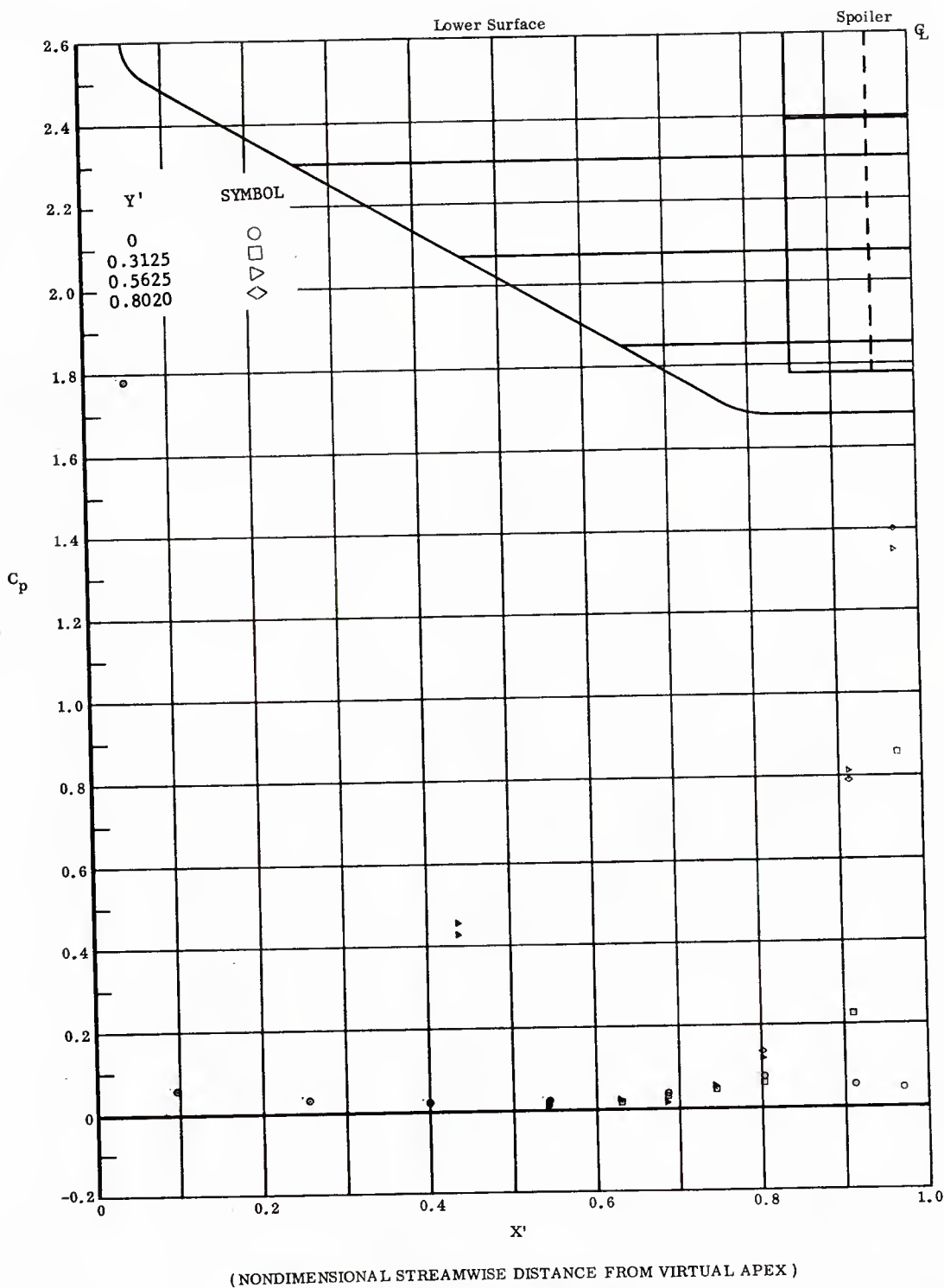
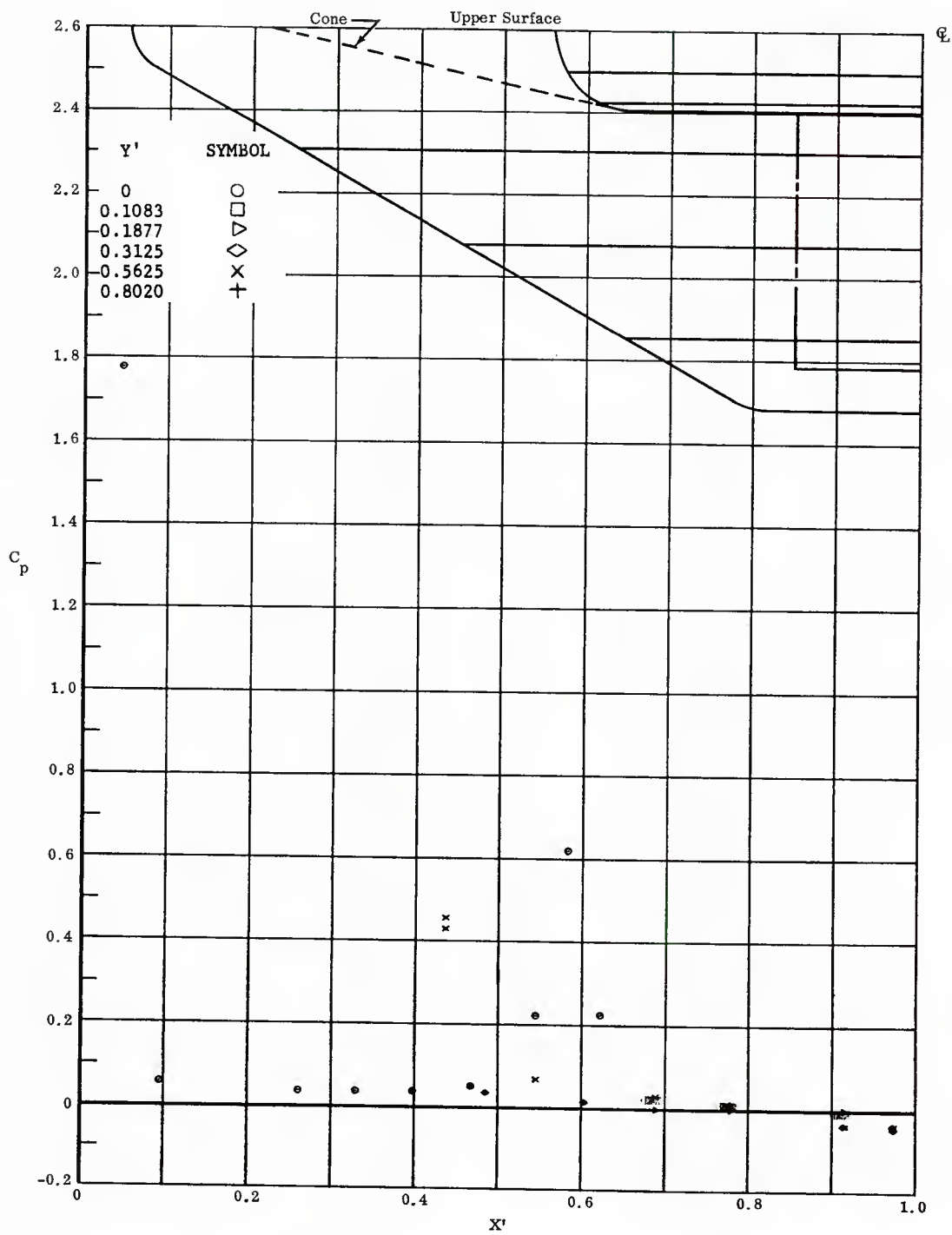


Fig. 27 Streamwise Pressure Distributions on Lower Surface; Left and Right Flaps Deflected  $+40^\circ$ ,  $\alpha = 0^\circ$ .



( NONDIMENSIONAL STREAMWISE DISTANCE FROM VIRTUAL APEX )

Fig. 27 Streamwise Pressure Distributions on Upper Surface; Left and Right Flaps Deflected +40,  $\alpha = 0^\circ$ .

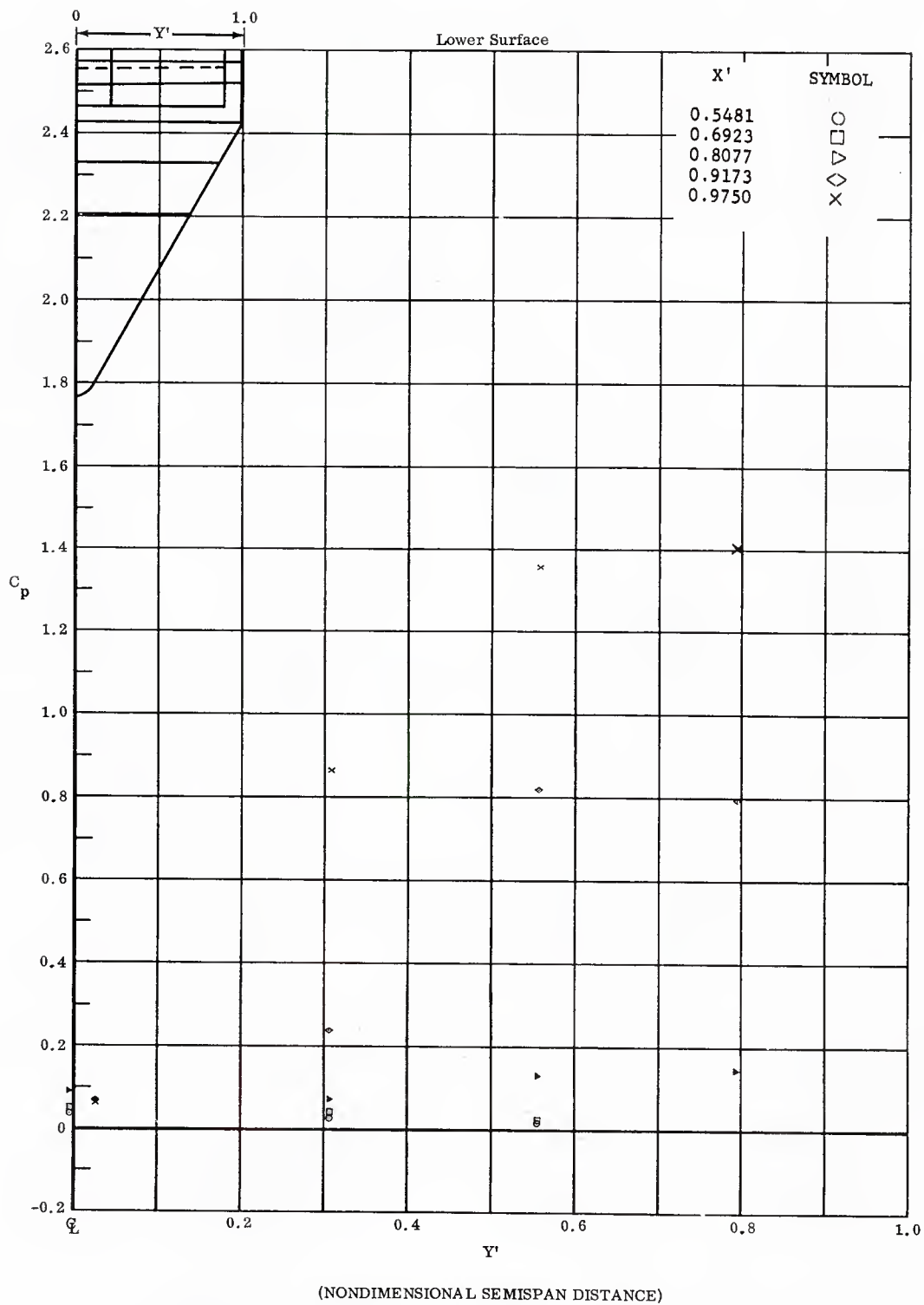


Fig. 27 Spanwise Pressure Distributions on Lower Surface; Left and Right Flaps Deflected  $+40^\circ$ ,  $\alpha = 0^\circ$ .

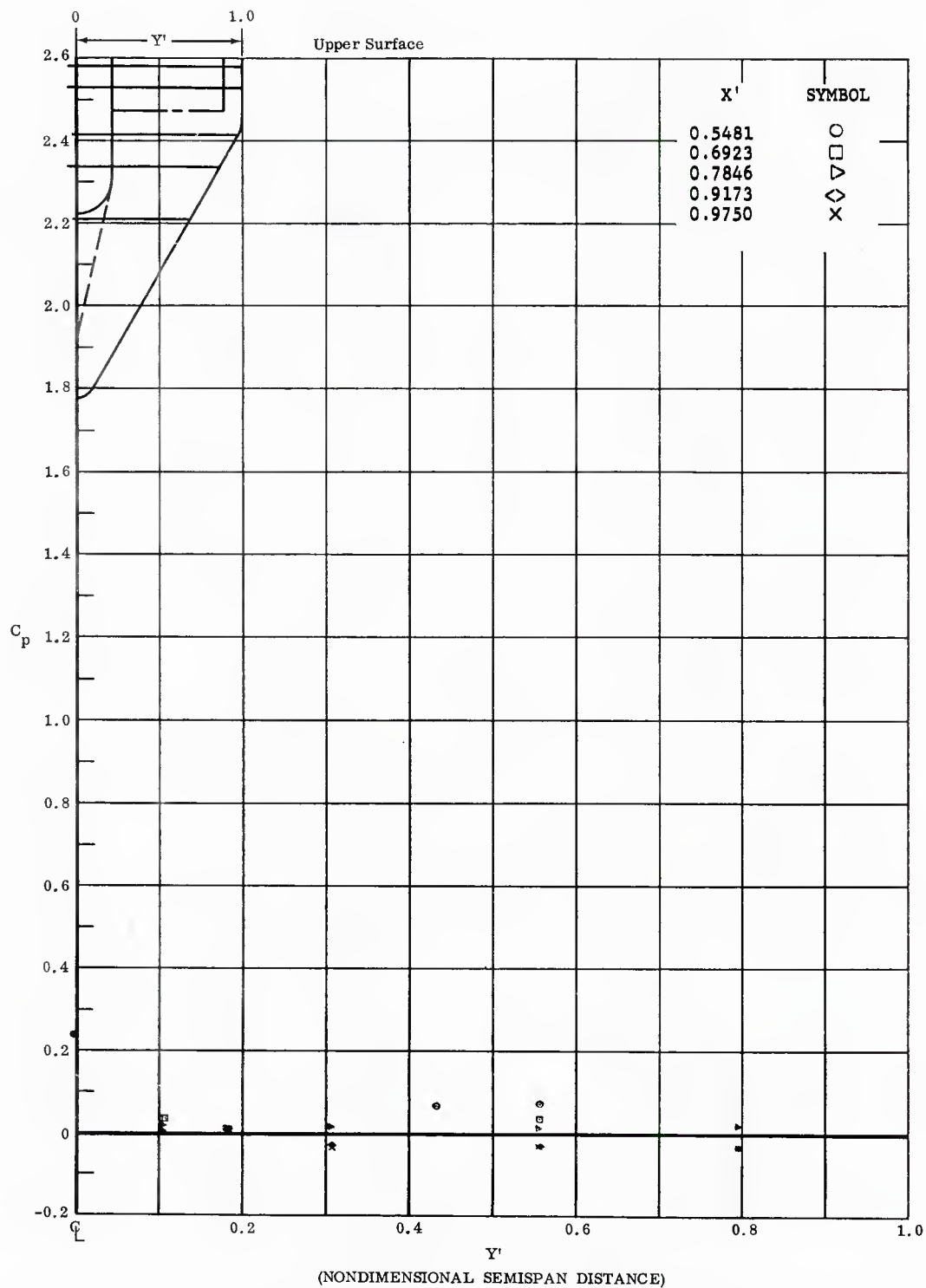


Fig. 27 Spanwise Pressure Distributions on Upper Surface; Left and Right Flaps Deflected  $+40^\circ$ ,  $\alpha = 0^\circ$ .

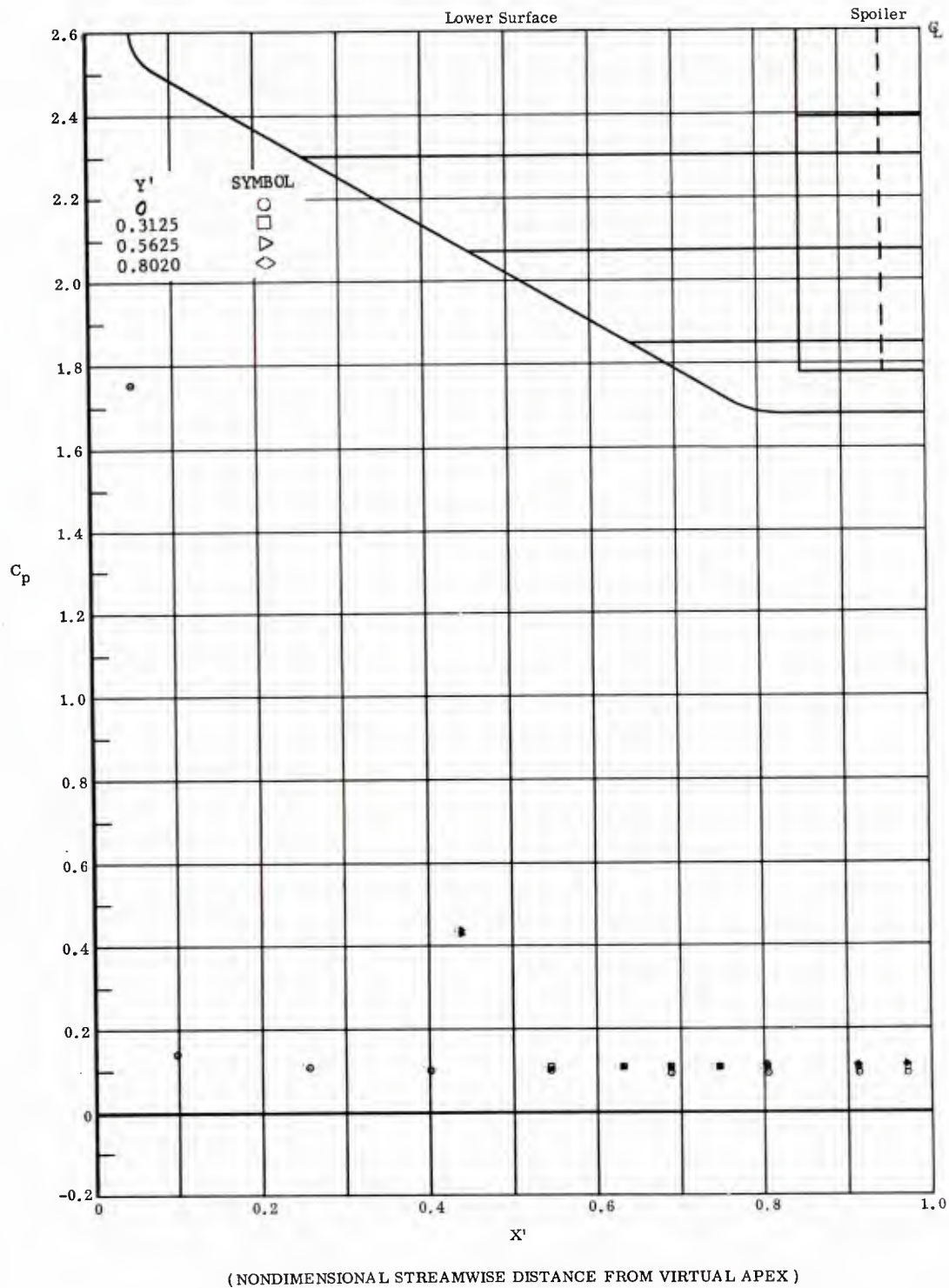
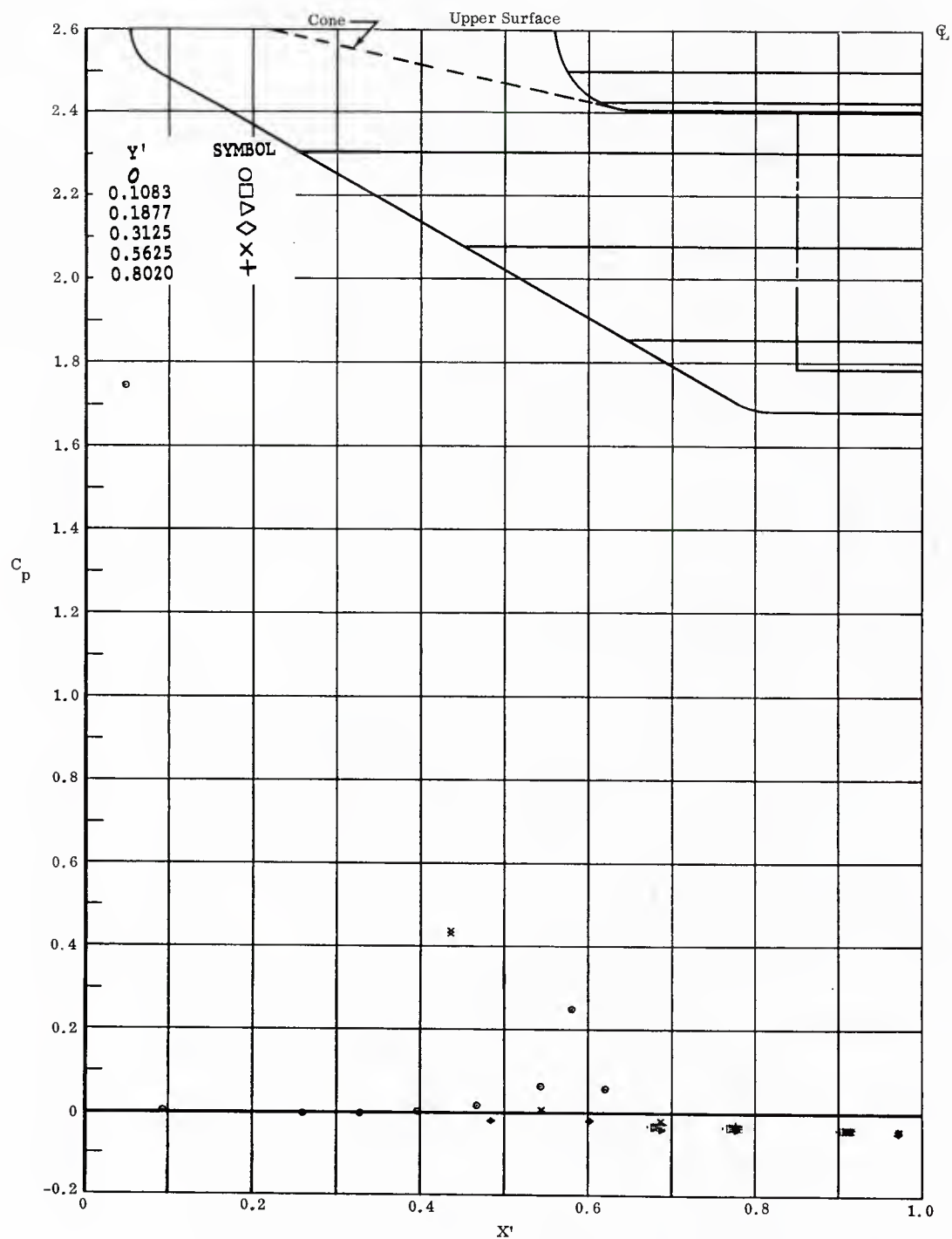


Fig. 28 Streamwise Pressure Distributions on Lower Surface; No Flap Deflections,  $\alpha = +10^\circ$ .



( NONDIMENSIONAL STREAMWISE DISTANCE FROM VIRTUAL APEX )

Fig. 28 Streamwise Pressure Distributions on Upper Surface; No Flap Deflections,  $\alpha = +10^\circ$ .

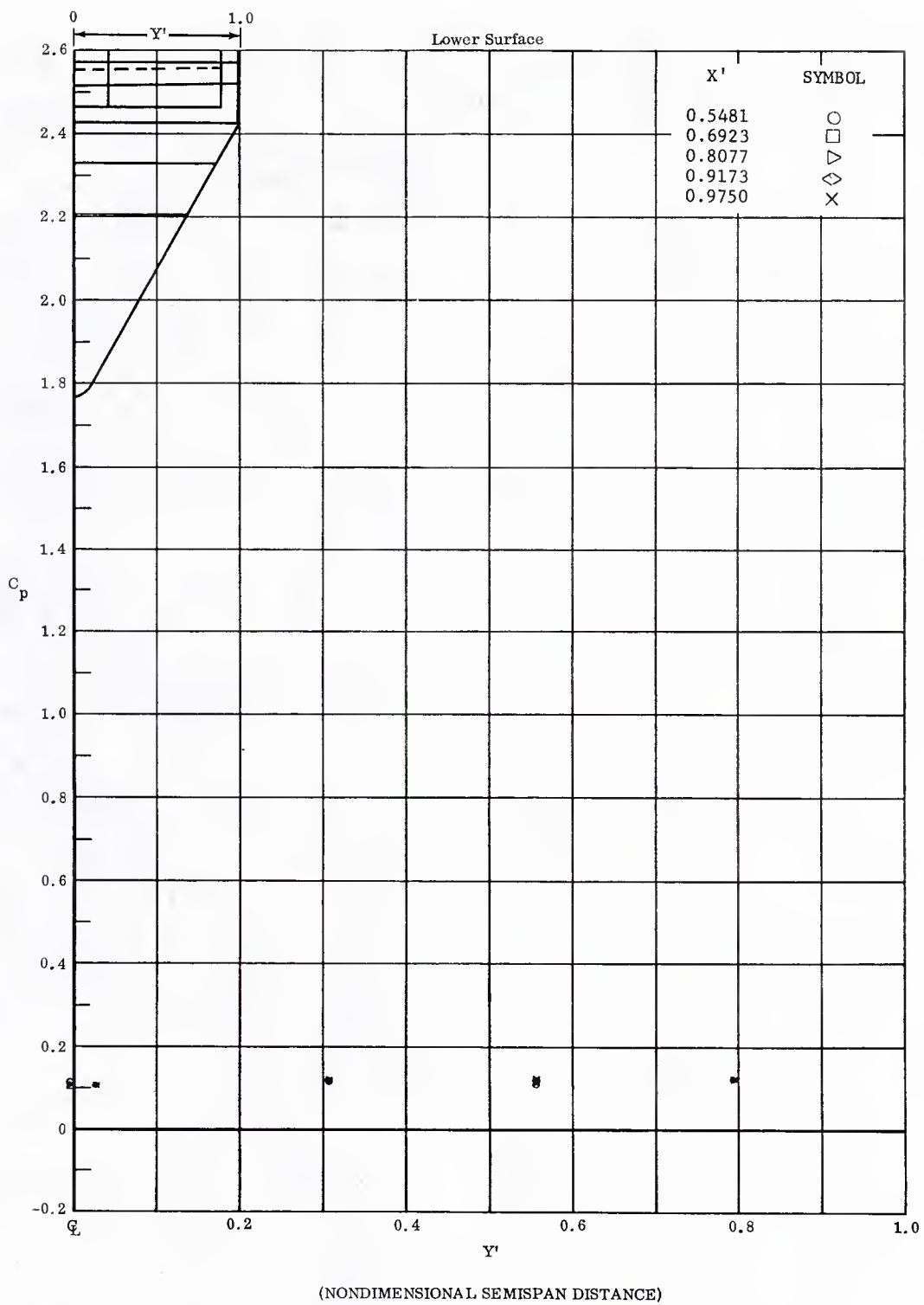


Fig. 28 Spanwise Pressure Distributions on Lower Surface; No Flap Deflections,  $\alpha = +10^\circ$ .



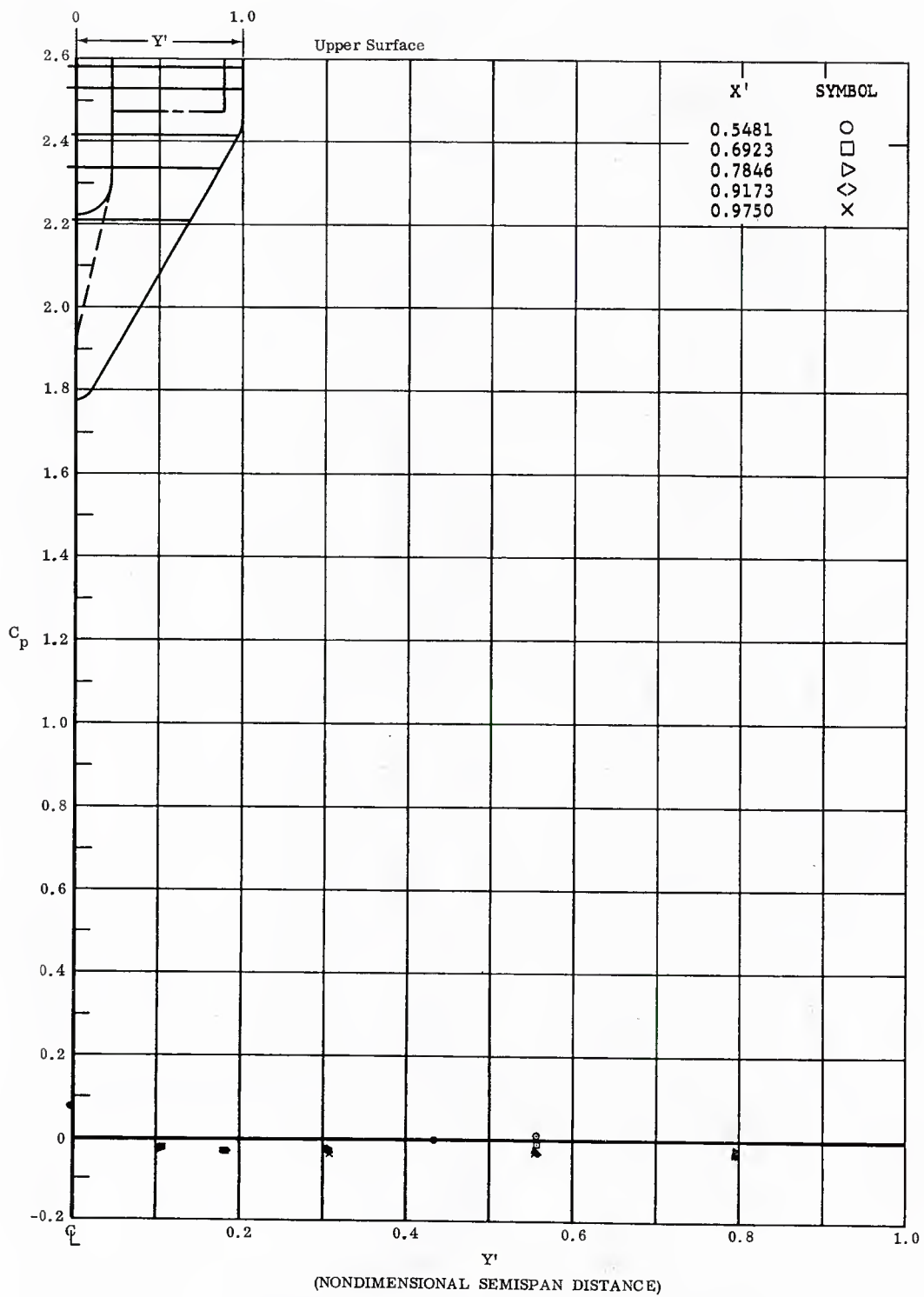


Fig. 28 Spanwise Pressure Distributions on Upper Surface; No Flap Deflections,  $\alpha = +10^\circ$ .

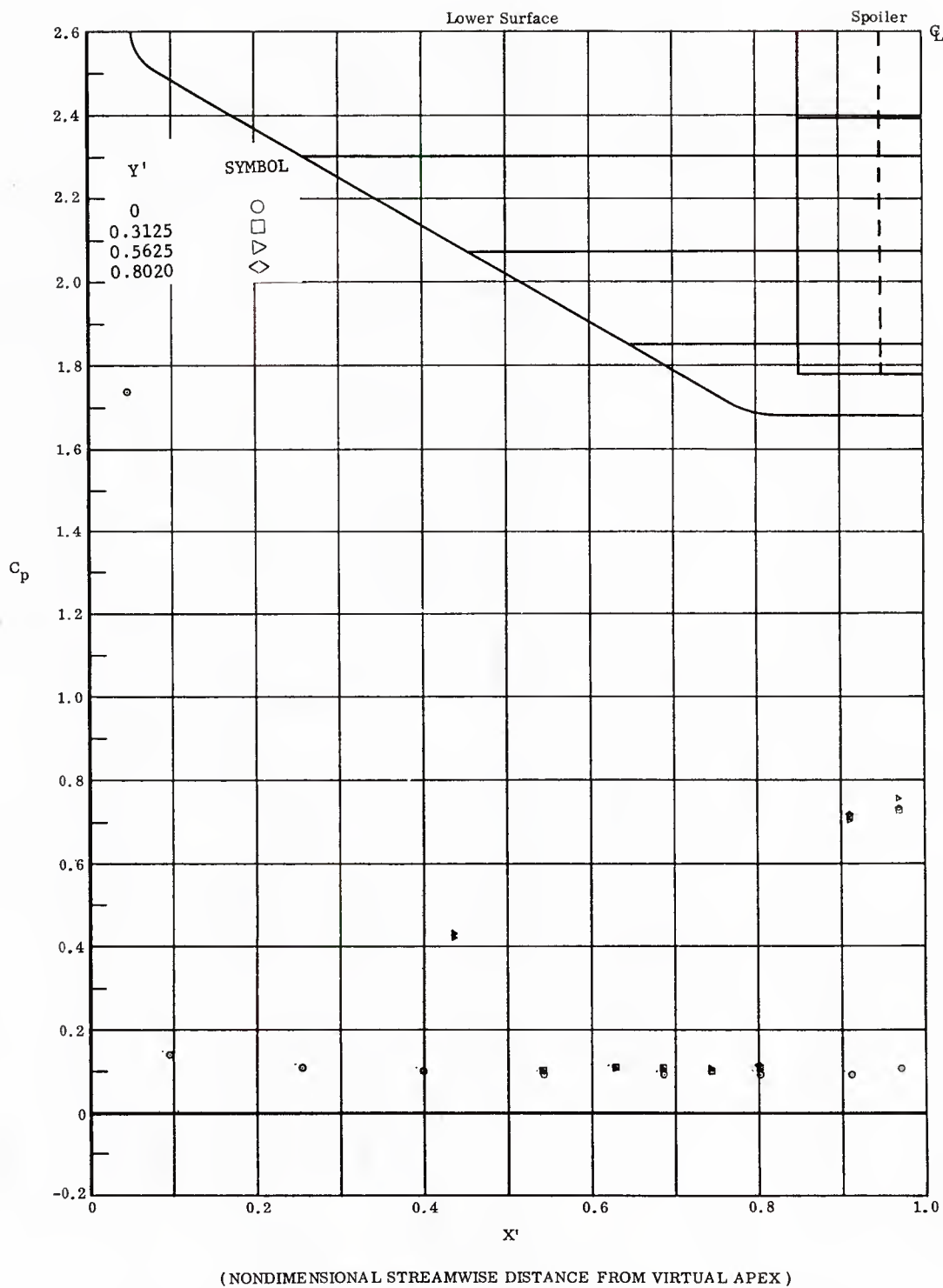
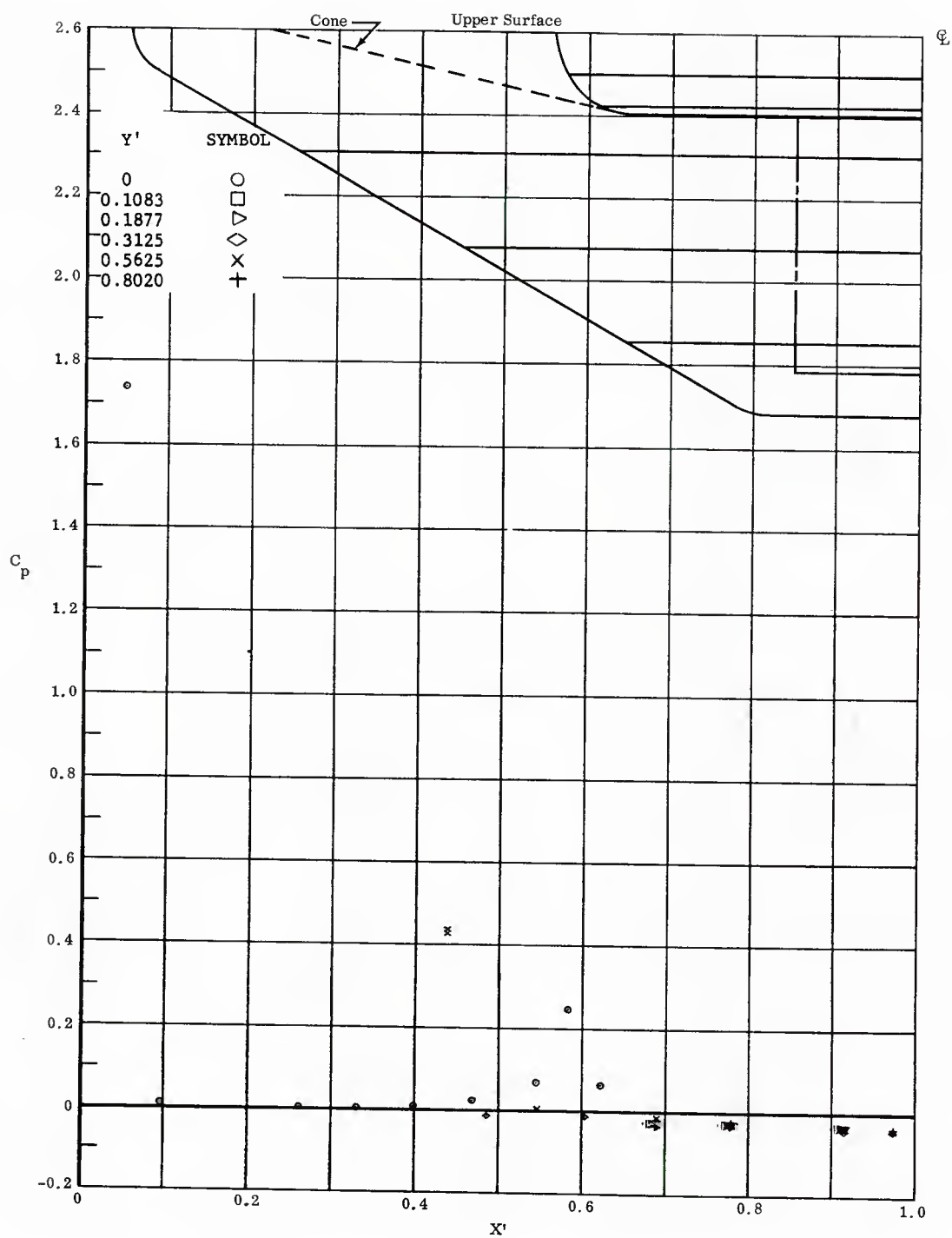


Fig. 29 Streamwise Pressure Distributions on Lower Surface; Left and Right Flaps Deflections  $+20^\circ$ ,  $\alpha = +10^\circ$ .



( NONDIMENSIONAL STREAMWISE DISTANCE FROM VIRTUAL APEX )

Fig. 29 Streamwise Pressure Distributions on Upper Surface; Left and Right Flaps Deflections  $+20^\circ$ ,  $\alpha = +10^\circ$ .

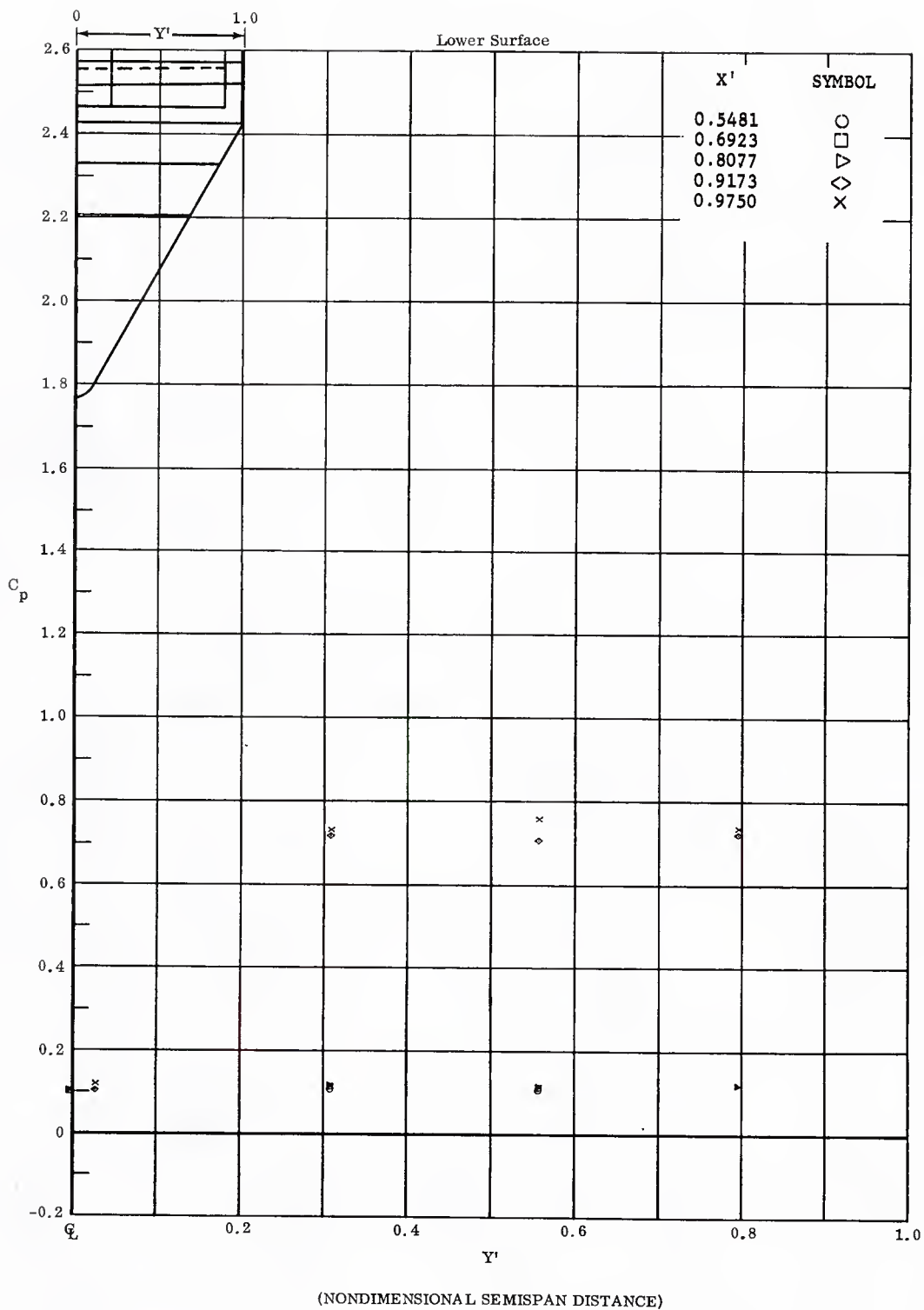


Fig. 29 Spanwise Pressure Distributions on Lower Surface; Left and Right Flaps Deflections  $+20^\circ$ ,  $\alpha = +10^\circ$ .

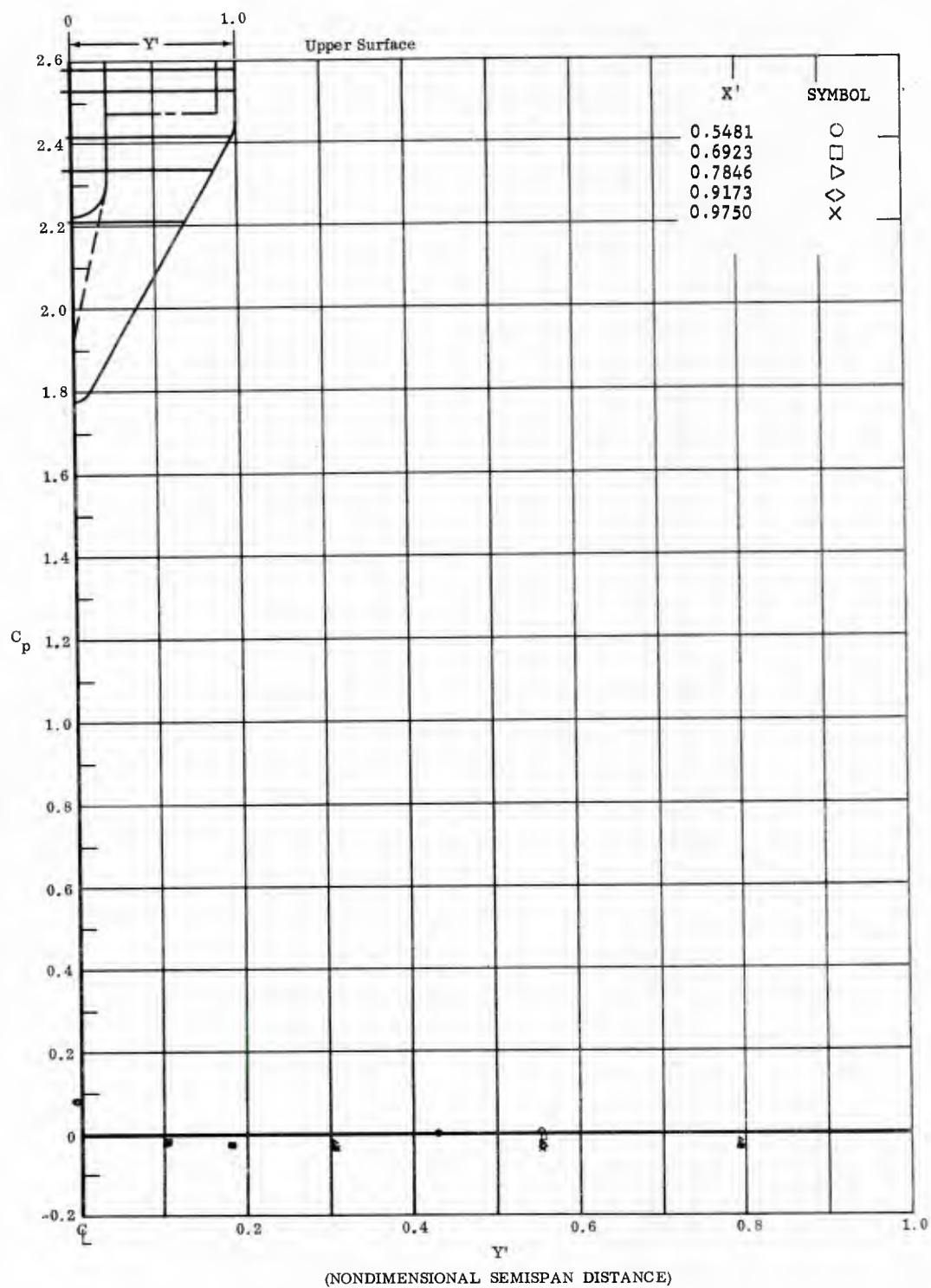


Fig. 29 Spanwise Pressure Distributions on Upper Surface; Left and Right Flaps Deflections  $+20^\circ$ ,  $\alpha = +10^\circ$ .

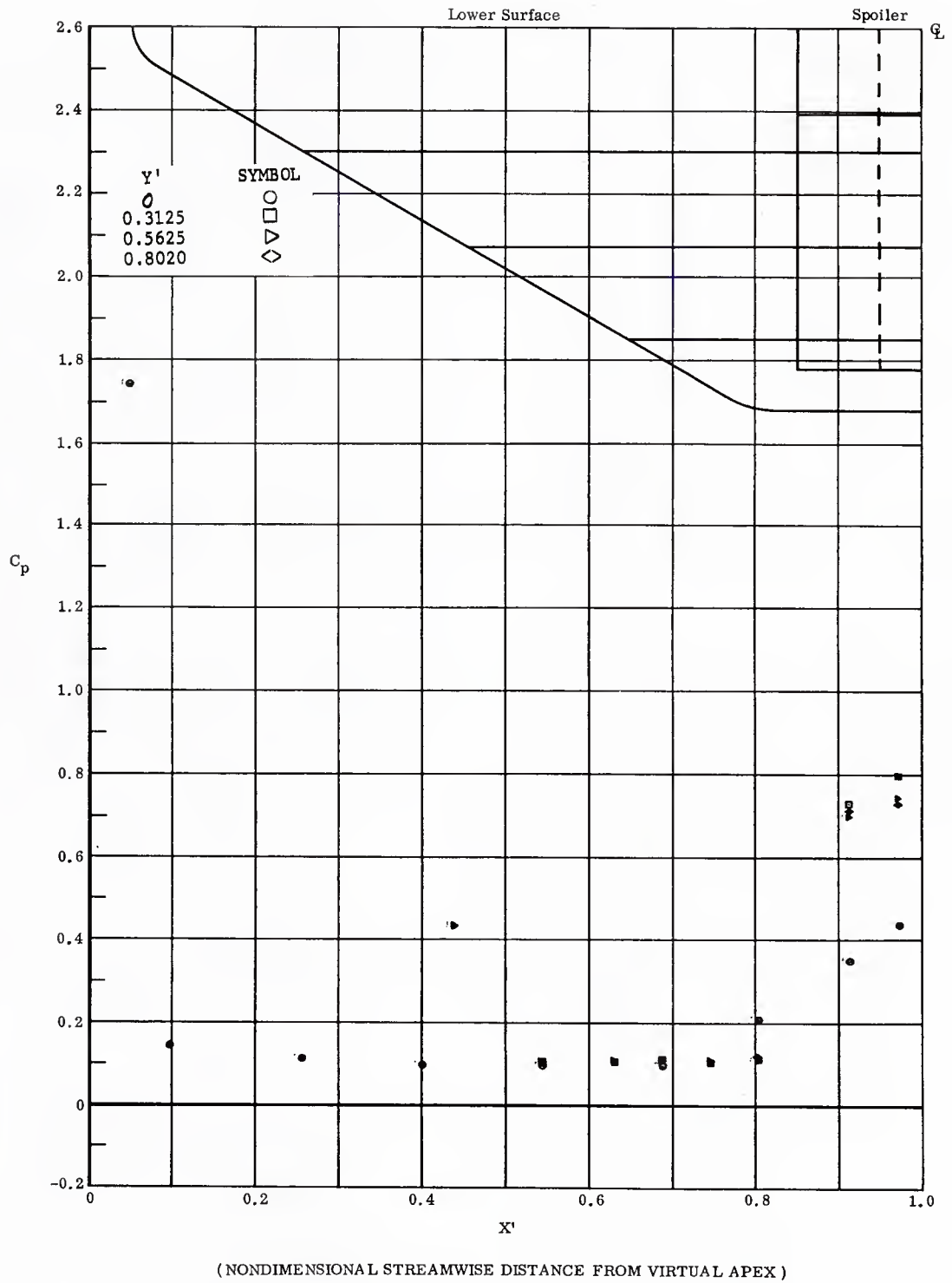
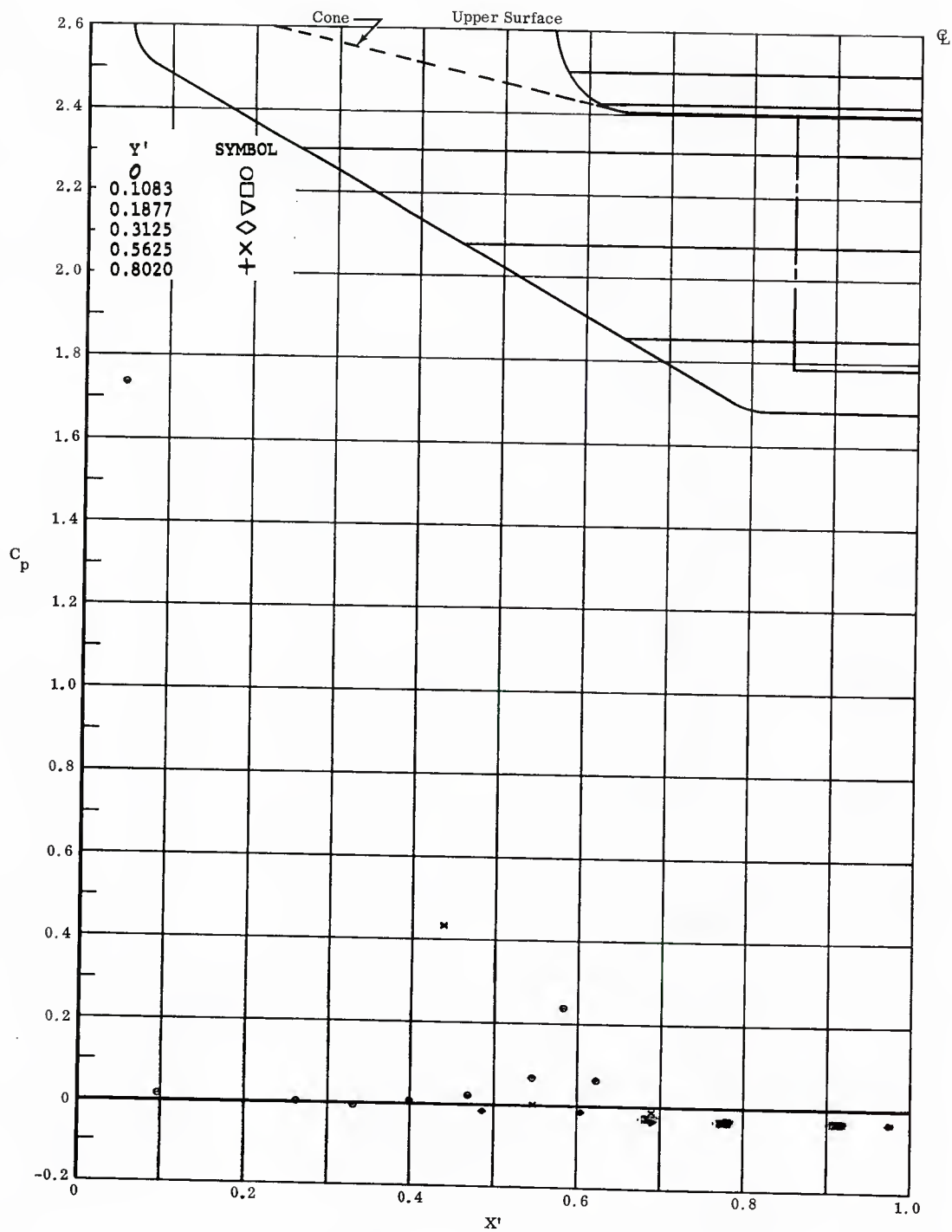


Fig. 30 Streamwise Pressure Distributions on Lower Surface; Center, Left and Right Flaps Deflected  $+20^\circ$ ,  $\alpha = +10^\circ$ .



( NONDIMENSIONAL STREAMWISE DISTANCE FROM VIRTUAL APEX )

Fig. 30 Streamwise Pressure Distributions on Upper Surface; Center, Left and Right Flaps All Deflected  $+20^\circ$ ,  $\alpha = +10^\circ$ .

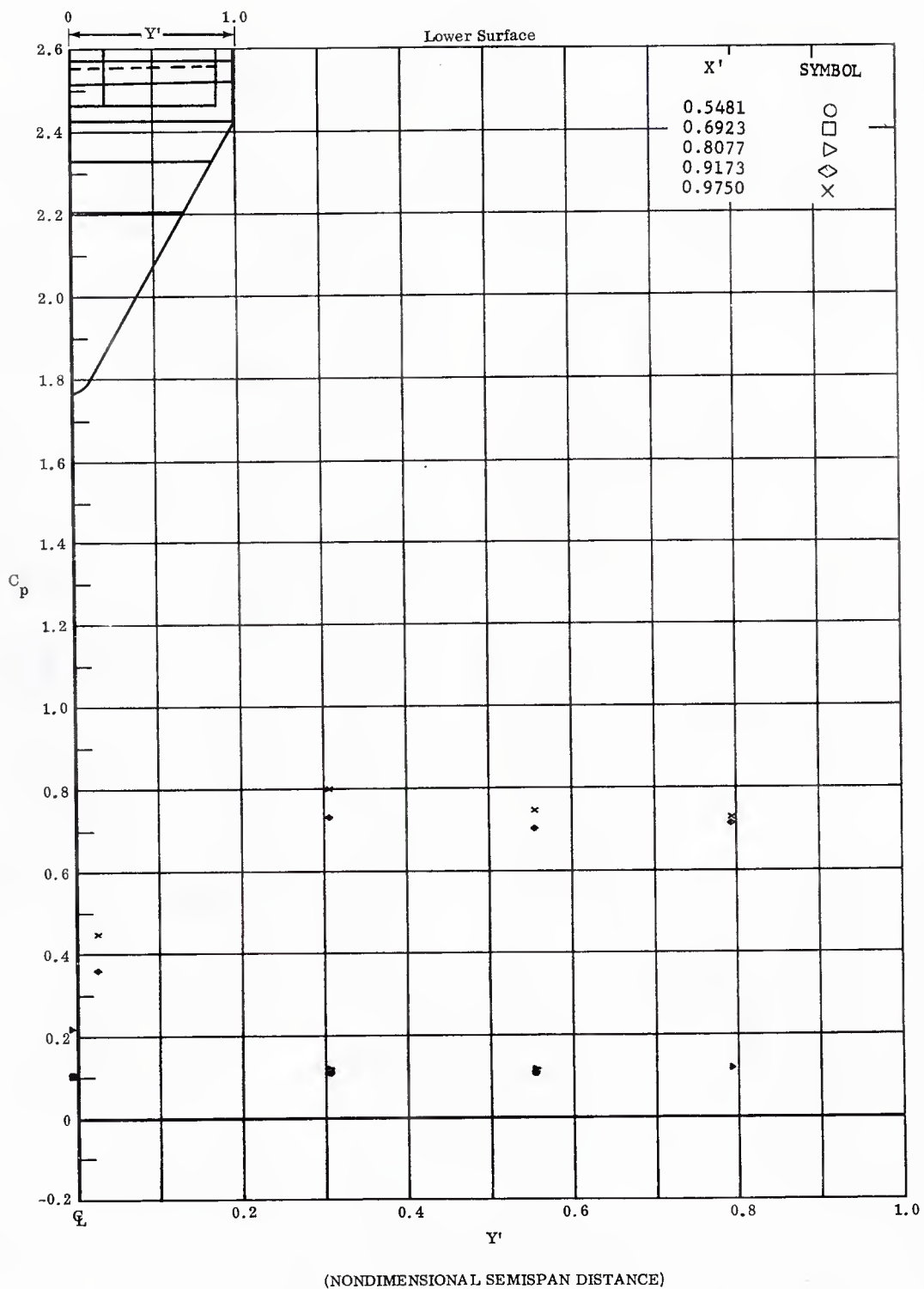


Fig. 30 Spanwise Pressure Distributions on Lower Surface; Center, Left and Right Flaps All Deflected  $+20^\circ$ ,  $\alpha = +10^\circ$ .



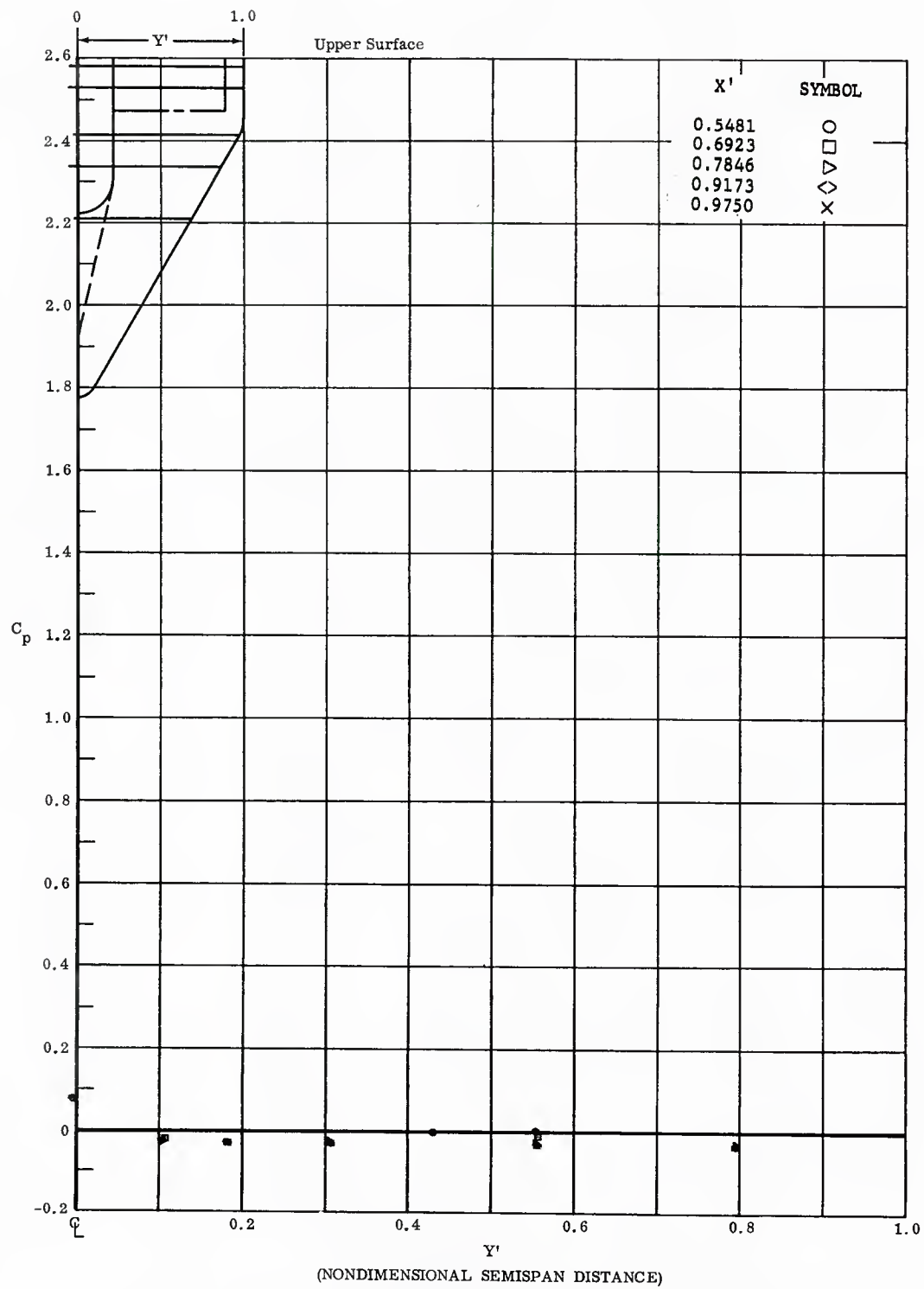


Fig. 30 Spanwise Pressure Distributions on Upper Surface; Center, Left and Right Flaps All Deflected  $+20^\circ$ ,  $\alpha = +10^\circ$ .

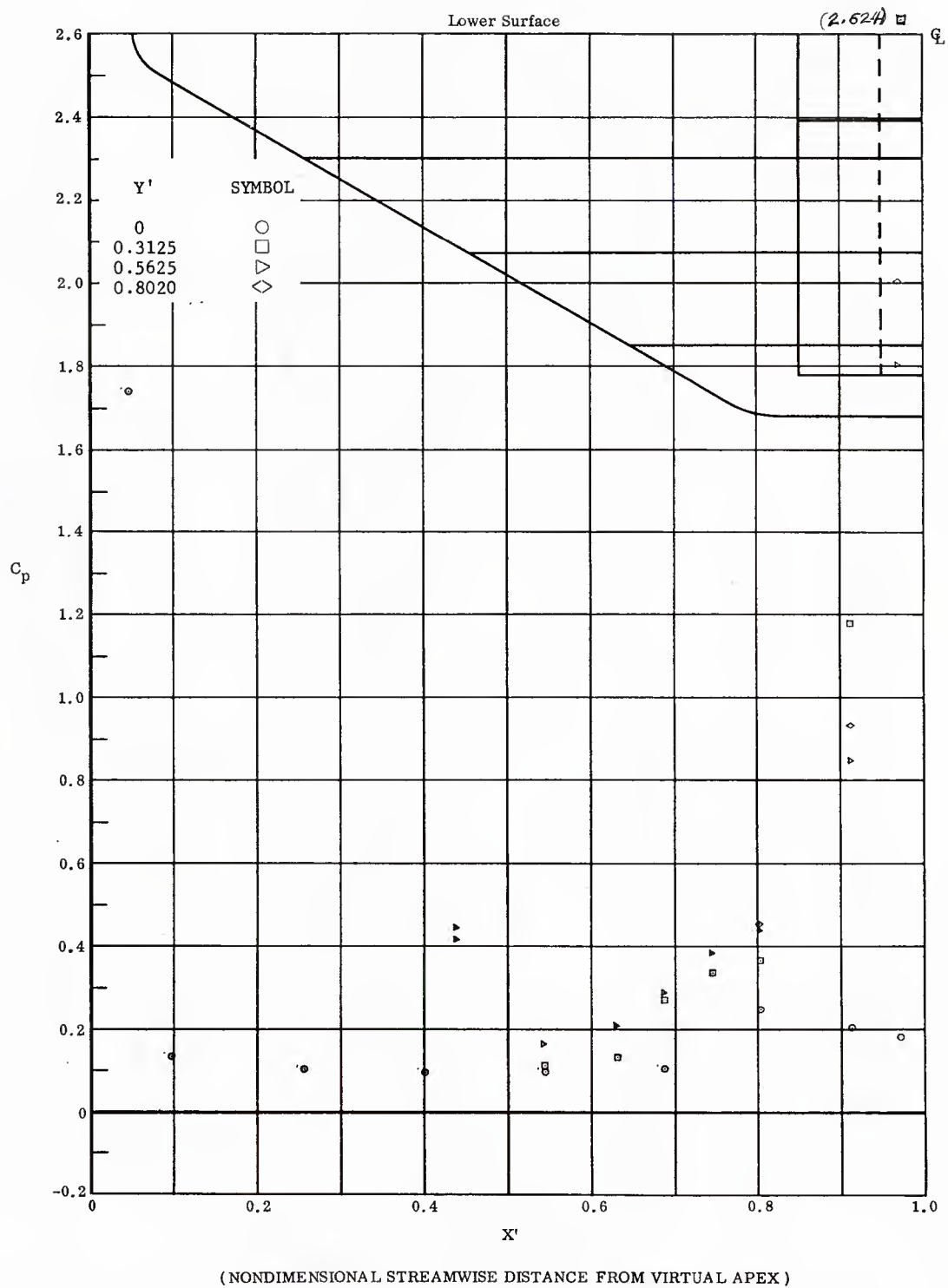
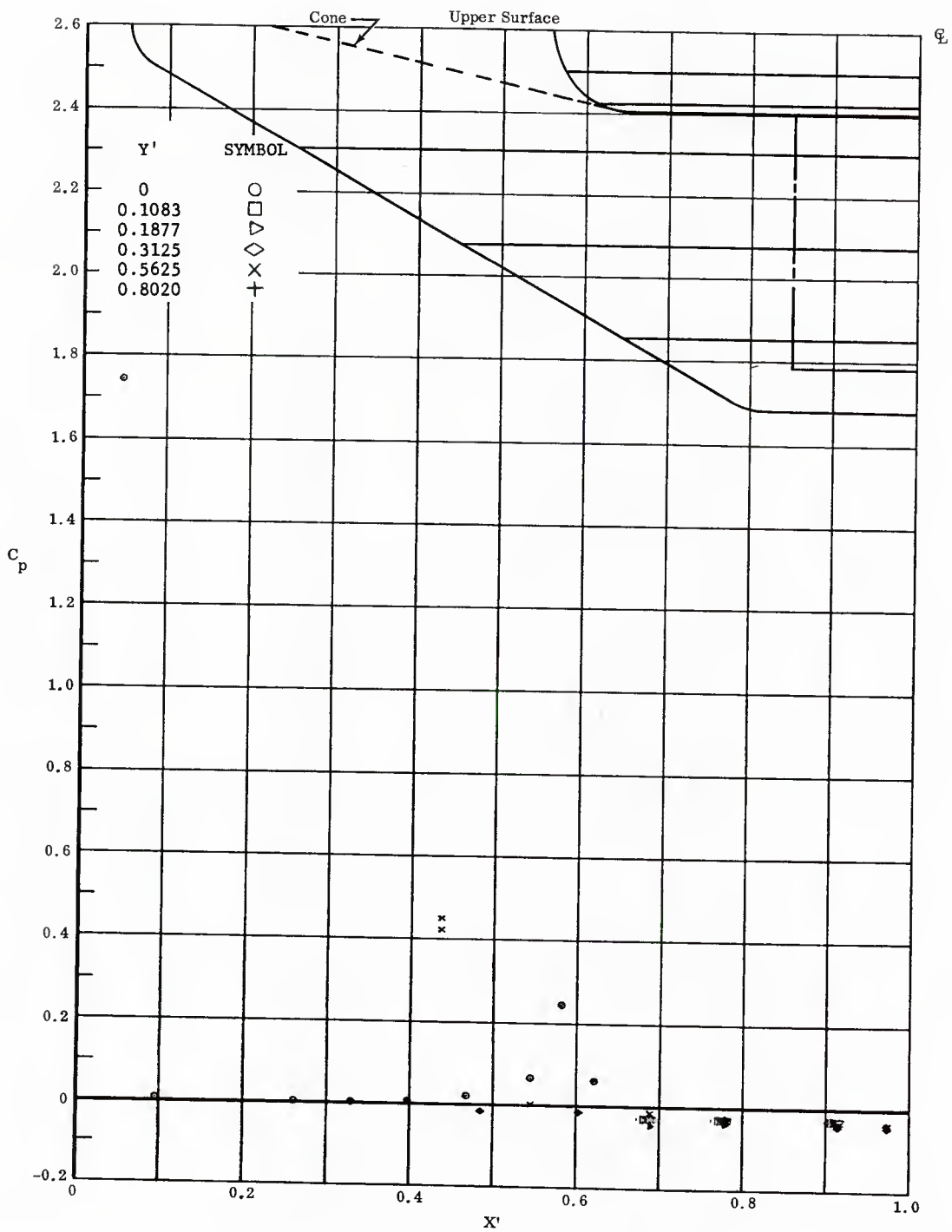


Fig. 31 Streamwise Pressure Distributions on Lower Surface; Left and Right Flaps Deflected +40°,  $\alpha = +10^\circ$ .



( NONDIMENSIONAL STREAMWISE DISTANCE FROM VIRTUAL APEX )

Fig. 31 Streamwise Pressure Distributions on Upper Surface; Left and Right Flaps Deflected  $+40^\circ$ ,  $\alpha = +10^\circ$ .

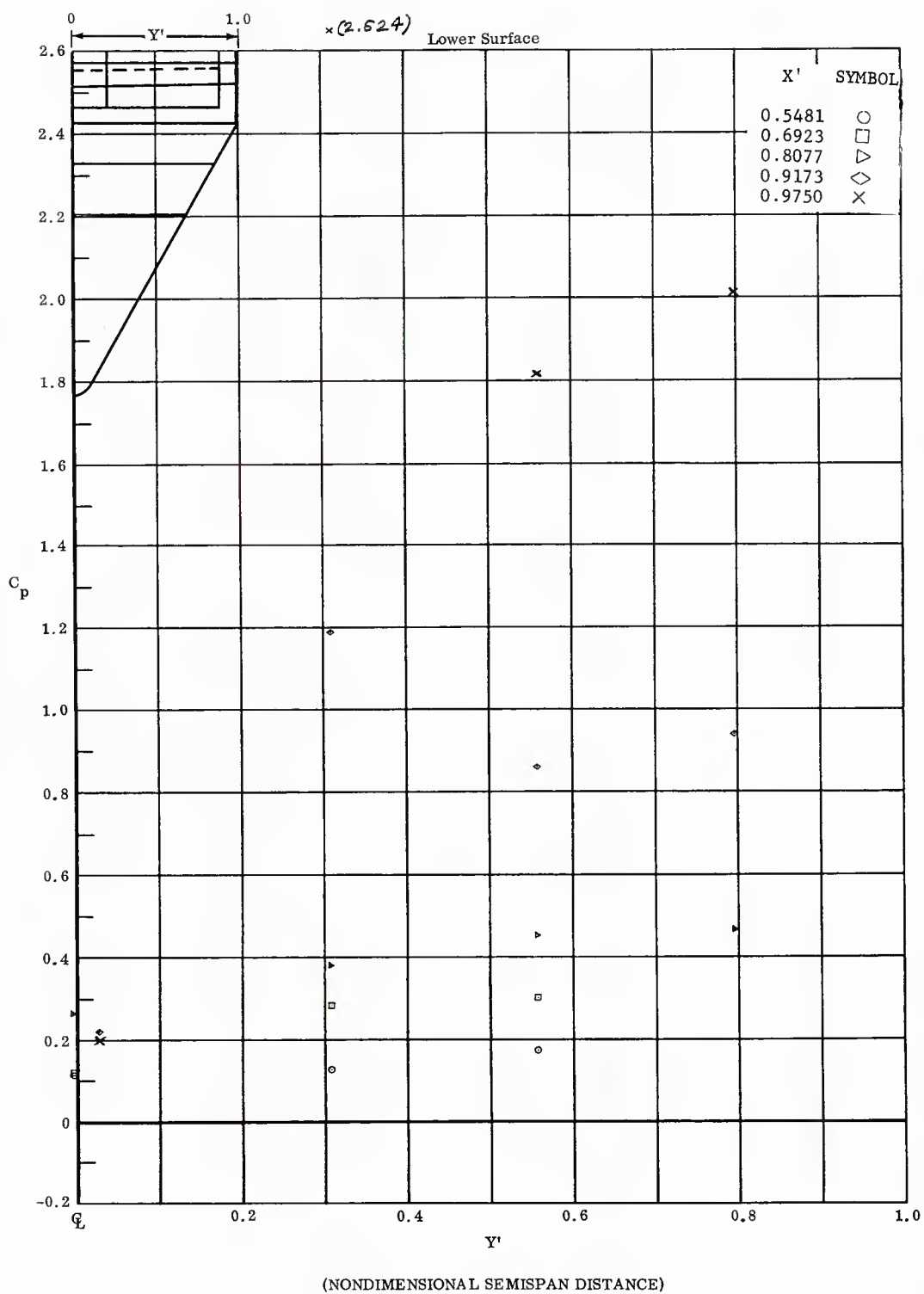


Fig. 31 Spanwise Pressure Distributions on Lower Surface; Left and Right Flaps Deflected  $+40^\circ$ ,  $\alpha = +10^\circ$ .

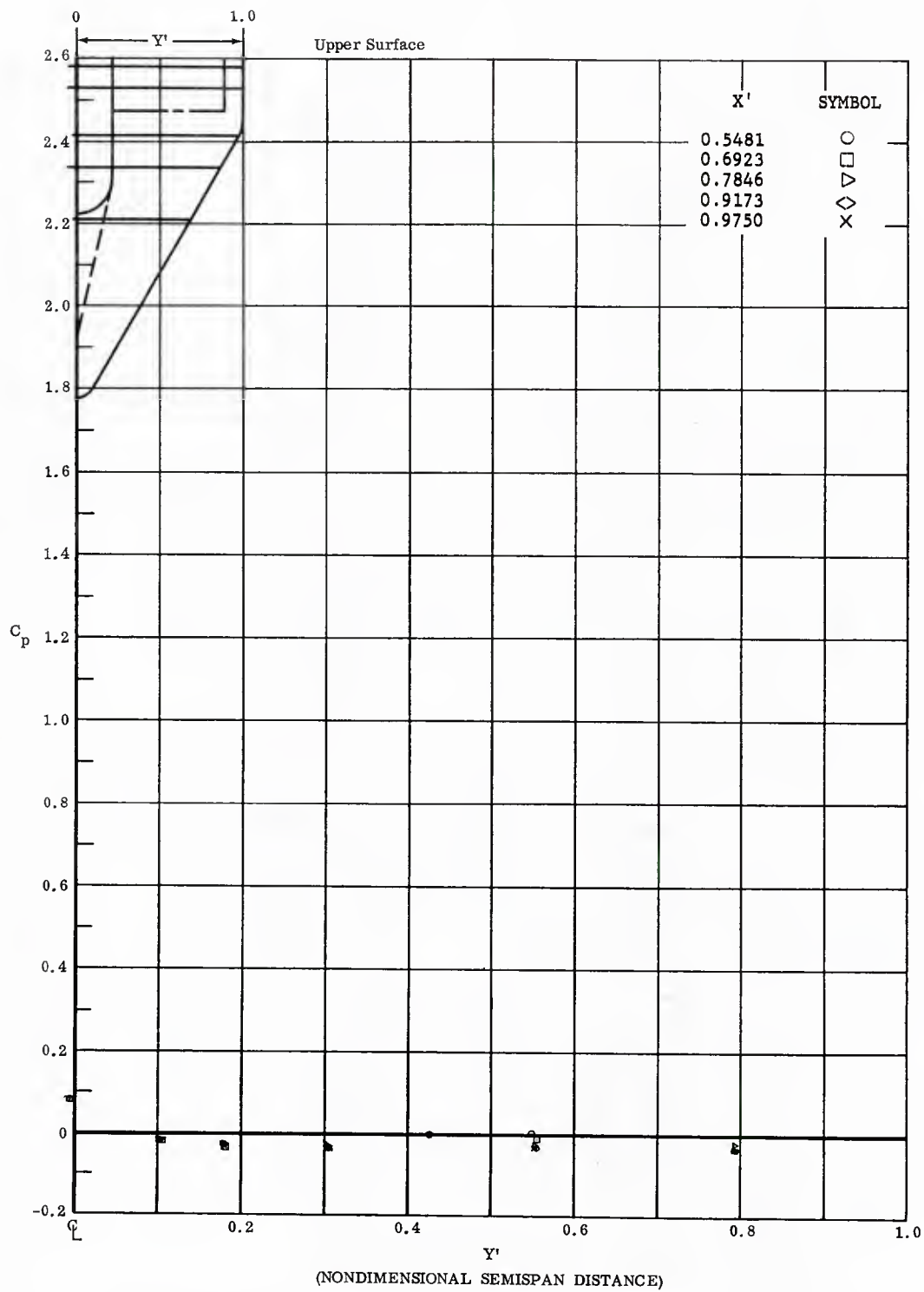


Fig. 31 Spanwise Pressure Distributions on Upper Surface; Left and Right Flaps Deflected  $+40^\circ$ ,  $\alpha = +10^\circ$ .

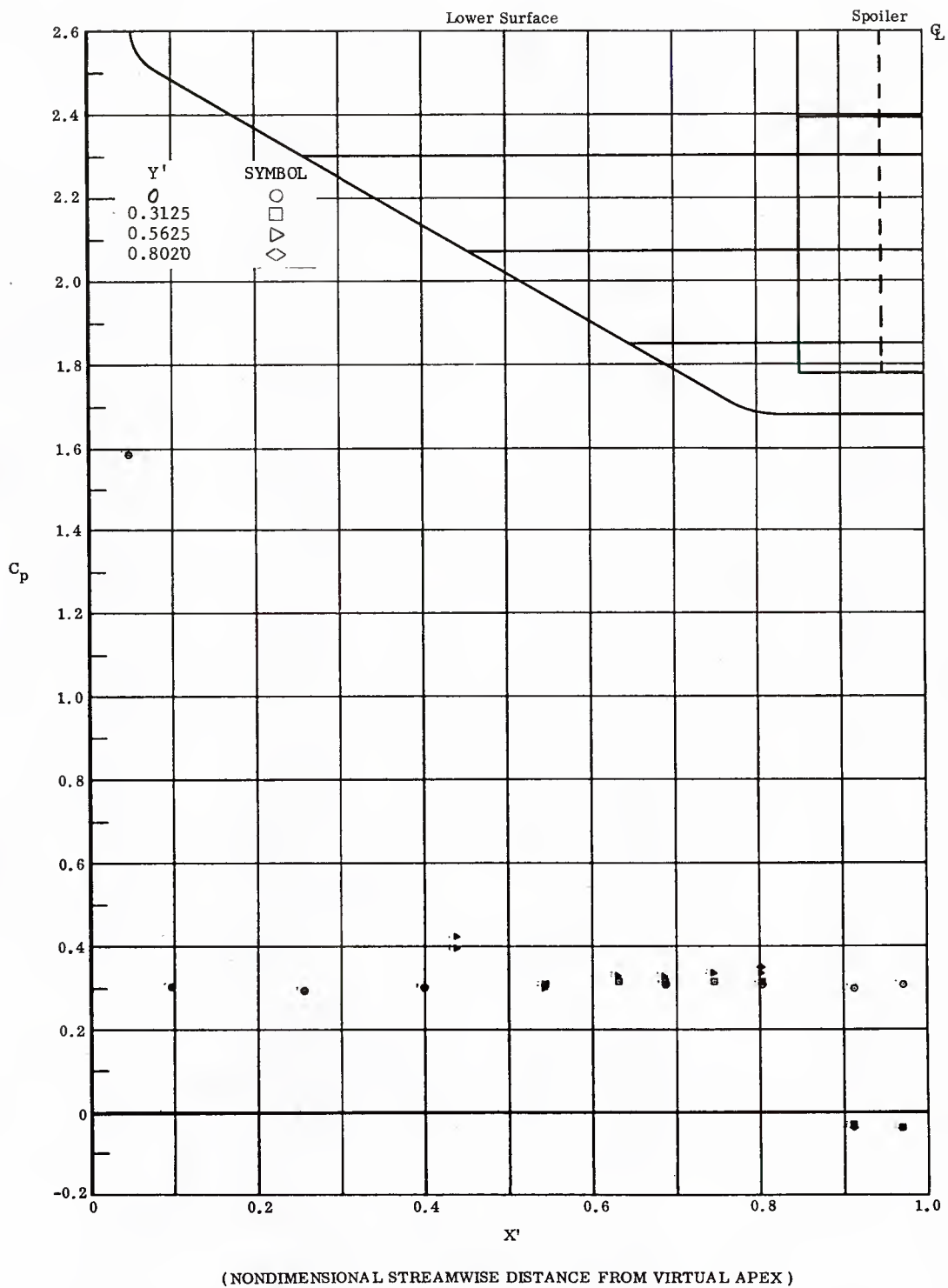
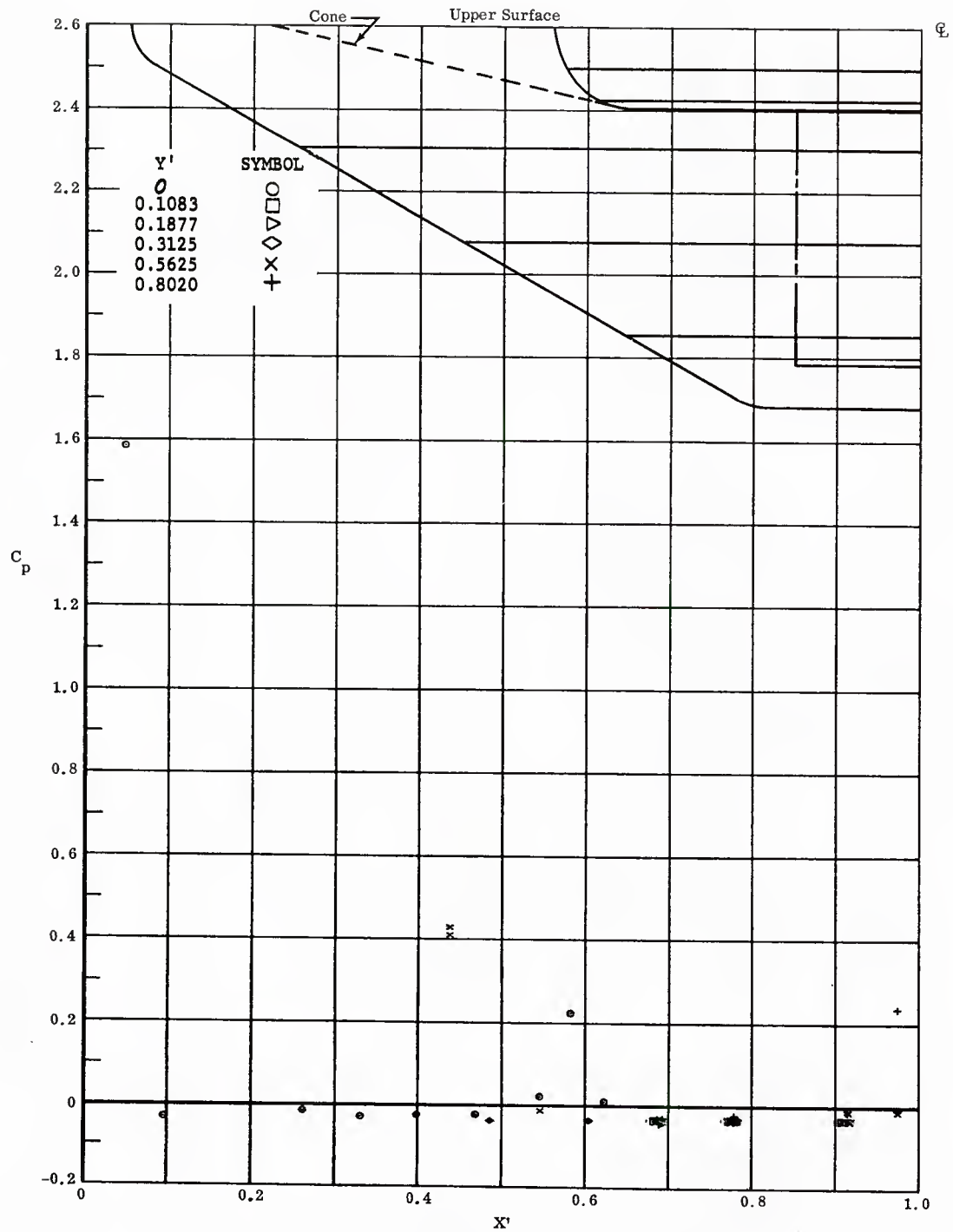


Fig. 32 Streamwise Pressure Distributions on Lower Surface; Left and Right Flaps Deflected  $-40^\circ$ ,  $\alpha = +20^\circ$ .



( NONDIMENSIONAL STREAMWISE DISTANCE FROM VIRTUAL APEX )

Fig. 32 Streamwise Pressure Distributions on Upper Surface; Left and Right Flaps Deflected  $-40^\circ$ ,  $\alpha = +20^\circ$ .

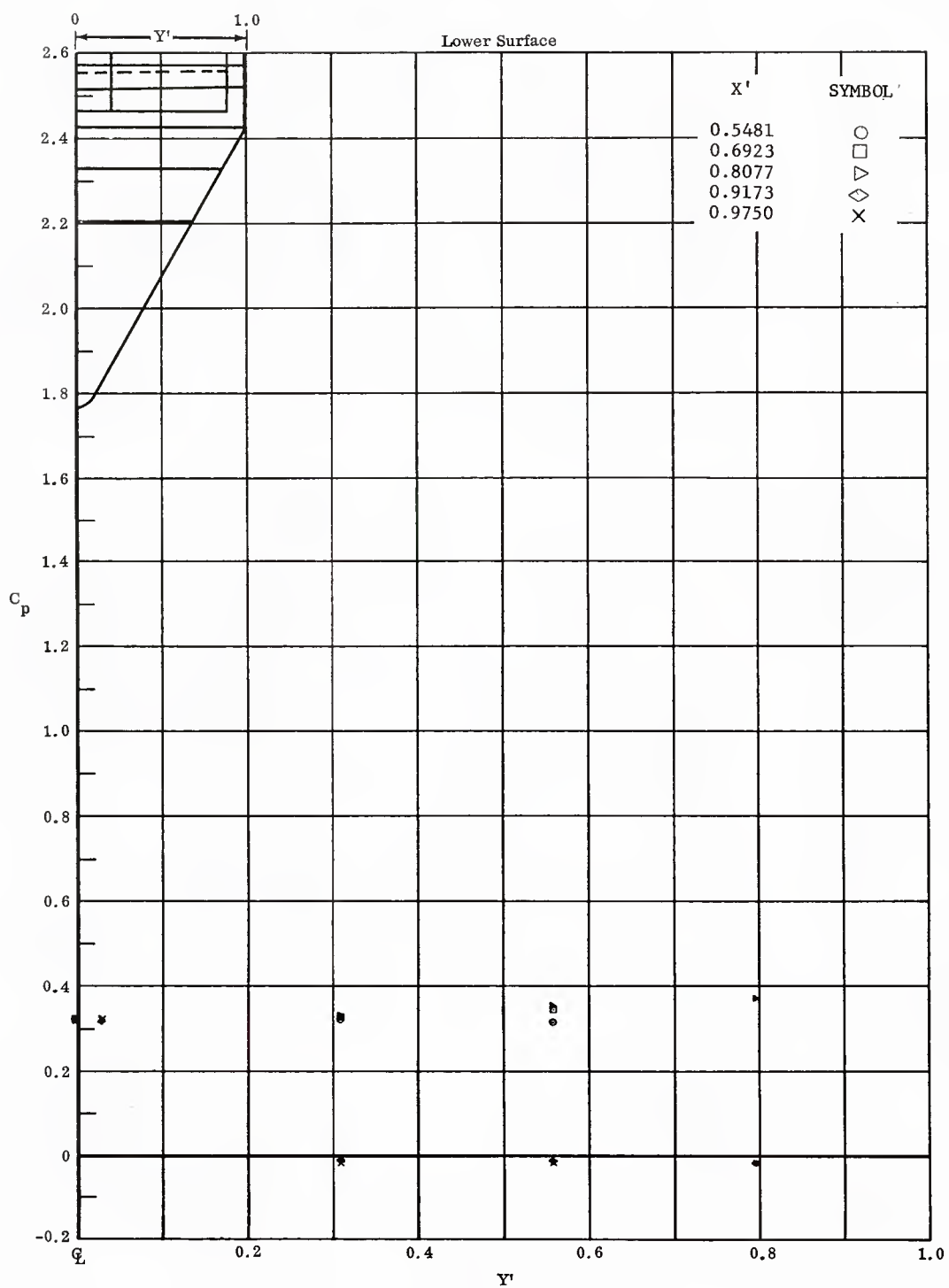


Fig. 32 Spanwise Pressure Distributions on Lower Surface; Left and Right Flaps Deflected  $-40^\circ$ ,  $\alpha = +20^\circ$ .



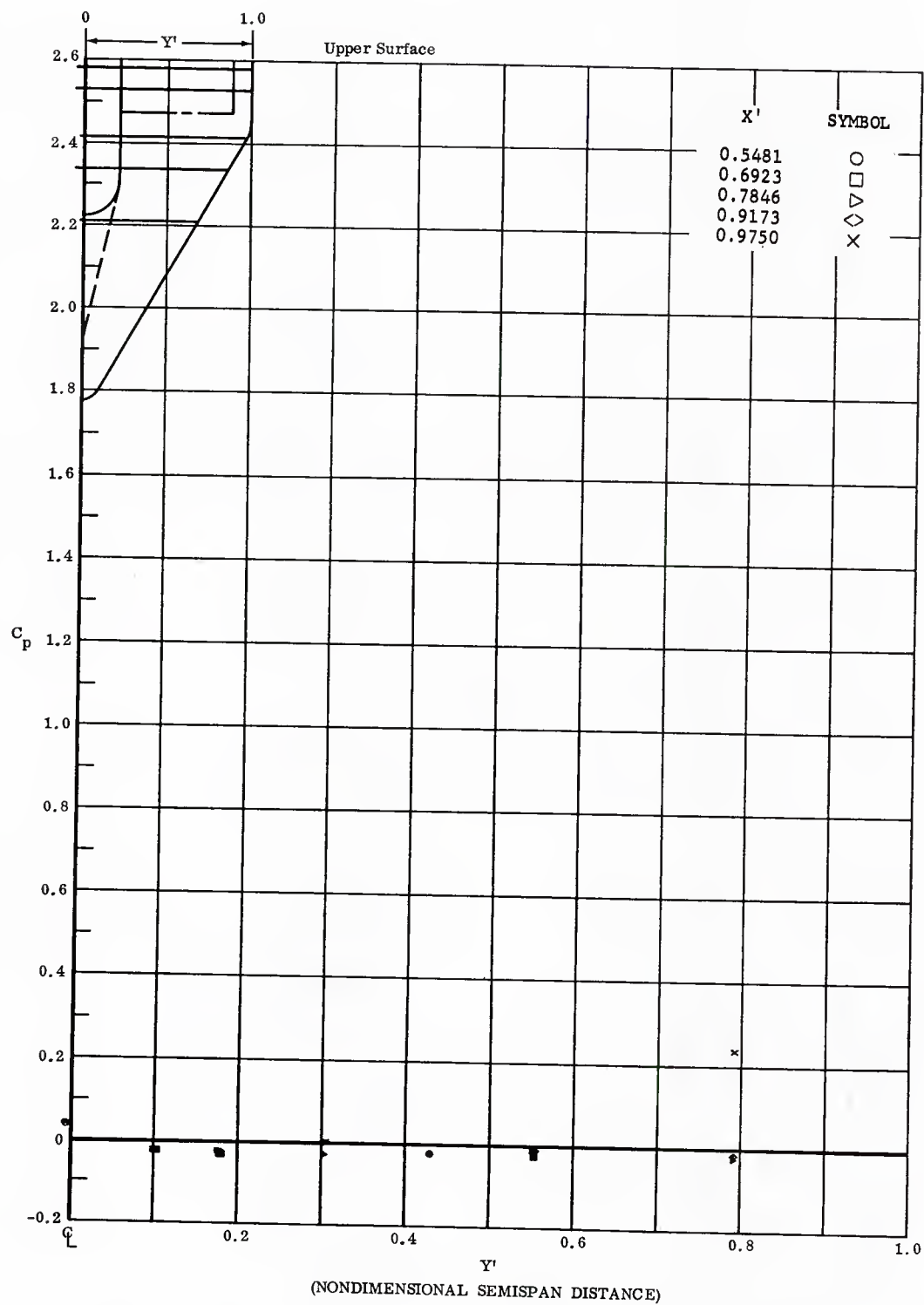
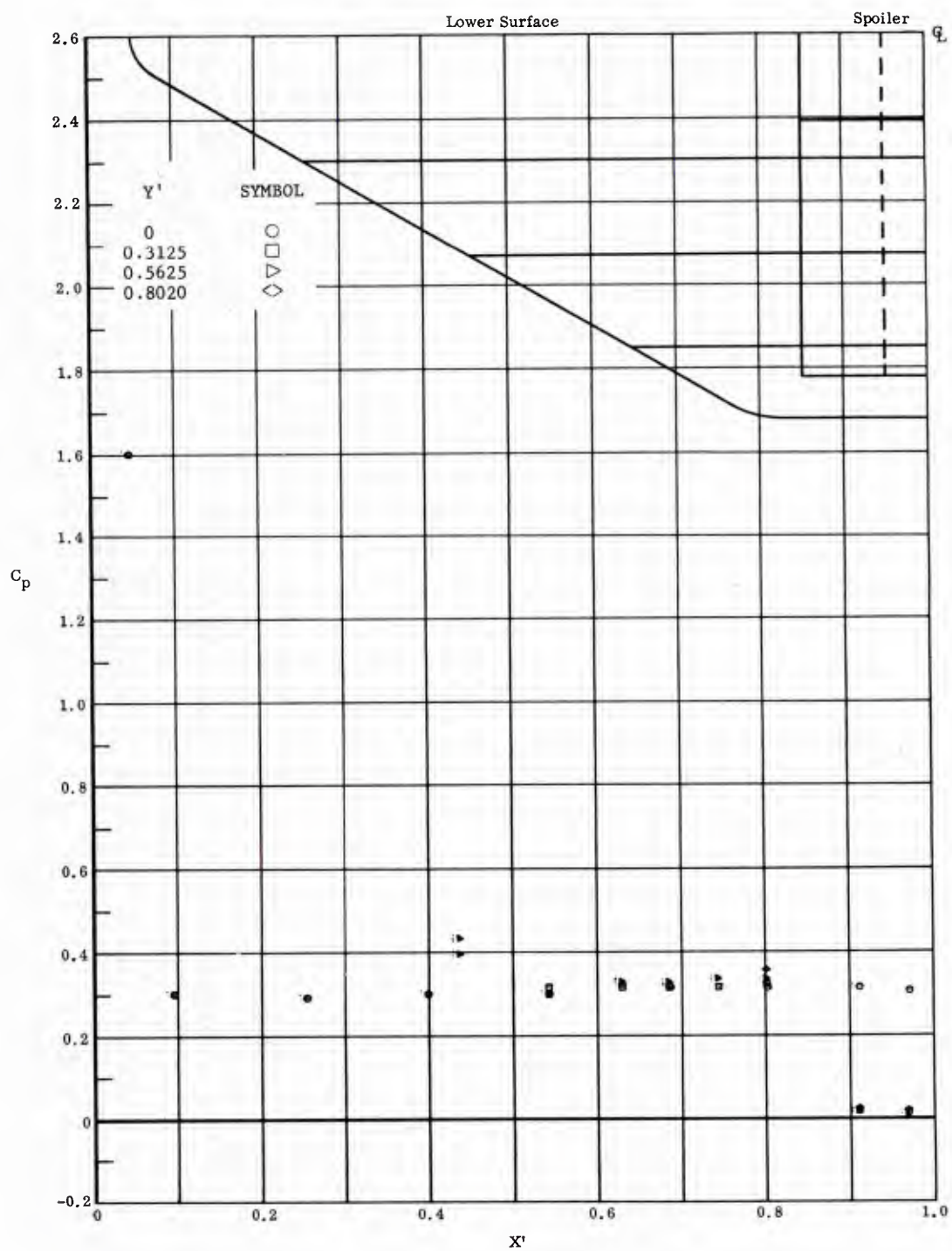


Fig. 32 Spanwise Pressure Distributions on Upper Surface; Left and Right Flaps Deflected  $-40^\circ$ ,  $\alpha = +20^\circ$ .



(NONDIMENSIONAL STREAMWISE DISTANCE FROM VIRTUAL APEX)

Fig. 33 Streamwise Pressure Distributions on Lower Surface; Left and Right Flaps Deflected  $-20^\circ$ ,  $\alpha = +20^\circ$ .

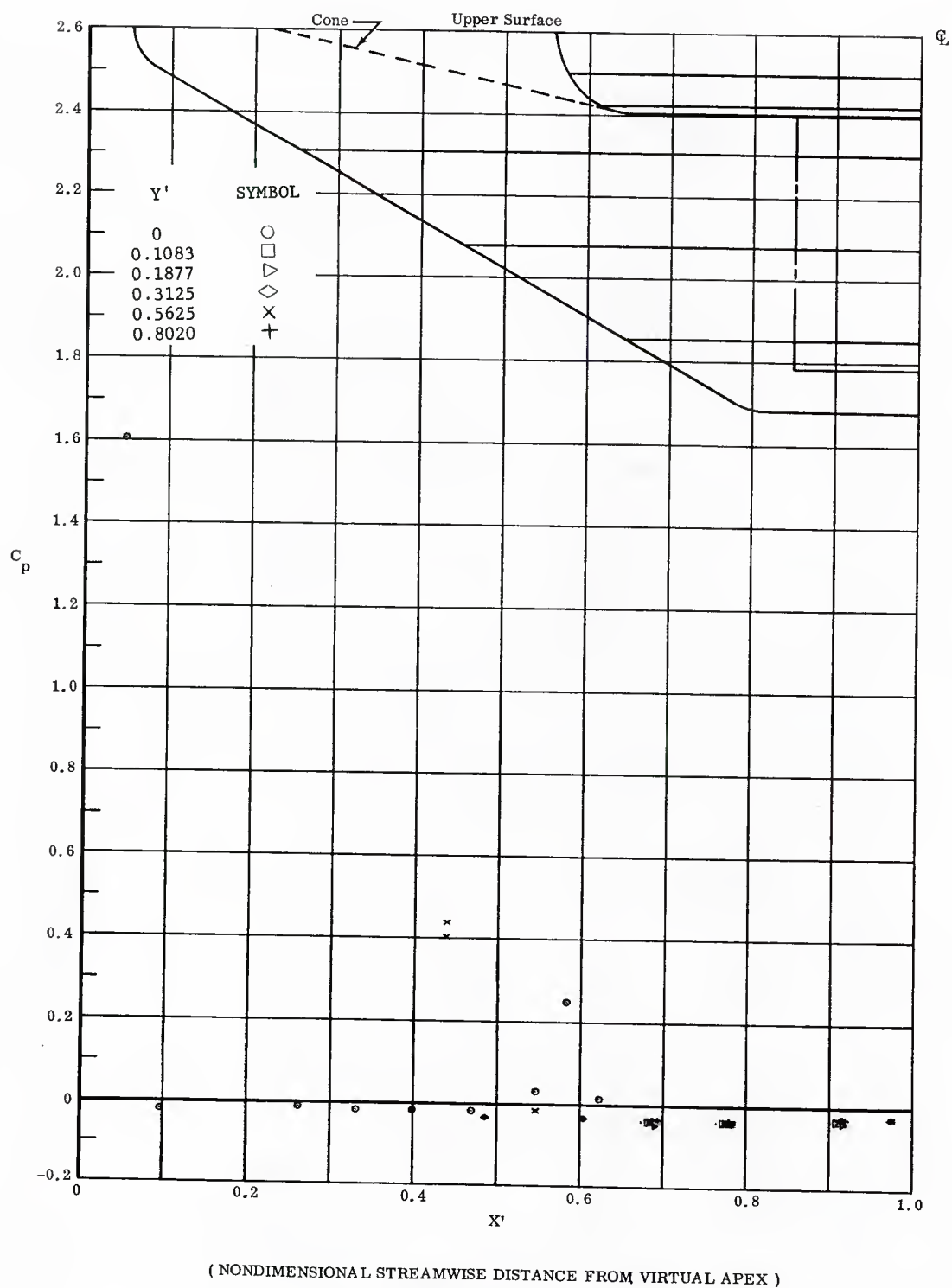
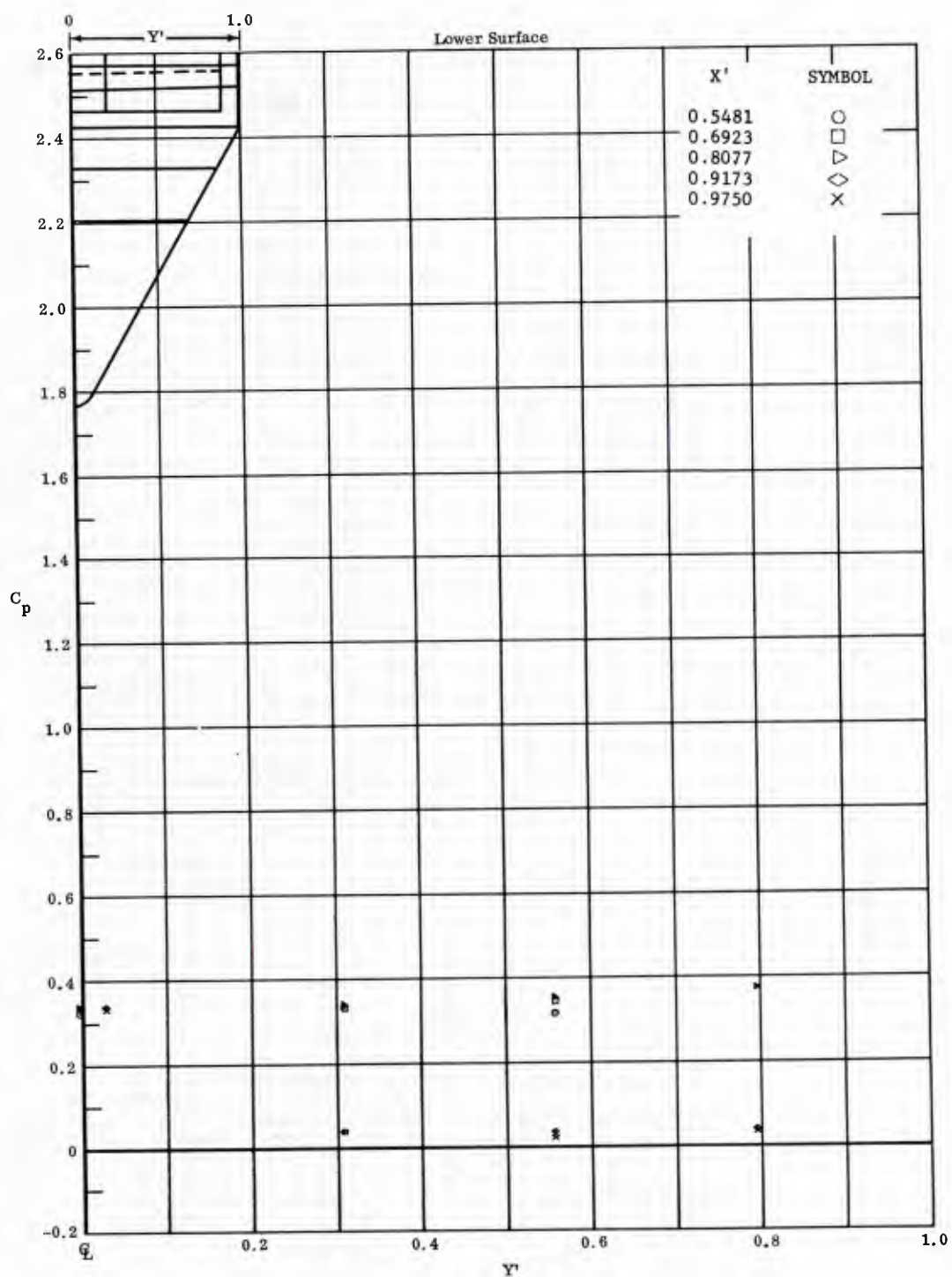


Fig. 33 Streamwise Pressure Distributions on Upper Surface; Left and Right Flaps Deflected  $-20^\circ$ ,  $\alpha = +20^\circ$ .



(NONDIMENSIONAL SEMISPAN DISTANCE)

Fig. 33 Spanwise Pressure Distributions on Lower Surface; Left and Right Flaps Deflected  $-20^\circ$ ,  $\alpha = +20^\circ$ .

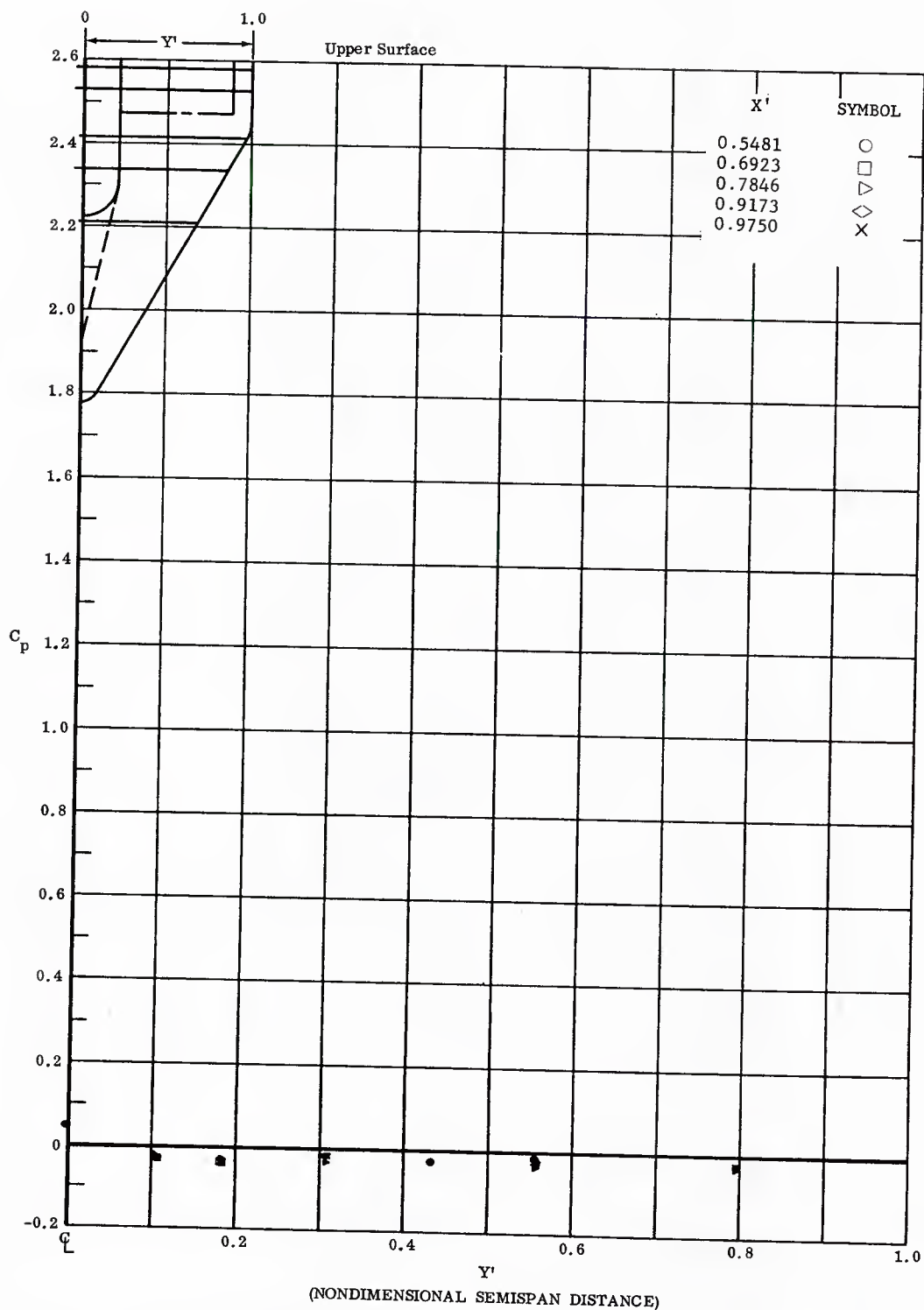


Fig. 33 Spanwise Pressure Distributions on Upper Surface; Left and Right Flaps Deflected  $-20^\circ$ ,  $\alpha = +20^\circ$ .

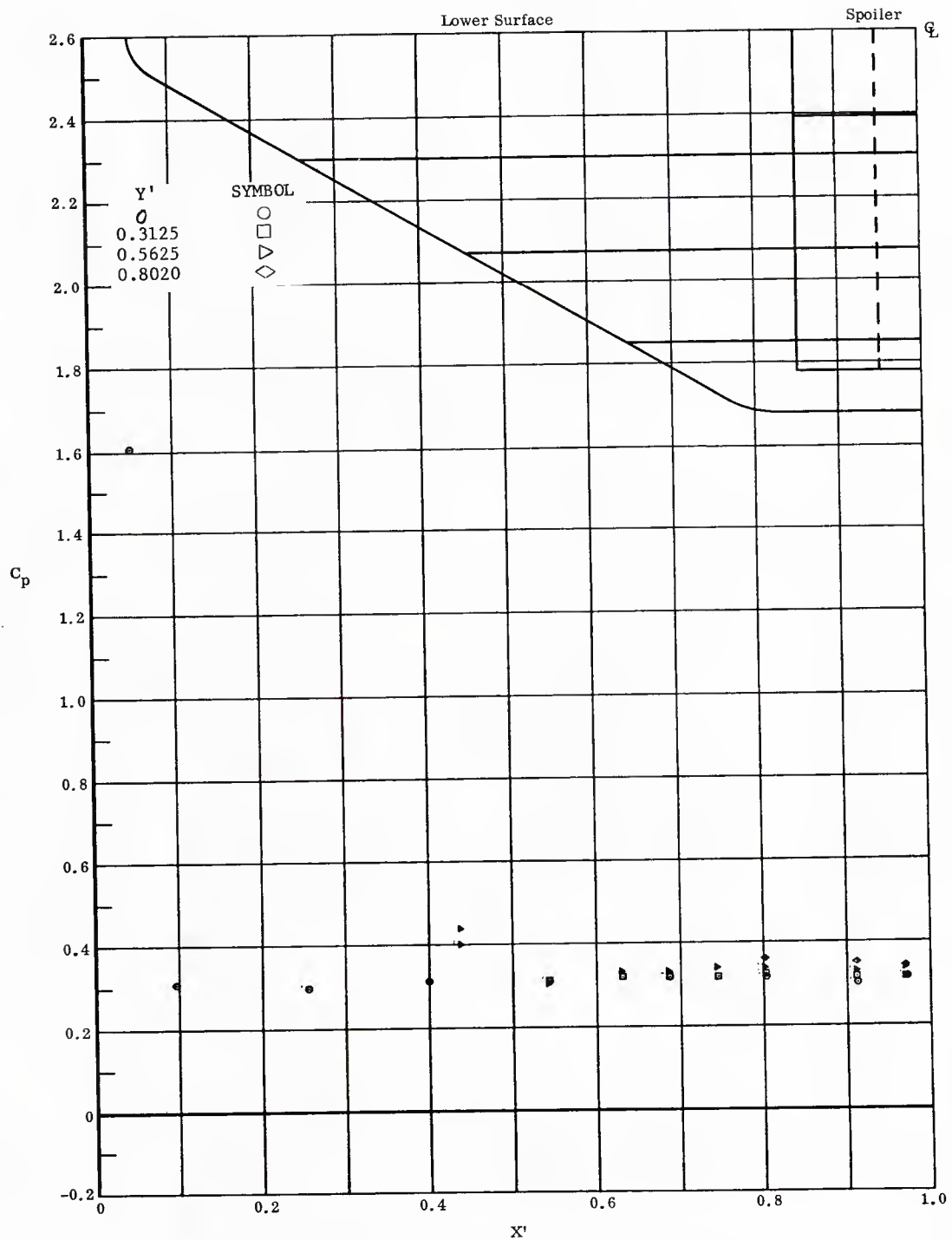
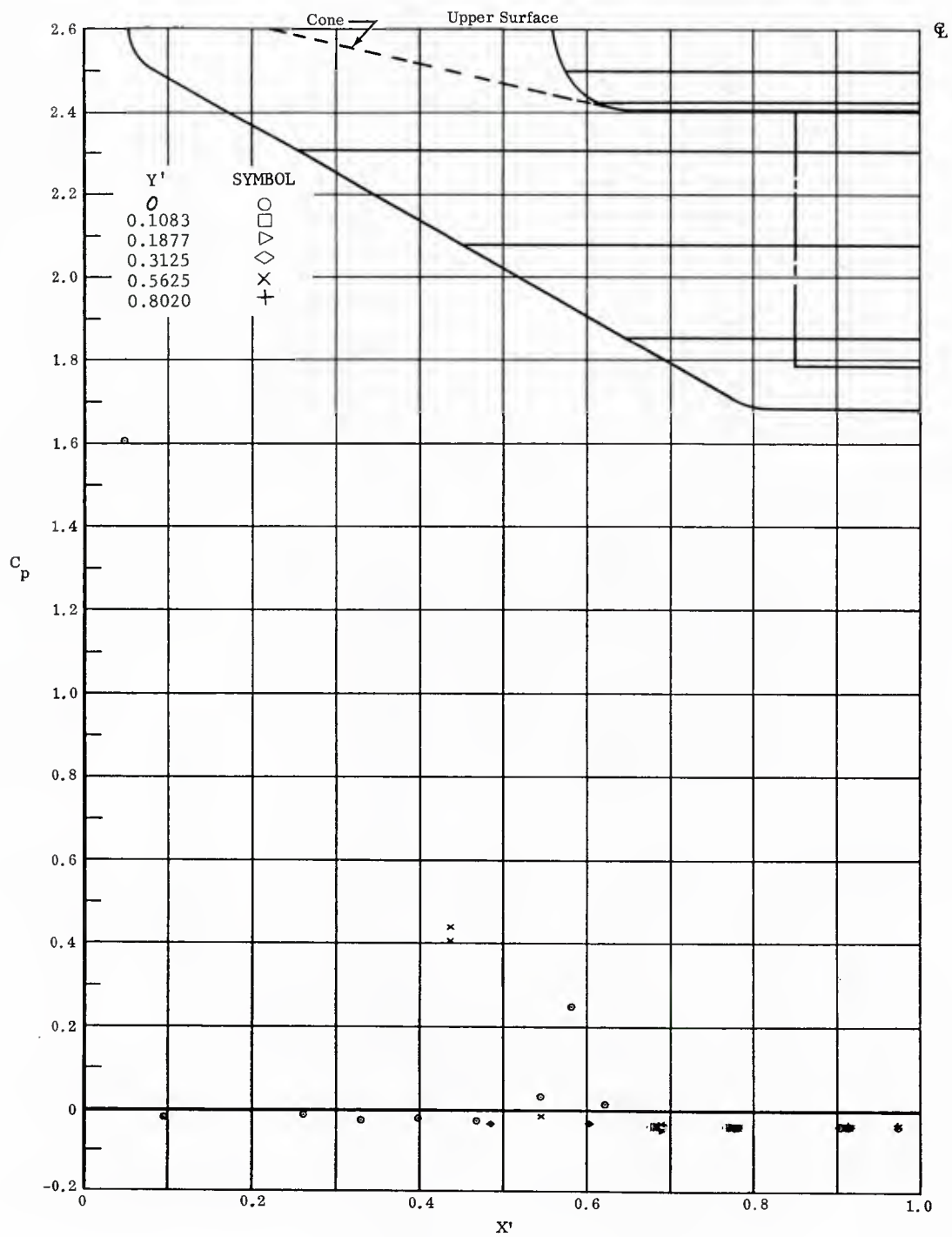


Fig. 34 Streamwise Pressure Distributions on Lower Surface; No Flaps Deflected,  $\alpha = +20^\circ$ .



( NONDIMENSIONAL STREAMWISE DISTANCE FROM VIRTUAL APEX )

Fig. 34 Streamwise Pressure Distributions on Upper Surface; No Flaps Deflected,  $\alpha = +20^\circ$ .

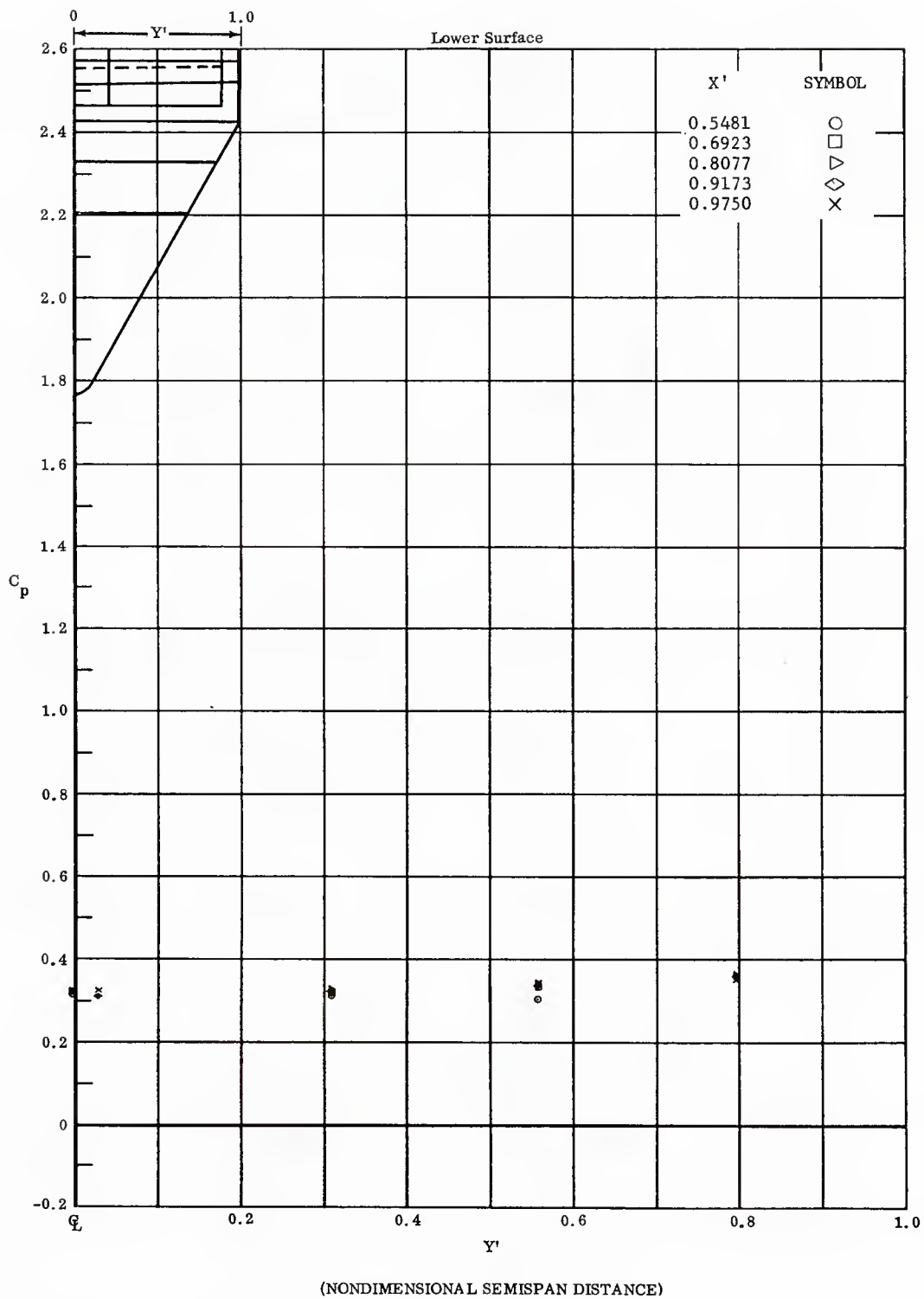


Fig. 34 Spanwise Pressure Distributions on Lower Surface; No Flaps Deflected,  $\alpha = +20^\circ$ .



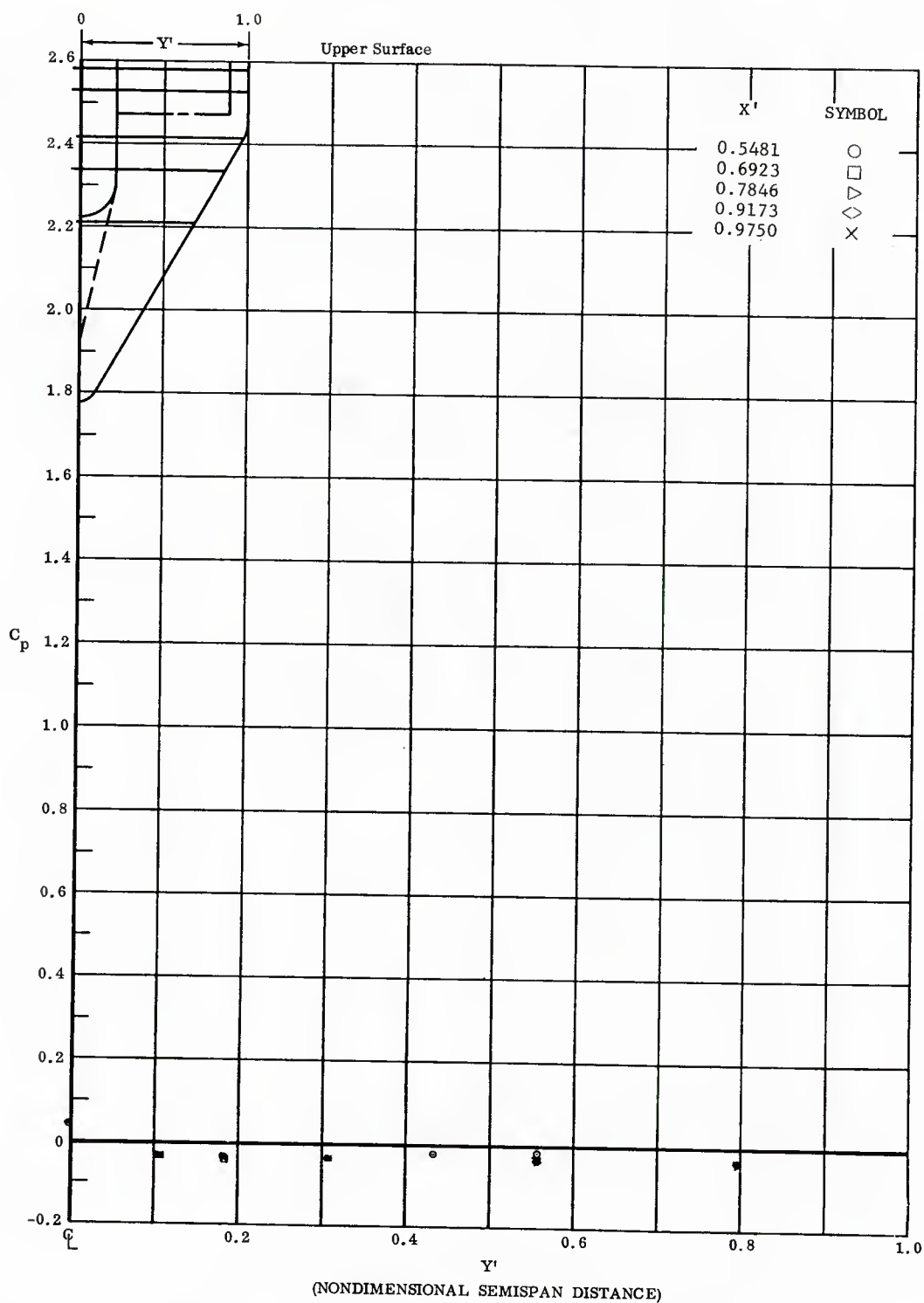


Fig. 34 Spanwise Pressure Distributions on Upper Surface; No Flaps Deflected,  $\alpha = +20^\circ$ .

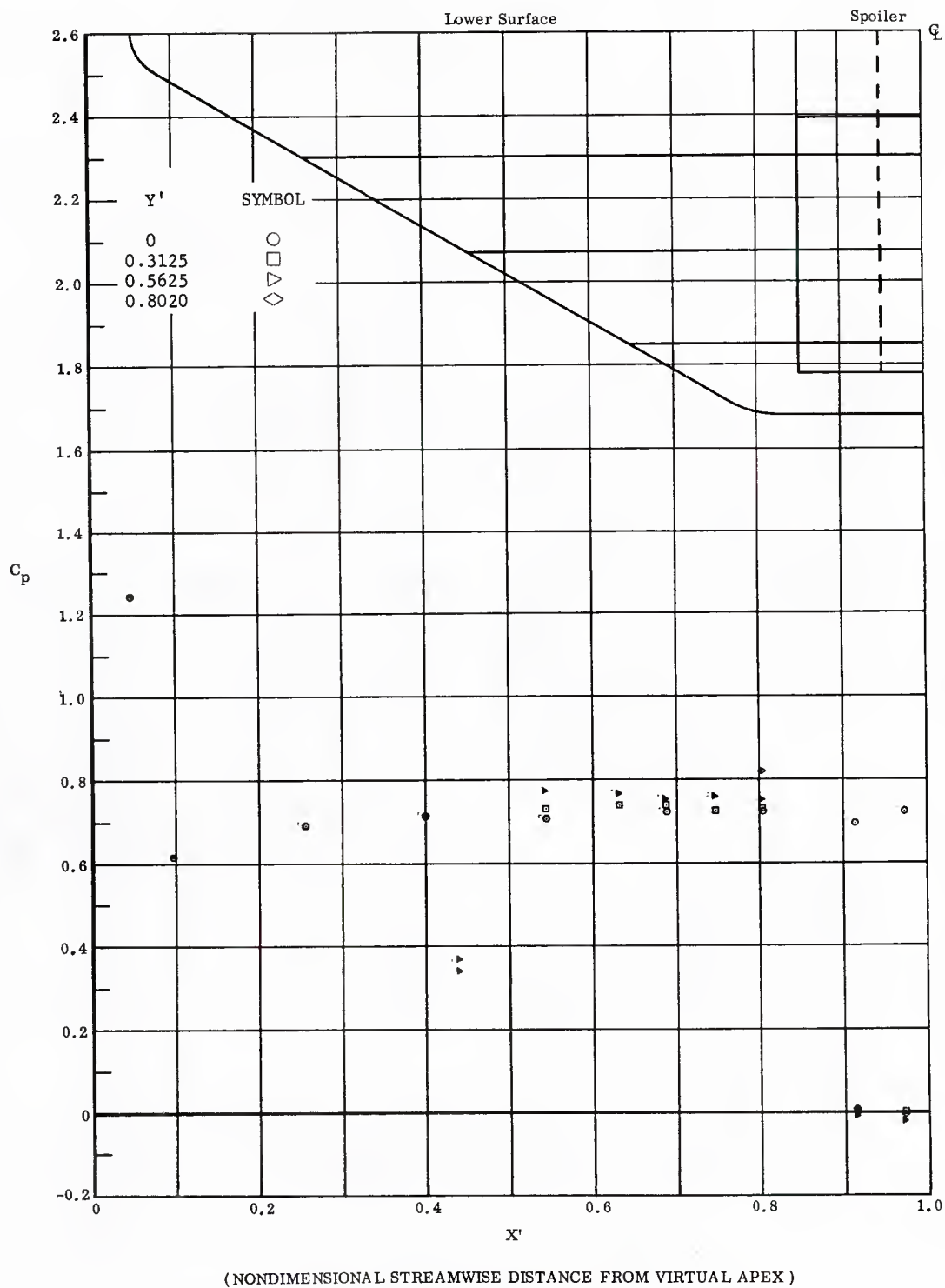
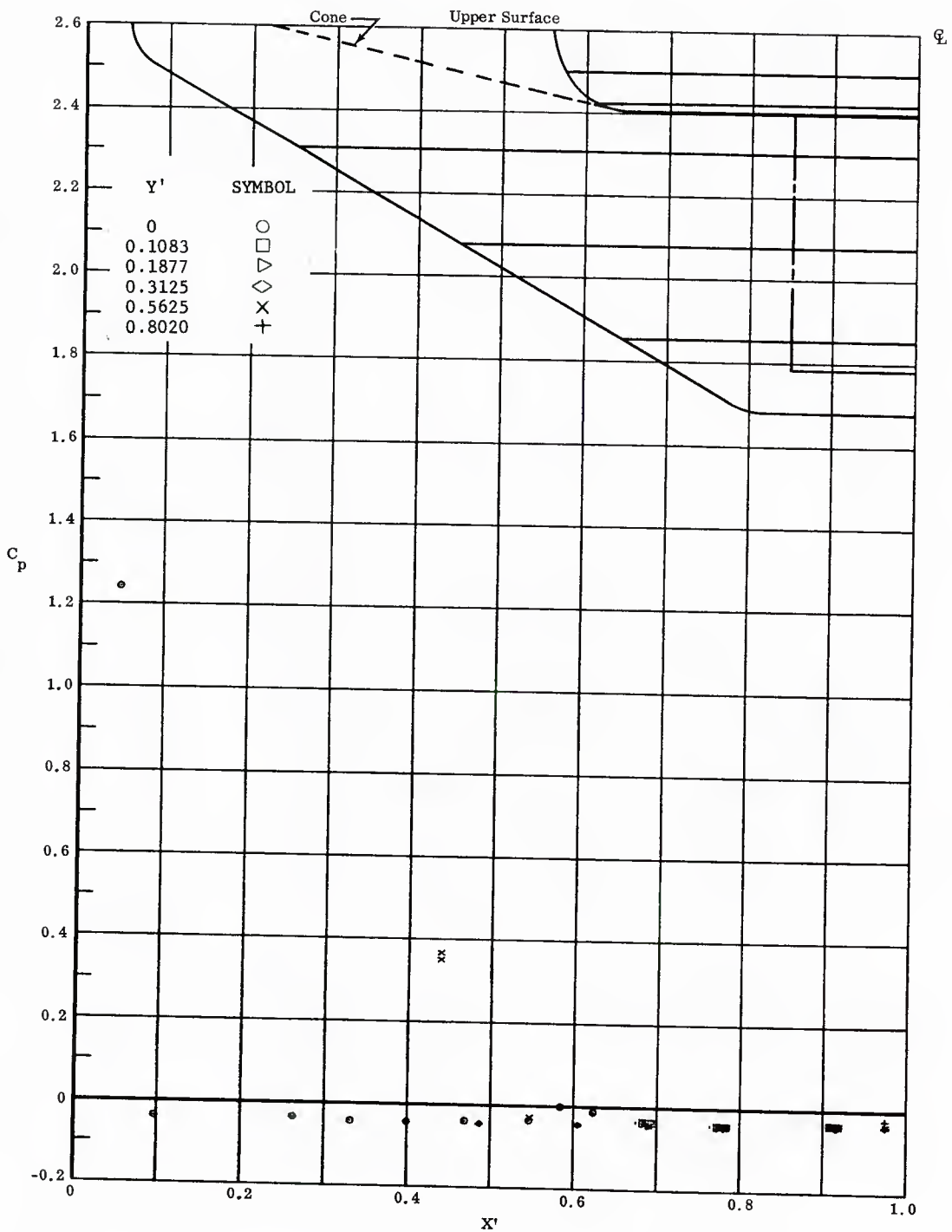


Fig. 35 Streamwise Pressure Distributions on Lower Surface; Left and Right Flaps Deflected  $-40^\circ$ ,  $\alpha = +33^\circ$ .



(NONDIMENSIONAL STREAMWISE DISTANCE FROM VIRTUAL APEX )

Fig. 35 Streamwise Pressure Distributions on Upper Surface; Left and Right Flaps Deflected  $-40^\circ$ ,  $\alpha = +33^\circ$ .

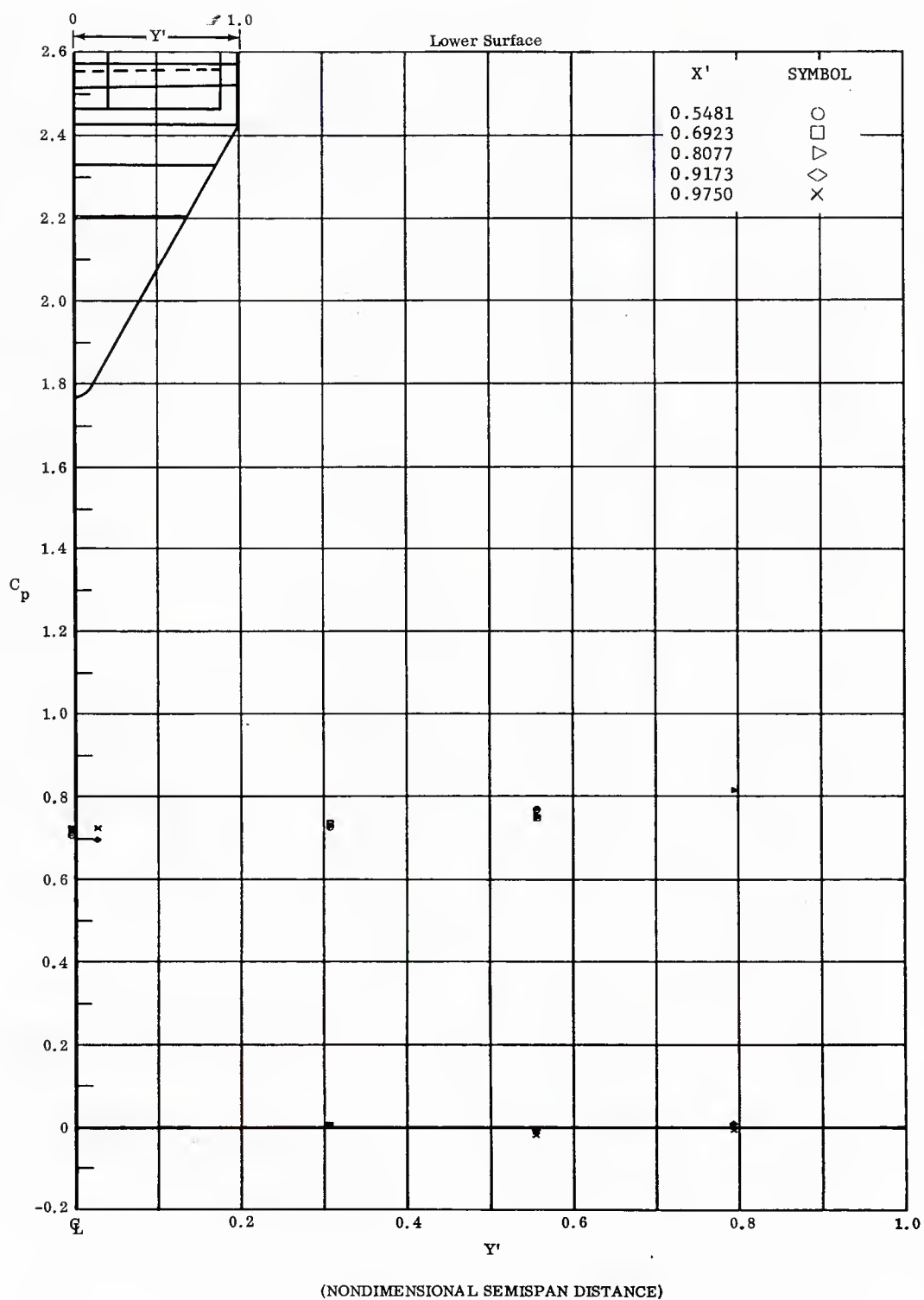


Fig. 35 Spanwise Pressure Distributions on Lower Surface; Left and Right Flaps Deflected  $-40^\circ$ ,  $\alpha = +33^\circ$ .

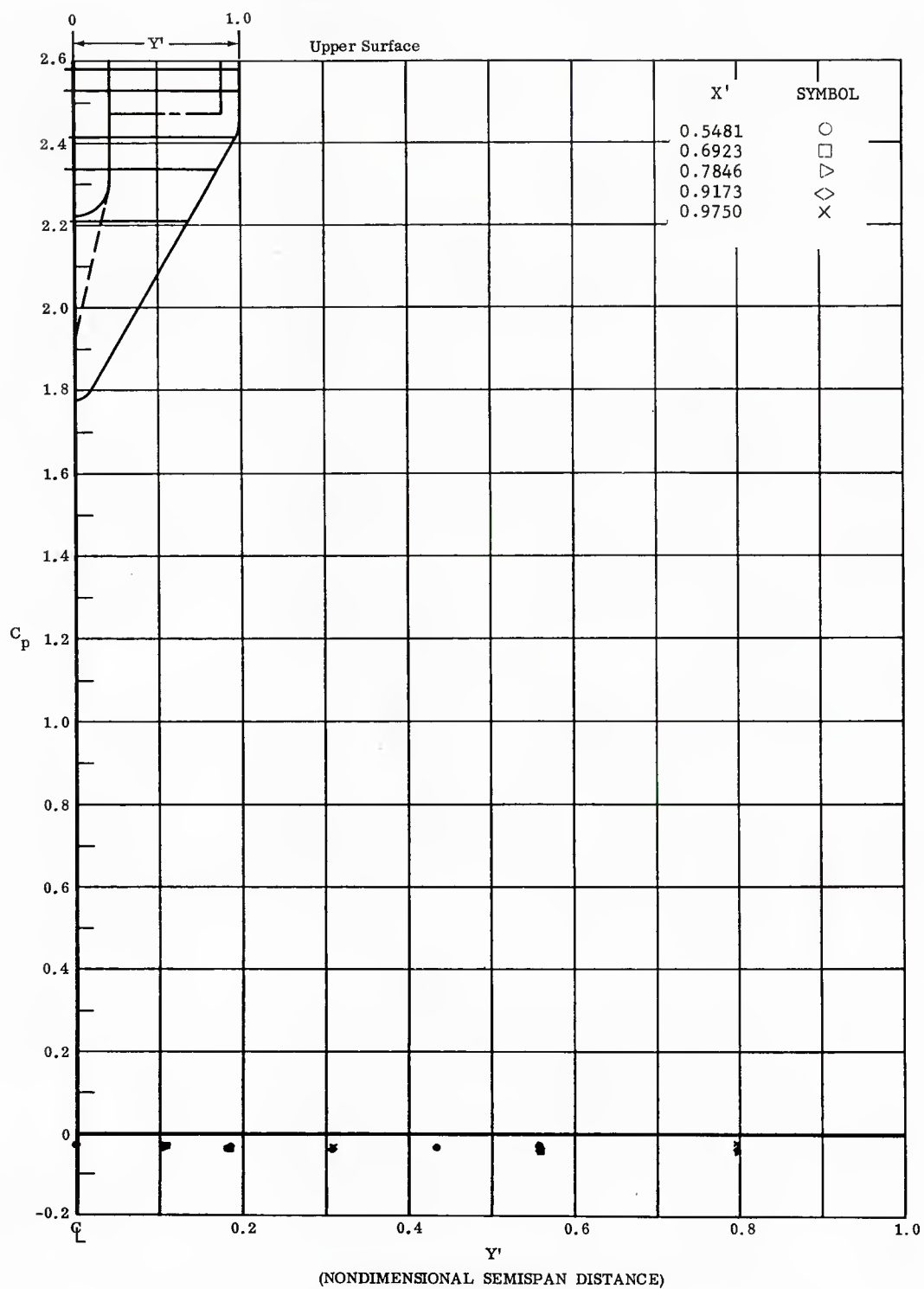


Fig. 35 Spanwise Pressure Distributions on Upper Surface; Left and Right Flaps Deflected  $-40^\circ$ ,  $\alpha = +33^\circ$ .

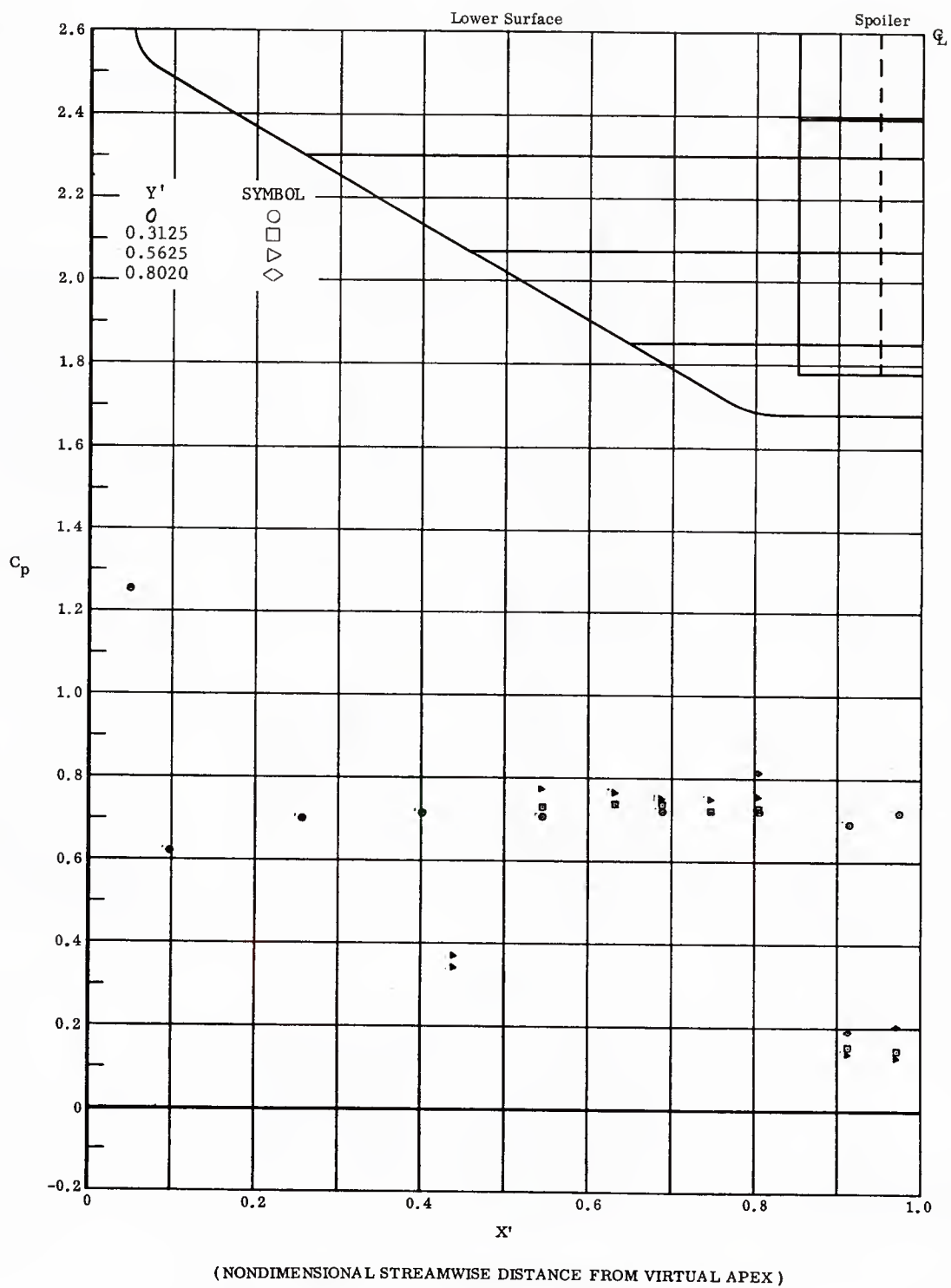


Fig. 36 Streamwise Pressure Distributions on Lower Surface; Left and Right Flaps Deflected  $-20^\circ$ ,  $\alpha = +33^\circ$ .

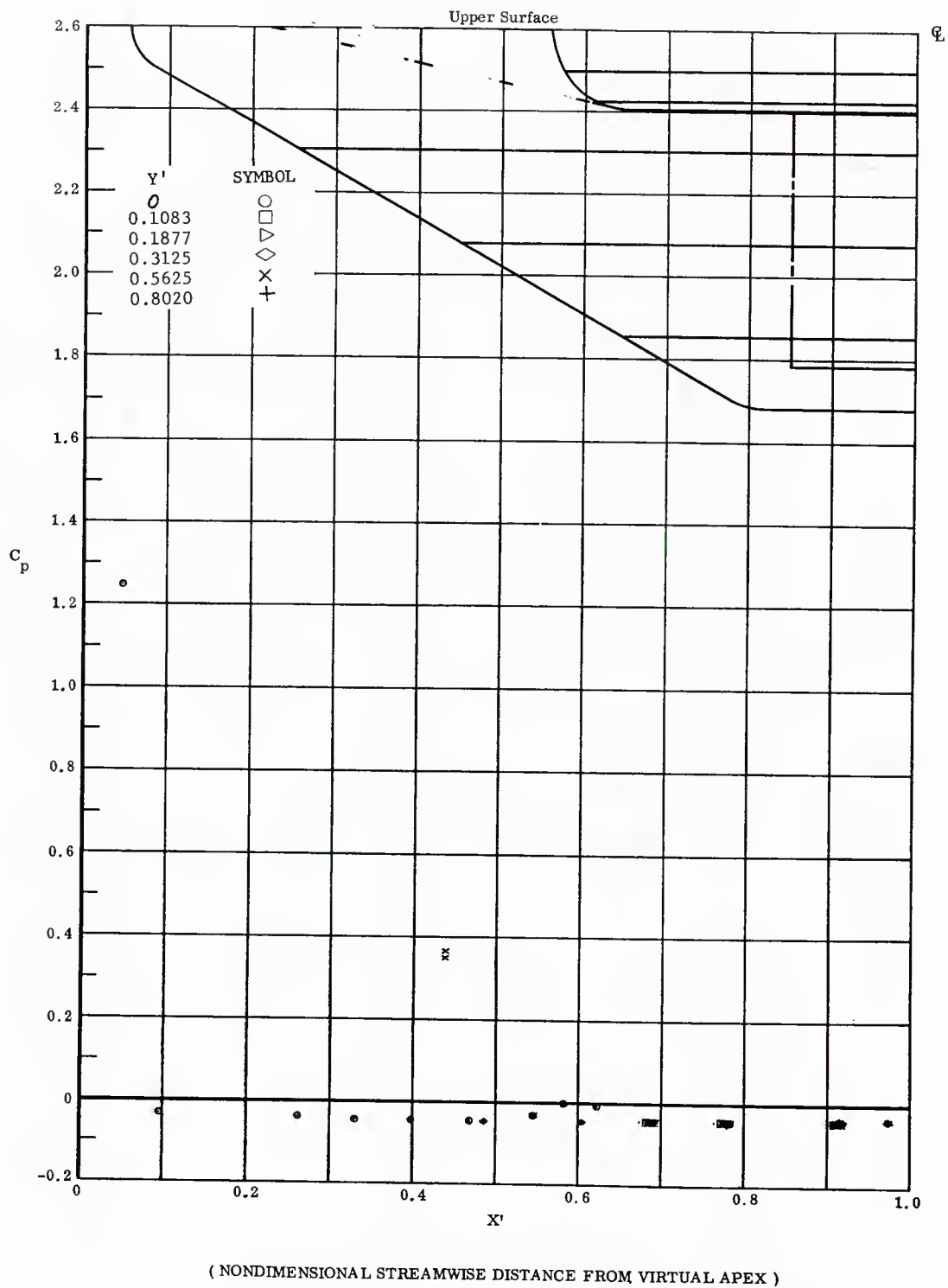


Fig. 36 Streamwise Pressure Distributions on Upper Surface; Left and Right Flaps Deflected  $-20^\circ$ ,  $\alpha = +33^\circ$ .

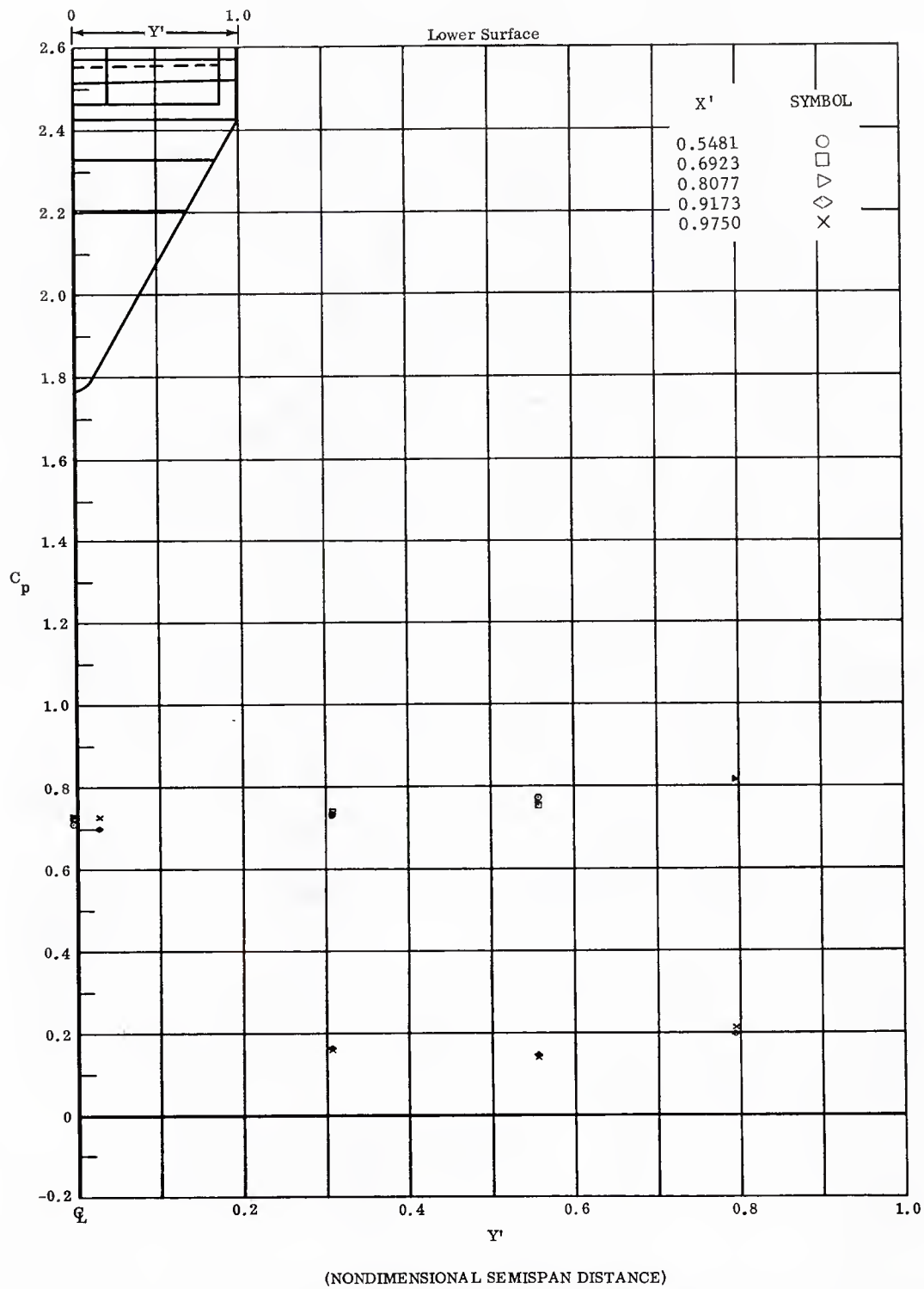


Fig. 36 Spanwise Pressure Distributions on Lower Surface; Left and Right Flaps Deflected  $-20^\circ$ .  $\alpha = +33^\circ$ .



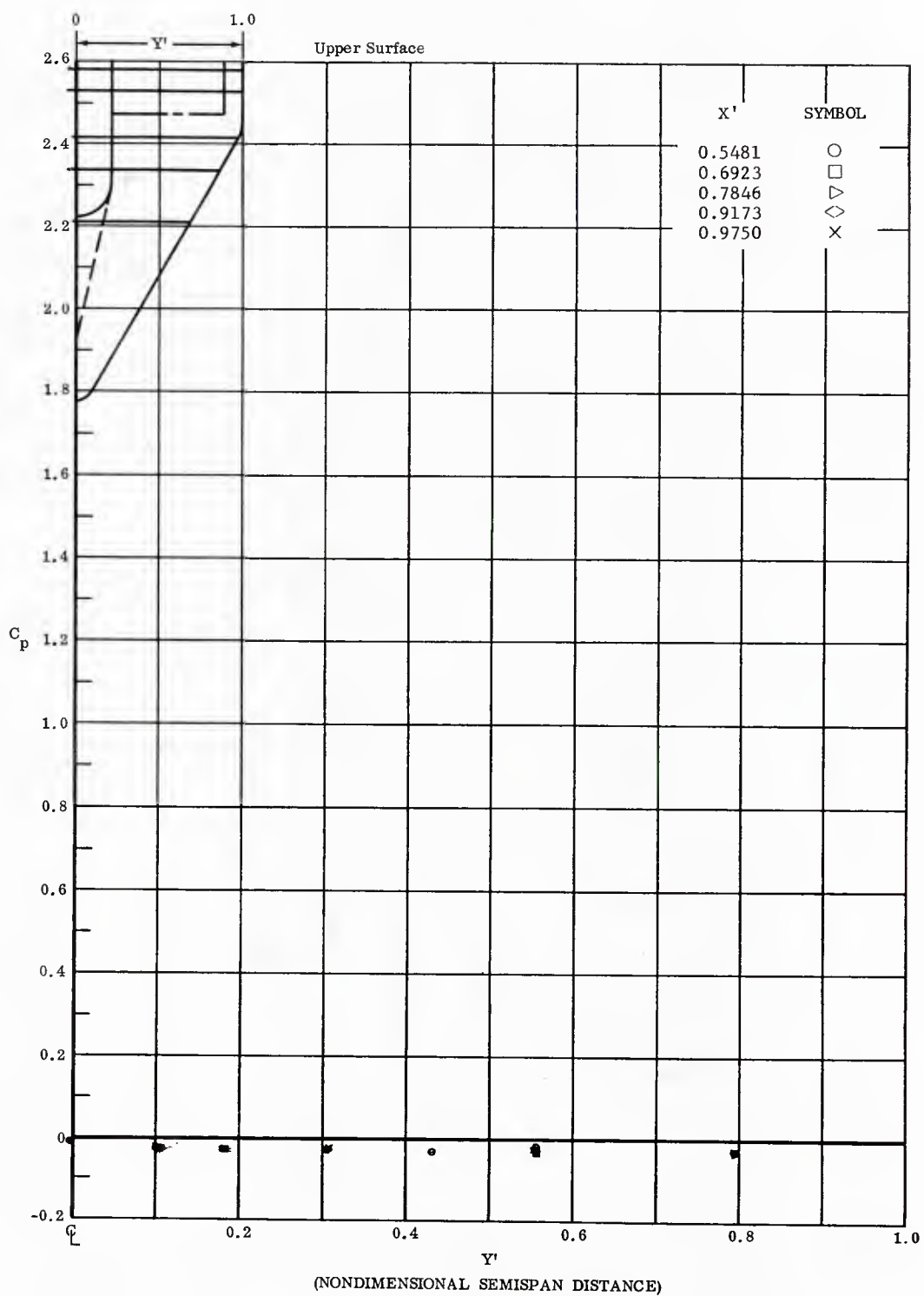


Fig. 36 Spanwise Pressure Distributions on Upper Surface; Left and Right Flaps Deflected  $-20^\circ$ ,  $\alpha = +33^\circ$ .

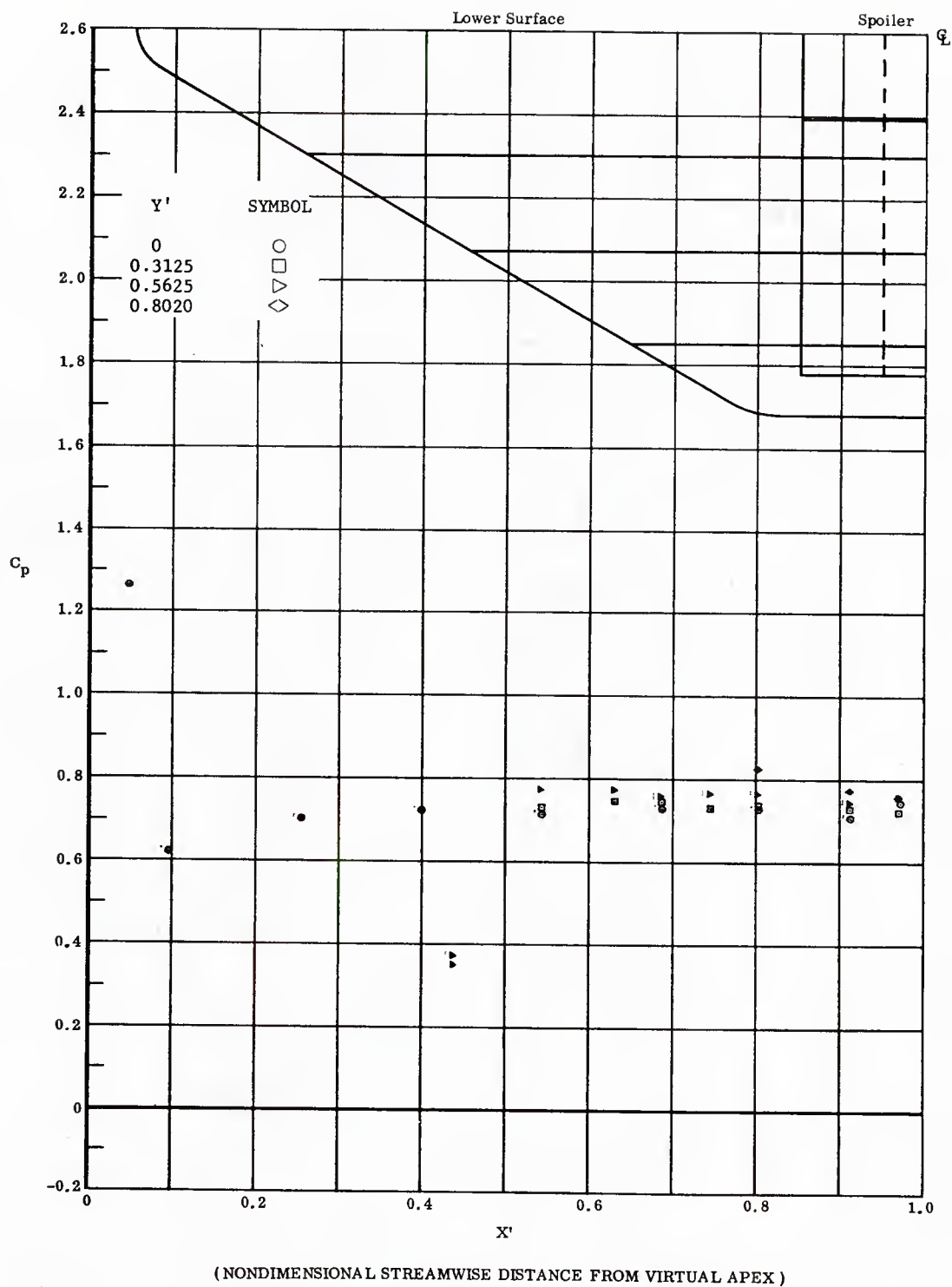
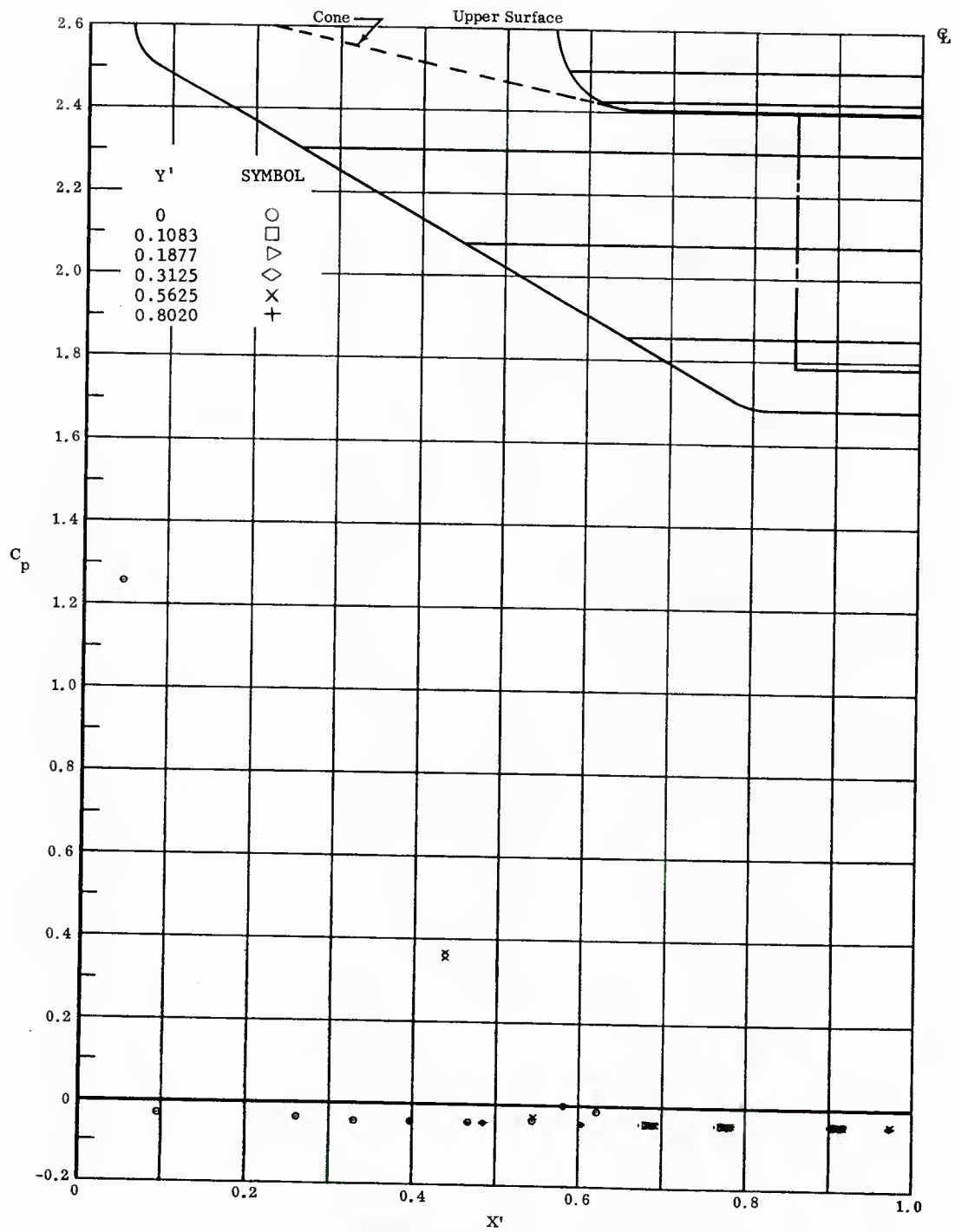


Fig. 37 Streamwise Pressure Distributions on Lower Surface; No Flap Deflections,  $\alpha = +33^\circ$ .



( NONDIMENSIONAL STREAMWISE DISTANCE FROM VIRTUAL APEX )

Fig. 37 Streamwise Pressure Distributions on Upper Surface; No Flap Deflections,  $\alpha = +33^\circ$ .

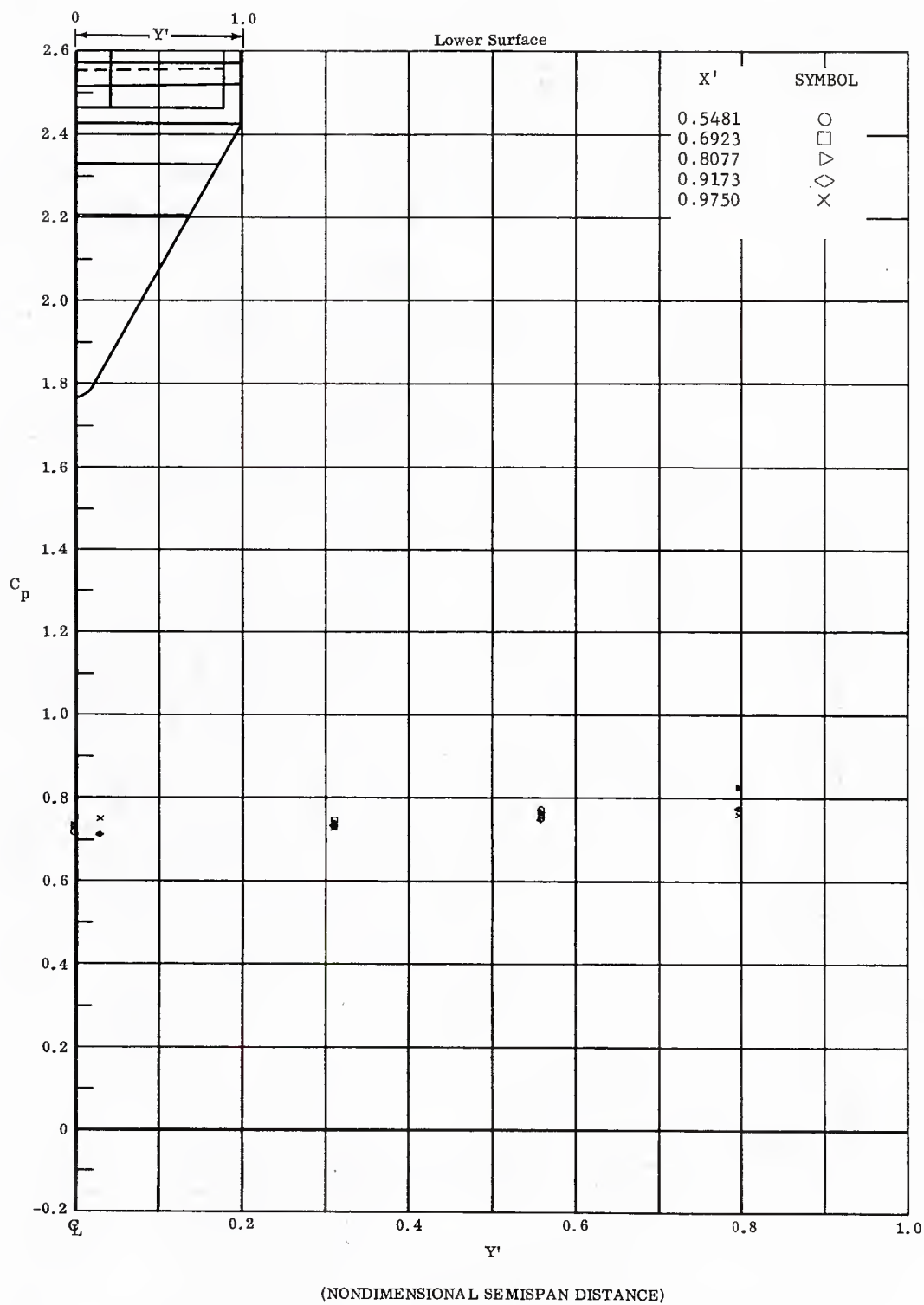


Fig. 37 Spanwise Pressure Distributions on Lower Surface; No Flap Deflections,  $\alpha = +33^\circ$ .

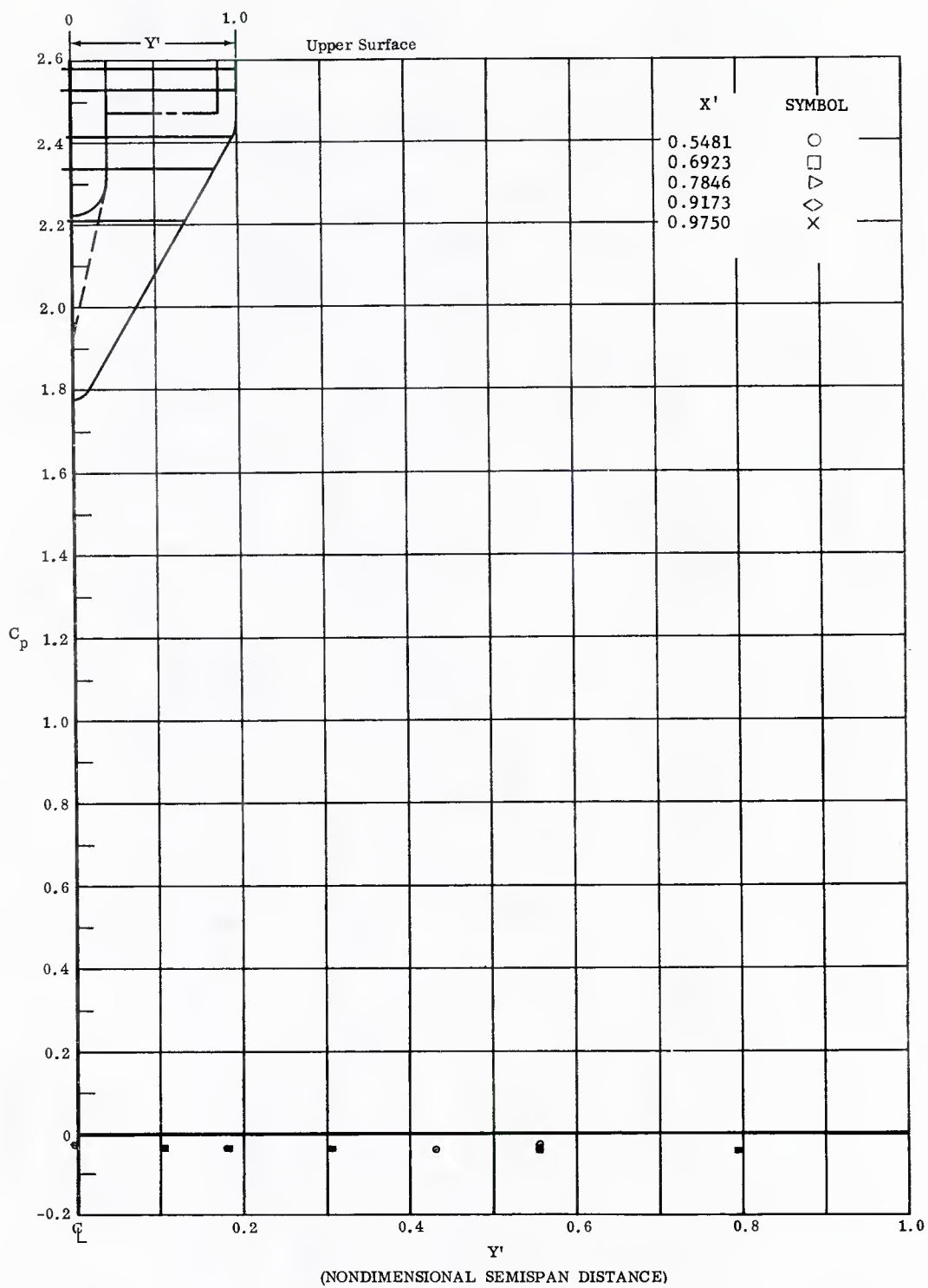


Fig. 37 Spanwise Pressure Distributions on Upper Surface; No Flap Deflections,  $\alpha = +33^\circ$ .

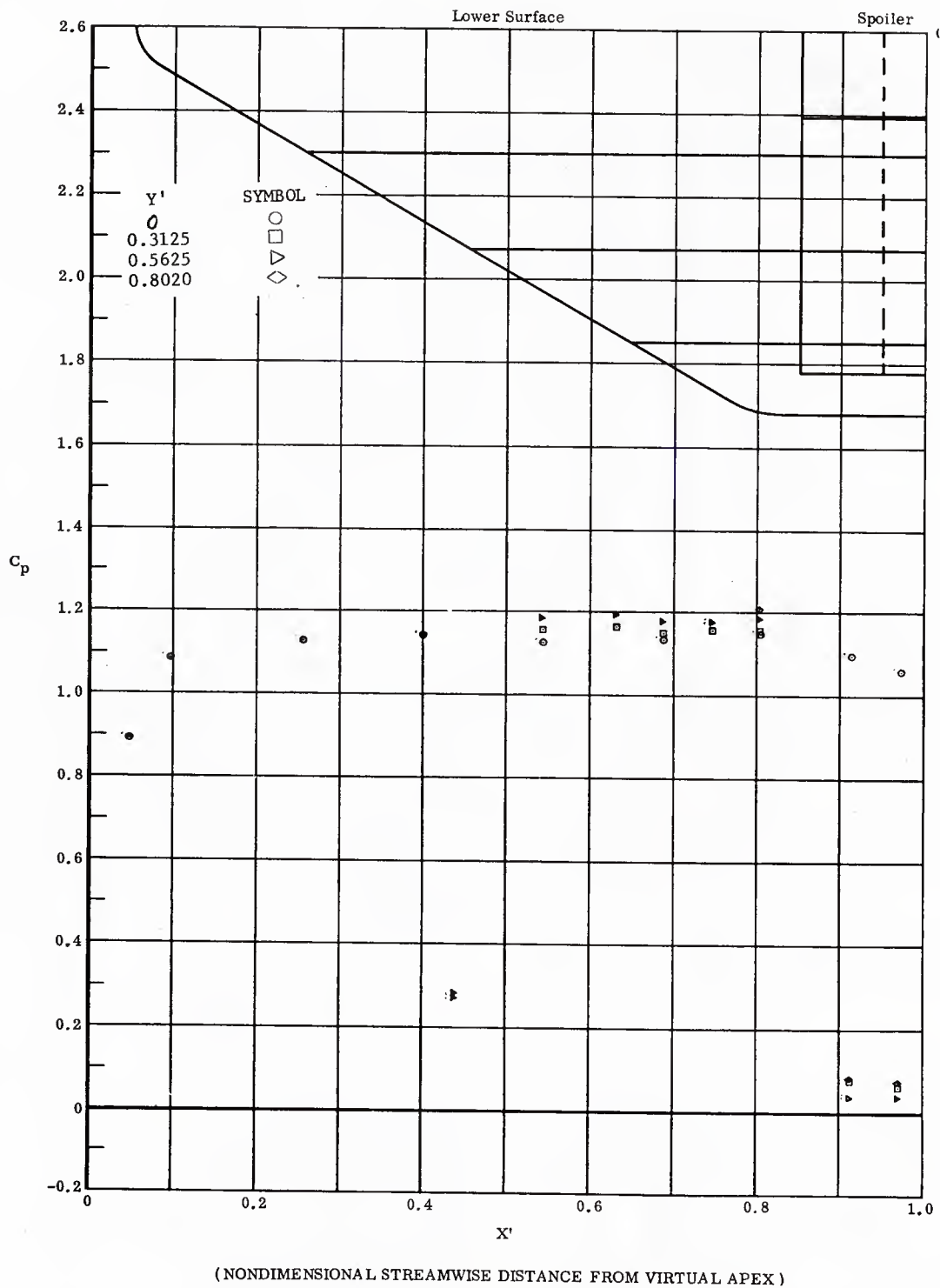
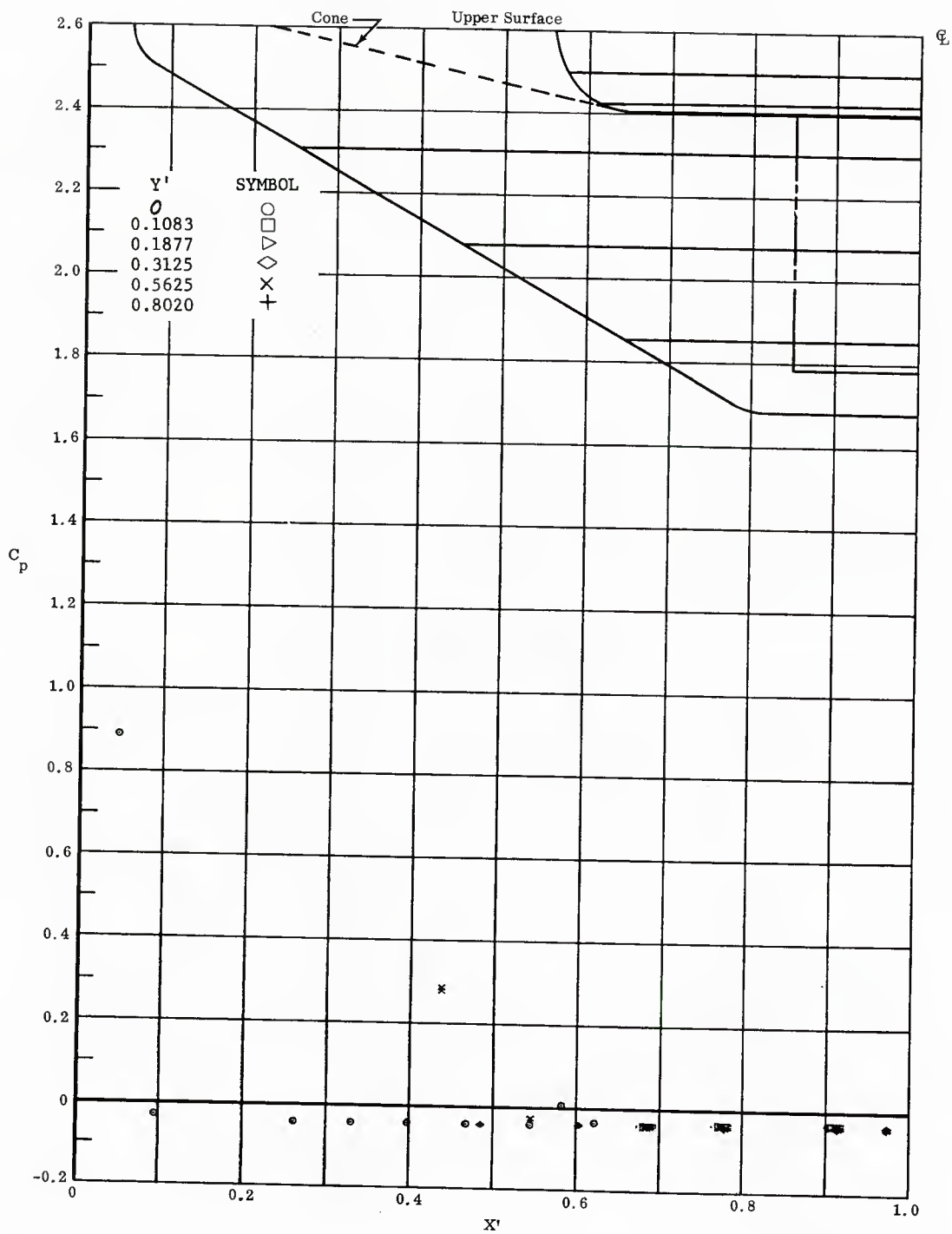


Fig. 38 Streamwise Pressure Distributions on Lower Surface; Left and Right Flaps Deflected  $-40^\circ$ ,  $\alpha = +45^\circ$ .



( NONDIMENSIONAL STREAMWISE DISTANCE FROM VIRTUAL APEX )

Fig. 38 Streamwise Pressure Distributions on Upper Surface; Left and Right Flaps Deflected  $-40^\circ$ ,  $\alpha = +45^\circ$ .

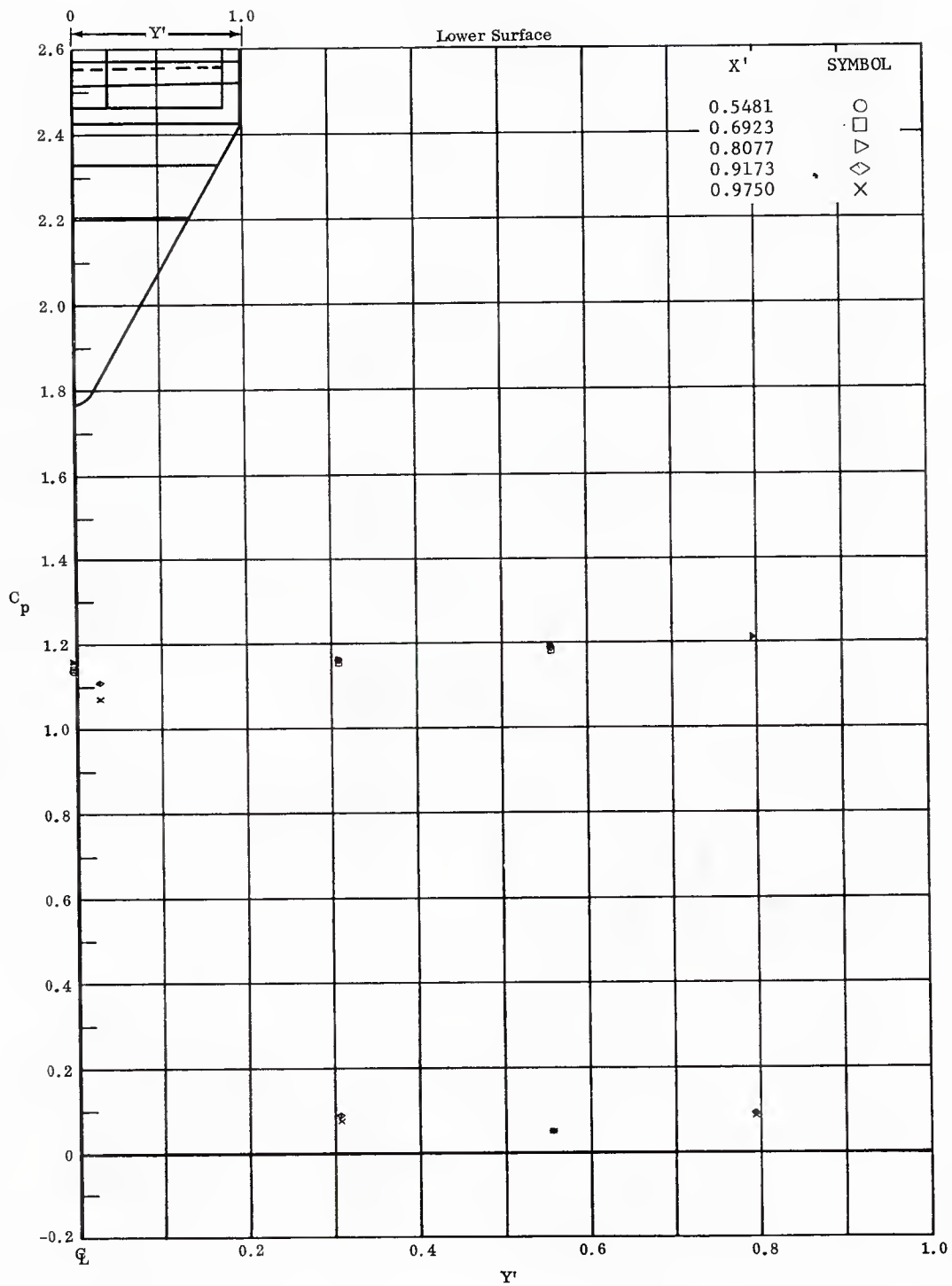


Fig. 38 Spanwise Pressure Distributions on Lower Surface; Left and Right Flaps Deflected  $-40^\circ$ ,  $\alpha = +45^\circ$ .



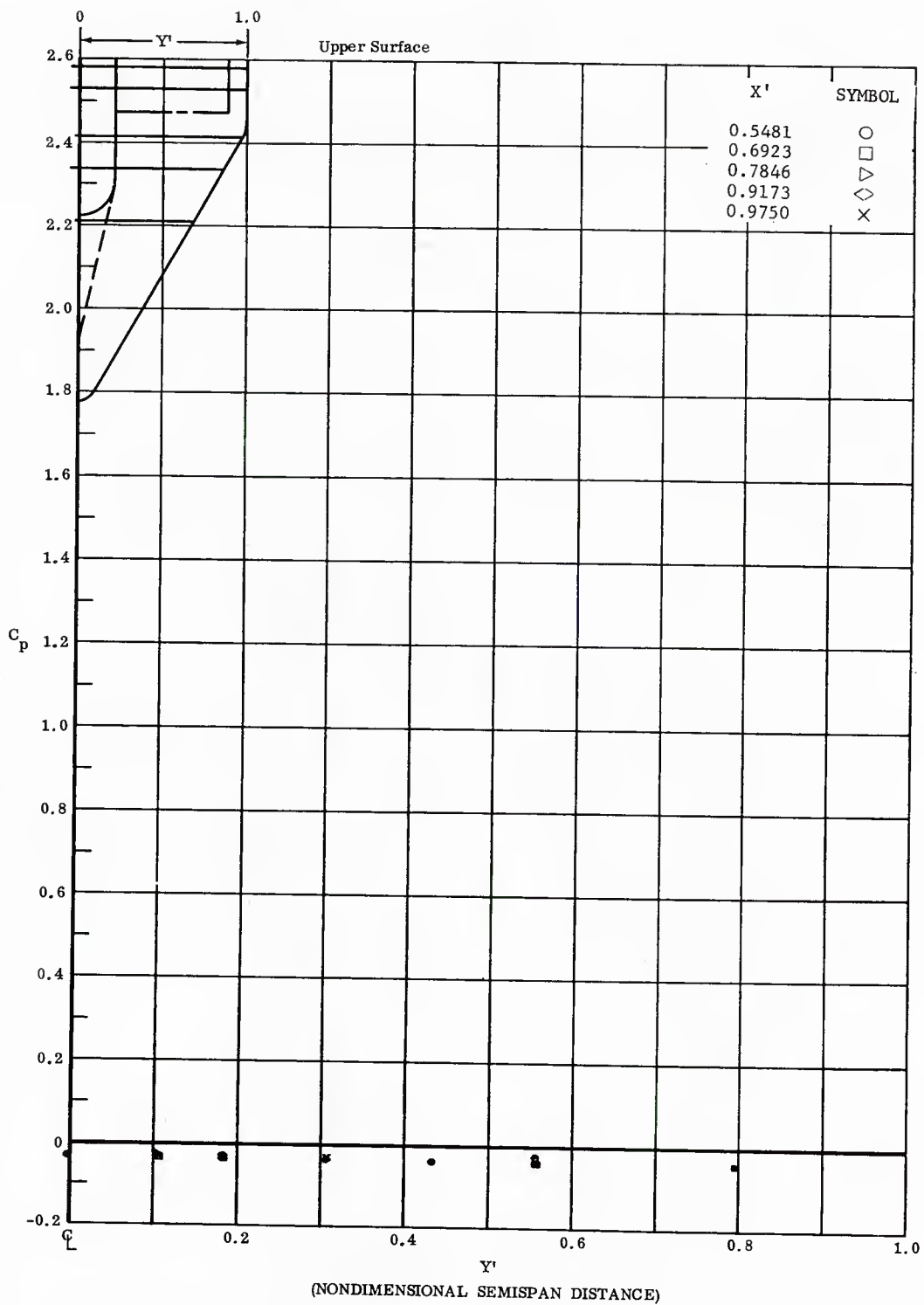


Fig. 38 Spanwise Pressure Distributions on Upper Surface; Left and Right Flaps Deflected  $-40^\circ$ ,  $\alpha = +45^\circ$ .

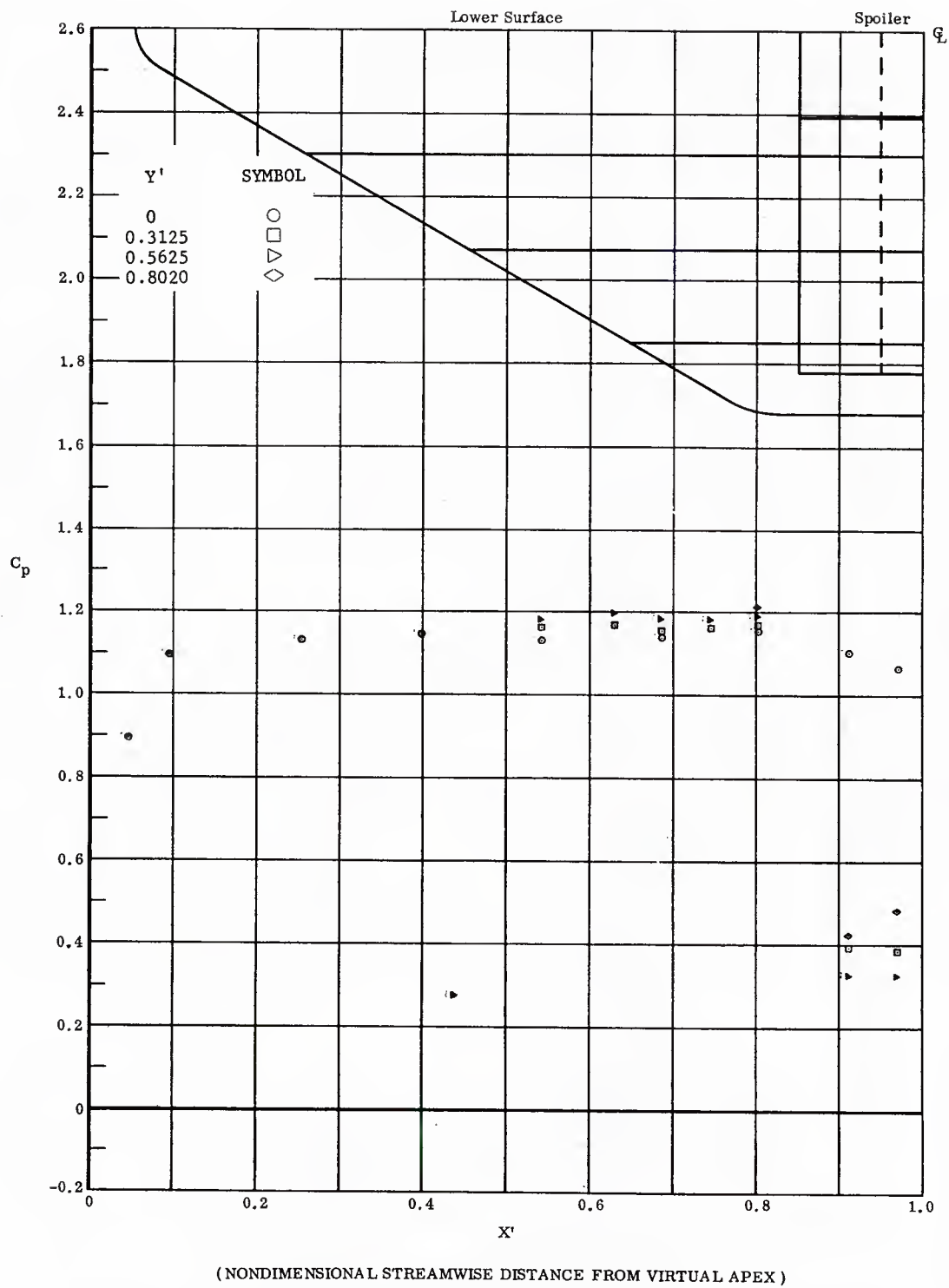
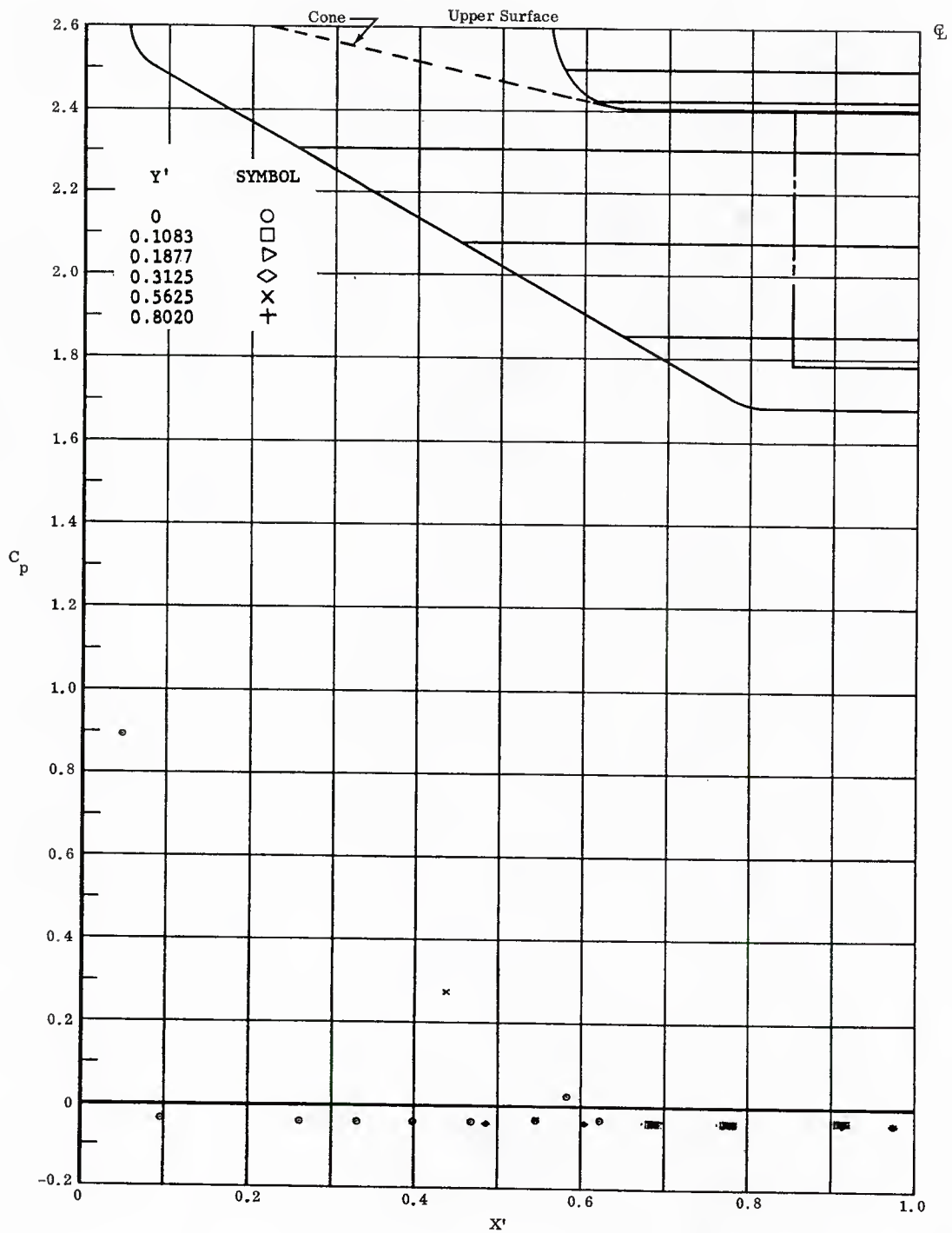
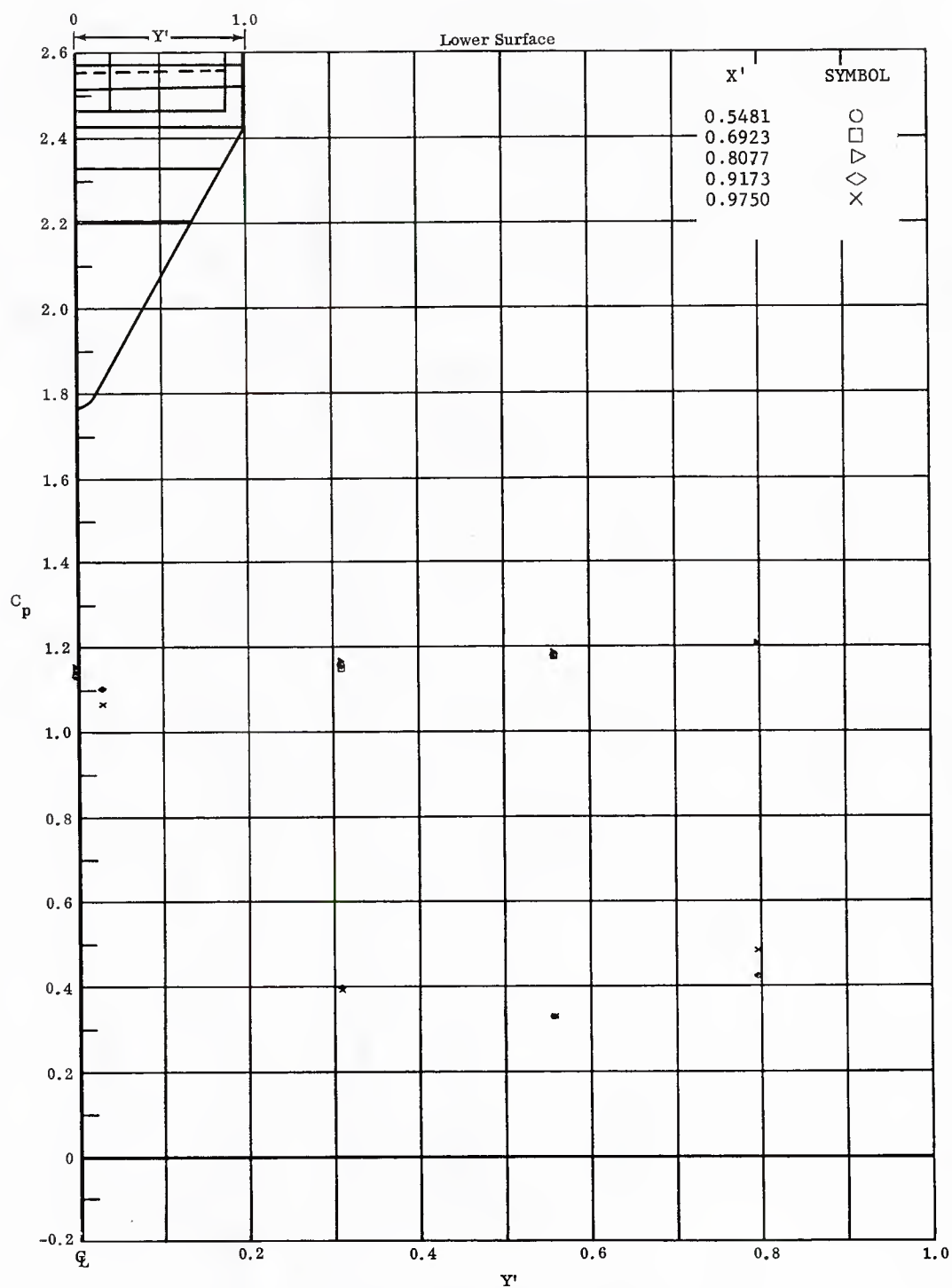


Fig. 39 Streamwise Pressure Distributions on Lower Surface; Left and Right Flaps Deflected  $-20^\circ$ ,  $\alpha = +45^\circ$ .



( NONDIMENSIONAL STREAMWISE DISTANCE FROM VIRTUAL APEX )

Fig. 39 Streamwise Pressure Distributions on Upper Surface; Left and Right Flaps Deflected  $-20^\circ$ ,  $\alpha = +45^\circ$ .



(NONDIMENSIONAL SEMISPAN DISTANCE)

Fig. 39 Spanwise Pressure Distributions on Lower Surface; Left and Right Flaps Deflected  $-20^\circ$ ,  $\alpha = +45^\circ$ .

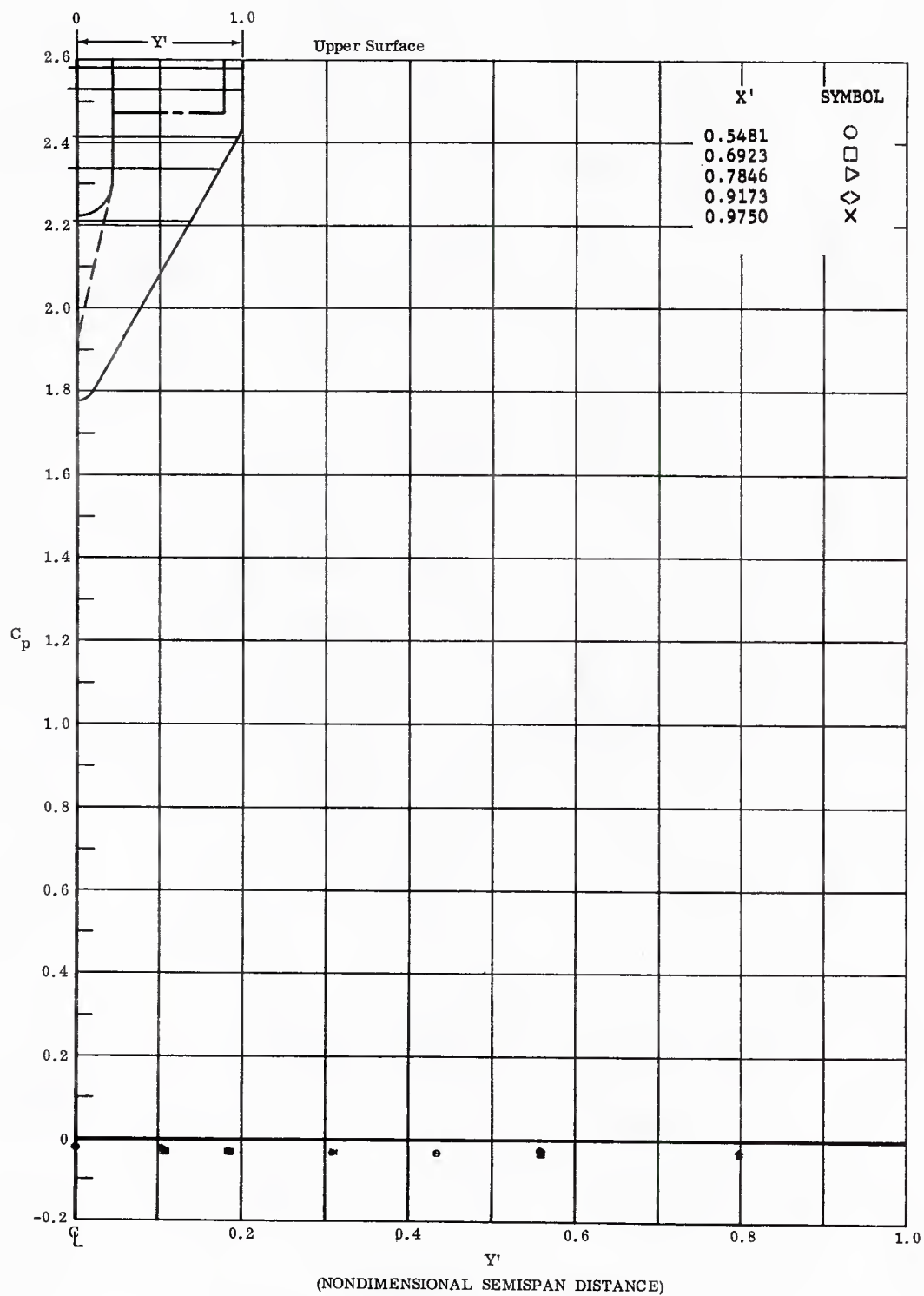


Fig. 39 Spanwise Pressure Distributions on Upper Surface; Left and Right Flaps Deflected  $-20^\circ$ ,  $\alpha = +45^\circ$ .

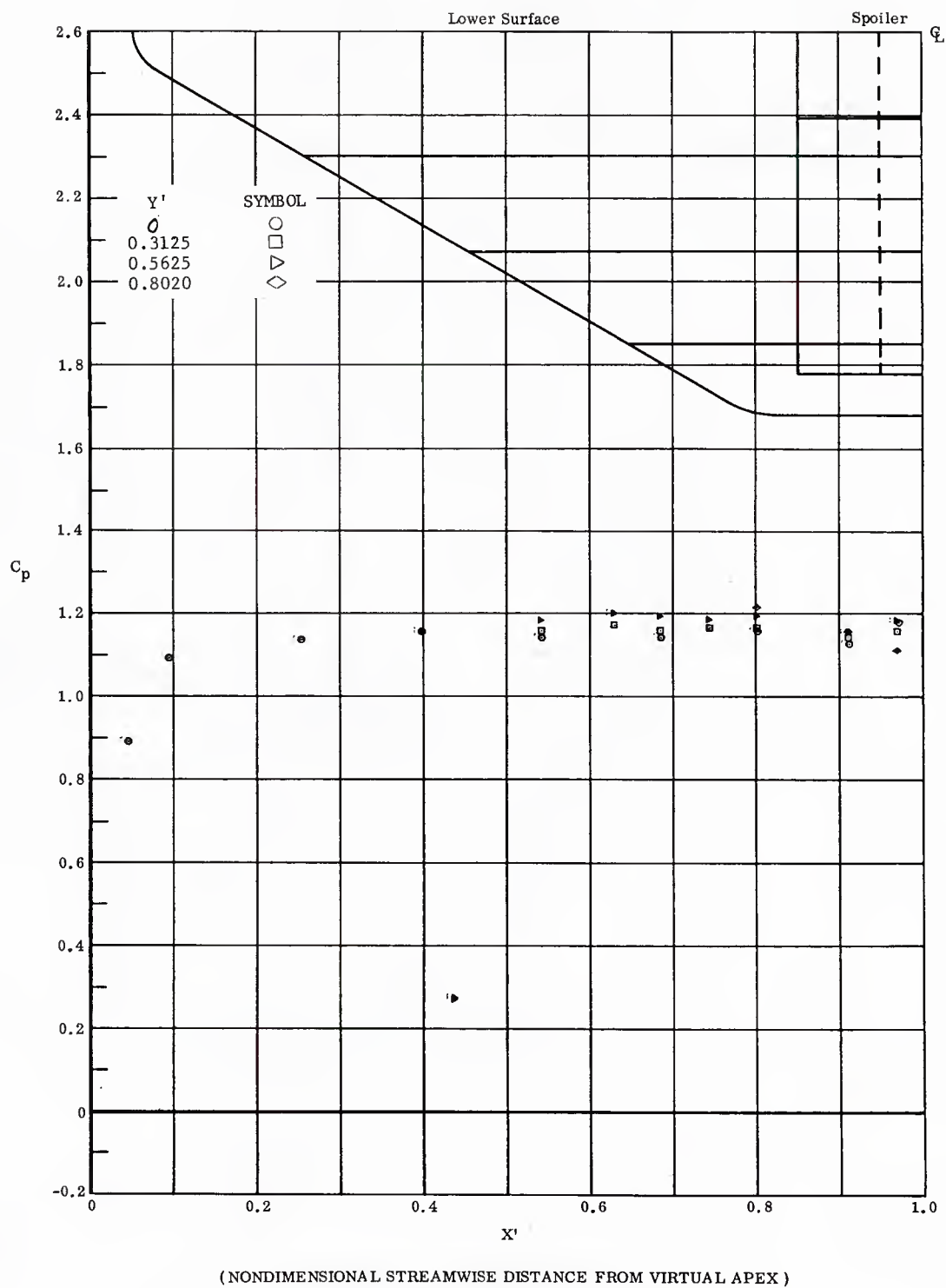


Fig. 40 Streamwise Pressure Distributions on Lower Surface; No Flap Deflections,  $\alpha = +45^\circ$ .

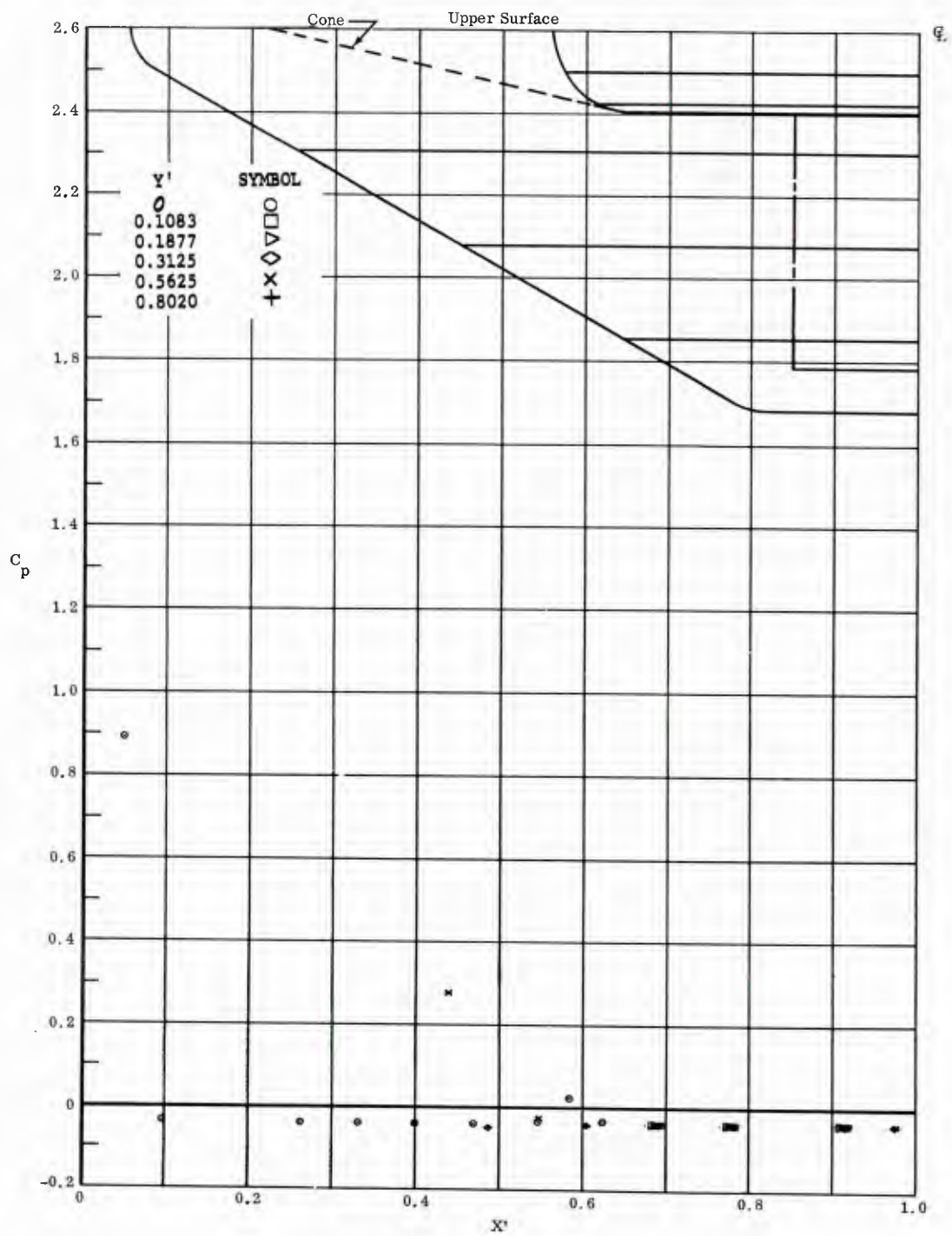


Fig. 40 Streamwise Pressure Distributions on Upper Surface; No Flap Deflections,  $\alpha = +45^\circ$ .

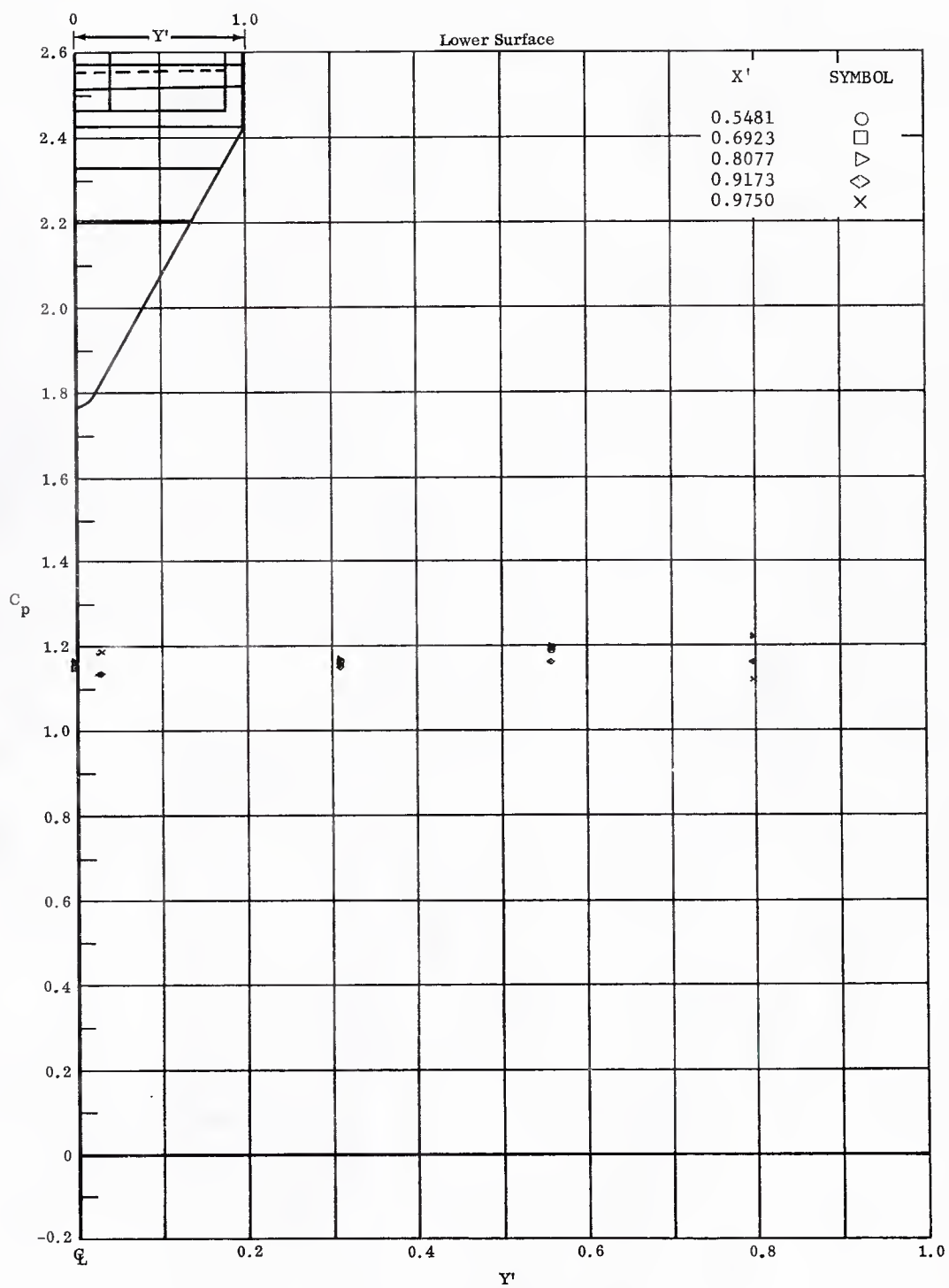


Fig. 40 Spanwise Pressure Distributions on Lower Surface; No Flap Deflections,  $\alpha = +45^\circ$ .



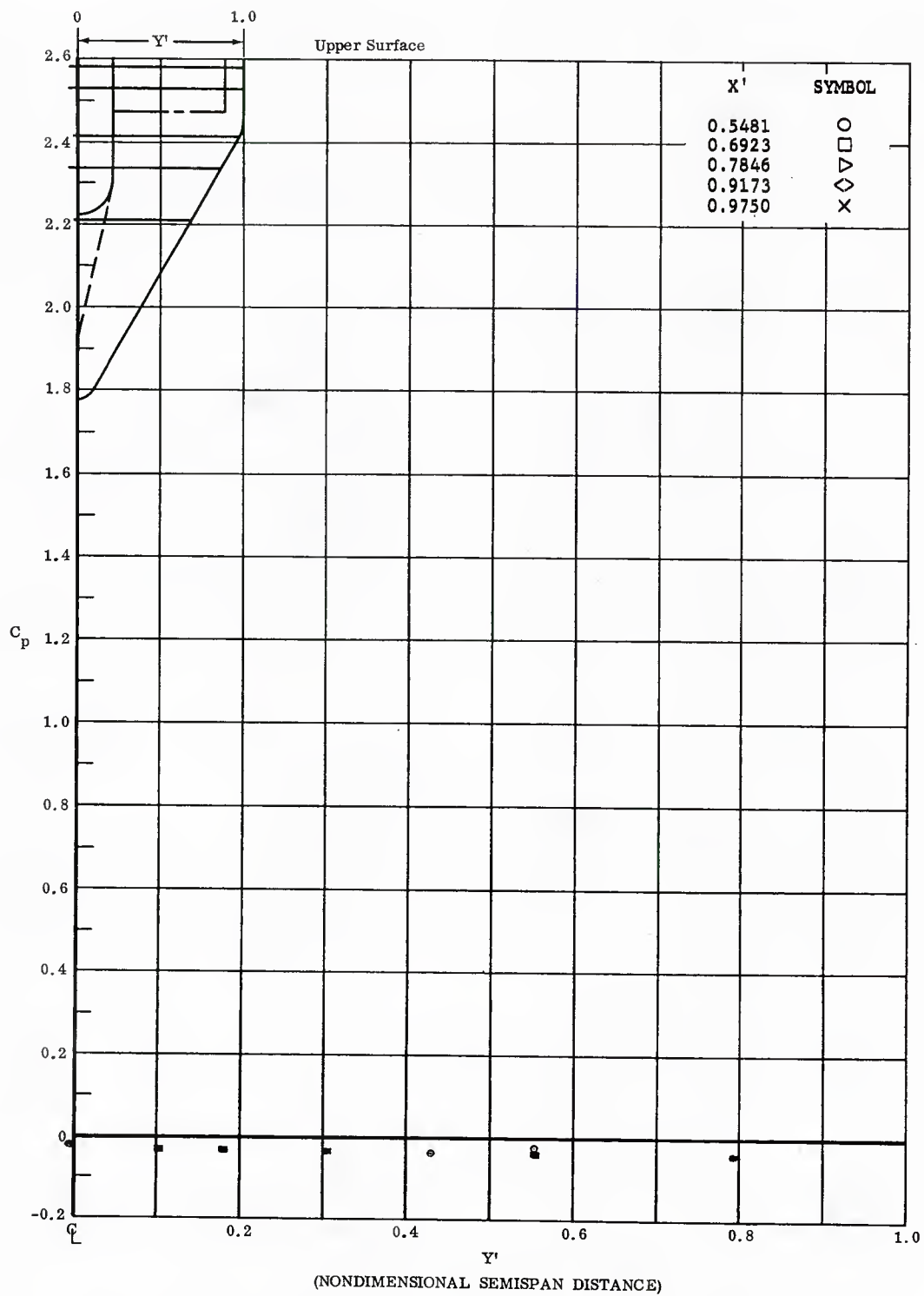


Fig. 40 Spanwise Pressure Distributions on Upper Surface; No Flap Deflections,  $\alpha = +45^\circ$ .

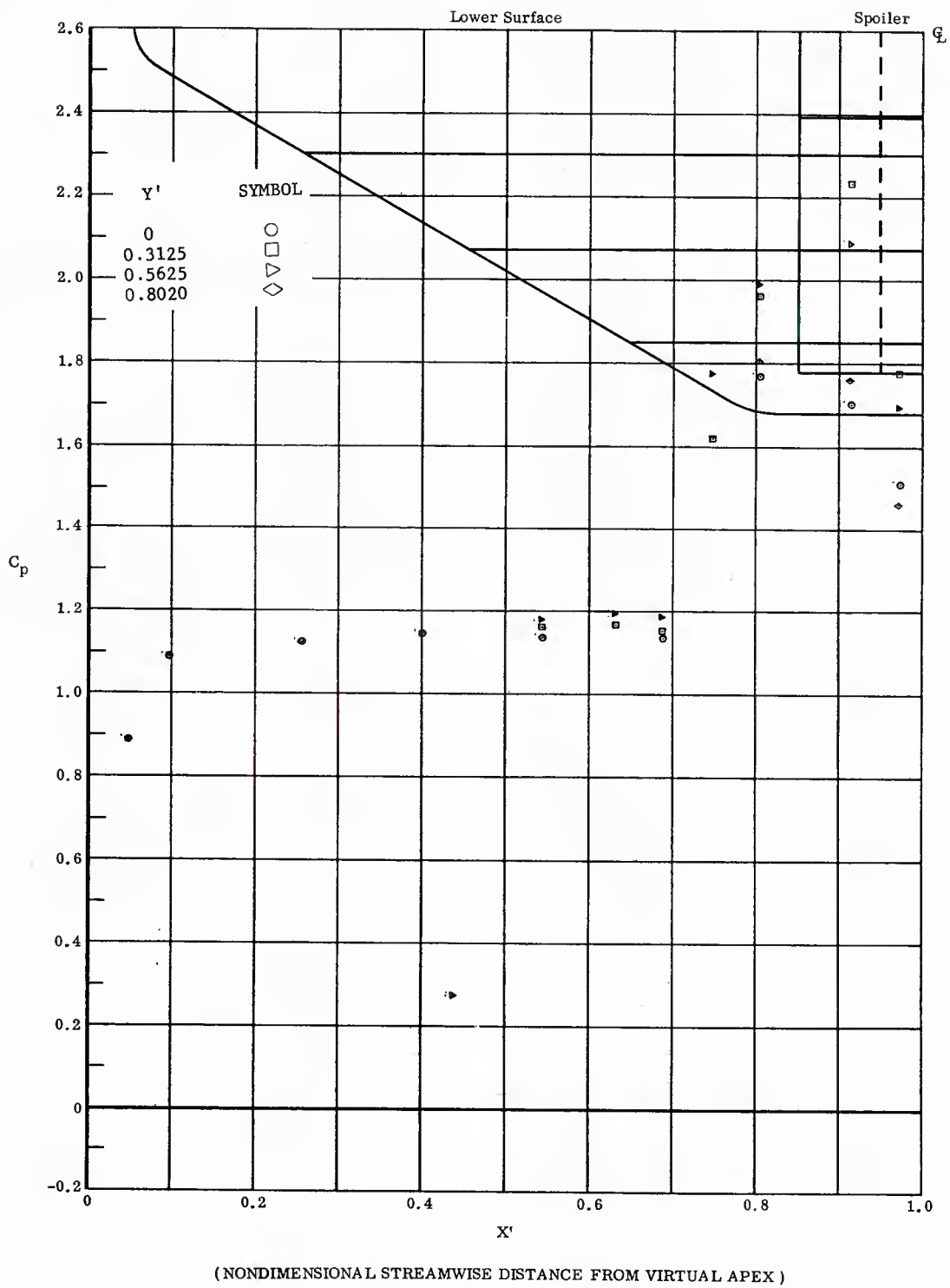
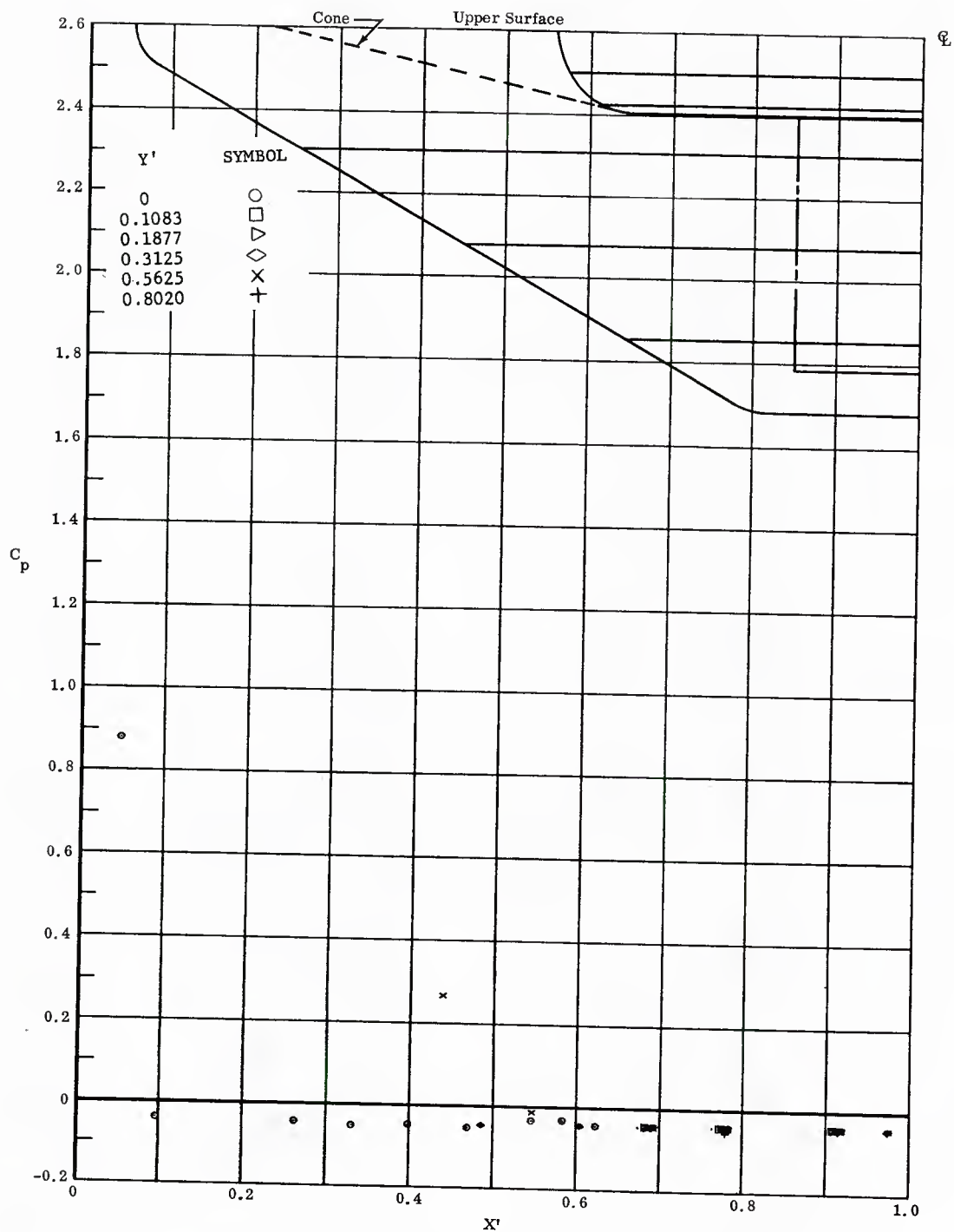


Fig. 41 Streamwise Pressure Distributions on Lower Surface; Left and Right Flap Deflections  $+20^\circ$ ,  $\alpha = +45^\circ$ .



( NONDIMENSIONAL STREAMWISE DISTANCE FROM VIRTUAL APEX )

Fig. 41 Streamwise Pressure Distributions on Upper Surface; Left and Right Flap Deflections  $+20^\circ$ ,  $\alpha = +45^\circ$ .

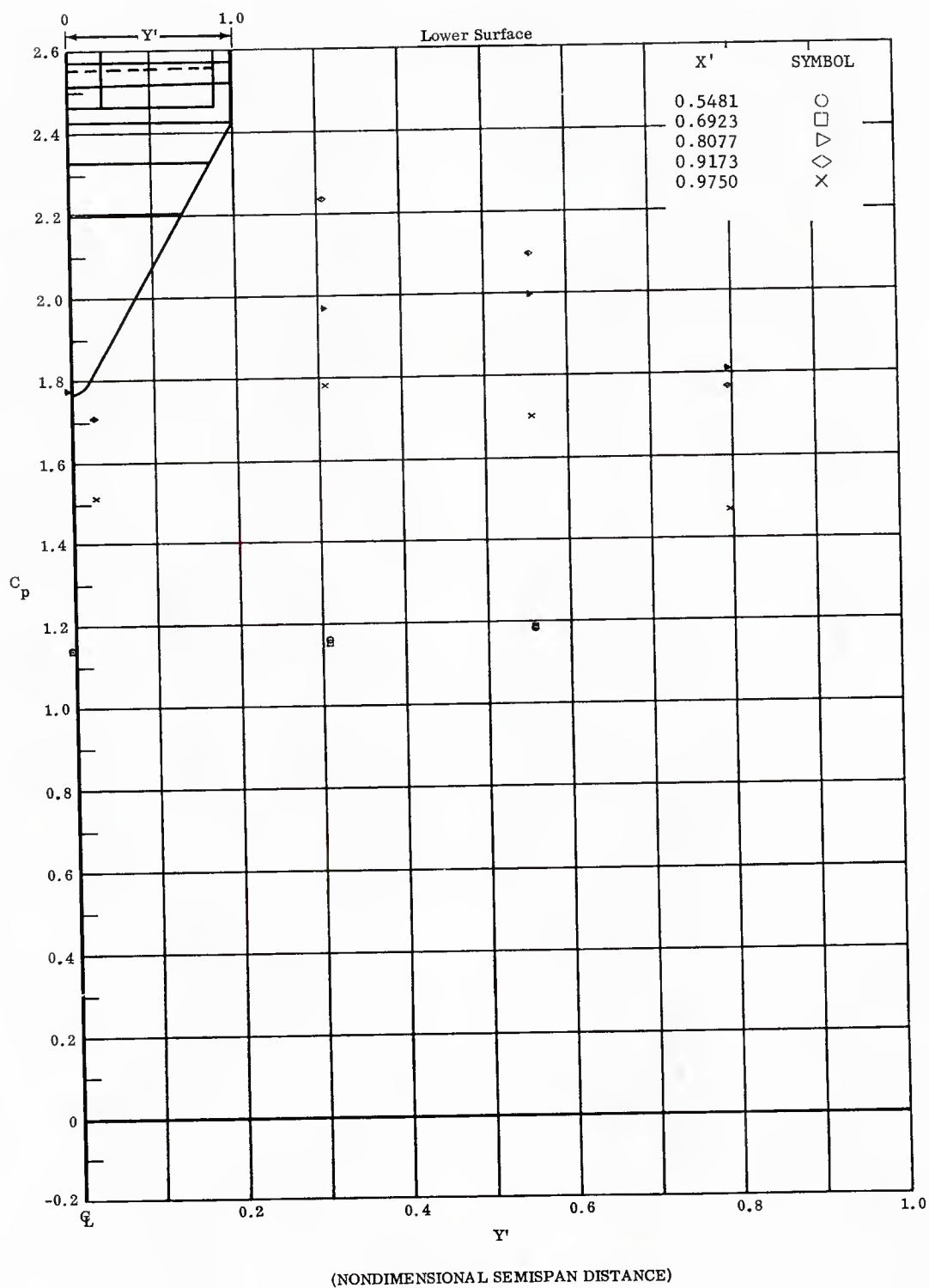


Fig. 41 Spanwise Pressure Distributions on Lower Surface; Left and Right Flap Deflections  $+20^\circ$ ,  $\alpha = +45^\circ$ .

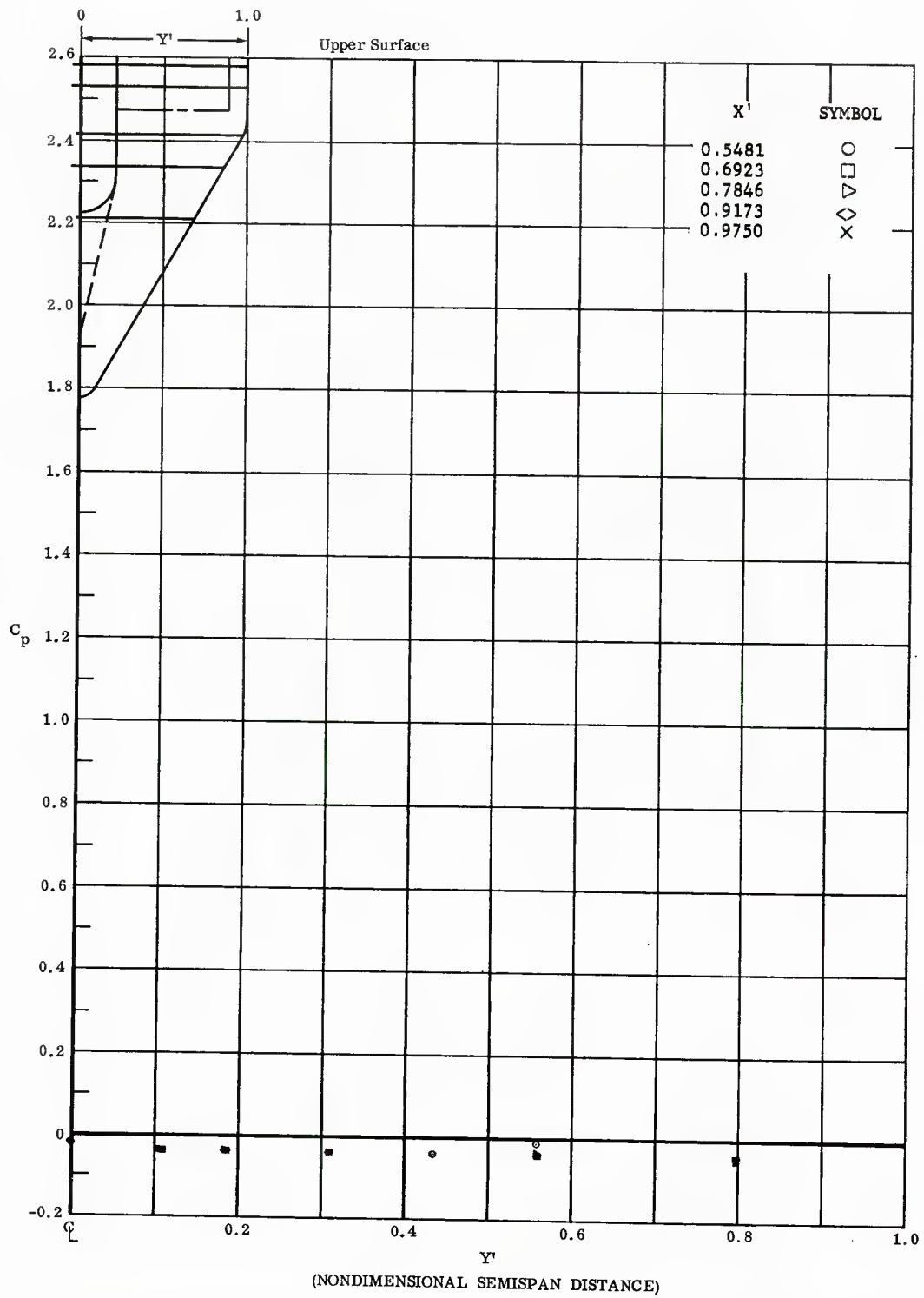


Fig. 41 Spanwise Pressure Distributions on Upper Surface; Left and Right Flap Deflections  $+20^\circ$ ,  $\alpha = +45^\circ$ .

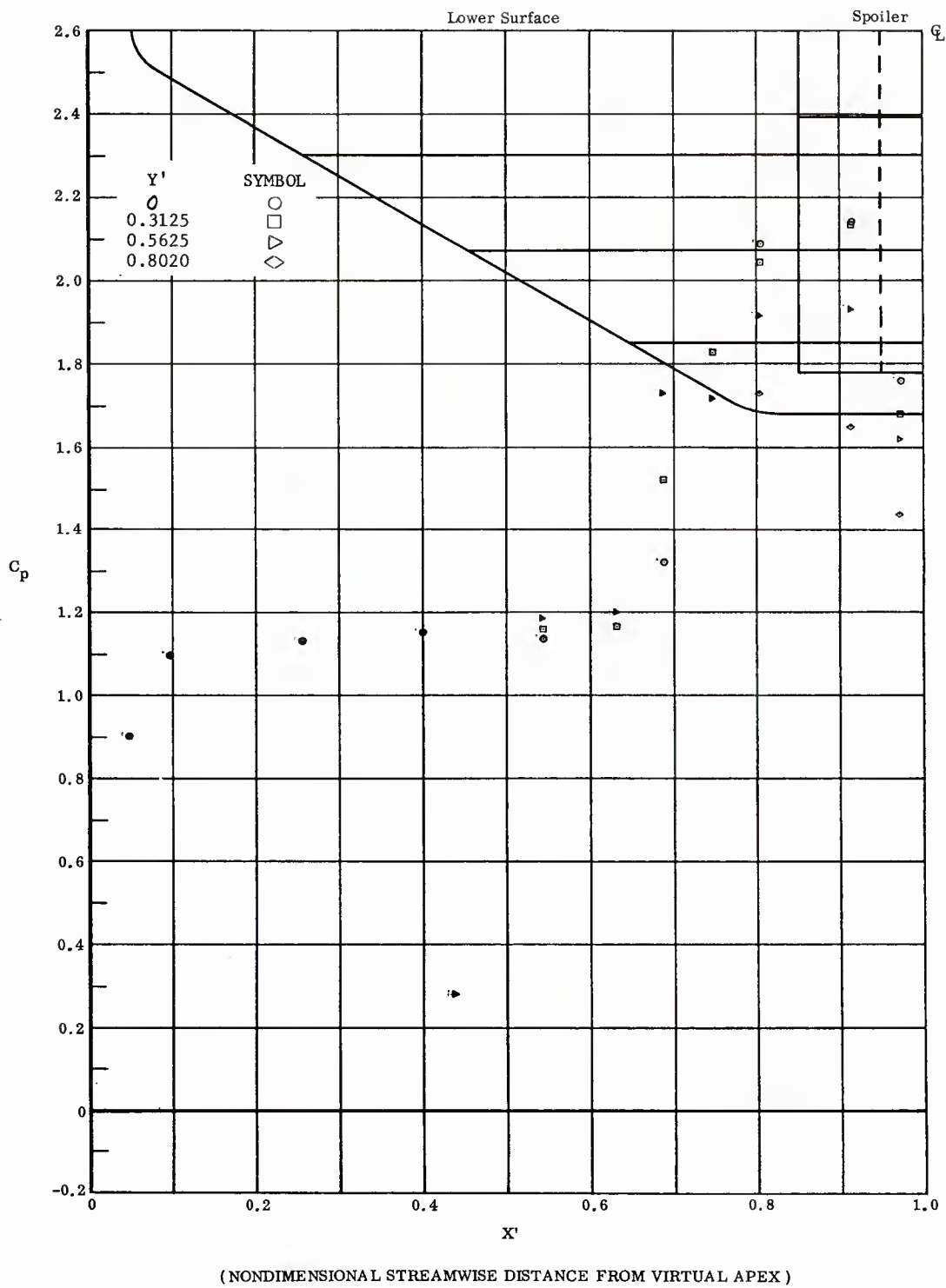
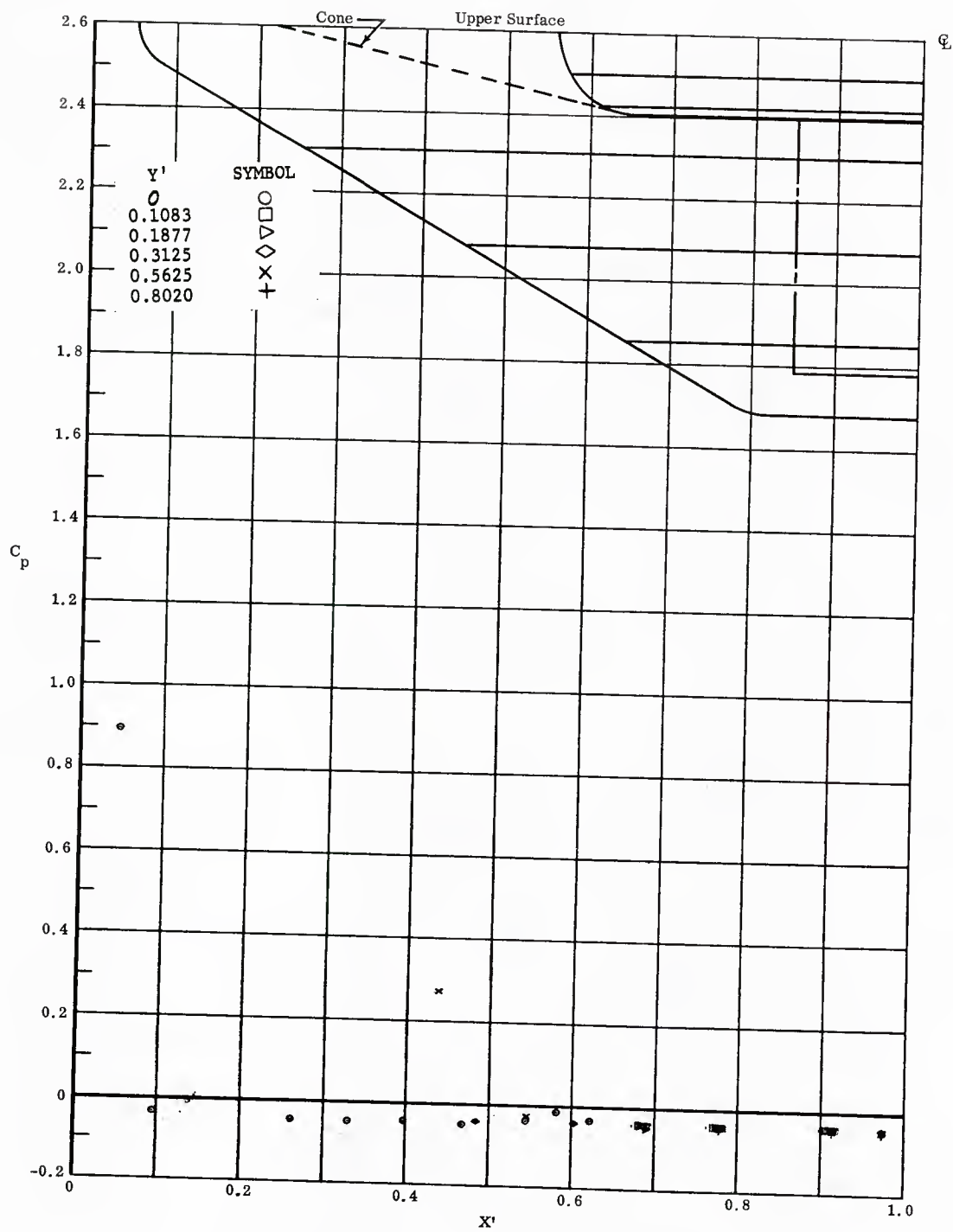


Fig. 42 Streamwise Pressure Distributions on Lower Surface; Center, Left and Right Flaps All Deflected  $+20^\circ$ ,  $\alpha = +45^\circ$ .



( NONDIMENSIONAL STREAMWISE DISTANCE FROM VIRTUAL APEX )

Fig. 42 Streamwise Pressure Distributions on Upper Surface; Center, Left and Right Flaps All Deflected  $+20^\circ$ ,  $\alpha = +45^\circ$ .

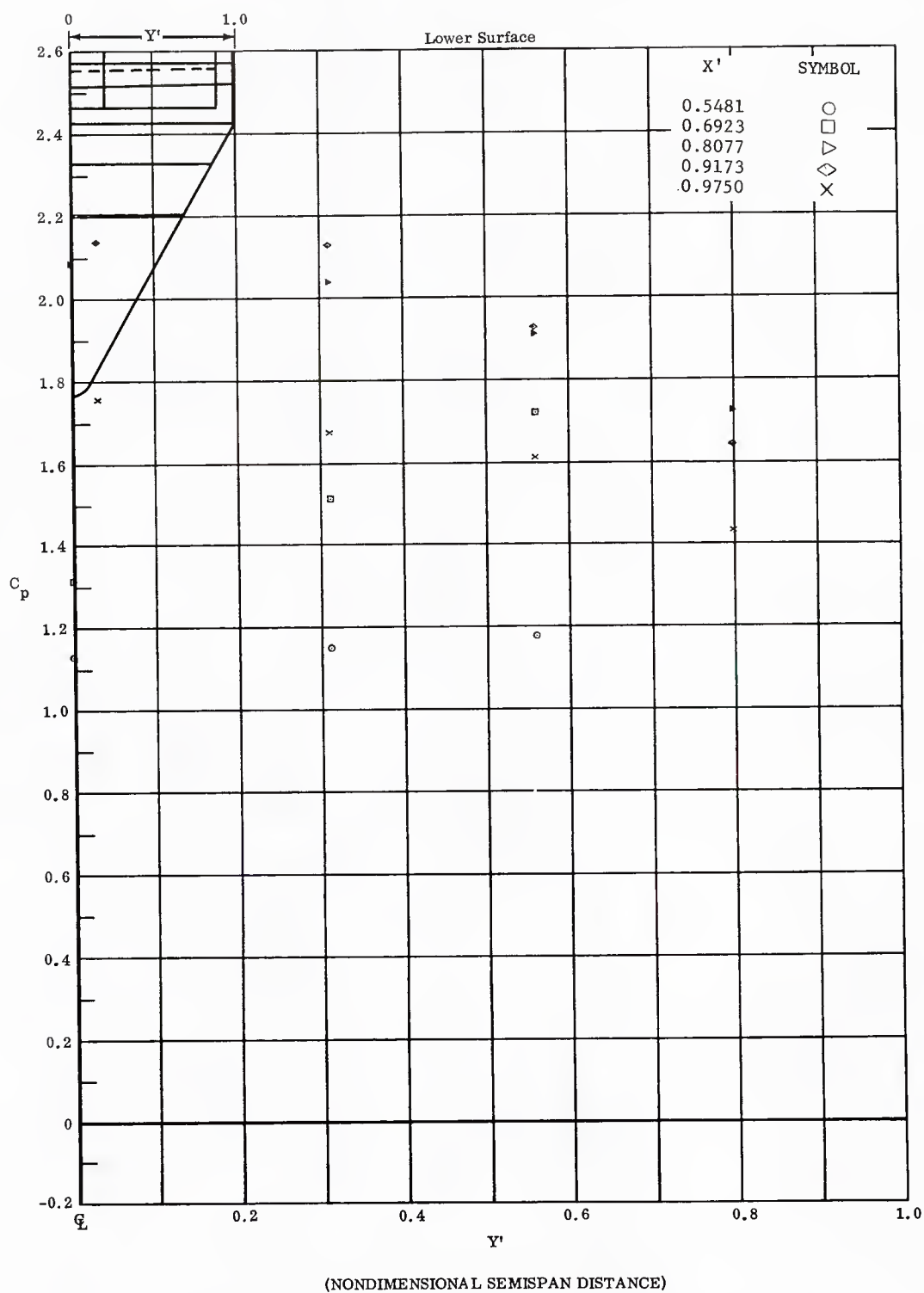


Fig. 42 Spanwise Pressure Distributions on Lower Surface; Center, Left and Right Flaps All Deflected  $+20^\circ$ ,  $\alpha = +45^\circ$ .



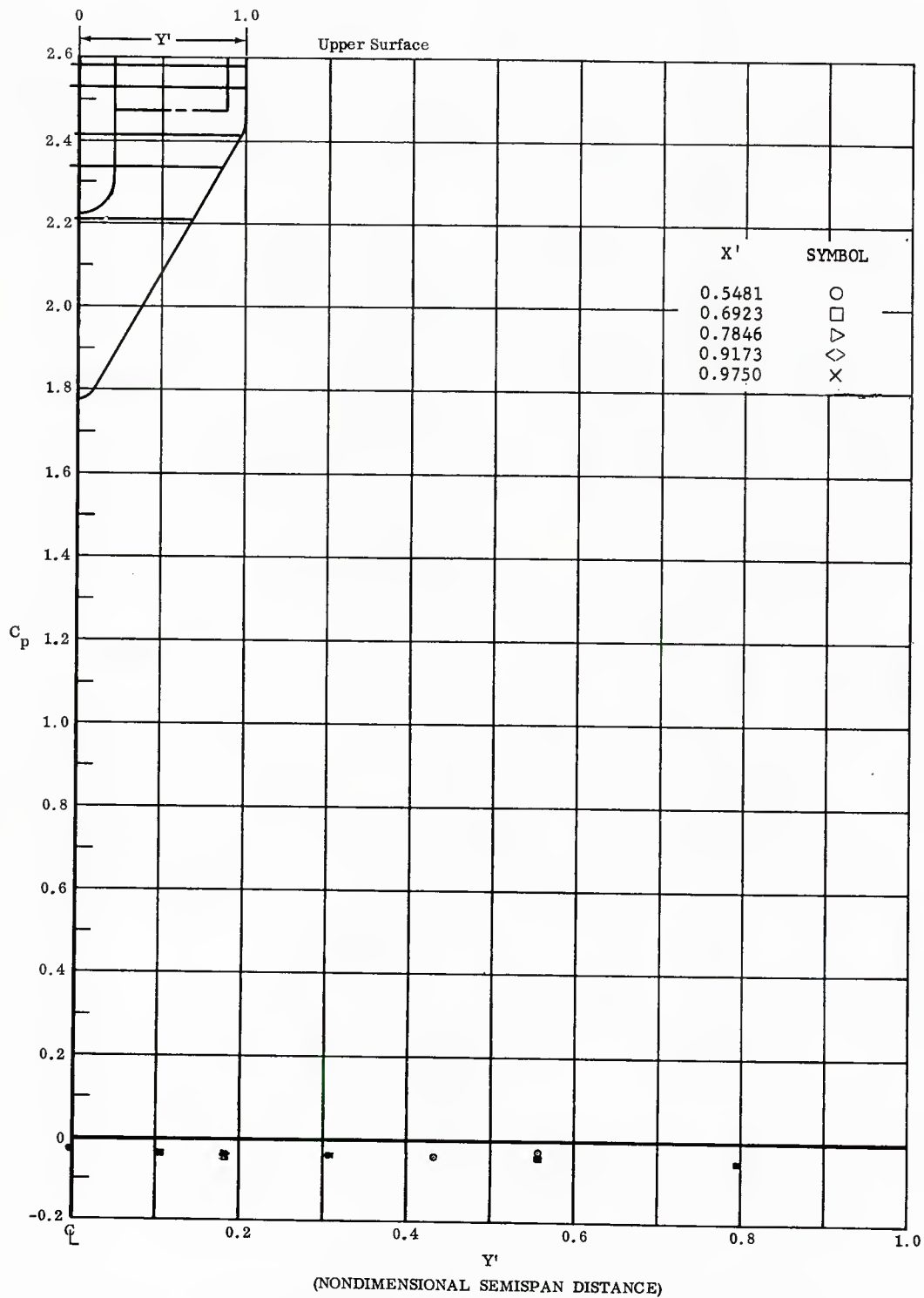


Fig. 42 Spanwise Pressure Distributions on Upper Surface; Center, Left and Right Flaps All Deflected  $+20^\circ$ ,  $\alpha = +45^\circ$ .